Author:
O'Brien, Harry

Title:
Advances in Iron-Catalysed Cross-Coupling Reactions

Methodology and Mechanism

Advances in Iron-Catalysed Cross-Coupling Reactions: Methodology and Mechanism

Harry Melville O'Brien

A dissertation submitted to the University of Bristol in accordance with the requirements for the award of the degree of Doctor of Philosophy in the Faculty of Science

School of Chemistry

August 2018

Abstract

The replacement of noble metal complexes with cheap, sustainable and non-toxic iron complexes as catalysts for cross-coupling reactions continues unabated. The significant advancement in methodology seen in the last decade has been accompanied by elegant mechanistic studies; vital for further reaction development.

The development of reactions which work with milder coupling partners is paramount. Organoboron reagents are particularly useful, and accordingly there has been great progress in the development of iron-catalysed Suzuki cross-coupling reactions. However, the cross-coupling between an aryl halide and an aryl boron reagent, a Suzuki biaryl cross-coupling, has not yet been achieved with iron-catalysis under mild conditions. Here, it is shown that the barrier to success has been in the activation of the aryl halide bond. This has been overcome by installation of an *ortho N*-pyrrole amide directing group (Scheme i). Notably, mechanistic studies reveal that the *N*-pyrrole amide works by tethering the iron-catalyst to the electrophile *via* π-coordination, and a single electron transfer process to afford an amino ketyl radical appears to be responsible for activation of the aryl halide bond.

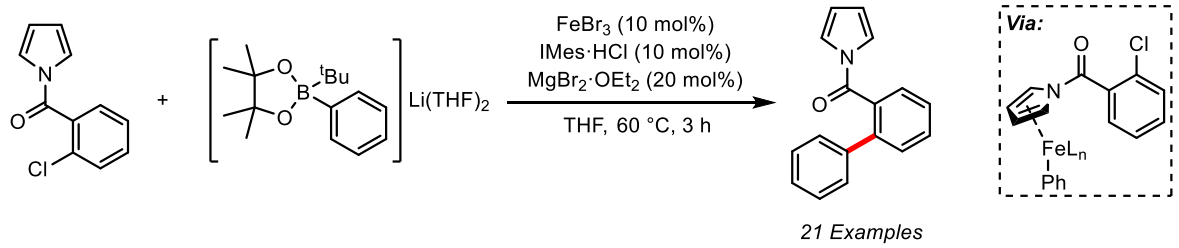

Scheme i: Iron-catalysed Suzuki biaryl cross-coupling *via* π-pyrrole coordination.

Asymmetric iron-catalysed cross-couplings are extremely rare, and the seminal example suffers from a restrictive electrophile scope. The enantioconvergent iron-catalysed cross-coupling of an unactivated alkyl halide substrate has been investigated to broaden the scope of this methodology.

Finally, a combined synthetic and mechanistic study was conducted to compare the activity of an *N*-heterocyclic carbene ligand with its *N*-heterocyclic germylene analogue in iron-catalysed cross-couplings (Figure i); affording insights into the role of carbene ligands in iron-catalysis.

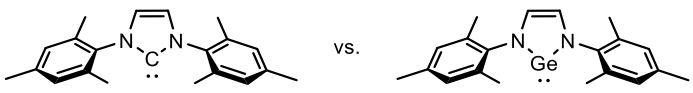

Figure i: A vis-à-vis comparison of an *N*-heterocyclic carbene and *N*-heterocyclic germylene.

Acknowledgements

First and foremost, I would like to thank my supervisor Robin Bedford for his wealth of ideas, encouragement and passion for chemistry which has made my PhD so enjoyable. Being able to pursue my own ideas whilst under the guidance of someone who is always genuinely excited to hear the next result is an opportunity not everyone is so lucky to receive. I still remember our first meeting and just knowing that Robin was who I wanted to work for; I was not wrong either. My industry supervisor Andrew Stark has given me a fantastic insight into the industrial side of chemistry, giving me perspective on how all our hard work fits into the larger picture. I am particularly thankful for his efforts to make my placement at AstraZeneca so rewarding. Finally, I would like to thank Masaharu-sensei for allowing me to spend a wonderful 10 weeks in his lab in Japan.

Thank you to Alex, Hope, Liam and Elliott; all of whom made my first home, and thus my time in Bristol, a truly memorable four years.

I would also like to thank the members of the Bedford group, past and present, who have made my second home a fantastic place to work in: Michelle, Tom, Oscar, Antonis, David, Stephen, Sanita, Carolina, Mattia, Soneela, Harry and Ben. Also the members of the Bower group; Matt, Phillippa, Olivia and Lauren who have been great people to share our lab space with. The undergraduate students who I have supervised and mentored over these four years: Katie, Charlotte, Roman, Leyla and Phil. Advising you all taught me more than you may have realised.

And finally, thank you to everyone for being especially understanding when I made a little too much of an unwanted side-product.

Abbreviations

General

δ	chemical shift
aq.	aqueous
br	broad
cat.	catalyst
d	doublet
ee	enantiomeric excess
equiv.	equivalent
er	enantiomeric ratio
ESI	electrospray ionisation
GC	gas chromatography
h	hour
HAAD	high-angle annular dark-field
HRMS	high resolution mass spectrometry
IR	infrared
J	coupling constant
KIE	kinetic isotope effect
LUMO	lowest unoccupied molecular orbital
m	multiplet
m.p.	melting point
m/z	mass-to-charge ratio
M^+	parent molecular ion
mol	mole
MS	mass spectrometry
n.d.	not detected
NMR	nuclear magnetic resonace
ppm	parts per million
q	quartet

Reagents and Solvents

^{n}BuLi	*n*-butyllithium
^{i}BuOH	*iso*-butanol
DCC	*N*,*N*'-dicyclohexylcarbodiiminde
DIPAMP	1,2-bis[(2-methoxyphenyl)(phenylphosphino)]ethane
DMAP	4-dimethylaminopyridine
DMF	dimethylformamide
dpbz	1,2-bis(diphenylphosphino)benzene
dppe	1,2-bis(diphenylphosphino)ethane
dppp	1,3-bis(diphenylphosphino)propane
dvtms	1,3-divinyltetramethyldisiloxane
Et_3N	triethylamine
Et_2O	diethyl ether
EtOAc	ethyl acetate
EtOH	ethanol
HMPA	hexamethylphosphoramide
IMes	1,3-bis-(2,4,6-trimethylphenyl)imidazol-2-ylidene
IPr	1,3-bis-(2,6-diisopropylphenyl)imidazol-2-ylidene
KOAc	potassium acetate
KOMe	potassium methoxide
MeOH	methanol
NHC	*N*-heterocyclic carbene
NMP	*N*-methyl-2-pyrrolidone
PCy_3	tricyclohexylphosphine
PEG	poly(ethylene glycol)
PPh_3	triphenylphosphine
SciOPP	spin-control-intended *ortho*-phenylene bisphosphine
SIMes	1,3-bis-(2,4,6-trimethylphenyl)imidazol-2-ylidene

R	residual group
r.t.	room temperature
s	singlet
STEM	scanning transmission electron microscopy
t	triplet
TEM	transmission electron microscopy
Temp.	temperature
TLC	thin layer chromatography
SIPr	1,3-bis-(2,6-diisopropylphenyl)imidazol-2-ylidene
TEMPO	2,2,6,6-tetramethylpiperidine 1-oxyl
TASF	tris(dimethylamino)sulfonium difluorotrimethyl silicate
THF	tetrahydrofuran
TMSCl	chlorotrimethylsilane

Substituents

acac	acetylacetonate
^{t}Bu	*tert*-butyl
Et	ethyl
Me	methyl
Mes	mesityl
Ph	phenyl
^{i}Pr	*iso*-propyl
Tol	tolyl
Tf	triflate
Ts	tosyl
X	halide

Declaration

I declare that the work in this dissertation was carried out in accordance with the requirements of the University's *Regulations and Code of Practice for Research Degree Programmes* and that it has not been submitted for any other academic award. Except where indicated by specific reference in the text, the work is the candidate's own work. Work done in collaboration with, or with the assistance of, others, is indicated as such. Any views expressed in the dissertation are those of the author.

Harry Melville O'Brien

August 2018

Contents

Chapter 1
Introduction

1.1 Transition Metal-Catalysed Cross-Coupling Reactions: Methodology

The ability to selectively form a new C-C bond between an organic halide, or related substrate, and an organometallic reagent in the presence of sub-stoichiometric transition metal-catalysts has irrevocably changed the way chemists approach synthesis. When the two organic moieties from the organic halide and organometallic reagent are different from one another, the reaction is termed 'cross-coupling'. A general scheme for this transformation is given in Scheme 1.1. The importance of cross-coupling was demonstrated by the award of the 2010 Nobel Prize in chemistry to Richard F. Heck, Akira Suzuki and Ei-ichi Negishi for their contributions to palladium-catalysed cross-couplings.[1]

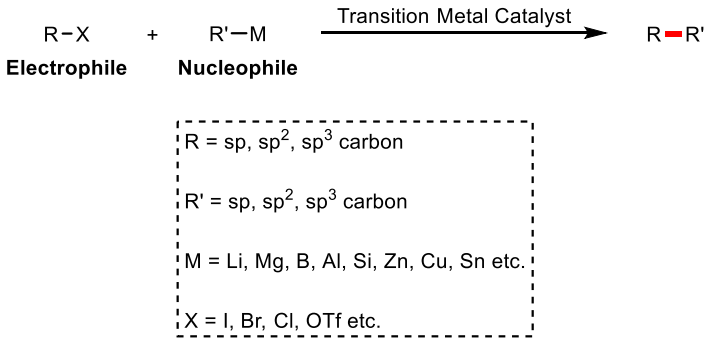

Scheme 1.1: Cross-coupling of two different organic fragments by a transition-metal catalyst.

The development of transition-metal catalysed cross-coupling reactions began with stoichiometric metal-mediated homocouplings from around 150 years ago.[2] Indeed, it is due to investigations into organometallic chemistry that progression towards using catalytic amounts of transition metals for organic synthesis occurred. For example, as early as 1905 Ullmann showed that sub-stoichiometric quantities of copper could promote C-O bond formation,[3] having reported just a few years earlier the dimerisation of 2-bromonitrobenzene mediated by 2 equivalents of copper.[4]

It was Job who reported the first transition metal-catalysed C-C coupling in the 1920's, noting that a solution of phenylmagnesium bromide with $NiCl_2$ is able to 'absorb' CO, C_2H_4 and C_2H_2.[2] This discovery went (and remains) largely unnoticed, with Corriu later stating that 'this great chemist, who was in fact the grandfather of the chemistry we are talking about today in this symposium, was and is completely unknown'.[5]

Instead, it is commonly accepted that the first example of a C-C cross-coupling reaction as depicted in Scheme 1.1 is attributed to Kharasch, who in 1941 published a series of papers on the effect of metal halides on the reactions between Grignard reagents and organic halides. A key example is the reaction between phenylmagnesium bromide and bromobenzene in the presence of different metal halide salts to produce biphenyl (Scheme 1.2).[6] Importantly, the coupling of two *different* organic moieties was also demonstrated.

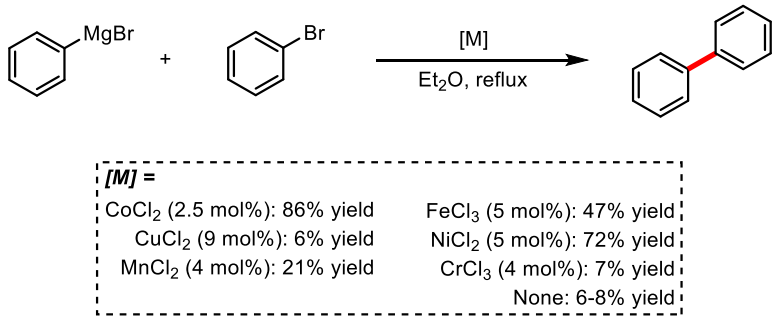

Scheme 1.2: Metal-catalysed cross-coupling of phenylmagnesium bromide with vinyl bromide.[6]

Although this demonstrated unequivocally that transition metals could be used as catalysts to form C-C bonds, the subsequent reactions developed by Kharasch,[7, 8] and also Meerwein,[9] were limited in their synthetic applicability. This was due to the lack of selectivity for the cross-coupled product, with homocoupling reactions severely affecting the yields of the desirable cross-coupling. It was in 1972 that Corriu[10] and Kumada[11, 12] overcame this limitation when both independently reported nickel-catalysed cross-couplings of aryl and alkenyl halides with Grignard reagents (Scheme 1.3a and 1.3b). Notably, Kumada used a nickel catalyst bearing a bidentate phosphine ligand to affect the best activity, setting the direction for the design of organometallic complexes as catalysts in cross-coupling chemistry for decades to come.

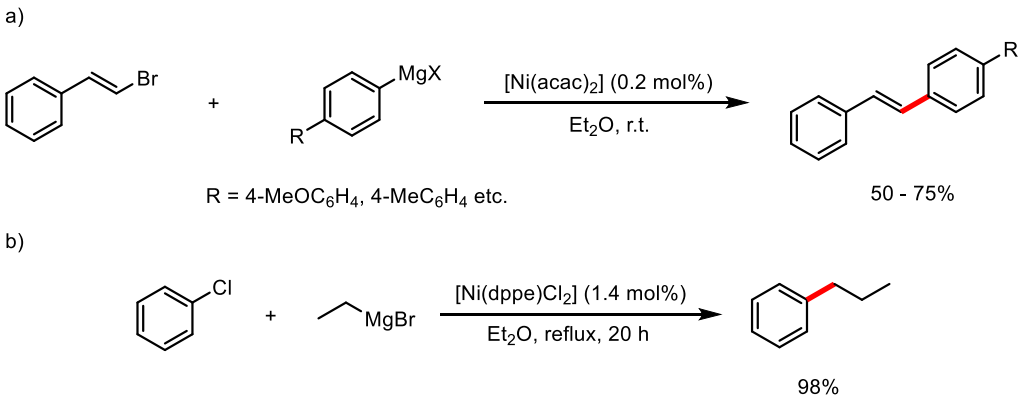

Scheme 1.3: Nickel-catalysed cross-coupling reactions between aryl and alkenyl halides with Grignard reagents reported by a) Corriu[10] and b) Kumada[11, 12].

1.1.1 The Genesis of Palladium Catalysis

The interest in palladium catalysts began when seven back-to-back publications were disclosed by Heck describing C-C bond forming reactions using arylmercury compounds with stoichiometric or catalytic Pd(II) (Scheme 1.4a).[13-19] In 1972, the same author described a process for the cross-coupling of styrene and iodobenzene under palladium-catalysis, known later as the Heck reaction (Scheme 1.4b).[20]

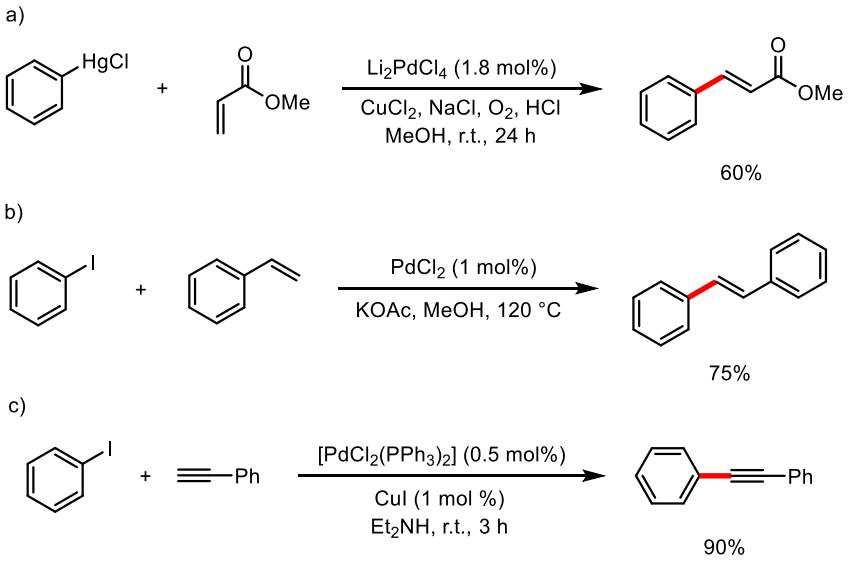

Scheme 1.4: The introduction of palladium catalysis by Heck utilising a) arylmercuric compounds,[13-19] later refined to what is known today as the Heck reaction (b).[20] The Sonogashira reaction (c) followed soon after.[21]

At this point, nickel, copper and palladium were the three main metals utilised in cross-coupling reactions.[22] However, the advantages of palladium catalysis soon became apparent. It replaced copper-based catalysts in the cross-coupling of acetylenes after being shown to work under exceedingly mild conditions, marking the birth of the Sonogashira reaction (Scheme 1.4c).[21] It also mostly replaced nickel in the cross-coupling of organomagnesium and organolithium reagents with organic halides;[23, 24] nickel being prone to allowing unwanted side reactions whereas the activity of palladium was more predictable.

With the choice of palladium-based catalysts becoming firmly rooted, attention turned to the different types of cross-coupling partner that could be utilised. This was born out of a desire to use less electropositive metals for the organometallic species to afford greater functional group tolerance. Subsequently, Negishi reported the palladium- and nickel-catalysed cross-coupling of organoaluminium reagents with organohalides (Scheme 1.5a).[25] However, it was the cross-coupling of organozinc reagents under palladium catalysis that earned Negishi his named reaction (Scheme 1.5b).[26, 27] Around the same time, Stille showed that organostannanes are also mild coupling partners (Scheme 1.5c).[28]

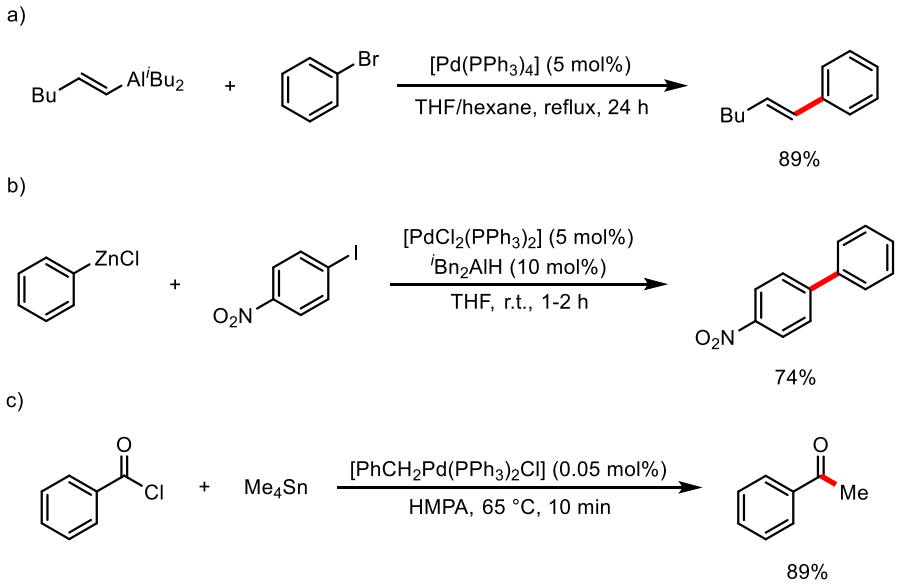

Scheme 1.5: The seminal reactions by Negishi: a) aluminium- and b) zinc-based organometallic cross-coupling partners.[25-27] The Stille reaction, using organostannanes (c) was developed soon after.[28]

Whilst the Negishi reaction tolerates a wide variety of functional groups, the organozinc reagents used in Negishi cross-couplings are sensitive to moisture, requiring inert atmosphere techniques to carry out the reactions. The organostannane cross-coupling procedures developed by Stille are exceptionally mild, however the toxicity of these reagents is concerning. What was needed was an organometallic cross-coupling partner that was highly active, functional group tolerant, bench-stable and non-toxic. All of these requirements were met by the utilisation of organoboron reagents, pioneered by Akira Suzuki (Scheme 1.6a).[29, 30] Since the polarity of the C-B bond is a lot lower compared to other organometallics, Suzuki reactions require a stoichiometric amount of base to 'activate' the nucleophile. This occurs by addition of the base in the vacant p-orbital on the boron atom, furnishing the more reactive 'ate' complex which allows for transmetallation to occur. A decade later, Hiyama showed how even more benign organosilicon reagents are competent cross-coupling partners (Scheme 1.6b).[31]

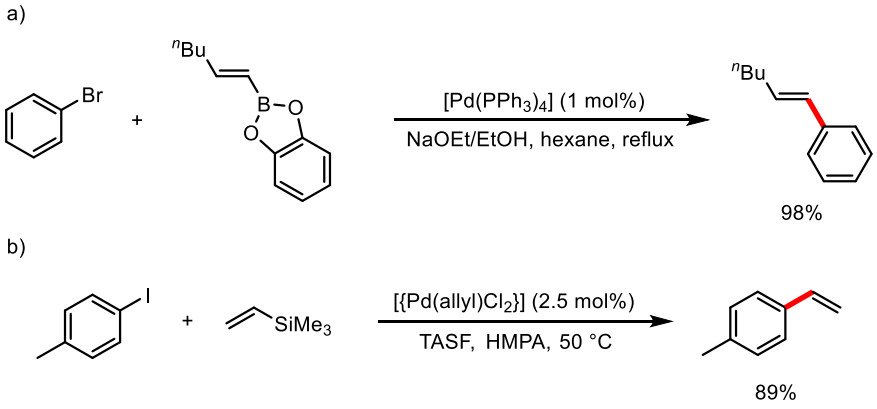

Scheme 1.6: The cross-coupling of a) organoboron reagents and b) organosilicon reagents pioneered by Suzuki[29, 30] and Hiyama[31] respectively.

Although organosilicon reagents are more environmentally friendly than organoboron reagents, today the Suzuki reaction is considered to be the most powerful method for C-C bond formation; it is easily the most widely used palladium-catalysed cross-coupling reaction. A recent survey found that of all the C-C bond forming reactions used in the pharmaceutical industry (including non-catalysed protocols e.g. Wittig olefination and Friedel-Crafts acylation), 40.2% of the reactions were Suzuki couplings, with the second most utilised reaction being Sonogashira couplings (18.4%).[32] Figure 1.1 demonstrates how palladium-catalysed cross-coupling reactions are used in the pharmaceutical industry (with the reactions often on the ton scale) and its utility in natural product synthesis. A comprehensive review of palladium-catalysed cross-couplings in natural product synthesis is given by Nicolau.[33]

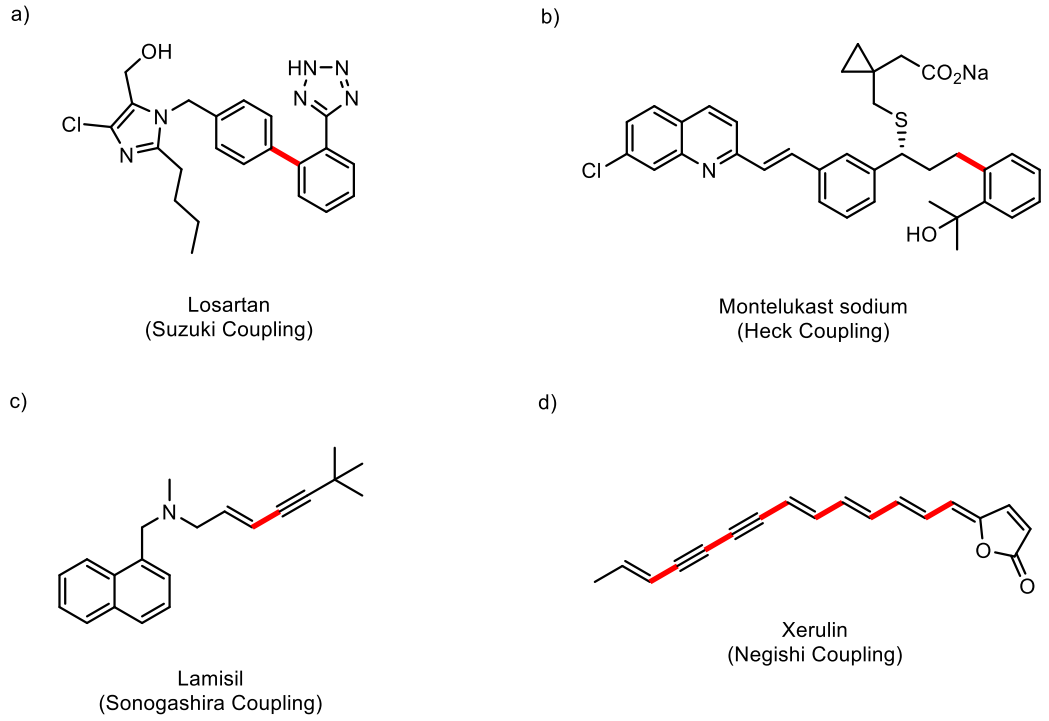

Figure 1.1: Examples of commercial drug molecules and natural products in which a C-C bond has been formed *via* a palladium-catalysed cross-coupling reaction (bond shown in red) including a) Losartan[34] for treatment of high blood pressure, b) Montelukast sodium[35] for the management of asthma symptoms and c) Lamisil,[36] an antifungal. Most impressive is the formation of six C-C bonds by Negishi couplings to produce the natural product Xerulin.[37]

Palladium-based catalysts have played a crucial role in the development of extremely powerful C-C bond-forming reactions under mild conditions with exceptional functional group tolerance. However, the amount of palladium that exists in the Earth's crust is in the region of parts per trillion, making it environmentally deleterious to extract (~ 6 g metal is produced per ton of ore). Naturally, this makes it an expensive commodity, especially as competing industries such as the automotive and electronics sectors rely on the metal. And whilst palladium-catalysts are used for the synthesis of various pharmaceutical compounds, issues concerning palladium's toxicity means that a pharmaceutical drug

intended for human consumption *via* an oral dose requires fastidious purification to meet a concentration limit of 10 ppm.[38]

In light of these issues, there has been a recent drive by chemists to find alternative metals to replace palladium in transition-metal catalysed cross-coupling reactions. Oddly enough, the metal which has come to light as the most popular replacement was overlooked when it was demonstrated to work superbly in Kumada-type reactions in the early 70's.

1.1.2 Dawn of the Iron Age

In 1971, Kochi described the cross-coupling reaction between alkenyl halides and Grignard reagents with simple iron halide salts.[39] The reactions provided the cross-coupled product in good to excellent yields with excellent stereoselectivity (Scheme 1.7).

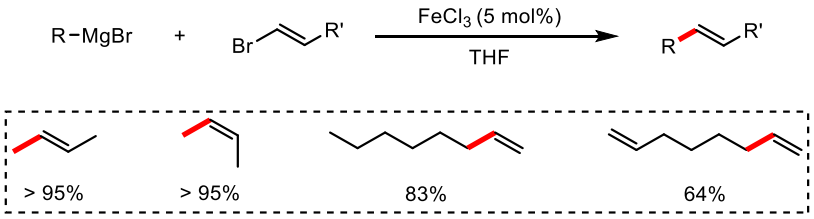

Scheme 1.7: Kochi's iron-catalysed cross-coupling reaction between Grignard reagents with vinyl and alkenyl halides.[39]

Kochi disclosed this seminal report a full year before the disclosure of Kumada and Corriu's nickel-catalysed cross-coupling reactions,[10, 11] yet the use of nickel- and palladium-based catalysts became popular instead. Consequently, the following decades only saw sporadic activity concerning iron-catalysed cross-couplings.[40-42] However, a resurgence in interest began following important publications by Cahiez[43] and Furstner[44, 45], both demonstrating that iron-catalysis was synthetically appealing and not just an academic curiosity (Scheme 1.8).

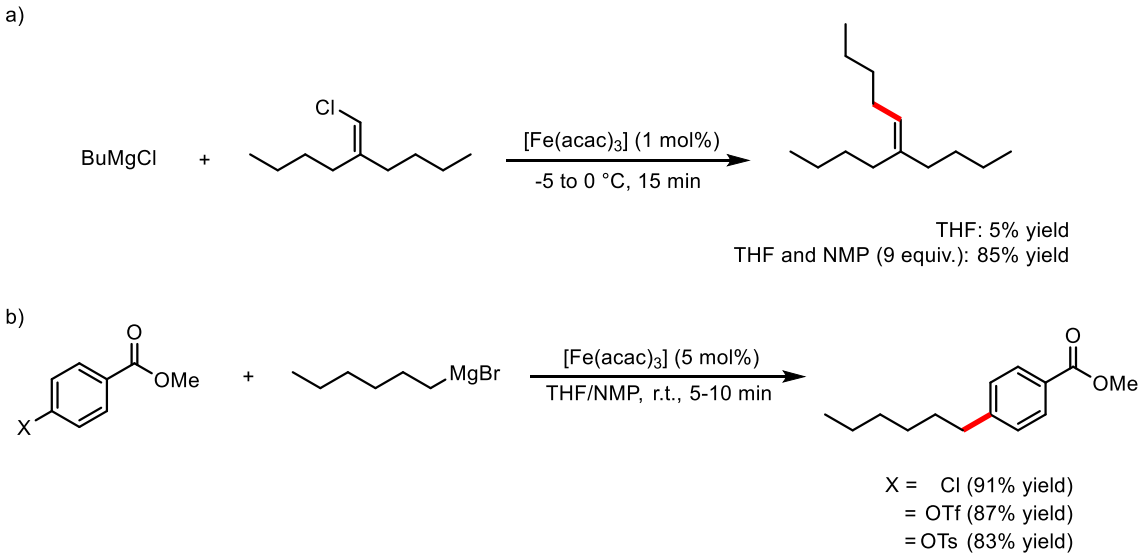

Scheme 1.8: Iron-catalysed cross-coupling reactions disclosed by a) Cahiez[43] and b) Fürstner[44, 45]. These protocols sparked explosive growth of new iron-catalysed cross-coupling reactions.

The first of these, by Cahiez in 1998 (Scheme 1.8a), showed how the addition of *N*-methyl-2-pyrrolidone (NMP) as a co-solvent supresses unwanted side-reactions in cross-couplings between Grignard reagents and alkenyl halides (halide = I, Br and Cl).[43] Cahiez's protocol expanded the scope of Kochi's iron-catalysed Kumada-type reaction, showing how a variety of functional groups such as esters, nitriles, aromatic or aliphatic halides and ketones can be tolerated. Later, in 2002, Fürstner demonstrated the iron-catalysed cross-coupling between alkyl or aryl Grignard reagents with aryl and heteroaryl chlorides, also utilising NMP as a co-solvent (Scheme 1.8b). The reaction proceeds under mild conditions tolerating ester, ether, nitrile, sulfonate, sulphonamides, thioether, acetal, alkyne and trifluoromethane groups. Furthermore, Fürstner also showed how tosylates and triflates may be utilised as leaving groups,[44] and that zincates and organomanganese nucleophiles are competent coupling partners.[45]

These early reports also demonstrated another interesting facet concerning iron-catalysis; that not only could Kumada-type cross-coupling reactions use inexpensive and toxically benign iron pre-catalysts, but that the activity compared to palladium-based systems could be strikingly different. For example, aryl chlorides, traditionally unproductive in palladium catalysis, are effective cross-coupling partners under iron-catalysis.[44] Soon, other groups became interested in the potential of iron-catalysed cross-coupling reactions and the field began to expand rapidly.

1.1.3 Iron-Catalysed Kumada Cross-Couplings

One of the advantages realised early on regarding iron-catalysed cross-couplings was that aryl Grignard reagents could be cross-coupled with alkyl halides with minimum amounts of alkene side-products being produced; the production of alkenes is a result of β-elimination and can occur rapidly under palladium catalysis.[46] Hayashi showed that the simple iron salt [$Fe(acac)_3$] was a capable pre-catalyst

for this transformation,[47] whereas Nakamura showed that $FeCl_3$ could be used to good effect when the aryl Grignard reagent was added slowly *via* syringe pump in the presence of stoichiometric amounts of *N,N,N',N'*-tetramethylethylenediamine (TMEDA) (Scheme 1.9).[48] Moreover, Nakamura's method worked well for unactivated alkyl bromides and chlorides. Bedford showed that Fe(III)-salen complexes were effective catalysts[49] whilst Fürstner and Martin showed that the ferrate complex $[Li(TMEDA)_2][Fe(C_2H_4)_4]$ was effective for a wide range of alkyl halides (Scheme 1.9).[50]

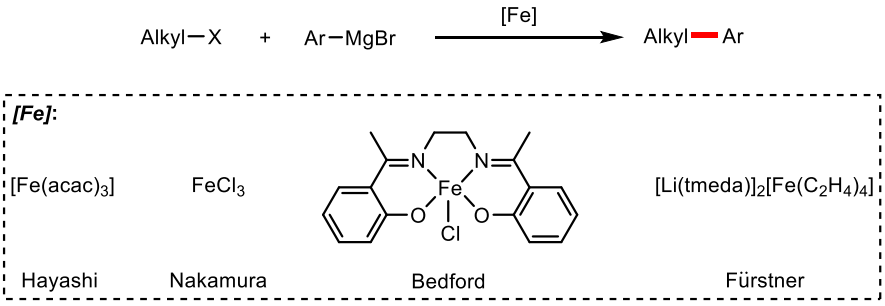

Scheme 1.9: Iron-catalysed cross-coupling of alkyl halides with aryl Grignards.

Bedford subsequently reported a simplified procedure which utilised simple iron salts with catalytic amounts of amine ligands (Scheme 1.10).[51] Unlike Nakamura's reaction, Bedford's protocol did not require slow addition of the Grignard reagent. Subsequently, Bedford then showed how a range of ligands types (phosphines, phosphites, arsines and *N*-heterocyclic carbenes (NHCs)) could also promote arylation of alkyl halides *via* Kumada-type couplings.[52]

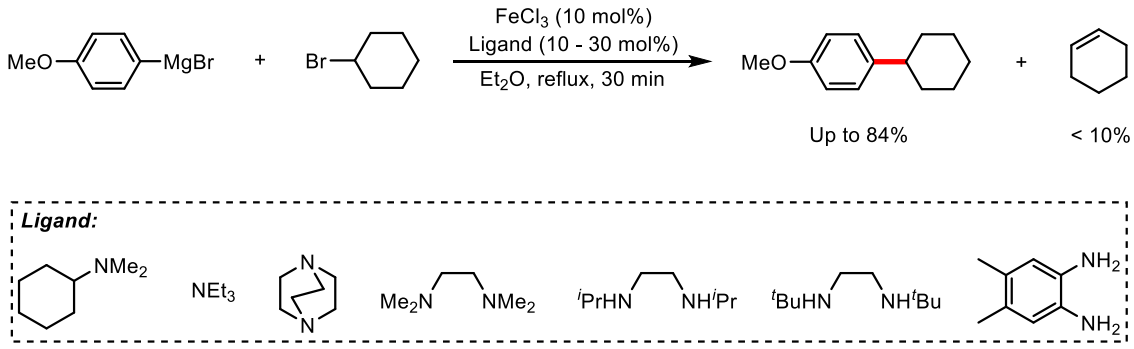

Scheme 1.10: Simplified iron-catalysed cross-coupling of aryl Grignard reagents with alkyl halides described by Bedford.[51] The reaction protocol was selective for the cross-coupled product, giving little of the β-eliminated alkene.

Having proved competent in alkyl halide and aryl Grignard cross-couplings, more challenging cross-coupling reactions with iron-catalysts were explored. One of the successful outcomes from this was aryl-aryl cross-couplings to form biaryls. The construction of biaryls is an important technology and is dominated by palladium catalysis.[53, 54] The difficulty with this transformation lies in the challenge of supressing the competitive homocoupling between two similar organic coupling partners. Nakamura overcame this issue by showing how a combination of Fe(III) fluoride salts with an NHC precursor

could supress the homocoupling side reactions, possibly due to the strong coordination of the fluoride to the iron catalyst (Scheme 1.11a).[55, 56] Later, Duong reported an effective Fe(III) alkoxide/NHC and $Fe(OTf)_2$/NHC system to supress unwanted side-reactions and afford the desired biaryls in up to excellent yields.[57, 58] A notable example of iron-catalysed Kumada biaryl cross-couplings is that of Jacobi von Wangelin who showed how a directing group effect of chlorostyrenes was able to mediate catalytic activity through transient π-coordination to the iron centre (Scheme 1.11b).[59]

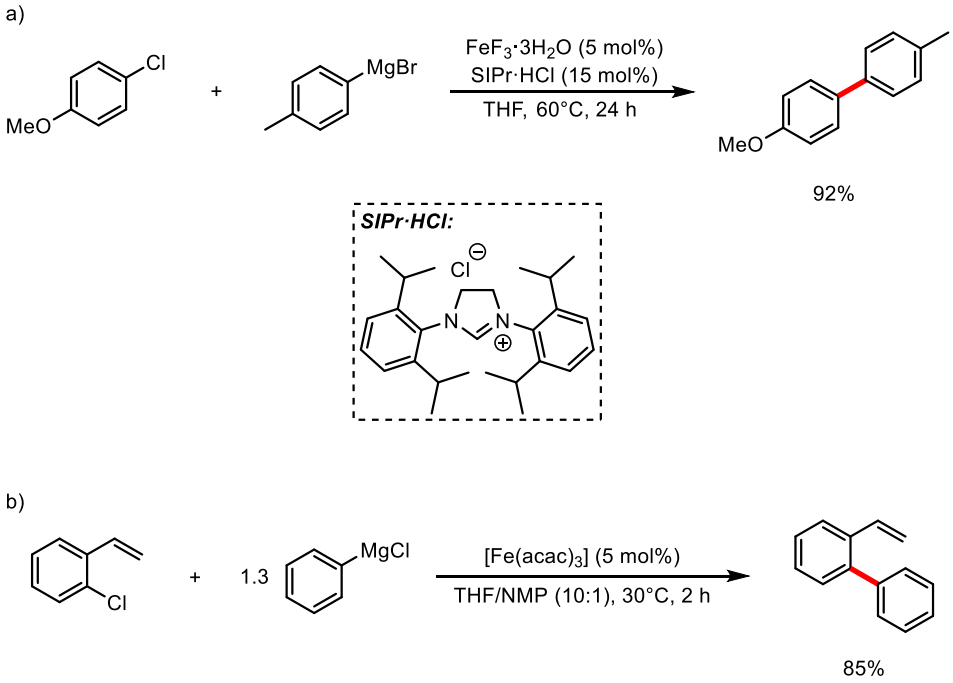

Scheme 1.11: a) Iron-catalysed biaryl cross-coupling by Nakamura[55] and b) Jacobi von Wangelin[59].

Compared to sp^2-sp^3 and sp^2-sp^2 cross-couplings, sp^3-sp^3 iron-catalysed Kumada-type cross-couplings are uncommon. The first example was reported by Chai and co-workers, using $Fe(OAc)_2$ and the wide bite angle bidentate phosphine Xantphos as a ligand (Scheme 1.12a).[60] However, the scope is limited to unfunctionalised alkyl halides. This was later improved by Cárdenas and co-workers who showed how (1,3-dioxan-2-ylethyl)magnesium bromide can be cross-coupled with a range of alkyl iodides. However, the reaction is still fairly limited in regards to the nucleophilic cross-coupling partner (Scheme 1.12b).[61] Overall, sp^3-sp^3 cross-couplings are still considered to be a challenge that has not been fully addressed.

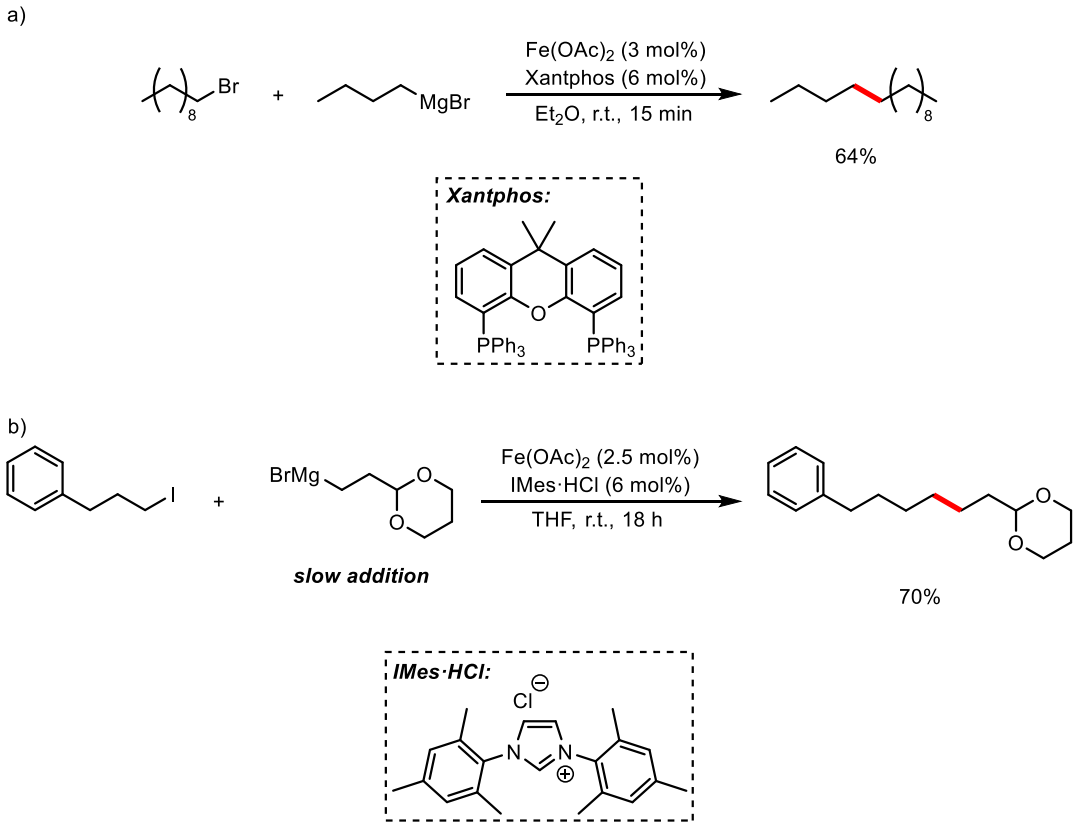

Scheme 1.12: Iron-catalysed sp^3-sp^3 cross-couplings reported by a) Chai[60] and b) Cárdenas[61].

1.1.4 Iron-Catalysed Negishi Cross-Couplings

Having established efficient methods for the cross-coupling of Grignard reagents, the exploitation of softer nucleophiles became a desirable goal due to the possibility of increased functional group tolerance. Fürstner showed early on that trialkylzincates were effective reagents before Kumada-type chemistry became popular.[45] Subsequently, Nakamura disclosed an $FeCl_3$-catalysed Negishi reaction between alkyl halides and diarylzinc reagents in the presence of stoichiometric TMEDA (Scheme 1.13a).[62] Crucial to the development was the preparation of the diarylzinc reagents; addition of two equivalents of phenylithium produces diarylzinc that is entirely unproductive, yet when two equivalents of phenylmagnesium bromide is used, the reaction proceeds almost quantitatively. A variety of (hetero)arylzinc reagents were effective in the reaction with alkyl halides bearing alkenyl, trimethylsilyl, alkynyl, ester and nitrile groups being well tolerated. Similar conditions could also be used for olefin synthesis (Scheme 1.13b), further demonstrating the wider scope of viable cross-couplings when softer organozincs are used.[63]

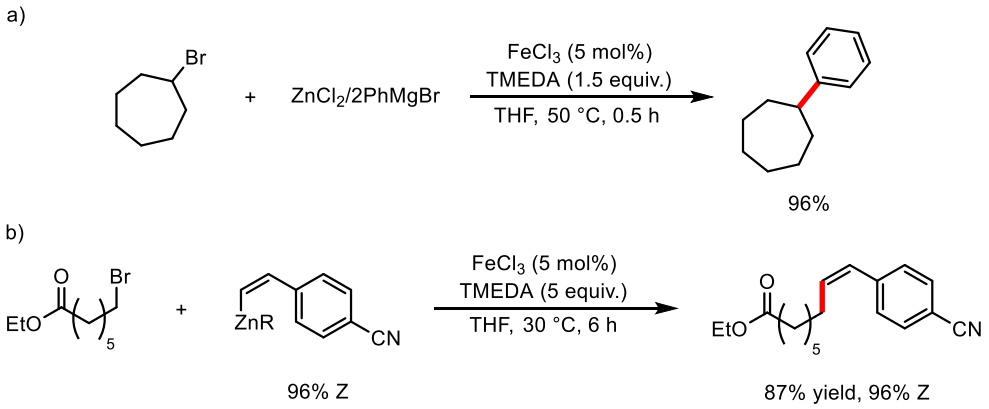

Scheme 1.13: Nakamura's iron-catalysed Negishi cross-couplings.[62, 63]

The requirement of stoichiometric additives (notably TMEDA) could be overcome by catalyst design, and bidentate phosphine ligands proved to be particularly useful in this respect. The first such example came when Bedford developed the cross-coupling between benzyl halides and phosphates with diarylzincs using the iron pre-catalyst [$FeCl_2(dpbz)_2$] (dpbz = 1,2-bis(diphenylphosphino)benzene) (Scheme 1.14).[64] Soon after, Nakamura expanded the scope of the Negishi reaction to achieve the synthesis of polyfluoroaromatic compounds, also utilising the ligand dpbz with iron salts and no additives.[65]

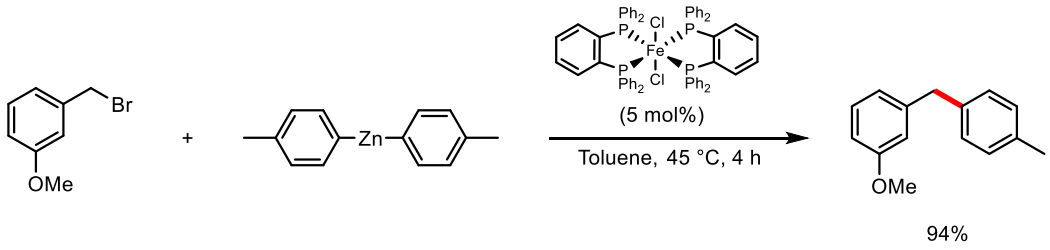

Scheme 1.14: Bedford's iron-catalysed Negishi cross-coupling using [$FeCl_2(dpbz)_2$].[64]

Unfortunately, dpbz is an expensive ligand which impedes the methodology (even when a cheap metal is being used). With this in mind, Bedford showed how dpbz could be replaced with the far cheaper and widely available bidentate ligand bis(diphenylphosphino)ethane (dppe) (Figure 1.2). This remarkable discovery evolved from detailed mechanistic studies which showed the ligand to form highly active systems when the correct iron pre-catalyst was used. More recently, Pringle showed that even more active pre-catalysts could be made by exploiting the bis(diarylphosphino)thiophene ligand (Figure 1.2), with conversion of the electrophile occurring twice as fast compared to when dpbz is used as a ligand.[66]

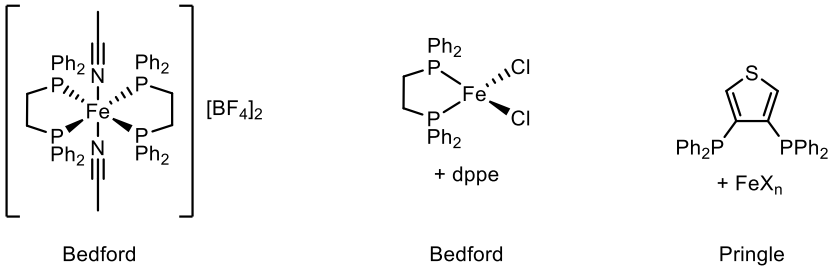

Figure 1.2: Active and pre-catalysts and ligands for the Negishi cross-couping.[66, 67]

1.1.5 Iron-Catalysed Suzuki Cross-Couplings

The potential of using cheap, non-toxic and sustainable iron catalysts with soft, non-toxic and environmentally friendly organoboron reagents for cross-coupling chemistry quickly became apparent. Iron-catalysed Suzuki chemistry was shown to be a tangible target by Bedford who demonstrated how bench-stable tetraarylborate salts could be used to arylate benzyl halides bearing ether, trifluoromethyl, ester, bromide and nitrile functionalities (Scheme 1.15).[68] The key to success was the employment of a co-catalytic organozinc reagent to facilitate transmetallation of the aryl group from the borate to the iron-centre. Unfortunately, there exists little in the way of variety concerning tetraarylborates, severely limiting the scope of the reaction.

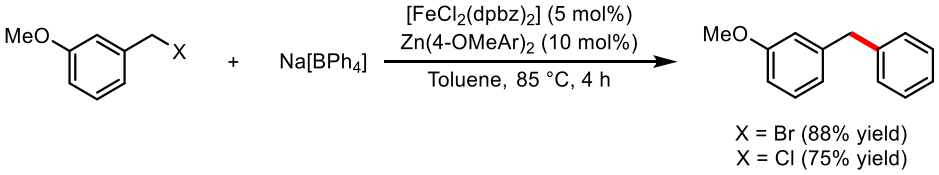

Scheme 1.15: Iron-catalysed cross-coupling of benzyl halides with tetraorganoborates.[68]

Nakamura expanded on this transformation by showing the competency of modular arylboronic acid pinacol esters activated with alkyl lithium reagents (Scheme 1.16).[69] Readily synthesised from the parent aryl boronic acids, the pinacol ester derivatives open the scope to a wide variety of cross-coupling partners. As with Bedford's disclosure, a co-catalytic amount of a metal halide salt was required for the reaction to proceed; in this case a 20 mol% loading of $MgBr_2$ was found to be optimal.

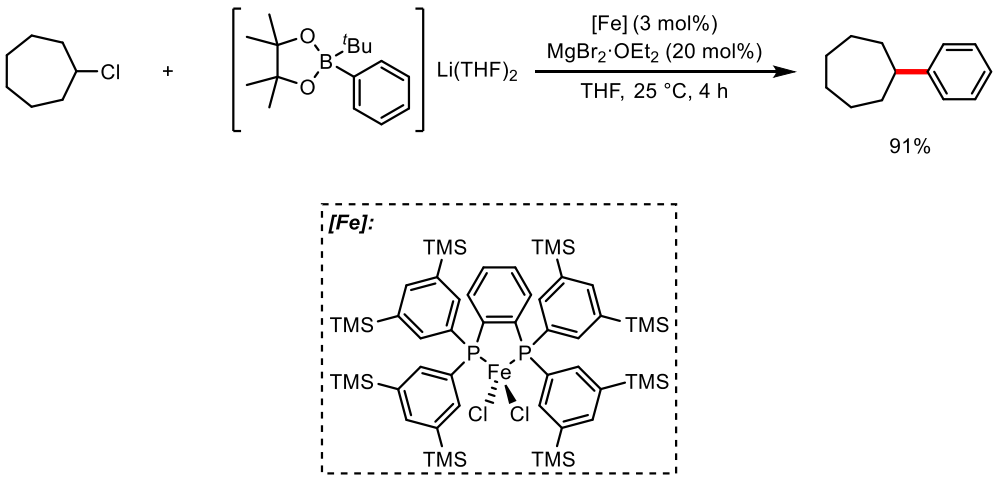

Scheme 1.16: Nakamura's iron-catalysed cross-coupling of arylboronic acid pinacol ester derivatives.[69]

Nakamura and co-workers employed an extremely bulky and synthetically challenging bidentate phosphine ligand on their iron-catalyst. Bedford later showed how the same transformation was possible when the cheap and readily available dppe ligand was used, but to the delight of the authors, it was found that in some cases no ligand is required. Later, the scope of the organoboron coupling partner was developed further when Bedford showed the effectiveness of trialkylborates in the Suzuki reaction (Scheme 1.17).[70] In this case, dpbz was the most effective ligand, with co-catalytic zincates also being required.

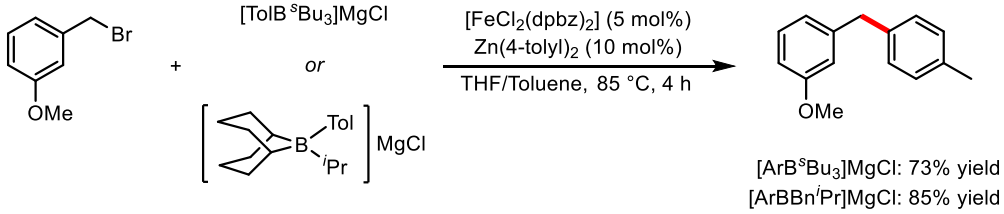

Scheme 1.17: Iron-catalysed cross-coupling of alkylborates.[70]

Alkyl-alkyl Suzuki cross-coupling was achieved by Nakamura using *iso*-propylmagnesium chloride-activated trialkylboranes which could be cross-coupled with unactivated alkyl halides using an $[Fe(acac)_3]$/Xantphos catalyst system (Scheme 1.18).[71] The addition of a metal halide salt was not required due to concomitant formation of magnesium salts during activation of the trialkylborane. The reaction displays good functional group tolerance and was shown to be effective for the synthesis of long chain fatty acid derivatives.

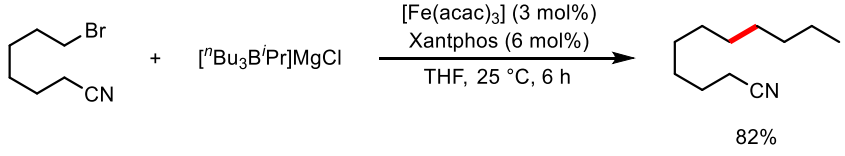

Scheme 1.18: Iron-catalysed alkyl-alkyl Suzuki cross-coupling.[71]

Whilst these reactions represent the current state-of-the-art iron-catalysed Suzuki couplings, the technology is still reliant on the use of moisture-sensitive (and often pyrophoric) alkyllithium and alkylmagnesium activators. Traditional activating agents (for example hydroxide bases) have so far been shown to be ineffective.[69] Aryl-aryl Suzuki couplings have also proven to be a challenging task, with only partial activity having described so far (see Section 2.1).

1.1.6 Applications of Iron-Catalysed Cross-Coupling Reactions

Of all types of iron-catalysed cross-coupling protocols, the Kumada variants are the most developed. As discussed, significant progress has been made with Negishi and Suzuki chemistries, and examples of aluminium Negishi-type,[70, 72] Sonogashira[73-76] and Heck[77, 78] reactions also exist (however these have been far less developed). Although the Kumada-type chemistry relies on moisture sensitive Grignard reagents, this technology has already shown promise in scale-up, medicinal and sustainable technologies.[79] A particularly impressive example of a multi-kilogram scale Kumada-type reaction was reported by Gangula for the synthesis towards the selective renin inhibitor aliskiren (Scheme 1.19).[80] The desired product was isolated in high yield whilst maintaining stereoselectivity. Notably, NMP (traditionally used as a co-solvent) could be used at a substoichiometric loading.

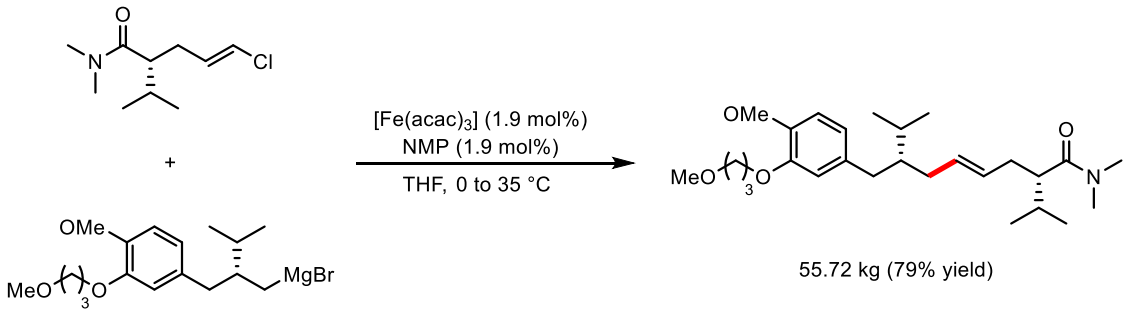

Scheme 1.19: Multi-kilogram iron-catalysed Kumada cross-coupling.[80]

The adoption of iron-catalysis by medicinal chemists is also encouraging. Lee and co-workers reported an iron-catalysed alkylation of a functionalised chloropyridazine to afford an SGLT2 inhibitor (potential antidiabetic compounds - Scheme 1.20).[81] The conditions were based on those developed by Fürstner.[45] Most noteworthy is the selectivity of the reaction; alkylation occurring at the 2-chloropyradizine position whilst in the presence of a chloroarene, which would be difficult to achieve under palladium catalysis.

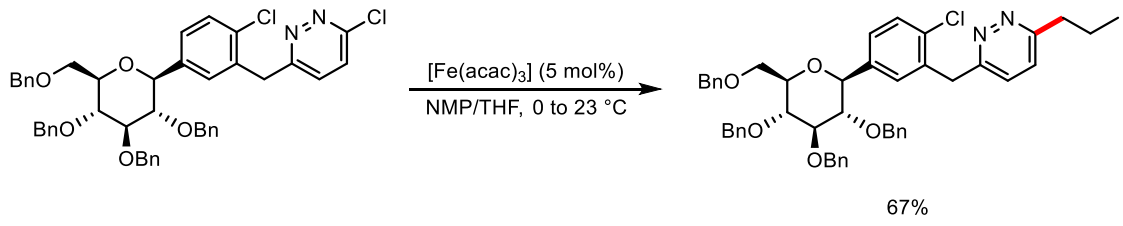

Scheme 1.20: Iron-catalysed alkylation to produce an SGLT2 inhibitor by Lee and co-workers.[81]

Finally, a protocol towards more synthetically sustainable iron-catalysed cross-couplings has been recently described by Szostak and co-workers.[82] Ethereal solvents Et_2O and THF are commonly employed in iron-catalysed cross-coupling reactions, however these are not considered environmentally sustainable. 2-Methyltetrahydrofuran (2-MeTHF) is a green and eco-friendly solvent and it was shown that aryl chlorides and tosylates react with organometallic reagents in this solvent under mild conditions. Furthermore, selected reactions were found to be expediently scaled up, showing 2-MeTHF to have potential as a sustainable solvent for iron-catalysed cross-couplings.

Overall, iron-catalysed cross-coupling reactions now cover almost the whole spectrum of reaction types developed with palladium in the 1970's, with the notable exception of Suzuki biaryl cross-coupling. Whilst there is still a way to go in regards to developing milder and more functional group tolerant reactions, the foundations have been well laid for further development. If the development of new and improved iron-catalysed cross-coupling reactions is to continue unabated, then an in-depth understanding of the mechanisms by which these transformations occur is paramount. Unfortunately, due to the low stability of catalytic intermediates, paramagnetic nature of many organometallic iron complexes and prevalence of single electron transfer processes (SET), this can be challenging to obtain. Encouragingly, many innovative mechanistic studies have emerged alongside the synthetic evolution of new iron-catalysed cross-coupling reactions, paving the way for further synthetic development. These mechanistic investigations will be discussed next.

1.2 Transition Metal-Catalysed Cross-Coupling Reactions: Mechanisms

The elementary steps for palladium-catalysed cross-couplings are well established and a generic catalytic cycle is shown in Figure 1.3. Following the generation of an active Pd(0) species, the first step that occurs is oxidative addition of the organohalide to generate a Pd(II) intermediate. The addition of the second coupling partner occurs *via* transmetallation from the organometallic reagent with concomitant liberation of metal halide salt. The cross-coupled product is then furnished by reductive elimination, regenerating the active Pd(0) catalytic species.

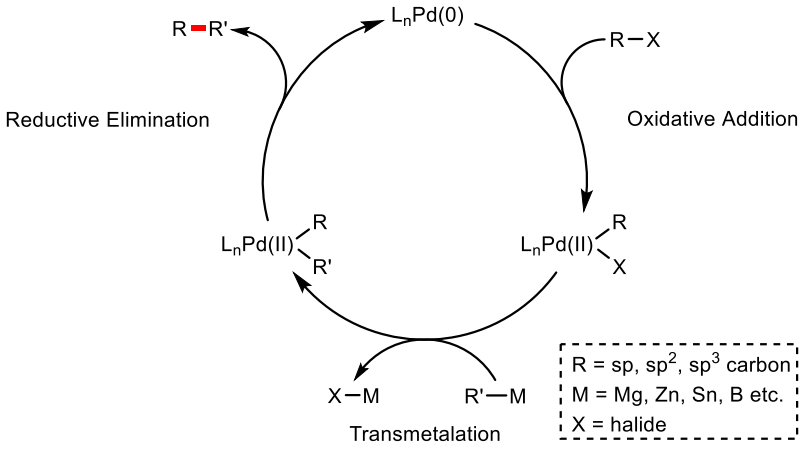

Figure 1.3: Generic catalytic cycle for palladium-catalysed cross-couplings.

The same manifold does not occur in iron-catalysed cross-couplings. For example, whereas palladium-catalysed cross-couplings occur by elementary two-electron reductive/oxidative steps, iron may instead operate *via* single-electron transfer (SET) processes. Nakamura observed this when stereochemical probes *trans*- and *cis*-1-bromo-4-*tert*-butylcyclohexane both formed more stable *trans*-arylated **1** from identical reaction conditions, suggesting the formation of an alkyl radical (Scheme 1.21a).[48] For a similar reaction, Bedford and co-workers performed a 'radical clock' experiment using (bromomethyl)cyclopropane as a substrate (Scheme 1.21b).[51] Ring-opened alkene 4-phenylbutene was obtained, strongly supporting the generation of an alkyl radical. If the cross-coupling operates *via* a traditional two-electron oxidative addition pathway, (cyclopropylmethyl)benzene would be furnished instead.

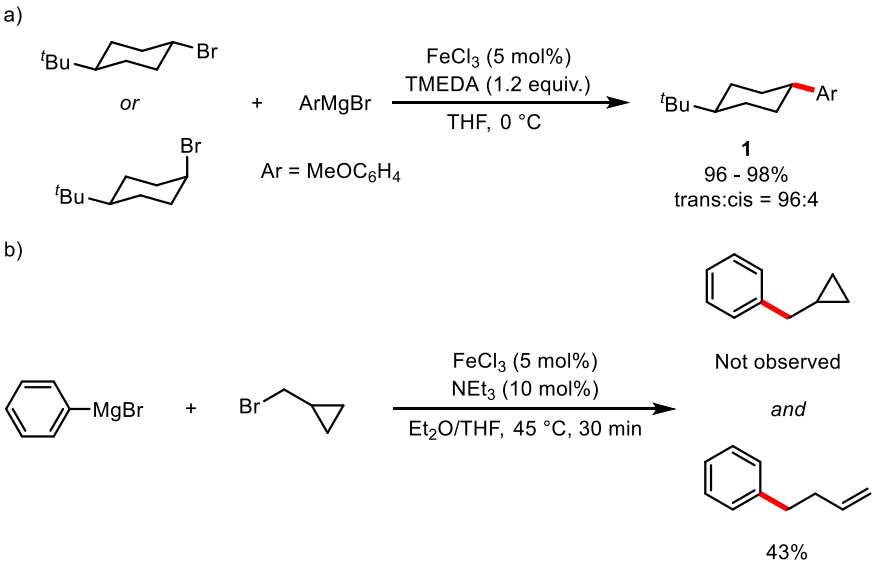

Scheme 1.21: Radical probe reactions by a) Nakamura[48] and b) Bedford[51].

Another divergence from the general palladium catalytic cycle is that ligands and additives are not always coordinated to the iron-centre during catalysis. In Nakamura's iron-catalysed Kumada cross-coupling, the stoichiometric addition of TMEDA is vital for the suppression of unproductive side reactions.[48] Nagishima probed the mechanism with the cross-coupling of bromooctane and mesitylmagnesium bromide (MesMgBr) as a model reaction.[83] The reaction with such a bulky Grignard reagent is uncharacteristic of the developed protocol, affording the cross-coupled product in only 32% yield after 18 h at room temperature. However, the sterically demanding mesityl groups allow for the isolation of otherwise unstable organoiron species. Thus, Nagishima and co-workers could isolate complexes **2** and **3**. The reaction of **2** with 2 equivalents of bromooctane forms complex **3** with 76% formation of cross-coupled product. The reaction of **3** with MesMgBr forms **2**. Finally, **3** reacts with bromooctane much slower than **2**. Based on these observations, a catalytic cycle was proposed (Figure 1.4).

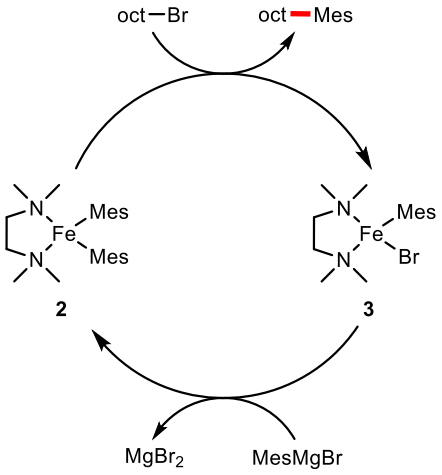

Figure 1.4: Catalytic cycle with complexes **2** and **3**.[83]

Stoichiometric reactions can give valuable insight into the reactivity of isolated organoiron complexes. Yet in a catalytic reaction, excesses of coupling reagents exist: for Nakamura's Kumada-type reaction, the ratio of iron to Grignard reagent is 1:20. Bedford showed that for a mixture of either $FeCl_2$ or $FeCl_3$ with eight equivalents of MesMgBr in the presence of TMEDA, the homoleptic Fe(II) 'ate' species $[Fe(Mes)_3]$ (**4**) is the sole observable species by paramagnetic ^1H NMR spectroscopy.[84] Homoleptic **4** was shown to not only be competent for the cross-coupling of bromooctane, but crucially reacted *faster* with bromooctane than **2**. Bedford proposed that the role of TMEDA in the reaction is to instead act as a 'chaperone', stabilising off-cycle species and preventing catalyst decomposition (Figure 1.5).

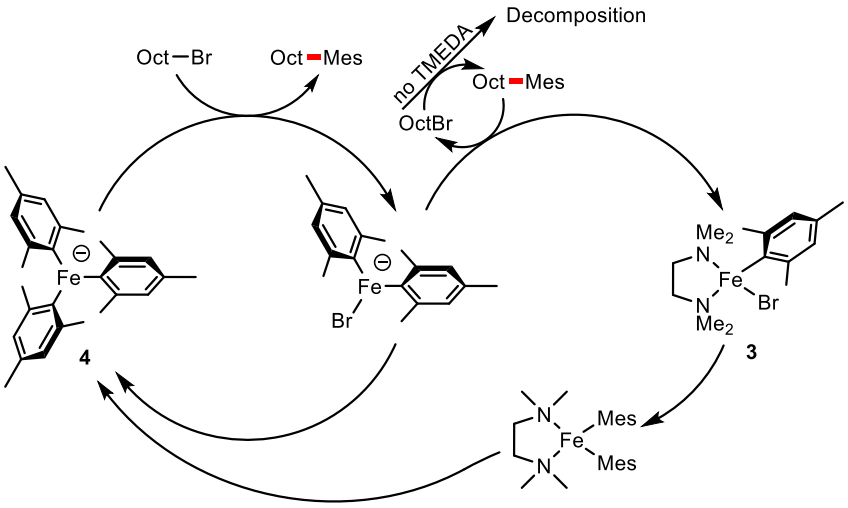

Figure 1.5: Bedford's revised catalytic cycle for the cross-coupling of bromooctane with MesMgBr.[85]

NMP is another additive commonly employed to supress unproductive side reactions. Often used as a co-solvent, a vast excess is present in catalytic mixtures. NMP is a strong oxygen donor and as such a suitable ligand for iron. Holland and co-workers isolated an Fe/NMP complex from the reaction of 3 equivalents $FeCl_2(THF)_{1.5}$ with 8 equivalents NMP to afford the two iron species-containing complex $[Fe(NMP)_6][FeCl_3(NMP)]_2$ (Figure 1.6a).[86] The isolated complex proved to be a competent pre-catalyst in a Kumada cross-coupling reaction, however an active pre-catalyst does not mean that it is the active species in the reaction. Indeed, using *in situ* spectroscopy techniques, Neidig showed that reactions of $[Fe(acac)_3]$ and methylmagnesium bromide under catalytically relevant conditions in THF/NMP mixtures actually produces homoleptic Fe(II) 'ate' $[FeMe_3]_2[Mg(NMP)_6]$ as the major species (Figure 1.6b).[87] Thus, NMP interacts with the magnesium cations instead of iron.

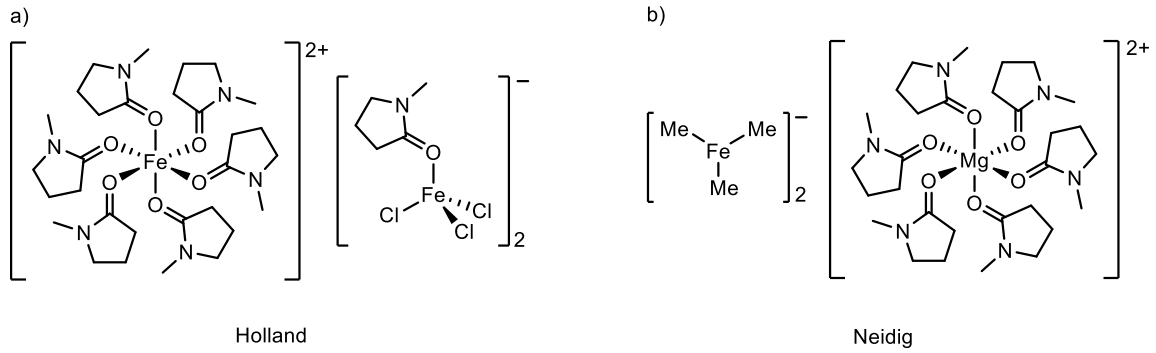

Figure 1.6: a) $[Fe(NMP)_6][FeCl_3(NMP)]_2$ reported by Holland[86] and b) $[FeMe_3]_2[Mg(NMP)_6]$ reported by Neidig[87].

What about more strongly coordinating ligands? As discussed, both phosphines and NHC's can be exploited to promote cross-couplings. Both ligand types are strong σ-donors, and as may coordinate to iron. Both Neidig[88] and Bedford[85] have shown that a range of bidentate phosphine iron complexes will form complex **4** in the presence of an excess of MesMgBr. However, **4** is in equilibrium with bisaryl or dimeric monoaryl complexes, depending on the phosphine present (Scheme 1.22). Where the equilibrium lies depends on the stability of the chelated iron complex. Kinetic studies show that for the primary catalytic cycle, the phosphine ligands appear to be coordinated to iron, particularly in protocols where the Grignard is added slowly, disfavouring the formation of **4**. The case with NHC ligands has been less defined. Tonzetich showed that alkyl ligand scrambling can occur upon the addition of 1 equivalent of benzyl Grignard reagent to a well-defined three-coordinate Fe(II) NHC complex.[89] However, the authors did not describe the speciation of the mixture with an excess of Grignard reagent as would be present in a catalytically relevant mixture.

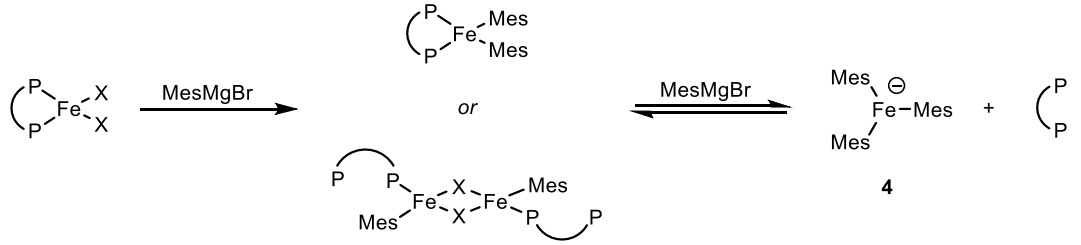

Scheme 1.22: Equilibrium between **4** and mono- and bis-aryl phosphine complexes.[85]

In the palladium cycle shown in Figure 1.1, the lowest oxidation state of the catalyst is Pd(0). From this, the entire cycle can be built from the known elementary redox reactions. A robust and generic mechanistic model cannot be built without knowing what the lowest relevant oxidation state of the metal is. To date, Fe(-II), Fe(-I), Fe(0), Fe(I) and Fe(II) have all been proposed as the lowest active catalyst oxidation state for cross-coupling reactions.[85]

Fe(-II) was suggested by Fürstner and co-workers for couplings between Grignard reagents and alkyl halides. Bogdanović had shown the formation of "inorganic Grignard" reagents from the reaction of

Mg(0), alkyl halide and $FeCl_2$ in a ratio of 25/4/1.[90] This forms 4 equivalents of Grignard in the presence of iron which reacts to furnish an iron species of formal composition $[Fe(MgX)_2]$. From this, Fürstner proposed the catalytic cycle shown in Figure 1.7.[45] However, the formation of $[Fe(MgX)_2]$ requires the presence of an excess of the powerful reductant Mg(0), which would not be present in a representative cross-coupling reaction.

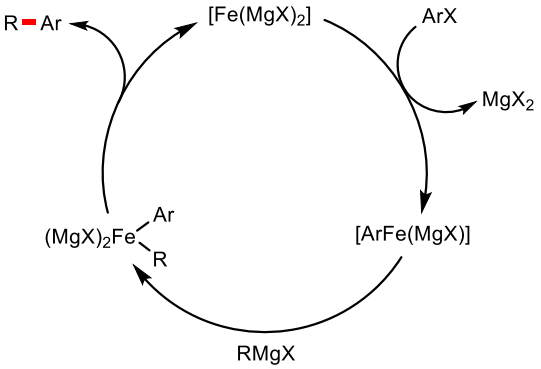

Figure 1.7: Proposed Fe(-II)/Fe(0) manifold by Fürstner.[45]

Later, Fürstner and co-workers prepared complexes of Fe(0), Fe(I), Fe(II) and Fe(III), all bearing cyclopentadienyl (Cp) or 1,2,3,4,5-pentamethylcyclopentdienyl (Cp*) ligands (Figure 1.8). These were shown to be outperformed in the cross-coupling of phenylmagnesium bromide with methyl-4-bromocrotonate by an Fe(-II) complex which *did not* bear either a Cp or Cp* ligand. Thus, Fürstner concluded that Fe(-II) must be the lowest oxidation state in the catalytic cycle. However, there are two issues with Fürstner's interpretation:

1) Cp or Cp* are not representative of the ligands most commonly exploited in iron-catalysed cross-couplings.
2) Using an Fe(-II) complex which is not analogous to the other complexes makes the premise internally inconsistent. If the Cp ligands *don't* perturb the activity, then the Cp-containing Fe(0) complex should be a highly active pre-catalyst; it is actually the worst. Therefore, the assumption that Cp is a valid model to compare with Cp-free complexes is not true.

In the decade since, there has been scant evidence to support the Fe(-II) manifold, and little evidence exists overall for the concurrence of sub-zero valent species. Indeed, a recent report by Fürstner on the reaction of cyclohexylmagnesium chloride with FeX_n (X = acac or Cl, n = 2 or 3), far from showing reduction to Fe(-II), shows disproportionation and production of an Fe(IV) cyclohexyl 'ate' complex.[91]

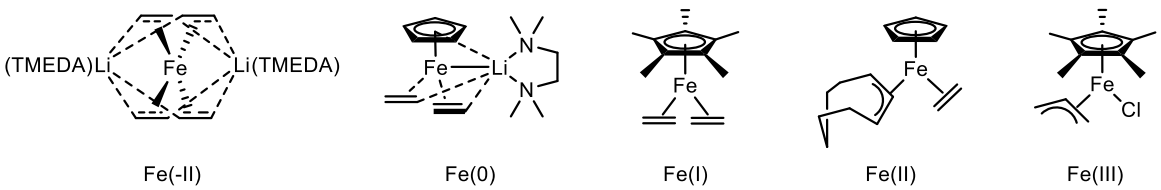

Figure 1.8: Model complexes of Fe(-II), Fe(0), Fe(I), Fe(II) and Fe(III).[92]

Fe(0) is accessible under a variety of catalytically relevant conditions. In many cases, reduction to Fe(0) affords Fe(0) nanoparticles rather than homogeneous complexes. Indeed, Bedford has shown that pre-formed iron-nanoparticles stabilised by poly(ethylene glycol) display excellent catalytic activity.[93] In cases where iron nanoparticles are catalytically active, whether or not the catalysis occurs on the particle surface is still unknown. Another possibility is that the nanoparticles could in fact be acting as an off-cycle reservoir for a highly competent soluble catalyst, with Bedford having shown that the drop-wise addition of a nanoparticle mixture to alkyl bromide results in the formation of a homogeneous solution.[84] It is likely that the organoiron complex formed from this reaction has a higher oxidation state than that of Fe(0), however more evidence is needed to fully delineate the role of iron nanoparticles in these reactions.

Overall, most studies point to the active oxidation state being higher than Fe(0). For a variety of cross-couplings, Fe(I) complexes have been shown to be readily accessible and also catalytically competent on kinetically relevant time-scales. Kochi first proposed Fe(I) to be the low oxidation state after observing an $S = ½$ species (corresponding to low-spin Fe(I)) in the EPR spectrum of a mixture of iron halide salts with methylmagnesium bromide.[94] This led Kochi to propose an Fe(I)/Fe(III) cycle as shown in Figure 1.9a. The identity of the $S = ½$ species remained a mystery for 40 years and was revealed by Neidig to be a mixed valence iron-cluster of the formula $[MgCl(THF)_5][Fe_8Me_{12}]$ (**5**).[95] Intriguingly, **5** turns out to only produce minimal quantities of cross-coupled product when reacted with a representative electrophile, meaning that the hunt for the active species in Kochi's reaction continues.

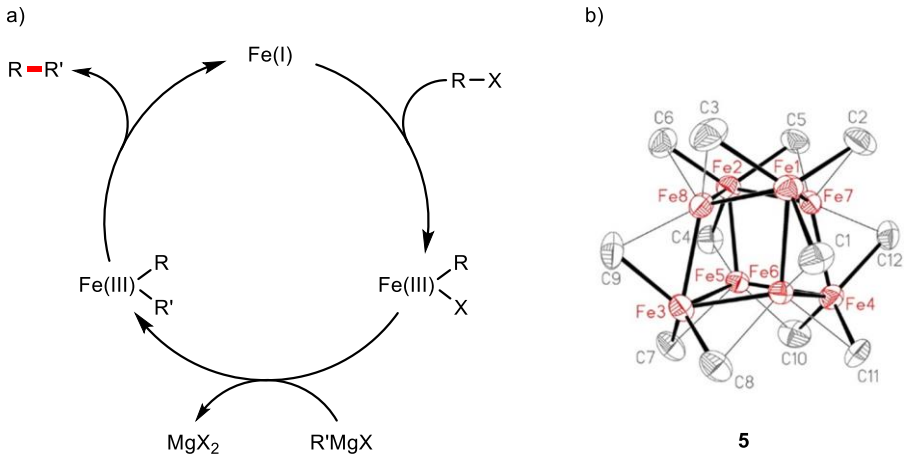

Figure 1.9: a) Proposed Fe(I)/Fe(III) cycle proposed by Kochi[94] and b) the identity of the observed $S = ½$ species[95].

Significant results have been gained by focussing on cross-coupling systems that make use of bidentate phosphine ligands, particularly dppe and dpbz which are effective in a variety of different cross-couplings. Another benefit of investigating phosphine-containing systems is that smaller, more representative nucleophilic reagents may be investigated. In the Negishi cross-coupling reaction, Bedford showed that the reaction of $[FeCl_2(dpbz)_2]$ with a diarylzinc reagent reduces the iron to

oxidation states below Fe(I).[96] What is important to note, however, is that in the time-scale for the most productive cross-coupling, Fe(I) appears to be the bulk oxidation state of the metal. Bedford and co-workers then isolated complexes **6-8** as prospective intermediate species (Figure 1.10). EPR spectroscopy showed all three compounds to be low spin (S = ½), whilst DFT calculations confirmed that the Mulliken spin density of the unpaired electron sits predominantly on the iron atom. The isolated complexes proved to be competent pre-catalysts for the Negishi reaction, with **6** showing essentially the same kinetic profile as the pre-catalyst [$FeBr_2(dpbz)_2$] for cross-coupling. EPR spectroscopy of samples removed from catalytic reactions has also shown the presence of Fe(I)-phosphine containing complexes. The analogous dppe-containing Fe(I) complexes have also been isolated and examined in Suzuki-type reactions (see Section 3.1 for further discussion).[67, 97]

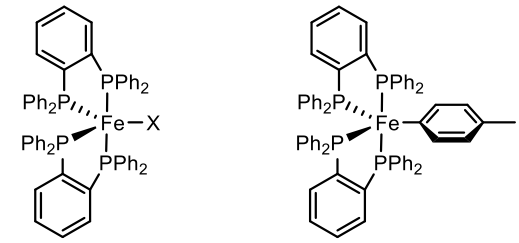

Figure 1.10: Fe(I) complexes **6-8** reported by Bedford.[96]

Finally, Fe(II) is also proposed to be the lowest oxidation state for a variety of transformations. Indeed, the formation of iron 'ate' species such **4** described above show that Fe(II) complexes are certainly accessible. Fe(II) 'ate' complexes formed from smaller, more representative, Grignard reagents have also been isolated and characterised.[84] However, these are often thermally unstable, and are likely to undergo disproportionation reactions upon warming to form iron species with oxidation states below Fe(II).[85] In the same way for Fe(I) complexes, bidentate phosphine ligands can stabilise Fe(II) reactive organoiron intermediates whilst also facilitating cross-coupling reactions under a variety of conditions. A particular phosphine ligand, the bulky 'spin-control-intended *ortho*-phenylene bisphosphine' (SciOPP) has been utilised by Nakamura in a variety of reactions.[69, 73, 98-100] This phenylene-bridged phosphine coordinates strongly to iron, with the steric bulk preventing the coordination of more than one ligand. Based on the likelihood of a radical-based mechanism from radical probe experiments, and lack of biphenyl production in a Suzuki reaction (which would occur from reductive elimination from the iron-centre, thus reducing it to oxidation states below Fe(II)), Nakamura has proposed a general Fe(II)/Fe(III) cycle for reactions utilising the bulky SciOPP ligand, shown in Figure 1.11.[69, 73, 98, 99].

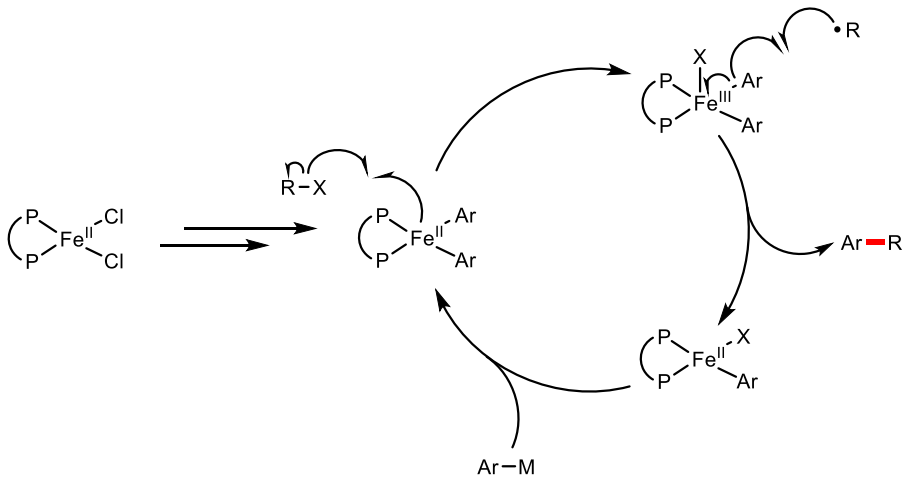

Figure 1.11: Proposed Fe(II)/Fe(III) cycle by Nakamura.[69]

Neidig has corroborated this proposal with extensive investigations using *in situ* spectroscopic techniques, coupled with the isolation and reactions of monoarylated and bisarylated SciOPP-containing organoiron complexes **9-12** (Figure 1.12). The reaction of [$FeCl_2$(SciOPP)] with MesMgBr forms complex **9**. This reacts with primary alkyl halides to produce **10** with concomitant formation of cross-coupled product. Alternatively, with smaller phenyl nucleophiles, whilst both complexes **11** and **12** may form in solution from reactions with [$FeCl_2$(SciOPP)] and phenyl nucleophiles, kinetic investigations show that monoarylated **12** is the predominant reactive species. Recently, Neidig showed that the proposed mechanism in Figure 1.11 is also likely for the iron-catalysed alkynylation of alkyl halides.[101]

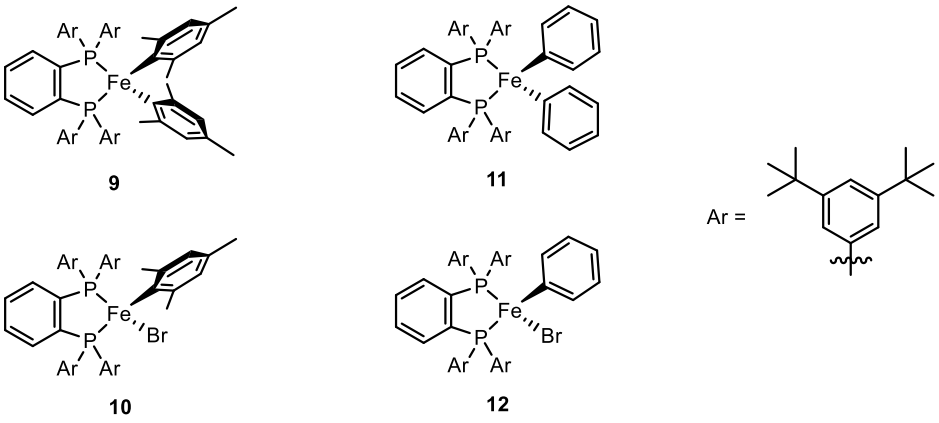

Figure 1.12: Fe(II)SciOPP complexes investigated by Neidig.[88, 102]

The difference in reactivity of smaller phosphines such as dpbz and dppe compared with bulkier ligands such as SciOPP illustrates how only small changes to the reaction conditions can vastly affect the operative mechanism. Current understanding points towards this being true for a variety of cross-couplings. Nevertheless, whilst this has frustrated attempts to build a generic catalytic cycle like that shown in Figure 1.1, great strides have certainly been made towards this goal.

1.3 Research Aims

Following a period of dormancy after Kochi's seminal report on an iron-catalysed cross-coupling reaction, research into this challenging area of synthesis continues with vigour. A variety of methods now exist for, in particular, effective Kumada-, Negishi- and Suzuki-type cross-couplings. These encouraging results show that it is indeed possible to mimic, or in some cases even out-perform, traditional palladium-catalysed methodologies. Where this has not yet been the case is in the construction of biaryl motifs using Suzuki-type conditions. In Chapter 2, the development of an iron-catalysed Suzuki biaryl cross-coupling reaction is charted. Also lacking are methods for enantioselective cross-couplings. In Chapter 4, the enantioconvergent cross-coupling of an unactivated alkyl halide is investigated.

Mechanistic understanding is key for the continual development of synthetic methodology. The low stability and paramagnetic nature of many organometallic iron complexes, coupled with single electron transfer events and the facile change between a variety of oxidation states makes the elucidation of these processes an arduous challenge. This has been met by a variety of elegant studies, showing that the nature of these reactions are particularly complicated. In Chapter 3, a variety of methods are utilised to gain a mechanistic understanding of the Suzuki biaryl cross-coupling reaction developed in Chapter 2. Finally, in Chapter 5 a comparison between an *N*-heterocyclic carbene ligand and its *N*-heterocyclic germylene analogue provides an interesting insight into both synthetic and mechanistic aspects of iron catalysis.

Chapter 2

Substrate-Directed Iron-Catalysed Suzuki Biaryl Cross-Coupling: Methodology

2.1 Introduction

When it comes to the construction of biaryl motifs, the palladium-catalysed Suzuki biaryl cross-coupling reaction is the methodology of choice for chemists in both academia and industry (Scheme 2.1).[30] This reaction is exploited in the synthesis of a range of commercial products including pharmaceuticals,[32] agrochemicals and materials.[34] Whilst palladium-based compounds are the most frequently used catalysts for facilitating the reaction between an aryl halide and the easily handled aryl boron reagent, recent efforts have focussed on replacing palladium with more benign, cheaper and abundant metals, with significant progress being made in the development of nickel-[103-108] and copper-[109-112] based catalysts.

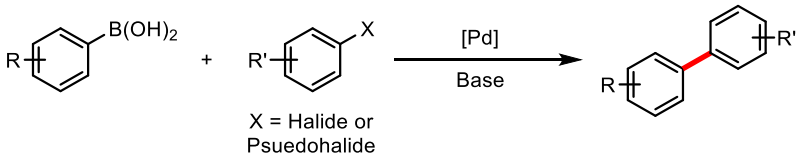

Scheme 2.1: Representative palladium-catalysed Suzuki biaryl cross-coupling reaction.

Replacing palladium-based catalysts with iron-based catalysts however is no easy feat, with very few examples of iron-catalysed Suzuki biaryl cross-coupling known (*vide infra*). Recently, there has been progress with cobalt-based catalysis which holds promise for the development of iron-based systems since the two metals can often display similar reactivity. The first example of this came from Chirik and co-workers who showed by mechanistic investigations into the transmetallation step between the cross-coupling of aryl triflates and heteroaryl boron reagents that cobalt pincer complexes could be used as effective catalysts (Scheme 2.2).[113]

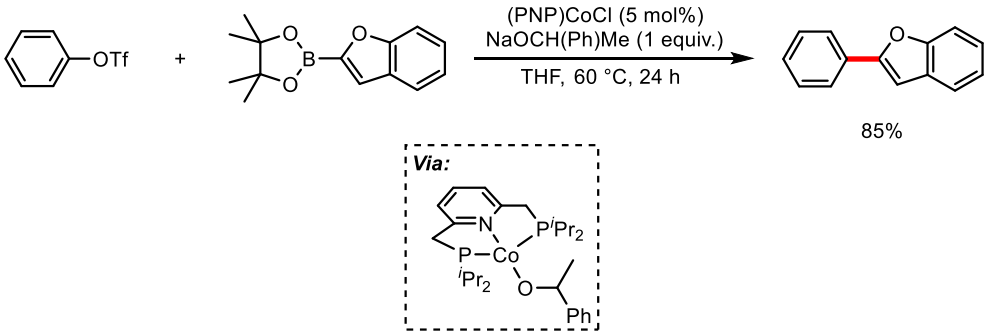

Scheme 2.2: Chirik's cobalt-catalysed Suzuki cross-coupling of aryl triflates and heteroaryl boronic esters.[113]

However, the very limited scope of organoboron reagents employed and the requirement for the leaving group to be a triflate impedes the utility of the reaction. This was later addressed by Duong who showed that the organoboron reagent phenylboronic acid neopentylglycol ester could be cross-coupled with (hetero)aryl halides (Scheme 2.3).[114] Again, the scope of the reaction is very limited when it comes to simple unactivated aryl halides, whereas a range of heteroarenes (particularly (halo)pyridines) can be utilised in this reaction with couplings proceeding in excellent yields.

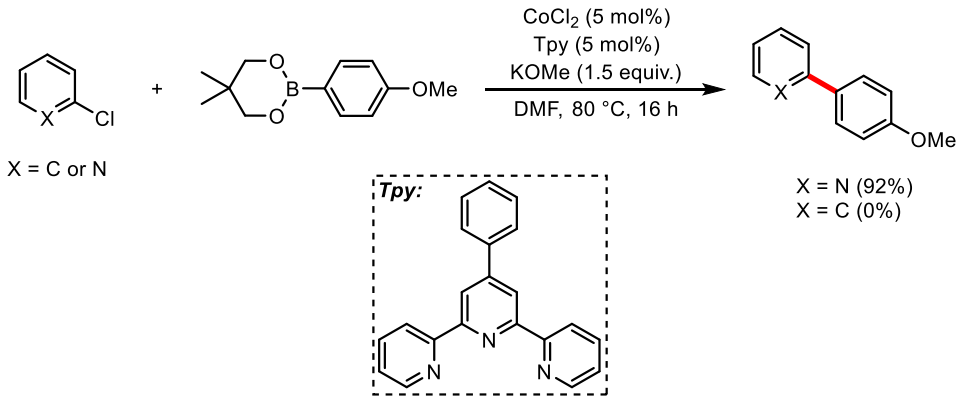

Scheme 2.3: Duong's cobalt-catalysed Suzuki biaryl cross-coupling of (hetero)aryl halides with aryl boronic esters.[114]

Concurrently, Bedford and co-workers reported their cobalt-catalysed Suzuki biaryl cross-coupling of simple unactivated aryl halides with ^{n}BuLi activated borates catalysed by $CoCl_2$ and the *N*-heterocyclic carbene (NHC) precursor SIPr·HCl (Scheme 2.4).[115] The reaction can tolerate a wide range of aryl halides under mild conditions, in particular aryl chlorides. Its synthetic utility was also demonstrated by the functionalisation of Edaravone, a drug administered to patients who have suffered from stroke and which has recently been approved for treatment of amyotrophic lateral sclerosis (ALS).[116, 117]

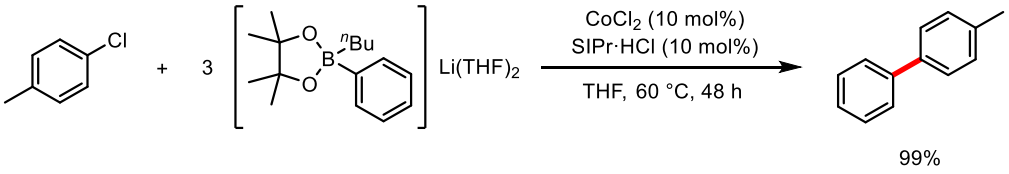

Scheme 2.4: Bedford's cobalt-catalysed Suzuki biaryl cross-coupling of aryl halides with alkyl lithium activated borate esters.[115]

With regard to using iron catalysts, however, there are few examples of aryl halide bond activation reactions that afford cross-coupling with organoboron reagents. Previous reports have been retracted from the literature due to issues with reproducibility,[118, 119] specifically due to the likelihood that palladium contamination effected the results,[120] whilst another example used pressures of 15 kBar to drive the reaction.[121] However, two known examples of Suzuki cross-coupling of (hetero)aryl halides occurring under mild conditions have been reported by Bedford. In the first instance, it was found that 2-bromopyridines may be arylated using bench-stable $Na[BPh_4]$ with co-catalytic zinc reagents (Scheme 2.5a).[68] The second example showed that when 2-halobenzyl halides were reacted with aryl boronates activated with ^{t}BuLi, the expected cross-coupling at the benzyl position was observed, along with the formation of small amounts of the diarylated product (Scheme 2.5b).[122] No cross-coupling at just the aryl position was achieved.

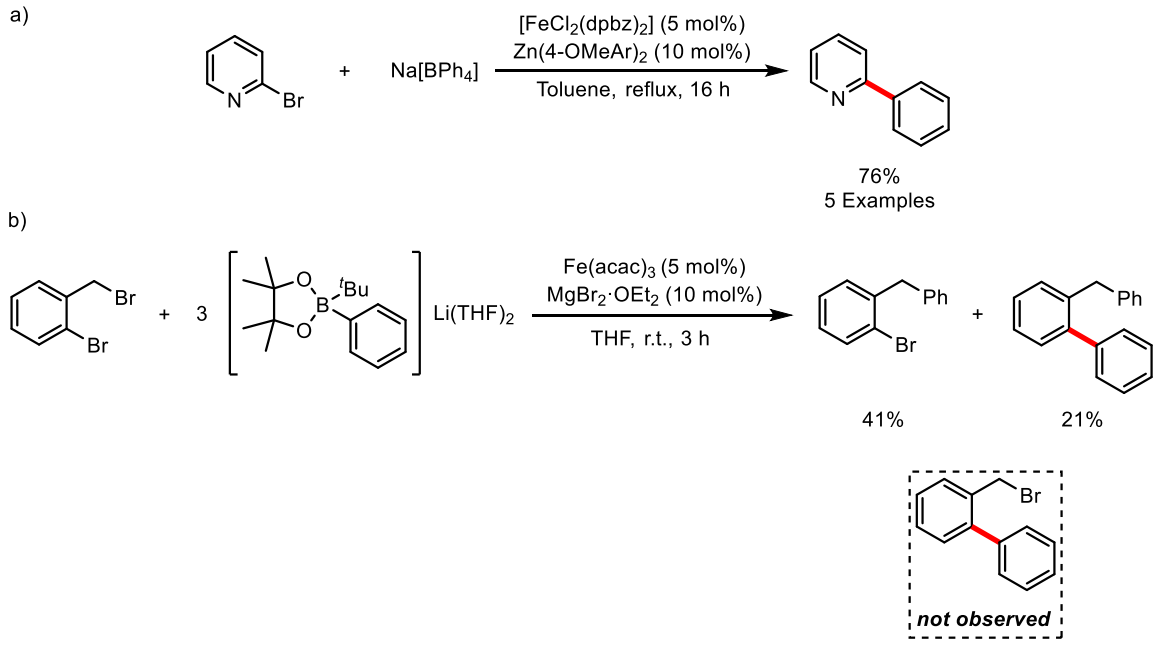

Scheme 2.5: a) Iron-catalysed Suzuki cross-coupling of 2-bromopyridines with $Na[BPh_4]$.[68] b) Iron-cataysed Suzuki biaryl cross-coupling of 2-halobenzylhalides.[122]

It appears that the barrier to success depends on activation of the aryl halide bond, which in the case of the 2-halobenzylhalides may be facilitated by a directing group effect. A similar effect was observed in a serendipitous discovery when attempting the dearomatisation of 2-methylindole amide **13** (Scheme 2.6).

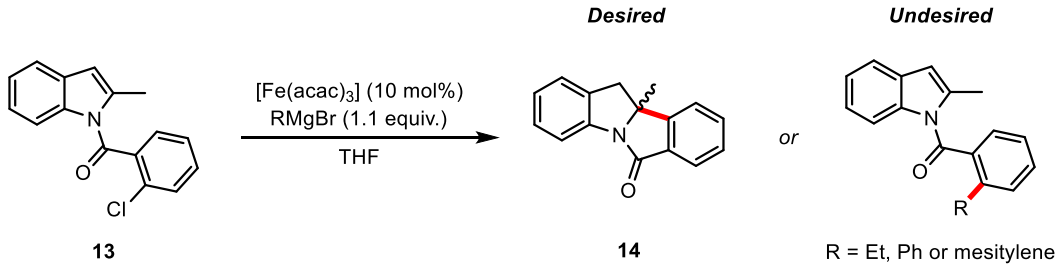

Scheme 2.6: Attempted iron-catalysed dearomatisation of **13** (products detected by GC-MS). Summer project student Charlotte Ellis undertook the investigation into the iron-catalysed dearomatisation of **13** under the author's supervision.

The addition of ethylmagnesium bromide (as an initiator) to a mixture of **13** and 10 mol% $[Fe(acac)_3]$ at room temperature failed to give the desired dearomatised product **14**, but instead gave the cross-coupled product at the aryl chloride position. Attempts to switch off this undesired reaction by using aryl Grignard reagents (since biaryl formation under iron-catalysis is usually challenging) failed, even when sterically demanding 2-mesitylmagnesium bromide was used as an initiator. This led to the proposition that the *N*-indole amide group was directing biaryl cross-coupling. A similar process was reported by Jacobi von Wangelin where it was shown that chlorostyrenes could direct iron-catalysed biaryl cross-coupling with aryl Grignard reagents (see Section 1.1.3).[59]

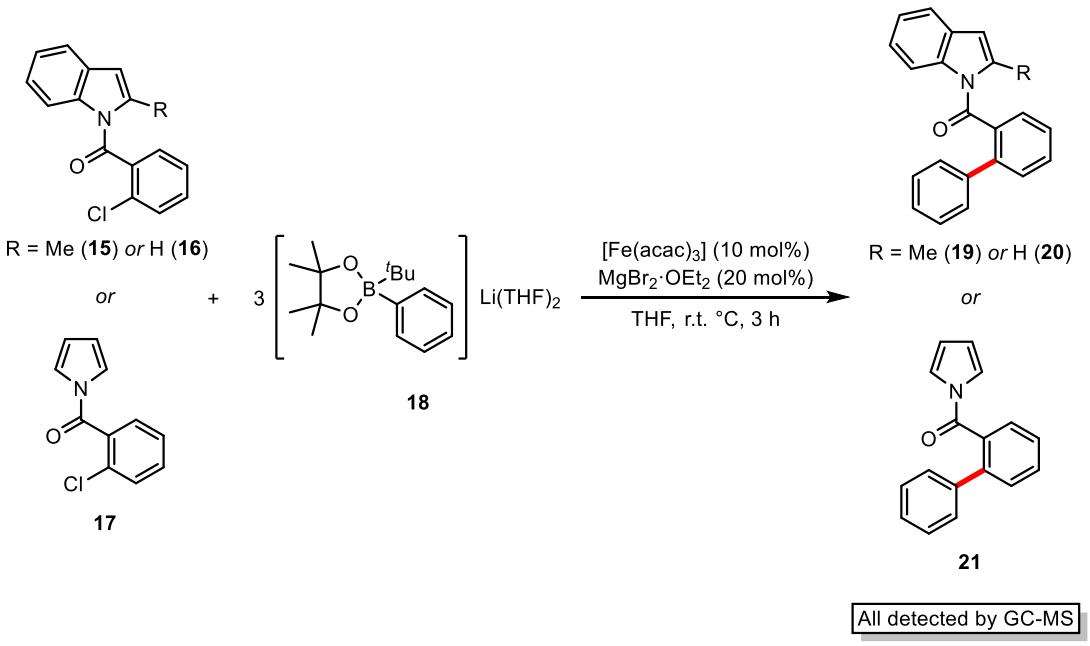

Scheme 2.7: Iron-catalysed Suzuki biaryl formation.

Intrigued by this unexpected outcome, aryl borate **18** was used in place of aryl Grignard reagents to examine the possibility of developing an iron-catalysed Suzuki biaryl cross-coupling (Scheme 2.7). To the authors delight, not only were *N*-indole amides **15** and **16** capable of directing biaryl formation, but also the *N*-pyrrole amide **17** (all detected by GC-MS). Invigorated by this outcome, the iron-catalysed Suzuki biaryl cross-coupling of *N*-pyrrole amide **17** with aryl borate **18** was pursued, the study of which follows.

2.2 Optimisation

Upon realisation that *N*-pyrrole amide substrate **17** and activated borate **18** could afford biphenyl **21** under iron-catalysis, optimisation of the reaction conditions began with a pre-catalyst and ligand screen, using the simple iron salt $FeBr_3$ as a pre-catalyst in the presence of co-catalytic $MgBr_2 \cdot OEt_2$ (20 mol%) in THF at room temperature (Table 2.1). When bidentate phosphine ligands 1,2-bis(diphenylphosphino)ethane (dppe) and 1,2-bis(diphenylphosphino)benzene (dpbz) were trialled, only trace or none of the desired cross-coupling product was detected (entries 2 and 3), resulting in poorer yield than when employing ligand-free conditions (entry 1). A similar result was obtained when using the bidentate amine *N,N,N',N'*-tetramethylethylenediamine (TMEDA) (entry 7). Suspecting that over-coordination of the metal was supressing activity, attention turned to monodentate phosphine ligands which led to an increase in activity (entries 4-6), with PPh_3 giving the highest yield (30%, entry 4).

Table 2.1: Optimisation of *N*-pyrrole amide directed iron-catalysed Suzuki biaryl cross-coupling.

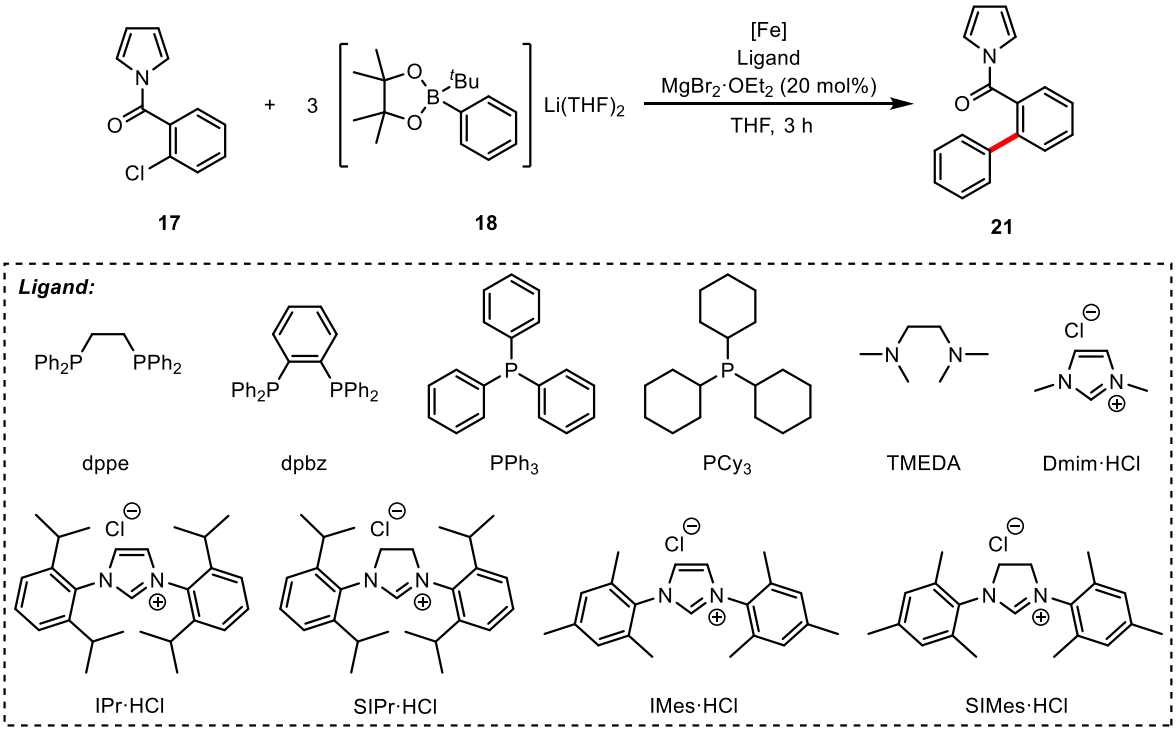

Entry	Pre-catalyst (mol%)	Ligand (mol%)	Temp. (°C)	Yield (%)[a]
1	$FeBr_3$ (10)	none	r.t.	16
2	$FeBr_3$ (10)	dppe (20)	r.t.	2
3	$FeBr_3$ (10)	dpbz (20)	r.t.	0
4	$FeBr_3$ (10)	PPh_3 (20)	r.t.	30

5	$FeBr_3$ (10)	PPh_3 (20)	60	19
6	$FeBr_3$ (10)	PCy_3 (20)	80	28
7	$FeBr_3$ (10)	TMEDA (20)	r.t.	1
8	$FeBr_3$ (10)	Dmim·HCl (20)	r.t.	0
9	$FeBr_3$ (10)	SIPr·HCl (20)	r.t.	3
10	$FeBr_3$ (10)	IPr·HCl (20)	r.t.	0
11	$FeBr_3$ (10)	SIMes·HCl (20)	r.t.	22
12	$FeBr_3$ (10)	IMes·HCl (20)	r.t.	27
13	$FeBr_3$ (10)	IMes·HCl (20)	60	73
14	**$FeBr_3$ (10)**	**IMes·HCl (10)**	**60**	**82**
15	$FeBr_3$ (5)	IMes·HCl (10)	60	55
16	$FeBr_3$ (15)	IMes·HCl (10)	60	69
17	$FeBr_2$ (10)	IMes·HCl (20)	60	73
18	$FeCl_2$ (10)	IMes·HCl (20)	60	68
19	FeF_3 (10)	IMes·HCl (20)	60	2
20	$[Fe(acac)_3]$ (10)	IMes·HCl (20)	60	19
21	$Fe(OTf)_2$ (10)	IMes·HCl (20)	60	19
22	$FeBr_3$ (10)	IMes (10)	60	80

Conditions: [Fe], ligand, $MgBr_2 \cdot OEt_2$ (0.025 mmol), **17** (0.125 mmol) and **18** (0.375 mmol) in THF for 3 h at the desired temperature. [a] Determined by GC analysis (dodecane internal standard). Roman Abrams assisted with the optimisation of the reaction as part of his undergraduate project supervised by the author.

Having observed how monodentate ligands gave higher activity than bidentate ligands and inspired by the works of Nakamura[55] and Duong[57] who showed that NHC precursors such as SIPr·HCl are effective ligands in iron-catalysed Kumada biaryl cross-coupling reactions, attention was turned to the use of NHC precursors. Whilst both SIPr·HCl and IPr·HCl proved inefficient in the reaction (entries 9-10), the less sterically demanding SIMes·HCl and IMes·HCl both proved to be competent, affording **21** in 22% and 27% yield respectively (entries 11 and 12). Gratifyingly, increasing the temperature to 60 °C whilst employing IMes·HCl as the ligand precursor increased the yield to 73% (entry 13). At this point, a screen of different iron salts was conducted with $FeBr_2$ and $FeCl_2$ giving essentially the same activity as $FeBr_3$ (entries 17 and 18). In stark contrast to Nakamura and Duong's Kumada biaryl systems

utilising NHC precursors, both FeF_3 (entry 19) and $FeOTf_2$ (entry 21) gave low yields. It was found that the loading of IMes·HCl could be lowered to 10 mol%, affording the cross-coupled product in 82% yield, however decreasing the loading of $FeBr_3$ to 5 mol% proved deleterious to the reaction (entry 15). Finally, the deprotonated NHC ligand, IMes, gave essentially the same activity as its precursor IMes·HCl (entry 22). Since IMes is extremely air- and moisture-sensitive, whereas its precursor IMes·HCl is bench-stable and easy to handle, it was decided to utilise NHC precursors for the remainder of the study.

Comparing entries 9-12 in Table 2.1, it appears that the difference in the electronics of the ligands (aromatic vs. non-aromatic 5-membered ring) has little effect on the outcome of the reaction, whereas the size of steric bulk on the *N*-aryl groups is critical (compare entries 9 and 11; 10 and 12). The requirement of *N*-aryl groups on the NHC precursor became apparent when Dmim·HCl was tested (entry 8). Grubbs has shown how reducing the bulk on the *ortho* positions of the *N*-aryl groups of IMes whilst increasing the bulk at the *meta* position can allow for more effective catalyst activity in ruthenium-catalysed olefin metathesis (Scheme 2.8).[123] Intrigued by this, the effects of altering the steric bulk on the *N*-aryl groups of the NHC precursor was explored further.

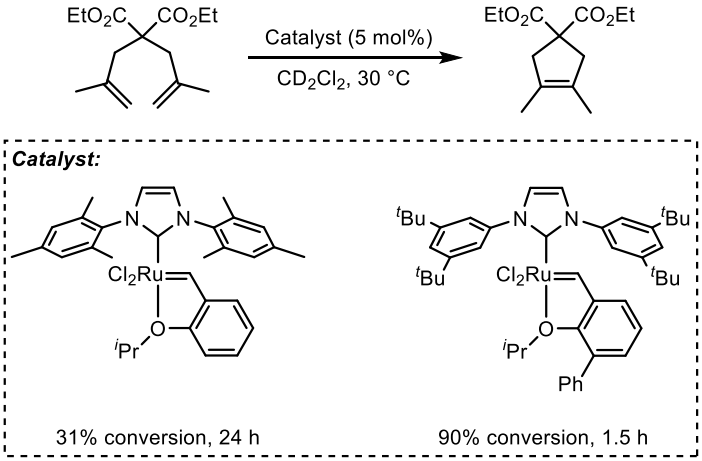

Scheme 2.8: Effect of *N*-aryl steric bulk in olefin metathesis.[123]

To test the importance of steric bulk on the *para* position of the *N*-aryl rings, the NHC precursor IXyl(2,6)·HCl was synthesised according to the procedure of Hintermann by condensation of 2,6-dimethylaniline with glyoxal in an isopropanol/water mixture at room temperature overnight to afford **22**. The impure crude starting material was then used directly for cyclisation using chlorotrimethylsilane (TMSCl) in EtOAc at 70 ºC for 2 h (Scheme 2.9).[124]

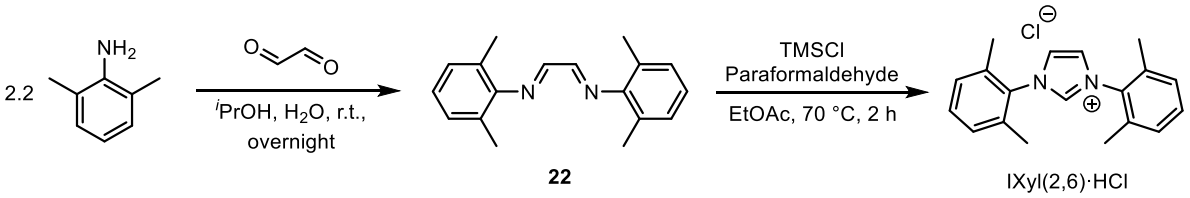

Scheme 2.9: Synthesis of IXyl(2,6)·HCl.

The synthesis of ITol·HCl, where small steric bulk at the *ortho* positions is present, was achieved following the procedure developed by Arduengo where the condensation and subsequent cyclisation of *p*-toluidine and glyoxal with paraformaldehyde and HCl occurs in a one-pot reaction to afford the desired product (Scheme 2.10).[125]

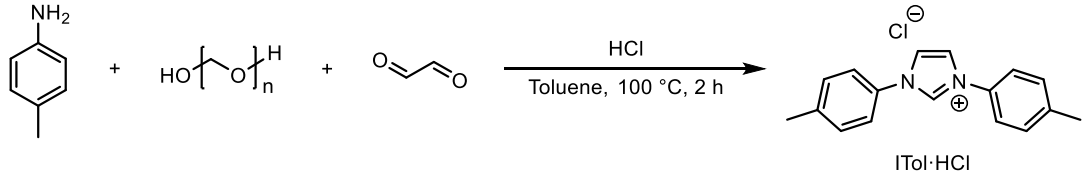

Scheme 2.10: Synthesis of ITol·HCl.

Whilst the synthesis of IXyl(2,6)·HCl and ITol·HCl were performed with relative ease, the synthesis of unknown IXyl(3,5)·HCl proved to be more demanding and revealed the capricious nature of NHC precursor synthesis. Initially, two different diazadienes were made from the condensation of 3,5-dimethylaniline with either glyoxal or 2,3-butanedione to afford **23** and **24** respectively (Scheme 2.11a).[126, 127] However, cyclisation of either diazadiene with paraformaldehyde and TMSCl as a chloride source failed to give the desired imidazolium salt (Scheme 2.11b).

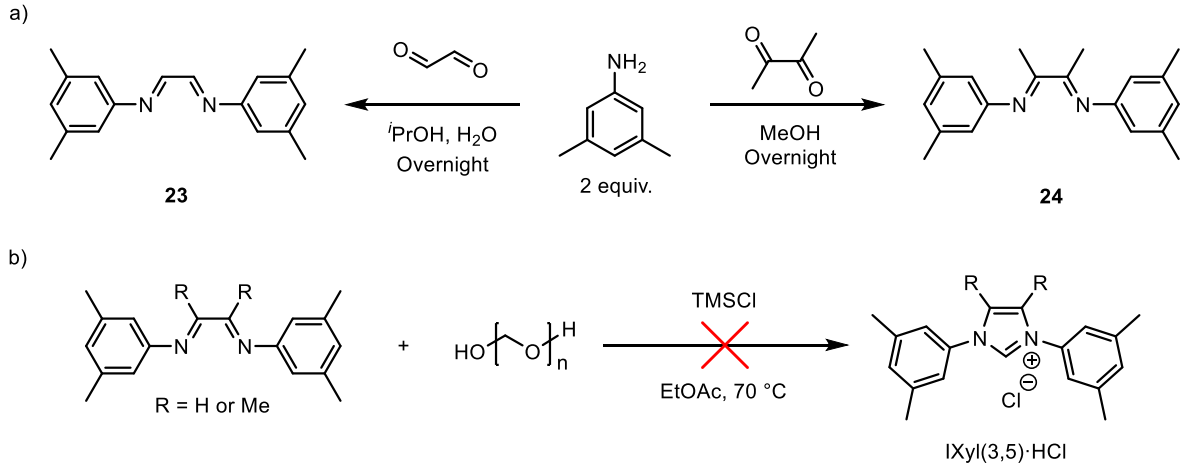

Scheme 2.11: a) Synthesis of diazadienes **23** and **24**. b) Attemped cyclisation of **23** and **24** with TMSCl.

Another attempt was made, following the one-pot procedure used by Arduengo to synthesise ITol·HCl, using either HCl as a chloride source or NH_4BF_4 to make the BF_4^- analogue, however neither reaction afforded the desired product (Scheme 2.12).

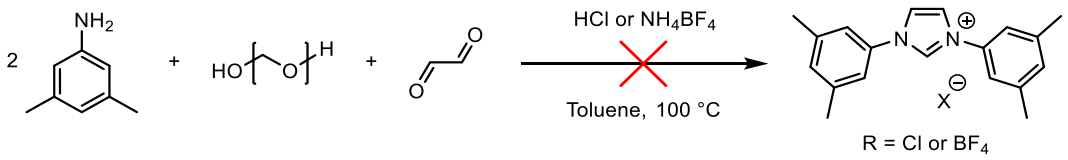

Scheme 2.12: Attempted synthesis of IXyl(3,5)·X (X = Cl or BF_4) following the method of Arduengo[125].

A brief appraisal of the literature revealed that although the synthesis of IXyl(3,5)·HCl has not been reported to date, the synthesis of the saturated analogue SIXyl(3,5)·HCl can be achieved when diazadiene **23** is reduced with $NaBH_4$ and subsequently protonated with 6M HCl to form the salt **25** in low yield which could be cyclised by stirring in neat triethyl orthoformate at 90 °C.[126] Carrying out this procedure afforded the desired ligand precursor (Scheme 2.13).

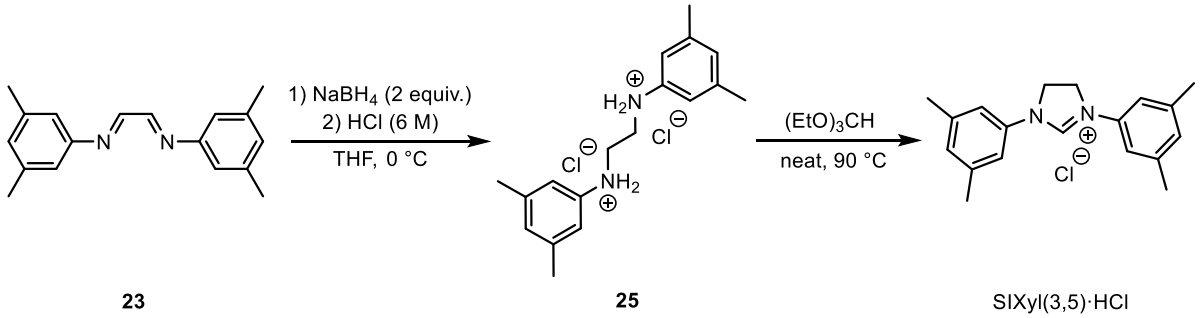

Scheme 2.13: Synthesis of SIXyl(3,5)·HCl.

As shown previously (Table 2.1), it was found that the electronic properties of the NHC precursor made little difference to the outcome of the reaction. Therefore, SIXyl(3,5)·HCl could still be used to gain insight into the steric requirements of the ligand. The synthesis of the least sterically demanding diaryl diazadiene **26** also turned out to be more difficult than envisioned, with the reaction between aniline and glyoxal affording intractable mixtures under a variety of conditions (Scheme 2.14). For this reason, this NHC precursor was not pursued further.

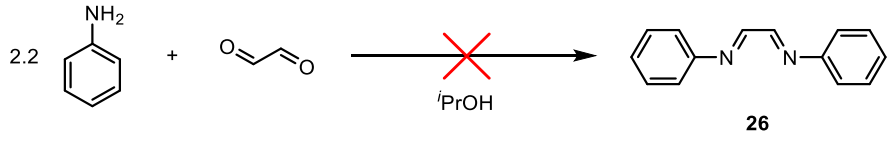

Scheme 2.14: Attempted synthesis of **26**.

With the NHC precursors IXyl(2,6)·HCl, SIXyl(3,5)·HCl and ITol·HCl in hand, these were tested under the optimised conditions at 20 mol% ligand loading (Table 2.2). Whilst the use of IXyl(2,6)·HCl afforded **21** with only a small decrease in yield compared to IMes·HCl (entry 1), reducing steric bulk in the *ortho* positions of the *N*-aryl ring proved to be deleterious to the reaction (entries 2 and 3). This demonstrates the requirement of modest steric bulk on the *ortho* positions of the *N*-aryl group of the ligand to afford good activity in the catalytic reaction.

Table 2.2: Effect of NHC precursor steric bulk in the cross-coupling reaction.

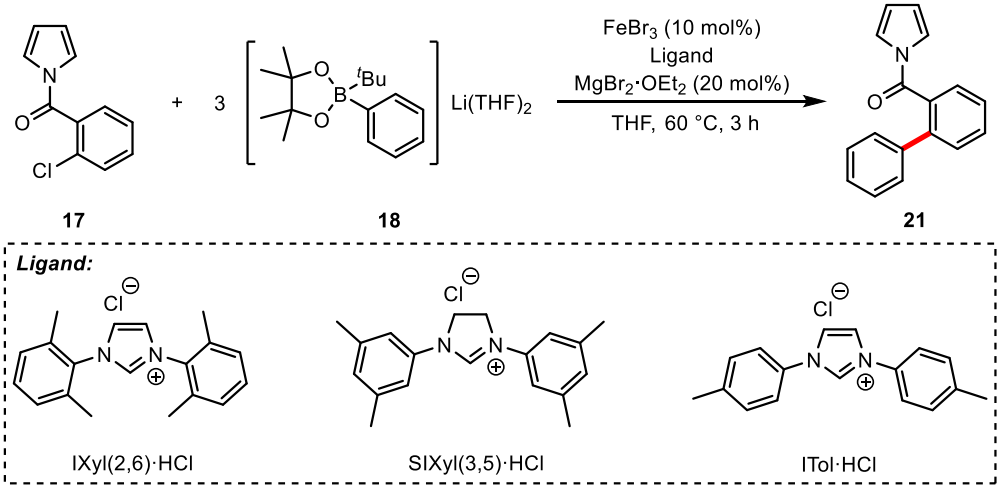

Entry	Ligand (mol%)	Yield (%)[a]
1	IXyl(2,6)·HCl (20)	67
2	SIXyl(3,5)·HCl (20)	29
3	ITol·HCl (20)	24

Conditions: $FeBr_3$ (0.0125 mmol), ligand (0.025 mmol), $MgBr_2{\cdot}OEt_2$ (0.025 mmol), **17** (0.125 mmol) and **18** (0.375 mmol) in THF for 3 h at 60 °C. [a] Determined by GC analysis (dodecane internal standard).

Having optimised the conditions for Suzuki biaryl cross-coupling of **21**, the effect of changing the halogen leaving group was probed (Table 2.3). Subjecting analogues of **17** to the reaction conditions showed that the 2-bromo analogue could be converted to the desired cross-coupled product **21** in a reasonable yield, albeit lower than with the chloride substrate (entry 2). Interestingly, it was observed that the production of the hydrodehalogenated product **27** increased when using the 2-bromo analogue. The selectivity for **21** was reduced further when the 2-iodo substrate was used, with an increased production of **27** observed. The 2-fluoro analogue showed the least activity with only a small amount of **21** being produced and no **27** observed. Taken together, it appears that the 2-chloro substrate offers the best activity and selectivity in the cross-coupling reaction. The facile activation of aryl chlorides in Suzuki cross-coupling reactions is highly desirable since aryl chlorides are far more widely commercially available and typically much cheaper than their bromide or iodide counterparts. Palladium-based catalysts are also often more sluggish with aryl chlorides compared with more activated aryl bromides and iodides.

Table 2.3: Effect of the halogen leaving group on the Suzuki biaryl cross-coupling.

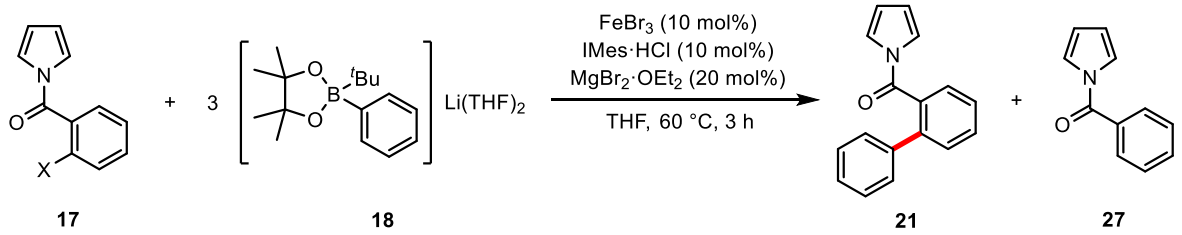

Entry	X	**21** (%)[a]	**27** (%)[a]
1	Cl	82	<5
2	Br	64	20
3	I	35	65
4	F	16	0

Conditions: $FeBr_3$ (0.02 mmol), ligand (0.02 mmol), $MgBr_2 \cdot OEt_2$ (0.04 mmol), substrate (0.2 mmol) and **18** (0.6 mmol) in THF for 3 h at 60 °C. [a] Determined by ^1H NMR analysis (1,3,5-trimethoxybenzene internal standard). Reactions performed by Mattia Manzotti.

Having determined the 2-chloro analogue to be the most active aryl halide, attention was turned to the loading of the borate **18** (Table 2.4). The use of 3 equivalents of borate **18** was shown to be necessary in both of Bedford's previous reports on iron- and cobalt-catalysed Suzuki biaryl cross-coupling. Here, it was found that reducing the nucleophile loading to 2.2 equivalents had no effect on the yield (entry 3). However, reducing the loading to 2 or 1.5 equivalents reduced productivity (entries 1 and 2). Throughout the entire study, pre-formed borate **18** was employed in the reaction and could be readily synthesised in 85% yield on a 30 g scale from phenylboronic acid pinacol ester and ^{t}BuLi. Pleasingly, using **18** formed *in situ* had little effect on the yield of the catalytic reaction.

Table 2.4: Effect of borate **18** loading on the Suzuki reaction.

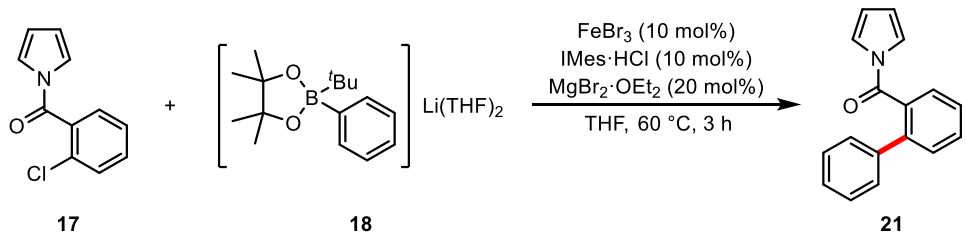

Entry	**18** (Equiv.)	Yield (%)[a]
1	1.5	64

2	2	77
3	2.2	82
4[b]	3	81

Conditions: $FeBr_3$ (0.02 mmol), IMes·HCl (0.02 mmol) $MgBr_2 \cdot OEt_2$ (0.04 mmol), **17** (0.2 mmol) and **18** in THF for 3 h at 60 °C. [a] Determined by ^1H NMR analysis (1,3,5-trimethoxybenzene internal standard). [b] Borate **18** prepared *in situ*.

Layering a saturated THF solution of **18** with hexane afforded single crystals of suitable quality for analysis by single crystal X-ray diffraction. The crystal structure of borate **18** is shown in Figure 2.1, confirming the identity of the nucleophile and showing the tetrahedral geometry of the boron atom. It is also apparent that the lithium counter ion coordinates to one of the oxygen atoms in the pinacol backbone, with two molecules of THF coordinating to the lithium atom.

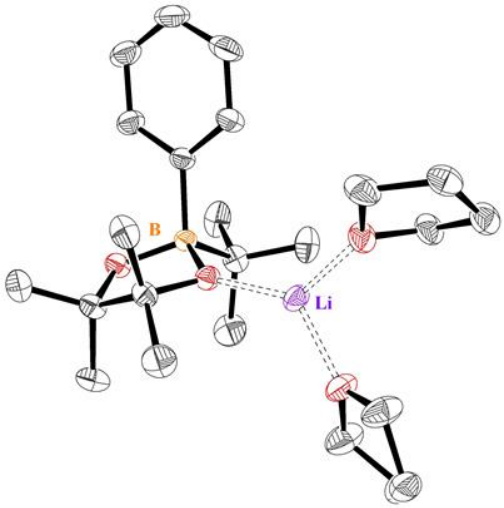

Figure 2.1: Single crystal X-ray structure of **18**. Ellipsoids depicted at 50% probability level with hydrogen atoms and disorder in THF ring omitted for clarity.

Finally, control experiments of the catalytic reaction were undertaken and showed that the presence of iron was necessary for the reaction to proceed (Table 2.5, entry 1). Meanwhile, high purity $FeBr_2$ gave a slight increase in performance and good productivity was observed when employing high purity $FeCl_3$ (entries 2 and 3). This indicates that impurities, in either the iron source or any other components of the reaction mixture, are unlikely to be responsible for the observed catalytic reactivity.

Table 2.5: Effect of iron source on the Suzuki biaryl reaction.

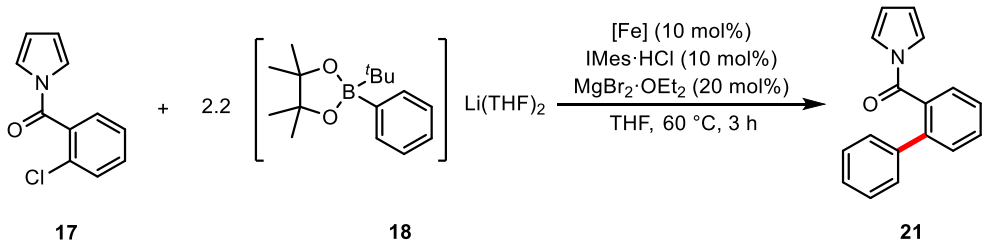

Entry	[Fe]	Yield (%)[a]
1	None	0
2	$FeCl_3$ (99.99% purity)	68
3[b]	$FeBr_2$ (99.999% purity)	84

Conditions: $FeBr_3$ (0.02 mmol), ligand (0.02 mmol), $MgBr_2{\cdot}OEt_2$ (0.04 mmol), **17** (0.2 mmol) and **18** (0.6 mmol) in THF for 3 h at 60 °C. [a] Determined by ^1H NMR analysis (1,3,5-trimethoxybenzene internal standard). [b] $FeBr_2$ and NHC-precursor stirred at 60 °C for 30 mins prior to addition of other reaction components.

2.3 Influence of the Directing Group

When the *meta* and *para* *N*-pyrrole amide substrates **28** and **29** were subjected to the reaction conditions neither *meta* or *para* arylated or hydrodehalogenated products were observed (Scheme 2.15). The lack of reactivity of *N*-pyrrole amide substrates **28** and **29** show that aryl chloride bond activation is likely achieved by a directing group effect.

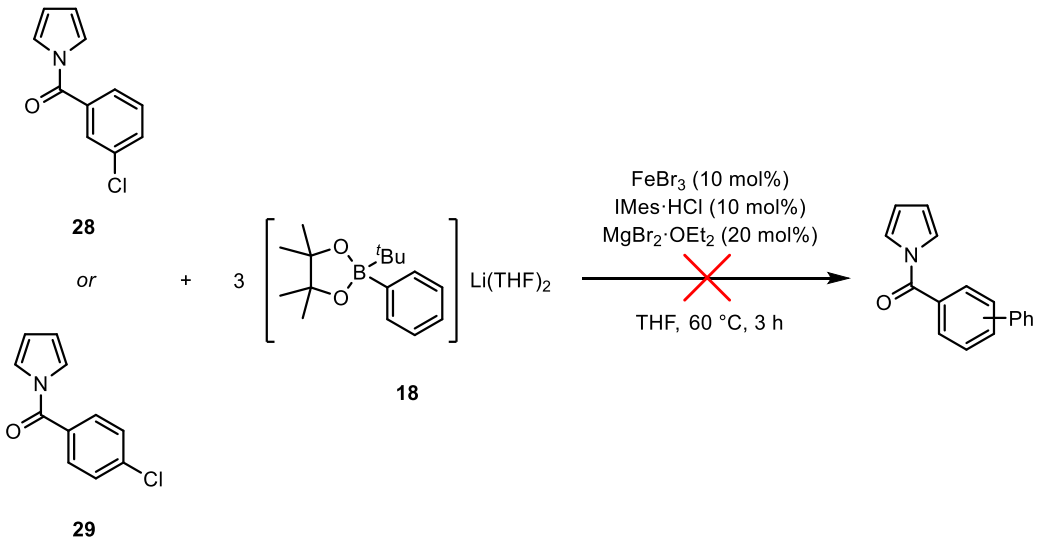

Scheme 2.15: Effect of the position of the directing group relative to the aryl chloride bond. Reactions performed by Mattia Manzotti.

In Bedford's earlier report on iron-catalysed Suzuki biaryl cross-coupling, more 'classic' directing groups such as tertiary amine, ether, ester, carbamate or imine functions failed to induce the desired cross-coupling reaction.[122] Upon the initial discovery of Suzuki biaryl cross-coupling it was found that *N*-indole amide is also a competent directing group (Section 2.1). Thus, a series of different amide-based directing groups were made to gain more insight into the influence of the directing group. As with the synthesis of **17**, *N*-indole (**30**) and *N*-pyrrolidine (**31**) amides were synthesised by deprotonation of indole or pyrrolidine with NaH and subsequently reacted with 2-chlorobenzoyl chloride to afford the desired *ortho*-directing aryl chlorides (Scheme 2.16a). Substrate **32** was synthesised from diphenylamine and benzoyl chloride using a modified procedure by Chen and co-workers (Scheme 2.16b),[128] whereas **33** was generated according to the procedure of Li and co-workers by amide coupling of aniline and 2-chlorobenzoic acid using *N*,*N*'-dicyclohexylcarbodiimide (DCC) with catalytic 4-dimethylaminopyridine (DMAP) (Scheme 2.16c).[129] Subsequent deprotonation of **33** with NaH and addition of *p*-toluenesulfonyl chloride afforded the protected amide **34** (Scheme 2.16c). Finally, **35** was made by reacting pyrazole with benzoyl chloride in the presence of catalytic Et_3N (Scheme 2.16d).

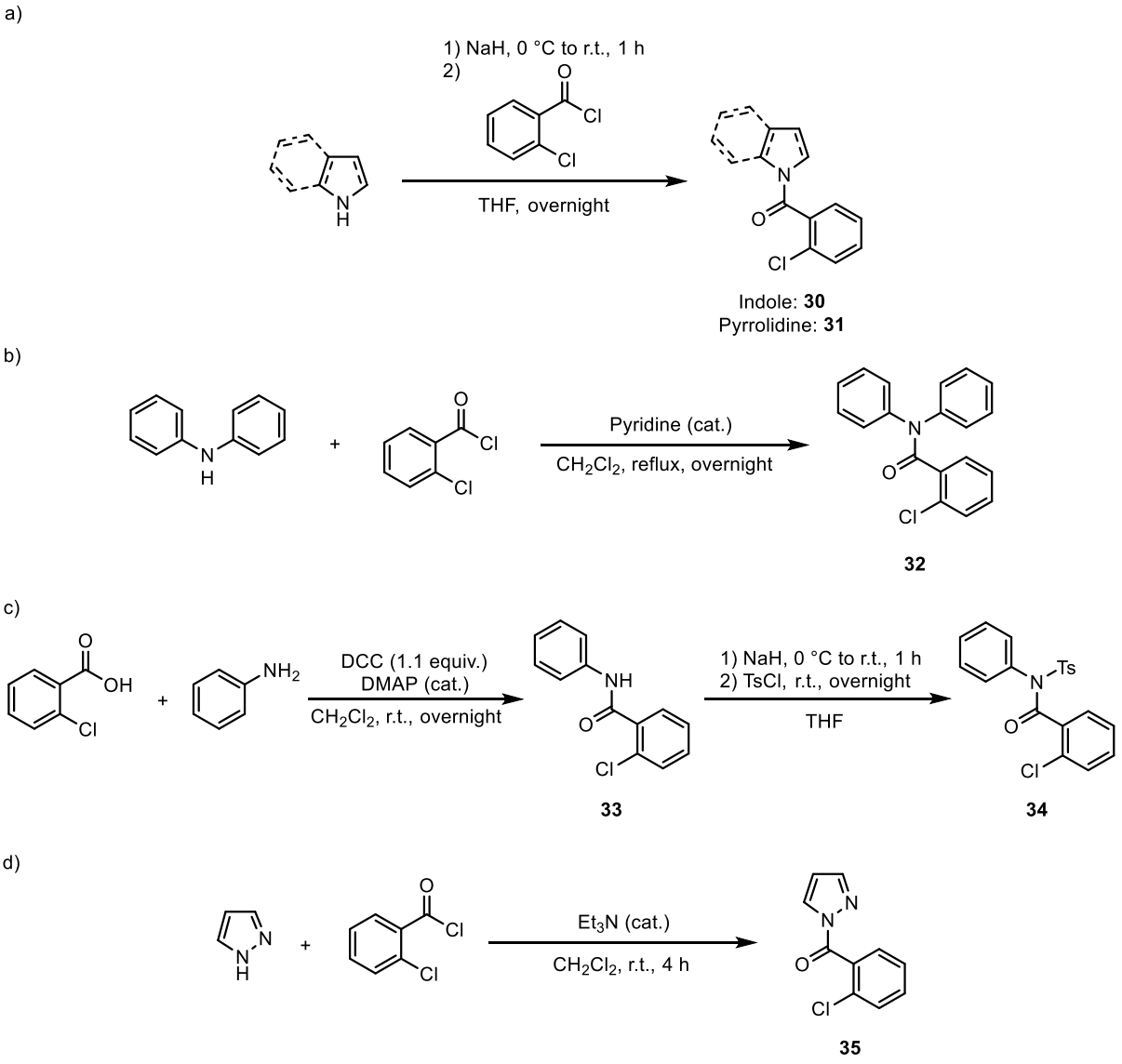

Scheme 2.16: Synthesis of substrates **30-35** with different amide directing groups.

The influence of the different directing groups on the reaction is shown in Scheme 2.17. *N*-indole amide proved to be capable of directing activation of the aryl chloride bond to afford structurally characterised **36** in 45% yield. Similarly, the *N*,*N*-diphenyl amide, **32**, afforded the desired cross-coupled product in modest yield (32%). Conversely, none of the substrates **31** and **33-35** were effective at directing aryl chloride bond activation. This survey suggests that aromaticity in the directing group is important, especially when comparing **17** with its saturated analogue **31**. This would also explain why substrates **30** and **32** are capable, to some extent, of being capable directing groups. When **33** was subjected to the reactions conditions, no conversion was observed. This could be due the deprotonation of the amide by the borate nucleophile **18** which would then be readily protonated upon quenching of the reaction. Protected **34** meanwhile showed conversion of the starting material but none of the desired arylated product **38**. Subjecting **35** to the optimised conditions only afforded trace amounts of the desired product (**40**).

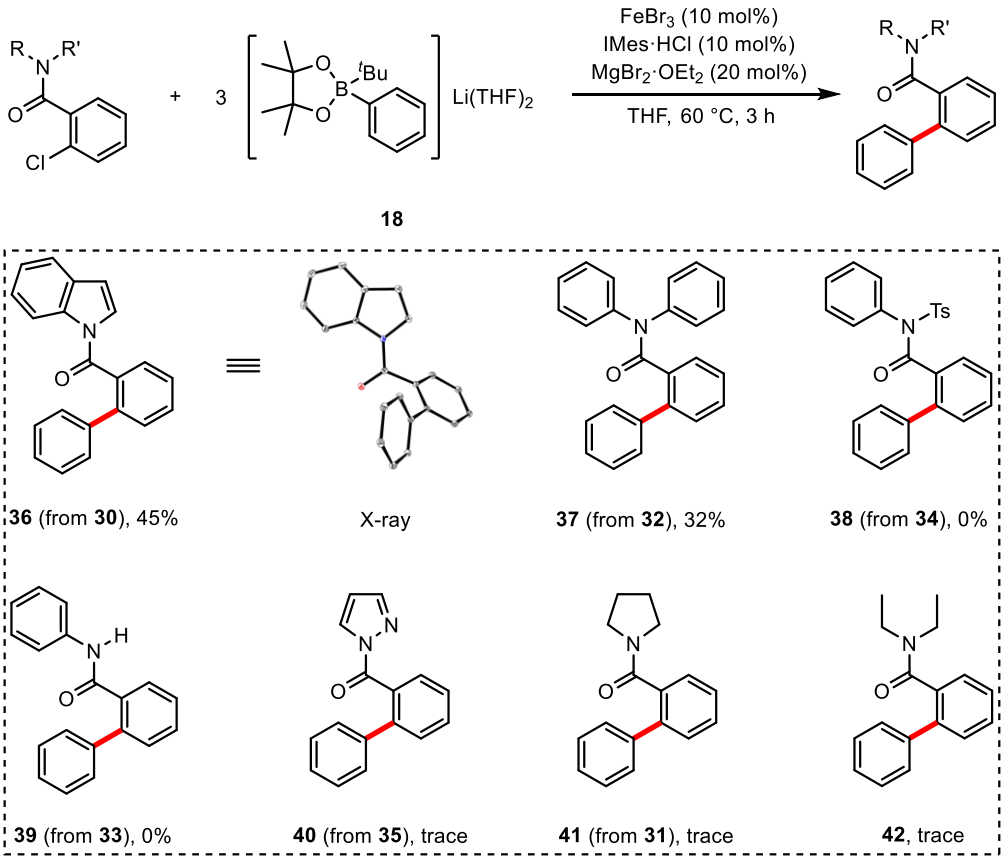

Scheme 2.17: Amide directing group scope. Yields determined by ^{1}H NMR analysis (1,3,5-trimethoxybenzene internal standard) with product identification confirmed by independent synthesis of the biaryl and/or GC-MS analysis.

GC-MS analysis of all the reaction mixtures from the amide scope showed the presence of 2-chlorobenzophenone (**43**) and (2-chlorophenyl)diphenylmethanol (**44**). The formation of **43** and **44** came as a surprise given the relative strength of amide bonds and the functional group tolerability associated with boron nucleophiles in catalysis. Recently, there has been a lot of interest in nickel-catalysed ketone synthesis from protected amides as an alternative procedure to Weinreb ketone synthesis.[130, 131] In particular, both *N*-pyrrole benzamide (**27**) and *N*-pyrazole benzamide have been shown to undergo oxidative addition at the C-N bond under palladium catalysis to afford ketones in the presence of aryl boronic acids.[132] An iron-catalysed variant would therefore be desirable; however, it was found that neither the presence of $FeBr_3$, IMes·HCl nor $MgBr_2{\cdot}OEt_2$ was required to generate **43** and **44** from the amine, suggesting that oxidative addition of the C-N bond to the iron-centre was not occurring in this case. The possibility of achieving this transformation catalyst-free offers the opportunity to broaden the scope of ketone synthesis from amides, especially with benzamides containing aryl halide bonds.

To investigate the potential of metal-free ketone synthesis from *N*-pyrrole amide **17** and borate **18**, a modest screen of conditions was investigated (Table 2.6). Whilst trace or none of **43** or **44** were detected in reactions under 60 °C (entries 1-3), small amounts were observed in reactions performed at 60 °C.

Increasing the temperature to 80 °C (entries 6-8) afforded modest amounts of **43** and **44**, which increased as the reactions were left longer, yet selectivity for **43** was not observed. Increasing the amount of **18** with respect to **17** was also found to afford modest amounts of the ketone and alcohol at 80 °C in 3 h (entries 9 and 10), but still with poor selectivity. Since no selectivity for **43** was observed, the metal-free ketone synthesis was not pursued further.

Table 2.6: Reaction between **17** and **18** to afford ketone **43** and alcohol **44**.

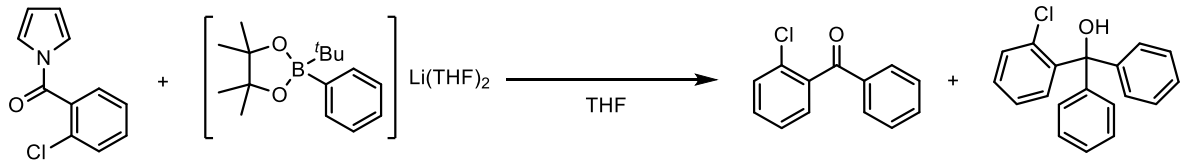

17 **18** **43** **44**

Entry	**18** (equiv.)	Temperature (°C)	Time (h)	**43** (%)[a]	**44** (%)[a]
1	1	r.t.	3	0	0
2	1	40	3	0	0
3	1	40	6	0	0
4	1	60	3	1	0
5	1	60	6	5	1
6	1	80	3	12	4
7	1	80	6	17	11
8	1	80	24	19	18
9	2	80	3	19	11
10	3	80	3	26	13

[a] Determined by GC analysis (dodecane internal standard).

Overall, probing the influence of the directing group showed that *N*-pyrrole amide was the most effective at allowing facile aryl chloride bond activation for the iron-catalysed Suzuki biaryl cross-coupling. It appears that aromaticity plays an important effect in the role of the directing group and that **17** is specially placed to tolerate the optimised reaction conditions. Under harsher reaction conditions, **18** can react with **17** to afford the corresponding ketone and alcohol, however attempts to optimise this process for the selective production of **43** were unsuccessful.

2.4 Scope and Limitations

To explore the scope and limitations of the reaction, borates **44-49** were prepared by addition of ^{t}BuLi to the parent boronic acid pinacol ester in either THF or hexane to afford phenyl borate salts containing alkoxy, alkyl, halogen, naphthyl and 2-methylthiophene[133] moieties in good yield (Scheme 2.18).

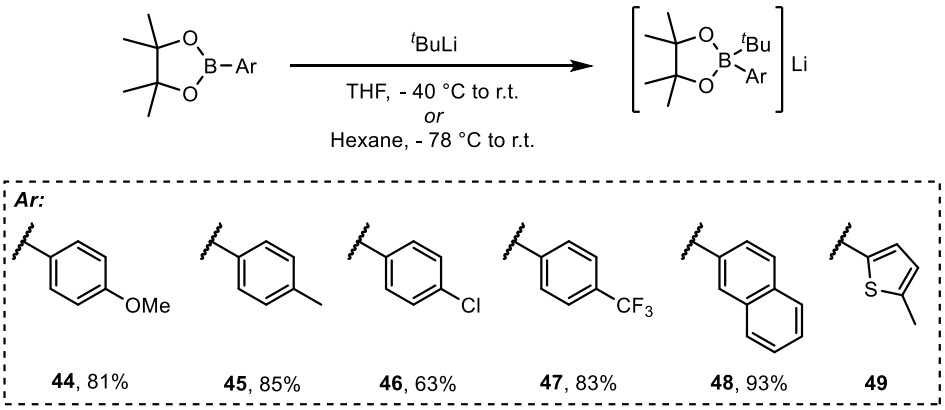

Scheme 2.18: Synthesis of borates **27-32**. Yields are of the isolated product. **49** is isolated with ~ 10% contamination of Li[Me-$C_4H_2S)_2$Bpin] – see Ref 133.

The synthesis was not amenable for all borate salts, however, with 4-cyanophenyl, 4-pyridine and 2-thiophene boronic acid pinacol esters not tolerating the addition of ^{t}BuLi (Scheme 2.19), forming intractable mixtures of product, starting material and unidentified compounds as determined by ^{1}H and ^{11}B NMR. This represents one of the major limitations in the current state-of-the-art iron-catalysed Suzuki cross-coupling reactions as ^{t}BuLi is the most commonly used activator for such transformations.

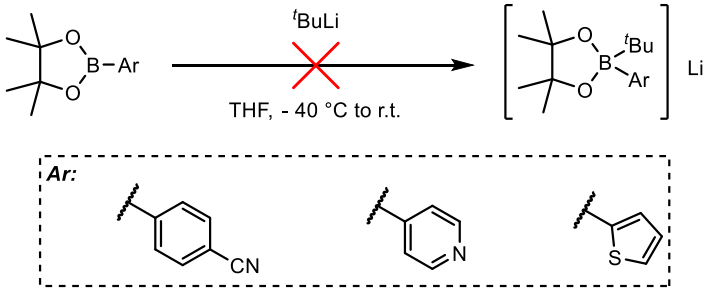

Scheme 2.19: Failed synthesis of 4-cyanophenyl, 4-pyridine and 2-thiophene borates.

Syntheses of a variety of aryl chlorides bearing the *ortho N*-pyrrole amide directing group were performed by deprotonation of pyrrole with NaH and reaction of the resulting anion with the commercially available functionalised benzoyl chloride in a simple one-pot reaction (Scheme 2.20a). Where the functionalised benzoyl chlorides were not readily available, a variety of the corresponding 2-chlorobenzoic acids were converted to the acid chloride by reaction with thionyl chloride. The acid chlorides obtained were used immediately, without purification, to afford the intended electrophile after reaction with deprotonated pyrrole (Scheme 2.20b).

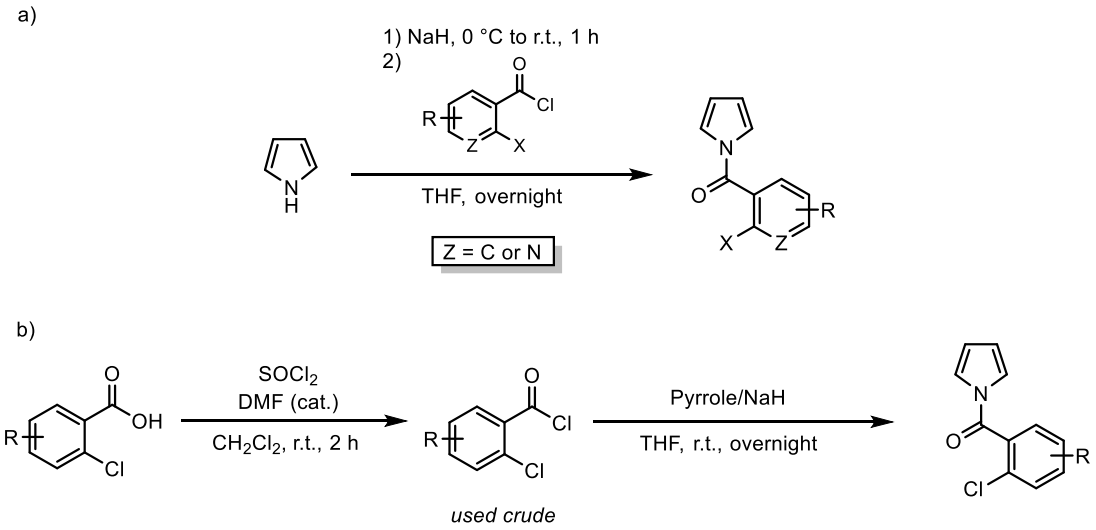

Scheme 2.20: Synthesis of aryl halide electrophiles for scope and limitation investigations.

With starting materials and optimised conditions in hand, the scope and limitations of the reaction were explored (Scheme 2.21). Using borate **18**, it was found that the reaction is tolerant of aryl chlorides bearing alkoxy (**50**-**52**), alkyl (**53**-**55**) and chloro (**58**) functional groups. Isolation of **58** not only lends credence to the suggestion that aryl chloride bond activation is dependent on a participating *ortho* directing group, but is also a useful orthogonal synthetic procedure which would be difficult to achieve with palladium catalysis. Gratifyingly, it was observed that a nitrile group on the aryl chloride could be accommodated (**57**), contrasting with Bedford's cobalt-catalysed Suzuki biaryl cross-coupling reaction where nitrile groups were not tolerated.[115] The production of **55** shows that having steric hindrance on the aryl chloride is tolerable. Disappointingly, an acetophenone group was not tolerated, with only trace amounts of **56** observed. Products resulting from arylation at the carbonyl group were detected by GC-MS, in line with previous observations of nucleophilic addition by activated borate **18** (Section 2.3).

Switching to the use of borate **44**, a range of biaryls could be isolated including bromo (**60**), fluoro (**61** and **62**), trifluoromethyl (**63**), tertiary amine (**64**) and thioether moieties (**65**). As before, isolation of **60** demonstrates a useful orthogonal process that would be difficult with traditional noble-metal catalysis. The production of fluorinated biaryls **61**-**63** is valuable owing to their importance in pharmaceuticals and functional materials. Isolation of tertiary amine **64** suggests that poisoning of the reaction by competitive lone pair donation from the amine to the iron-centre does not occur. Pleasingly, terphenyl **66** could be isolated in modest yield; the terphenyl moiety is found in immunosuppressive[134] and anti-fungal[135] agents. In general, it appears that placing the functional group either *meta* or *para* to the aryl chloride bond makes little difference to the activity of the catalysis, with both electron-rich and electron-poor aryl chlorides being well tolerated. Finally, heterocycle 2-chloropyridine could be arylated with **44** in modest yield to afford **67**.

When the thiophene borate **49** was used, none of the desired product, **68**, was obtained. However, 4-tolyl, 2-naphthyl and 4-chlorophenyl derived borates gave good to modest activity in the cross-coupling,

furnishing compounds **69**, **70** and **71** respectively. With regards to the borate nucleophiles, it appears that electron-rich aryl borates perform better than electron-poor aryl borates.

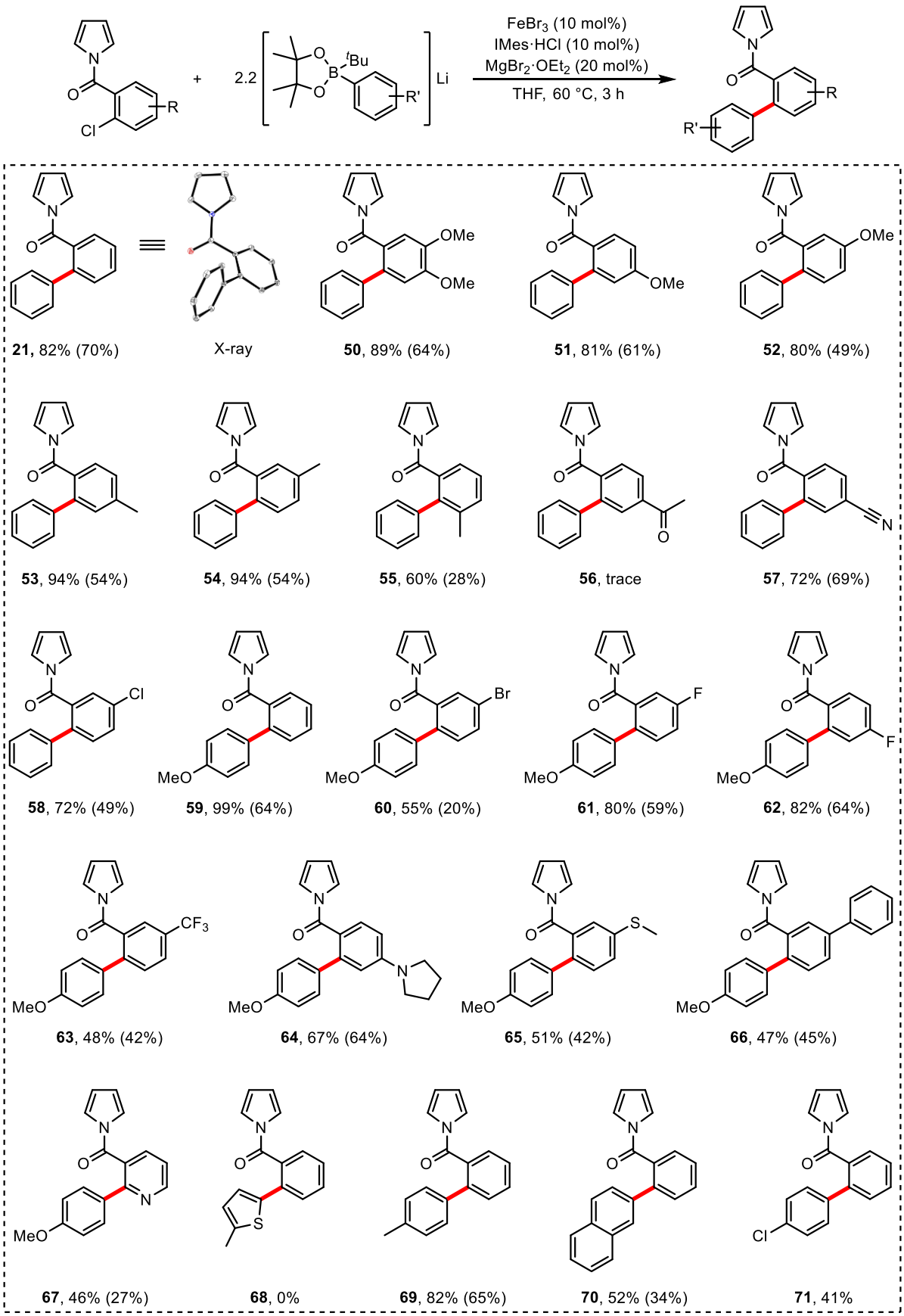

Scheme 2.21: Scope of iron-catalysed Suzuki biaryl cross-coupling. Yields determined by ^{1}H NMR analysis (1,3,5-trimethoxybenzene internal standard) with isolated yields in parenthesis.

Attempts to optimise the catalytic reaction between an electron-poor borate with **17** are summarised in Table 2.7. 4-Trifluoromethylphenyl borate **72** was chosen due to the extremely electron-withdrawing nature of the pharmaceutically privileged trifluoromethyl group. Intriguingly, when using isolated **72** no activity was seen (entry 1), whereas forming the nucleophile *in situ* furnished the desired product in moderate yield when the reaction was run under the previously optimised conditions (entry 2). Increasing the temperature proved to be deleterious to the yield (entry 3), whilst decreasing the temperature gave essentially the same activity (entry 4). Unfortunately, increasing the $FeBr_3$/IMes·HCl loading to 20 mol% only gave a small increase in the yield (entry 5).

Table 2.7: Optimisation of the Suzuki cross-coupling of **17** and **72**.

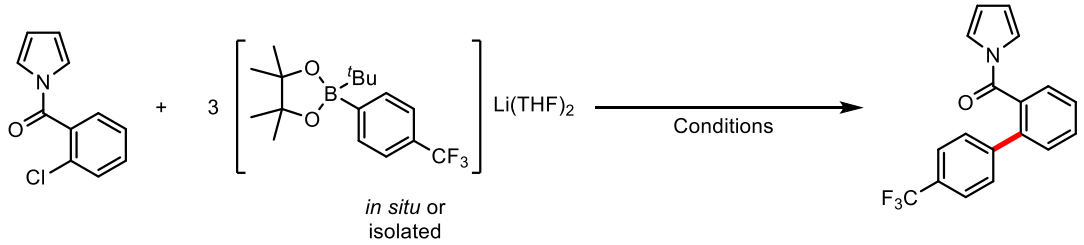

17 **72** **73**

Entry	Pre-catalyst (mol%)	Ligand (mol%)	Temp. (°C)	Yield (%)[a]
1[b]	$FeBr_3$ (10)	IMes·HCl (10)	60	0
2[c]	$FeBr_3$ (10)	IMes·HCl (10)	60	43
3[c]	$FeBr_3$ (10)	IMes·HCl (10)	40	44
4[c]	$FeBr_3$ (10)	IMes·HCl (10)	80	32
5[c]	$FeBr_3$ (20)	IMes·HCl (20)	60	54

Conditions: $FeBr_3$ (0.04 mmol), IMes·HCl (0.04 mmol), $MgBr_2{\cdot}OEt_2$ (0.08 mmol), **17** (0.4 mmol) and **72** (1.2 mmol) in THF for 3 h at 60 °C. [a] Determined by ^{1}H NMR analysis (1,3,5-trimethoxybenzene internal standard). Presence of the desired compound was also confirmed by GC-MS. [b] Reaction run twice with isolated borate. [c] Borate formed *in situ*.

2.5 Iron-Catalysed Suzuki Biaryl Cross-Coupling

Having demonstrated that installation of a directing group allows for a variety of biaryls to be accessed under the optimised reaction conditions, the extent to which a simple unactivated aryl halide could be arylated was investigated (Table 2.8). The reaction of **74** (synthesis carried out in hexane instead of THF) with the active catalytic system run in neat chlorobenzene at 100 °C for 2 nights furnished cross-coupled **76** in 20% yield with almost equal amounts of homocoupled **75** and **77** (entry 1). A modest screen of high boiling point solvents was conducted, with toluene, DMF and fluorobenzene each giving fewer amounts of homocoupled **75**, but with comparable amounts of **77** to **76** (entries 2-4). Running the reaction in hexafluorobenzene gave predominantly homocoupled **77** (entry 5). Finally, running the reaction in THF at 80 °C overnight afforded cross-coupled **76** in 17% yield, with **75** furnished in only 2% yield, but **77** in 16% yield (entry 6).

Table 2.8: Iron-catalysed Suzuki biaryl cross-coupling of chlorobenzene.

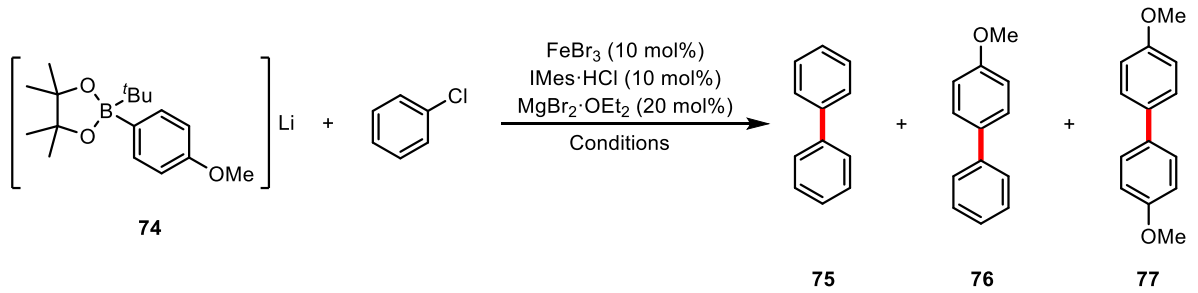

Entry	Solvent	Temperature (°C)	**75** (%)[a]	**76** (%)[a]	**77** (%)[a]
1	Neat	100[b]	10	20	16
2	Toluene	100[b]	4	17	20
3	DMF	100	3	23	34
4	Fluorobenzene	100	11	24	24
5	Hexafluorobenzene	100	1	7	28
6	THF	80	2	17	16

Conditions: $FeBr_3$ (0.01 mmol), IMes·HCl (0.01 mmol), $MgBr_2 \cdot OEt_2$ (0.02 mmol), chlorobenzene (0.1 mmol) and **74** (0.2 mmol) in the desired solvent overnight at the desired temperature. [a] Determined by GC analysis (dodecane internal standard). [b] Reaction run for 2 nights.

These data show that whilst aryl-halide activation without a directing group is feasible, harsher conditions are required, only furnishing modest amounts of the cross-coupled product. In all cases, significant homocoupling of the nucleophile was observed, showing that selectivity in the absence of a directing group is an issue. Conversely, fewer amounts of homocoupled **75** were observed in all cases

(expect for when the reaction was run in chlorobenzene, where increased homocoupling of the electrophile is likely due its vast excess), showing that activation of the aryl chloride bond is still the main barrier to success.

Finally, cross-coupling of 2-chloropyridine with **18** was also trialled under the optimised conditions, however, no cross-coupled product was observed (Scheme 2.22).

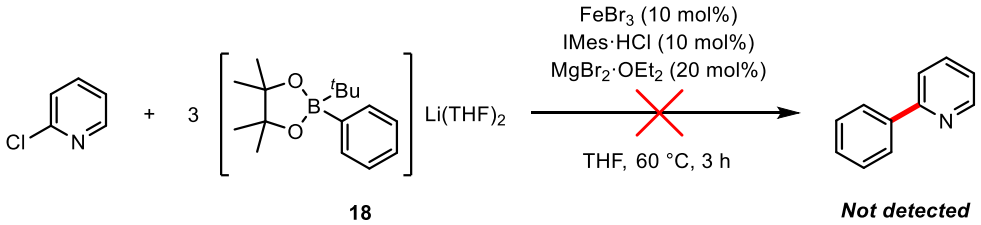

Scheme 2.22: Iron-catalysed Suzuki biaryl cross-coupling of 2-chloropyridine.

2.6 Cross-Coupling with Alternative Nucleophiles

Having found conditions to facilitate aryl chloride activation for Suzuki catalysis, the question arose of whether it was possible to broaden the scope beyond biaryl synthesis. Vinylation of aryl halides, like biaryl synthesis, is an sp^2-sp^2 cross-coupling process and has been achieved with both nickel- and palladium-catalysis,[136] however to this date there have been no reports on the use of iron-catalysis. Unfortunately, when borate **78** was subjected to the reaction conditions with *N*-pyrrole amide **17**, only trace amounts of the vinylated arene in the presence of unreacted **17** was observed by GC-MS analysis of the crude reaction mixture (Scheme 2.23). Similarly, ethylene borate **79** gave none of the desired cross-coupling.

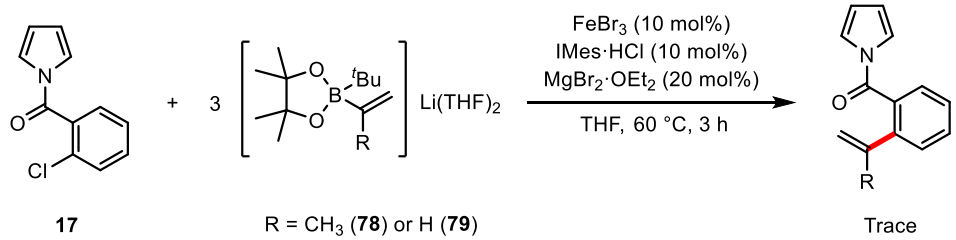

Scheme 2.23: Attempted vinylation of **17**.

Another transformation that is difficult to achieve under iron-catalysis is borylation of aryl halides. In 2014, Bedford[137] and Cook[138] disclosed their borylation of alkyl halides using iron-catalysis, although Bedford and co-workers found that their conditions were not amenable for simples aryl halides, only achieving low yields of phenylboronic acid pinacol ester (Scheme 2.24a). Later, Nakamura and co-workers developed conditions to allow borylation of aryl chlorides, however the scope of the reaction was limited to chloronaphthalenes and chlorobiphenyls, with chlorobenzene only affording the desired cross-coupling in 27% yield (Scheme 2.24b).[139]

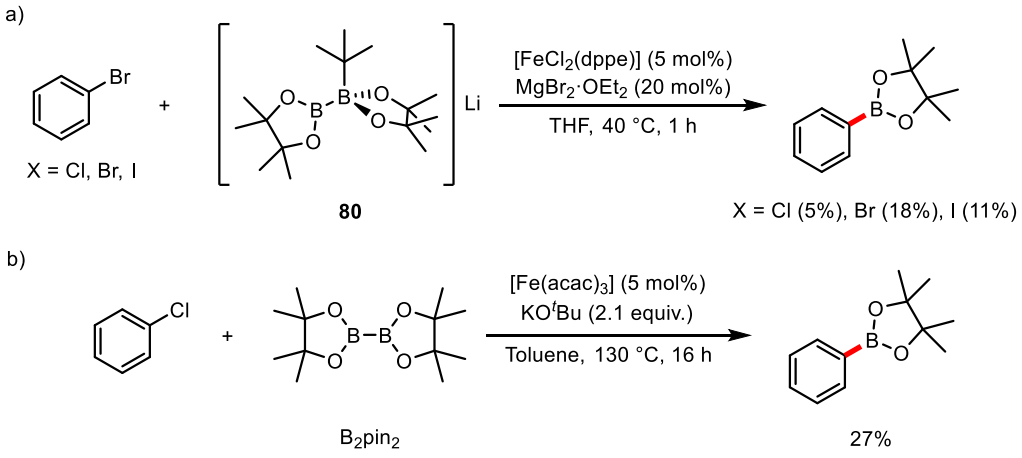

Scheme 2.24: a) Bedford's iron-catalysed borylation of aryl halides[137] and b) Nakamura's borylation of chlorobenzene[139].

To investigate whether the *N*-pyrrole amide directing group could aid borylation of aryl chlorides, conditions developed for the iron-catalysed Suzuki biaryl cross-coupling were trialled, as well as conditions developed by Bedford and co-workers for the borylation of alkyl halides using alkyl lithium activated B_2pin_2 (**80**) (Table 2.9). Unfortunately, in all cases none of the desired product was detected.

Table 2.9: Attempted iron-catalysed borylation of *N*-pyrrole amide **17**.

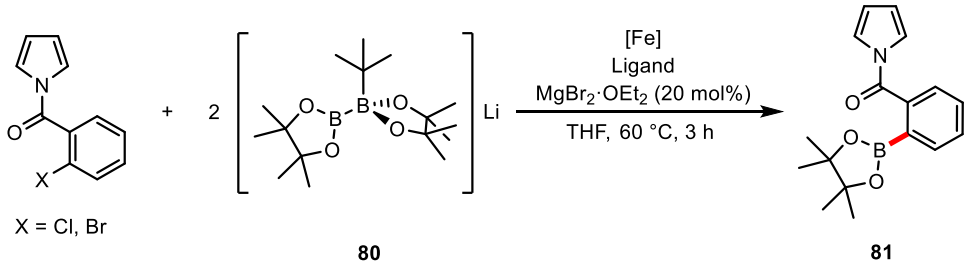

Entry	Pre-catalyst (mol%)	Ligand (mol%)	X	Yield (%)[a]
1	$FeBr_3$ (10)	IMes·HCl (10)	Cl	n.d.
2	$FeBr_3$ (10)	IMes·HCl (10)	Br	n.d.
3	$FeCl_2$ (5)	dppe (5)	Br	n.d.

Conditions: [Fe], ligand, $MgBr_2{\cdot}OEt_2$ (0.04 mmol), substrate (0.2 mmol) and **80** (0.4 mmol) in THF at 60 °C for 3 h. [a] Analysis by GC-MS.

2.7 Conclusions

In conclusion, it has been shown that installation of an *N*-pyrrole amide directing group allows for facile activation of *ortho* aryl chloride bonds in an iron-catalysed Suzuki biaryl cross-coupling (Scheme 2.25). *N*-pyrrole amide proved to be the most efficient group for directing catalysis and is easy to install onto the arene ring from a variety of commercially available benzoyl chlorides and benzoic acids. Whilst the transformation currently requires the presence of the directing group, it proves that iron-catalysed Suzuki biaryl cross-coupling is an achievable goal.

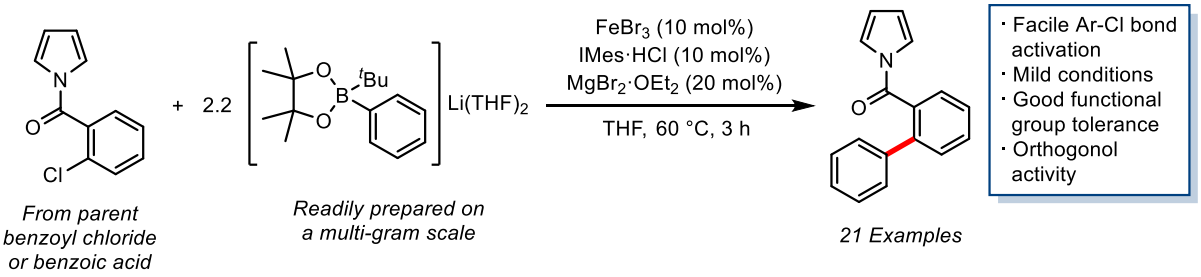

Scheme 2.25: Substrate-directed iron-catalysed Suzuki biaryl cross-coupling.

The mild conditions required for the transformation to take place, using $FeBr_3$ as a pre-catalyst with bench-stable NHC precursor IMes·HCl as ligand and co-catalytic $MgBr_2{\cdot}OEt_2$ in THF at 60 °C for 3 h allows for a variety of functional groups to be accommodated, with 21 examples of biaryls bearing the *N*-pyrrole amide function isolated. Currently, the process relies on phenylboronic acid pinacol esters to be activated with ^{t}BuLi which reduces the applicability of the reaction due to the limited tolerance for some functional groups on the arene of the nucleophile. Future endeavours should focus on utilising less aggressive activating agents such as those used in palladium-catalysed Suzuki cross-couplings (i.e. KO^{t}Bu). Meanwhile, attempts to utilise the *N*-pyrrole amide directing group for reactions that are currently difficult to achieve in iron catalyses such as vinylation and borylation of aryl halides proved unfruitful.

Clearly, a detailed mechanistic investigation would draw back the curtain on the underlying processes occurring during the reaction and may well subsequently prove vital to develop undirected aryl chloride bond activation (which under the optimised conditions yields the cross-coupled biaryl in low yield) and utilisation of the *N*-pyrrole amide directing group for other iron-catalysed transformations. These studies are the subject of the proceeding chapter.

Parts of this work have been published in *Nature Catalysis* **2018**, *1*, 429-437.

Chapter 3

Substrate-Directed Iron-Catalysed Suzuki Biaryl Cross-Coupling: Mechanism

3.1 Introduction

Whilst most mechanistic studies have focused on iron-catalysed Kumada-type reactions (see Section 1.2), the elucidation of analogous Suzuki-type mechanisms is still in its infancy. In 2014, Bedford and co-workers showed how arylation of alkyl, benzyl and allyl halides with aryl borates occurs when employing simple iron pre-catalysts under mild conditions.[97] Bidentate diphosphine ligands 1,2-bis(diphenylphosphino)ethane (dppe) and 1,3-bis(diphenylphosphino)propane (dppp) were found to be the most effective ligands for a variety of substrates. Focussing on the mechanism of the dppe-containing system, it was revealed that the Fe(II) pre-catalysts [$FeX_2(dppe)_2$] (X = Cl or Br) are reduced to the previously reported and structurally characterised Fe(I) complexes [$FeX(dppe)_2$] (X= Cl or Br) by aryl borate **18** in the presence of $MgBr_2$ (Scheme 3.1). Although the presence of $MgBr_2$ wasn't strictly required for the reduction, the amount of Fe(I) formed was significantly lower in its absence, suggesting that the metal halide salt facilitates transmetallation. Using initial rates studies, Bedford proposed that these species act as off-cycle resting states for a highly reactive, low coordinate Fe(I) species which activates the alkyl halide substrate. The reason for the requirement of the $MgBr_2$ salt was not fully delineated. Initial rates analysis showed an accelerating effect on the rate-determining step up until a 20 mol% loading of $MgBr_2$. At higher loadings of the salt however, a decrease on the initial rate was observed.

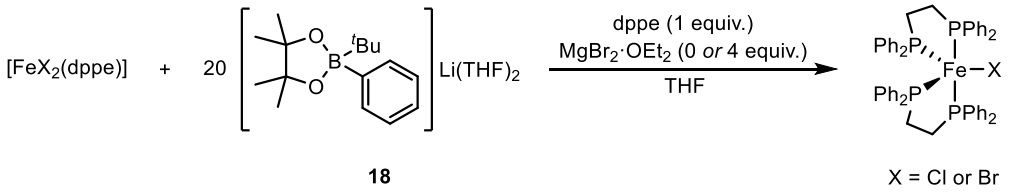

Scheme 3.1: Production of [$FeX(dppe)_2$] (X= Cl or Br) using borate **18**.[97]

One of the issues with mechanistic elucidation in iron-catalysed cross-couplings is the fact that even small changes in the catalytic system can have profound effects on reaction pathways and catalytic intermediates. In 2015, Neidig and co-workers[102] reported an elegant mechanistic study on Nakamura's[69] original iron-catalysed Suzuki cross-coupling reaction. The conditions are similar to those developed by Bedford and co-workers,[97] except the ligand employed in Nakamura's reaction is the 'bulky spin-control-intended *ortho*-phenylene bisphosphine' (SciOPP). The reaction of [$FeCl_2$(SciOPP)] with borate **18** in the presence of $MgBr_2$ yields the Fe(0) complex **82** (Scheme 3.2), in stark contrast to the bulk low oxidation state of iron species bearing dppe and dpbz ligands. Although accessible under the reaction conditions, the Fe(0) complex is too slow in catalysis to be an active species and thus is likely an off-cycle intermediate. Instead, Neidig proposed that phenylated Fe(II) species bearing the SciOPP ligand (Scheme 3.2) are the active species in catalysis. Again, the role of the metal halide salt was not elucidated.

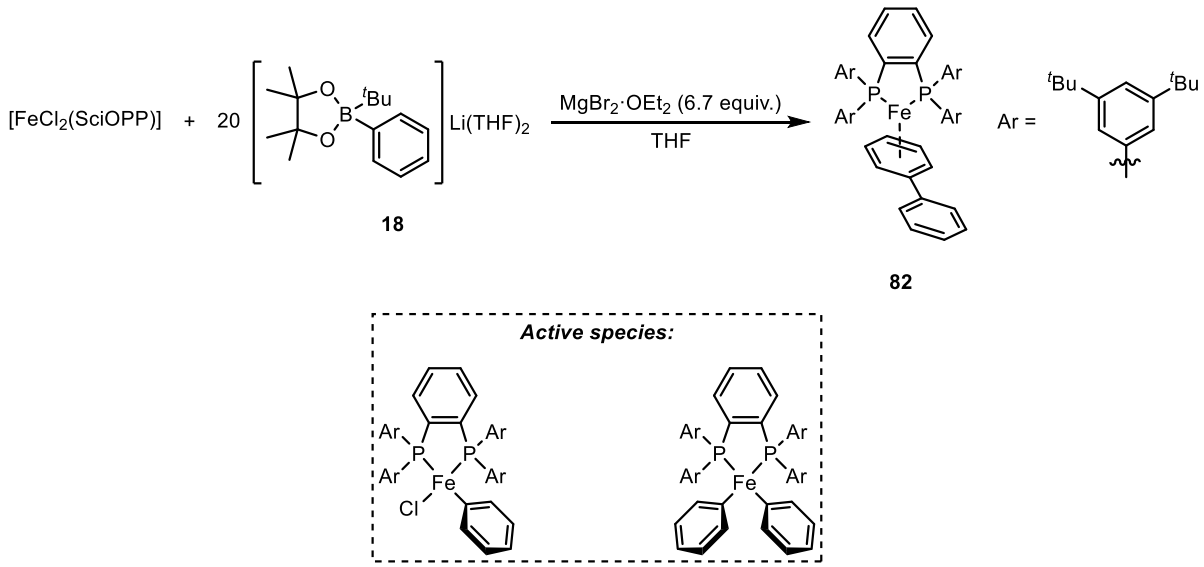

Scheme 3.2: Reduction to Fe(0) using **18** and proposed active species in Nakamura's Suzuki reaction.[69, 102]

Uncovering the specific role of additives such as $MgBr_2$, $ZnCl_2$ or $Zn(Ar)_2$ in iron-catalysed Suzuki reactions was attempted by Ingleson and co-workers by investigations into aryl transfer from borate species to iron complexes. Ingleson and co-workers found that alkoxide transfer to iron from aryl borate **83** was preferred over aryl transfer (Scheme 3.3),[140] showing how organometallic reagents such as ^{t}BuLi are required for boron-to-iron arene transmetallation.

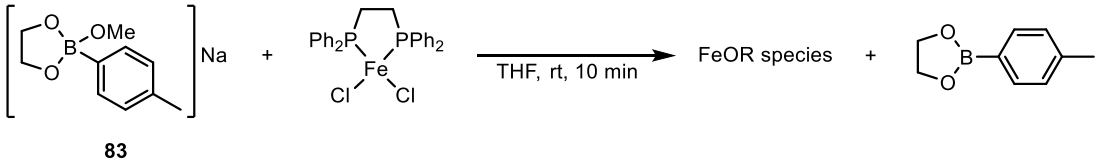

Scheme 3.3: Alkoxide transfer to iron from **83**.[140]

Subsequently, the design of trianionic ligands for aryl borates was undertaken to force aryl transfer from boron to iron.[141] However, when **84** (shown to be more nucleophilic than **18**) was reacted with $[FeCl_2(dppe)]$ + dppe, elevated temperatures were required to facilitate aryl transfer to iron (Scheme 3.4a). Conversely, using borate **18**, this could be achieved in minutes at ambient temperature (Scheme 3.4b).

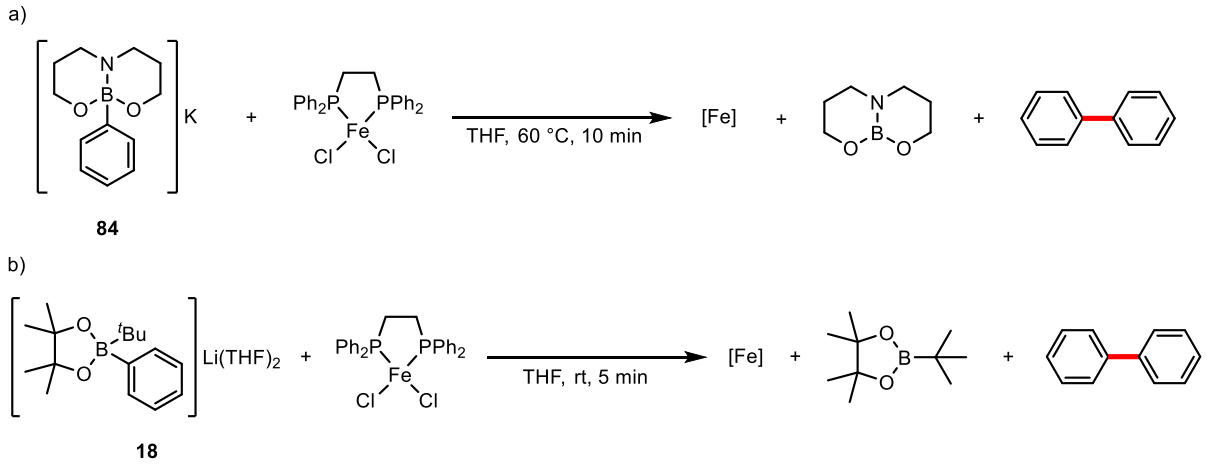

Scheme 3.4: Aryl transfer to iron from a) **18** and b) **84** without any additive.[141]

Having confirmed that that aryl transfer to iron could occur without any additives, **84** was used in the Suzuki arylation of cycloheptylbromide, with poor selectivity for the heterocoupled product observed when using zincate salts as additives. Having no additive or using $MgBr_2$ in the reaction failed to produce the homocoupled product under a range of conditions, in stark contrast to **18** which gives predominantly heterocoupled product with $MgBr_2$ as an additive. Furthermore, it was shown that with **84**, transmetallation to zinc could occur, but not to $MgBr_2$. The disparity between these results shows the intricacies of iron-catalysed Suzuki cross-couplings. The differences in product distribution are presumably due to the differences in rate between aryl transfer and the rest of the steps in the catalytic cycle which lead to heterocoupling. It is clear that the role of the additive in these reactions still needs to be defined.

In Chapter 2, the development of an iron-catalysed Suzuki biaryl cross-coupling reaction was described. Unlike most Suzuki-type reactions that have been reported with iron, bis-chelating phosphine ligands proved to be ineffective at promoting the reaction. Instead, the NHC-precursor IMes·HCl proved to be vital for high activity. The synthesis of well-defined iron complexes supported with NHC's have been of much interest over the last few years, with NHC complexes of Fe(0),[142-144] Fe(I)[145, 146] and Fe(II)[147-149] known, yet their role in iron-catalysed Suzuki reactions is yet to be fully explored. In this chapter, a variety of experiments are used to uncover the likely mechanistic manifold of the substrate-directed iron-catalysed Suzuki biaryl cross-coupling reaction developed in Chapter 2. The use of paramagnetic ^{1}H NMR, TEM, reaction poisoning, reaction screening and scope, kinetic analysis, kinetic isotope effects and computational chemistry allow for the proposition of a catalytic cycle and the role of both $MgBr_2$ and the *N*-pyrrole amide directing group.

3.2 Reduction of Iron with Activated Aryl Borate

As discussed previously, it has been shown that borate species can reduce iron complexes bearing phosphine ligands. To probe the lowest possible thermodynamically accessible oxidation state of iron under the Suzuki biaryl reaction conditions, a mixture of $FeCl_2$ and IMes was reduced with aryl borate **18** in the presence of $MgBr_2$. The formation of the known Fe(0) complex **85** was not detected upon analysis by ^{1}H NMR spectroscopy of the crude reaction mixture (Scheme 3.5). However, it worth noting that **85** can only be isolated in low yield from the reduction of $FeCl_2$ and IMes with KC_8, as reported by Ohki and Tatsumi.[144]

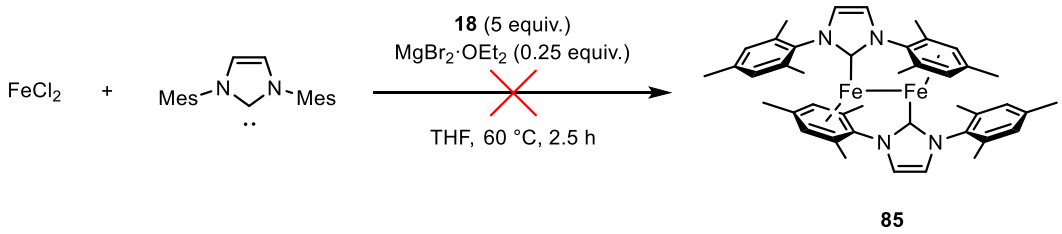

Scheme 3.5: Unobserved formation of **85** by the reduction of $FeCl_2$ with borate **18**.

Spiking the product mixture with 1,3-divinyltetramethyldisiloxane (dvtms) as a trapping reagent resulted in the formation of the Fe(0) complex **86**, indicated by the presence of the characteristic paramagnetic ^{1}H NMR signals at δ -10.7 ppm and δ -19.3 ppm.[143] Repeating the procedure with dvtms present during the addition of **18** led to the formation of **86** (Scheme 3.6), as characterised by ^{1}H NMR spectroscopy and X-ray crystallography (Figure 3.1b). This shows that borate **18** can reduce iron complexes bearing NHC ligands to low-valent species as observed with iron-phosphine compounds.[102] In the Suzuki cross-coupling reaction however, the NHC precursor IMes·HCl is used as a ligand instead of IMes. To see whether **18** is sufficiently basic to deprotonate the NHC precursor, the reduction was repeated using IMes·HCl, achieving the same result (Figure 3.1c). The presence of $MgBr_2$ was found not to be required for both the deprotonation and reduction processes (Figure 3.1d).

Complex **86** (synthesised according to Deng and co-workers)[143] proved to be a competent pre-catalyst in the Suzuki cross-coupling reaction, furnishing biaryl **21** in 73% yield. However, this does not mean that the active catalyst is an Fe(0) species, rather that Fe(0) complexes are certainly obtainable under the reaction conditions.

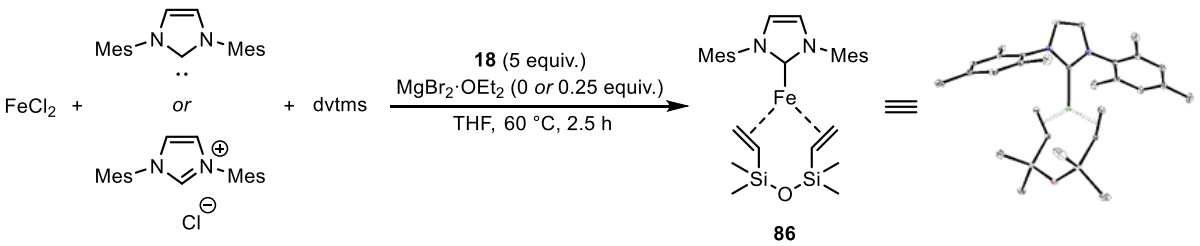

Scheme 3.6: Formation of Fe(0) complex **86** by reduction of $FeCl_2$ with **18**.

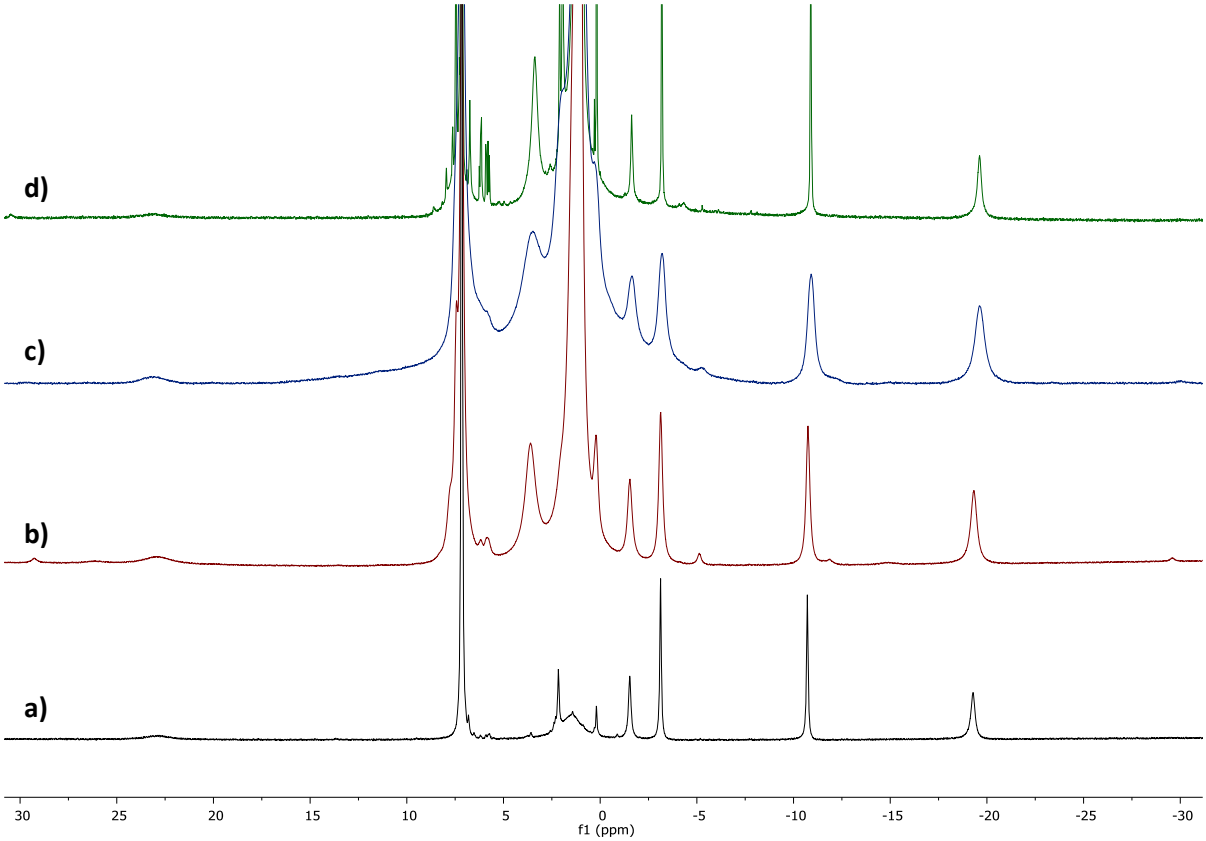

Figure 3.1: a) ^{1}H NMR spectrum of **86** synthesised according to Deng and co-workers[143] b) ^{1}H NMR spectrum of **86** synthesised by reduction of $FeCl_2$, IMes, dvtms and $MgBr_2{\cdot}OEt_2$ with **18**. c) ^{1}H NMR spectrum of **86** synthesised by reduction of $FeCl_2$, IMes·HCl, dvtms and $MgBr_2{\cdot}OEt_2$ with **18**. d) ^{1}H NMR spectrum of **86** synthesised by reduction of $FeCl_2$, IMes·HCl and dvtms with **18**.

In the absence of dvtms, it could be possible that reduction to Fe(0) causes any low coordinate intermediates formed to undergo aggregation to form iron nanoparticles. Bedford has previously shown that not only are iron nanoparticles formed in iron-catalysed Kumada and cross-coupling reactions, but that they are also catalytically competent pre-catalysts.[93] The presence of iron nanoparticles was also observed in iron-catalysed Suzuki cross-coupling reactions of alkyl, benzyl and allyl halides with borate **18**; however, in this case the formation of nanoparticles appears to only occur under ligand-free conditions.[97] Furthermore, it was found that the nature of the electrophile determines when the formation of nanoparticles occurs; in some cases before or after the cross-coupling reaction has completed. This draws to question whether such aggregates are indeed the actual catalytic species or are in fact catalyst resting states.

In the Suzuki biaryl reaction, the addition of borate **18** to the rest of the reaction components causes the reaction mixture to turn colourless, followed by a rapid darkening within 10 seconds. Removing an aliquot from the reaction mixture at 90 s (corresponding to ~ 30% yield (Section 3.4)) and drop-casting onto a 3 mm copper grid, it was shown by TEM analysis that the mixture contained a patchy network of deposited salts containing Fe, Mg, Br and Cl (Figure 3.2). EDX analysis and elemental mapping of

the salts showed that all elements present were homogeneously distributed throughout the structure, and that no electron-dense regions of Fe (or any other element) were present (Figure 3.3).

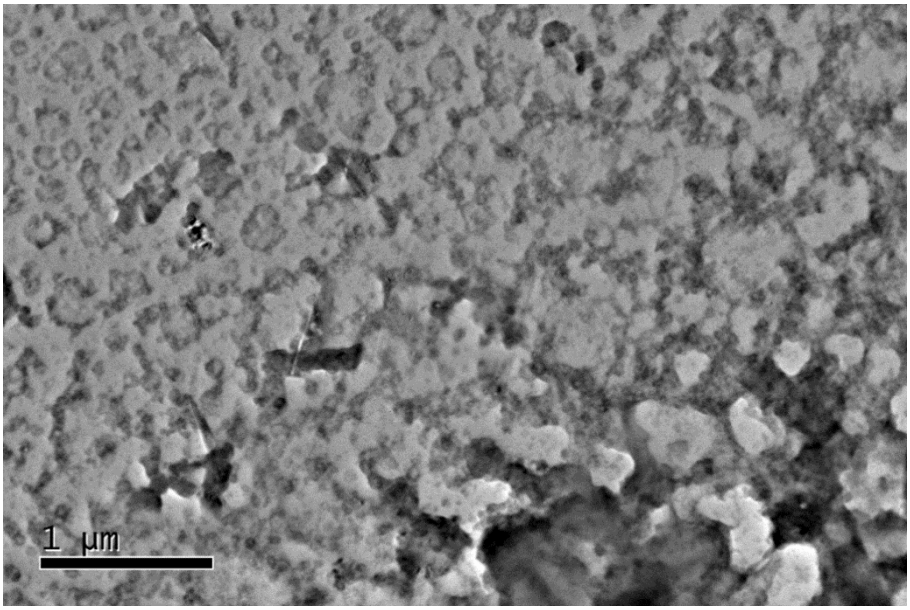

Figure 3.2: TEM image of aliquot withdrawn from the reaction mixture at 90 s. Samples prepared by the author, data collected and analysed by Dr Sean Davis.

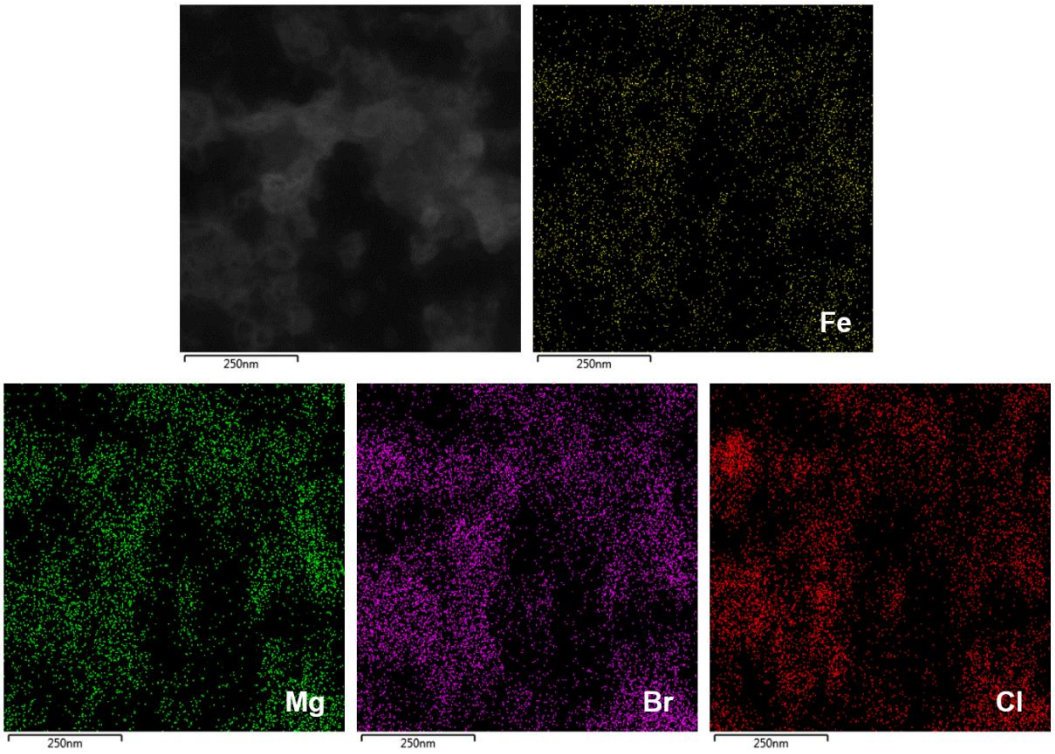

Figure 3.3: HAADF-STEM image of aliquot withdrawn from the reaction mixture at 90 s and corresponding elemental maps for Fe, Mg, Br and Cl. Samples prepared by the author, data collected and analysed by Dr Sean Davis.

To further probe whether iron nanoparticles are responsible for the catalytic activity, a Hg drop test was performed which had no effect on biaryl cross-coupling (Figure 3.4a). The Hg drop test originally introduced to probe whether reaction mixtures in platinum-group catalysis occur under a homogeneous or heterogeneous regime,[150] and the method has been exploited in selective poisoning tests in iron catalysis.[151] Any metal colloids present in the reaction mixture amalgamate and form alloys with Hg, and if these are the active catalytic species, production of **21** would be severely impeded. Figure 3.4b also shows the profile in the first 200 s of the mercury drop experiment, showing that the addition of mercury caused no change in rate.

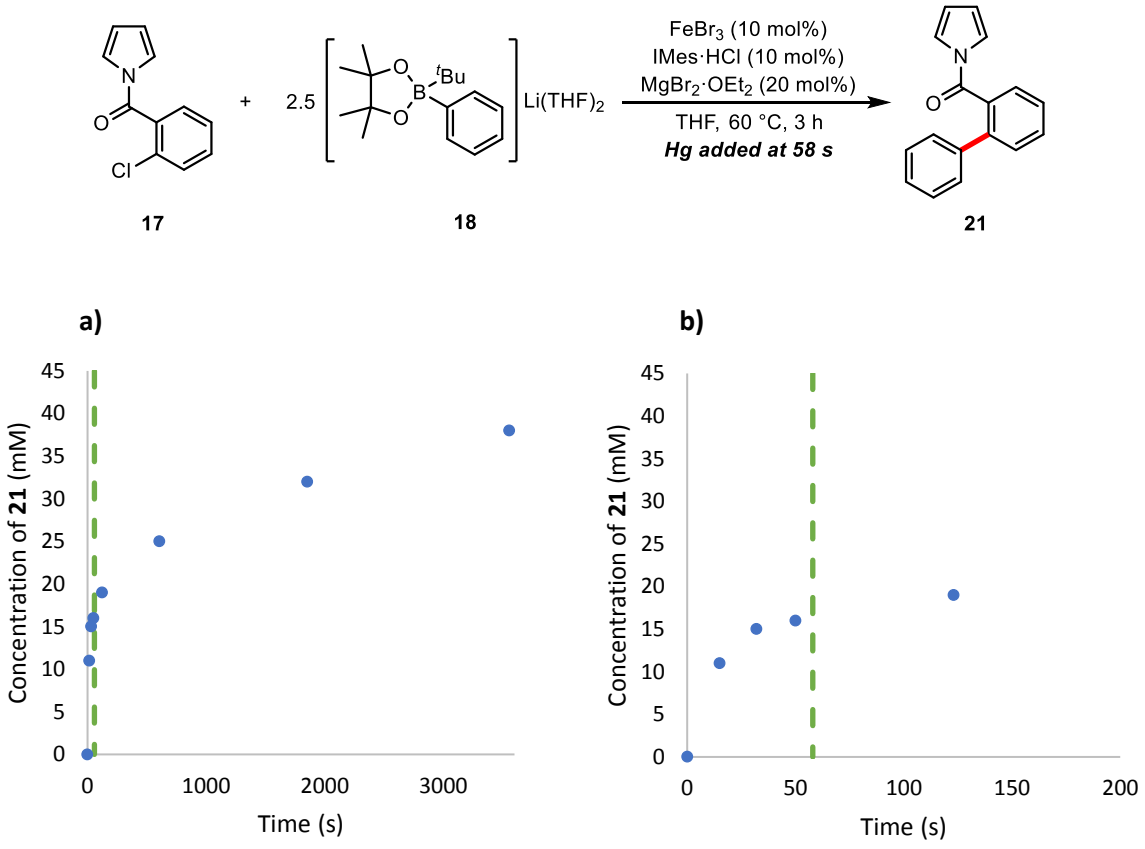

Figure 3.4: Effect of the addition of Hg at 58 s into the reaction mixture of the directed iron-catalysed Suzuki biaryl cross-coupling. a) Graph showing the production of **21** over the entire reaction period and b) within the first 200 s of the reaction.

Finally, using pre-formed iron nanoparticles supported with poly(ethylene) glycol (PEG) afforded **21** in only 9% yield, whilst using PEG as a ligand afforded **21** in 16% yield. With neither reaction giving better productivity than ligand-free conditions and the observation of a strong ligand dependence in the reaction, along with the evidence discussed above, it seems highly unlikely that iron nanoparticles are the active species in the cross-coupling and that homogeneous intermediates are responsible for the catalytic activity.

3.3 Role of $MgBr_2$

For the Suzuki biaryl reaction, a brief screen of alternative additives shows that a range of metal halide salts work to varying degrees of success (Table 3.1).

Table 3.1: Effect of alternative additives in the Suzuki biaryl cross-coupling.

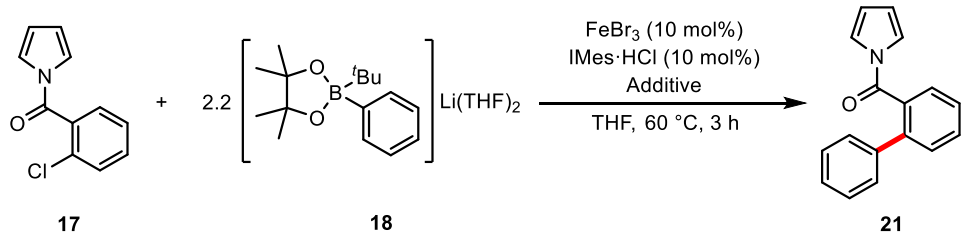

Entry	Additive (mol%)	Yield (%)[a]
1	LiBr (20)	5
2	LiBr (40)	0
3	NaBr (20)	40
4	NaBr (40)	36
5	KBr (20)	39
6	KBr (40)	35
7	$ZnBr_2$ (20)	23
8	$MgCl_2$ (20)	84
9	$AlBr_3$ (20)	76
10	$[NBu_4]Br$ (20)	0

Conditions: $FeBr_3$ (0.01 mmol), IMes·HCl (0.01 mmol), additive, **17** (0.1 mmol) and **18** (0.22 mmol) in THF for 3 h at 60 °C. [a] Determined by ^1H NMR analysis (1,3,5-trimethoxybenzene internal standard).

Whilst LiBr, NaBr, KBr and $ZnBr_2$ gave low to moderate activity (entries 1-7), $AlBr_3$ proved to be an effective additive, affording the cross-coupled product **21** in 76% yield (entry 9). Meanwhile, $MgCl_2$ (84%) offered essentially the same activity as $MgBr_2$. The lack of reactivity with $[NBu_4]Br$ here is perhaps likely due to the poor solubility of the salt under the reaction conditions. In the case of MgX_2 (X = Cl or Br), $ZnBr_2$ and $AlBr_3$, it is possible that formation of organo-main group metal intermediates occurs. These species could in turn transfer the phenyl group (liberated from the borate) to the iron centre in a transmetallation process. Indeed, magnesium, zinc and aluminium nucleophiles have been in exploited in iron-catalysed cross-coupling reactions before,[70] yet when $ZnPh_2/MgBr_2$ and

[Al(4-tol)$_4$]MgBr were used as nucleophiles, little or no cross-coupling was observed (Scheme 3.7).* Conversely, when phenylmagnesium bromide was used, the reaction gave **21** in 45% yield with significant biphenyl production (observed by GC-MS). However, in this case this is unsurprising since there already exists a precedent for iron-catalysed Kumada biaryl cross-coupling. Taken together, these results suggest that the role of the additive in the Suzuki biaryl reaction is not to facilitate transmetallation of the phenyl group to iron, but instead is more likely to be acting as a source of halide in the reaction.

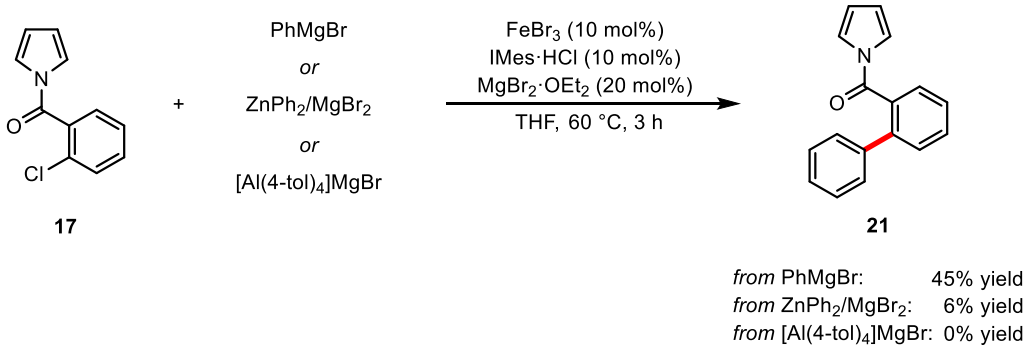

Scheme 3.7: Biaryl cross-coupling of **17** with alternative nucleophiles.

To gain a deeper understanding of the role of the additive, the effect on the production of **21** at different $MgBr_2$ loadings was investigated (Figure 3.5). In all cases a clear induction period of ~ 8 s was observed, coinciding with the reaction mixture turning colourless upon addition of **18** before darkening as production of **21** begins. The length of the induction period is independent of the concentration of the salt, showing that any process occurring in this induction phase does not require the additive.

* It is worth noting that the lack of activity is unlikely due to the excess of $MgBr_x$ present in these reactions since the optimised reaction furnishes **21** in 71% yield at a $MgBr_2$ loading of 80 mol%.

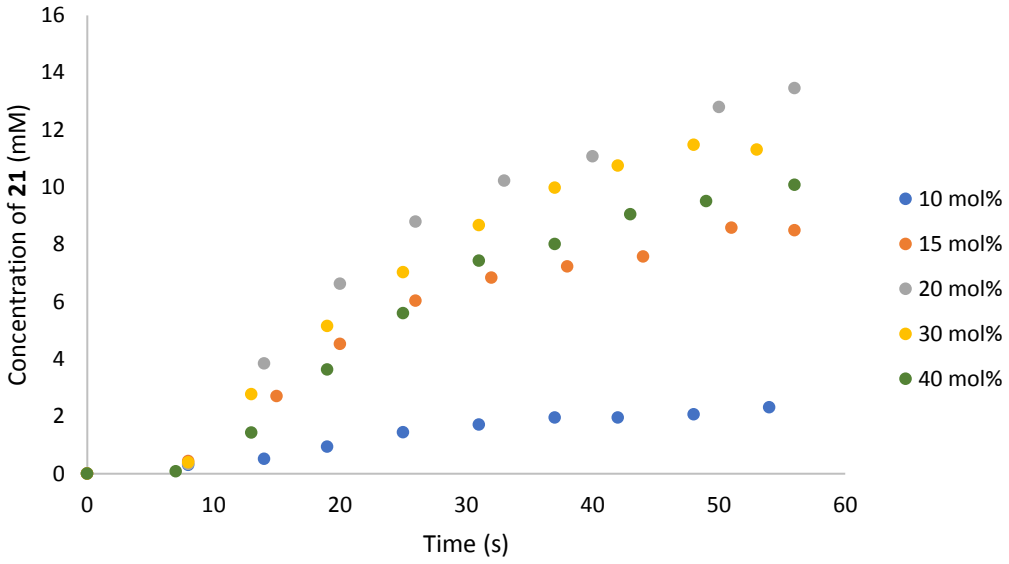

Figure 3.5: Formation of **21** over time at different concentrations of $MgBr_2$. Data collected by Mattia Manzotti.

The nature of this process was revealed by monitoring the formation of biphenyl during the course of the reaction at different concentrations of $MgBr_2$ (Figure 3.6). Here, it can be seen at all concentrations of $MgBr_2$ that by the end of the induction period most of the biphenyl made during the reaction has been produced.

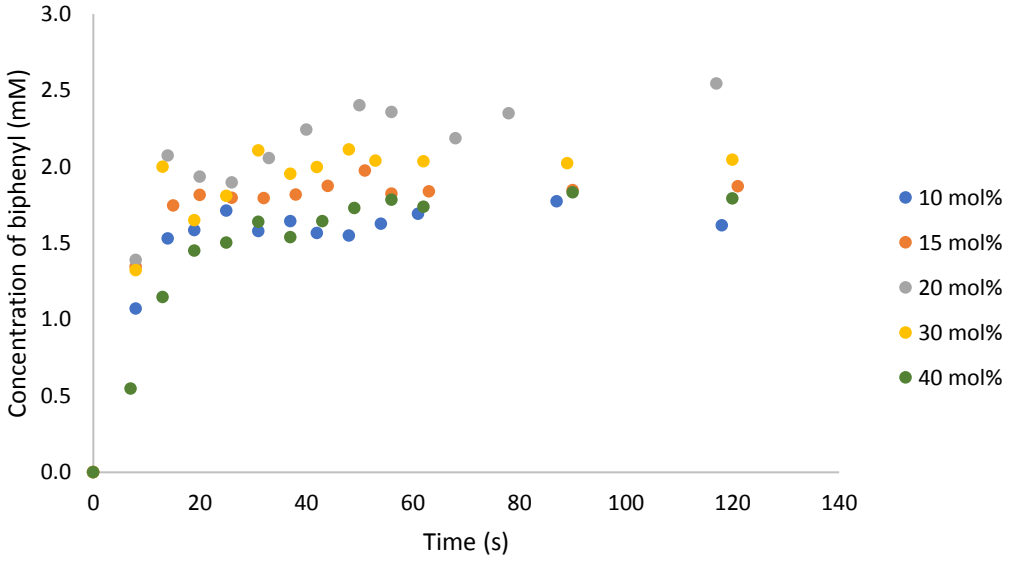

Figure 3.6: Formation of biphenyl over time at different concentrations of $MgBr_2$. Data collected by Mattia Manzotti.

The formation of biphenyl must occur by aryl transfer from **18** to the iron-centre. In this case, this appears to be independent of the concentration of the additive.[141] The subsequent elimination of biphenyl is a reductive process, liberating two electrons for every molecule of biphenyl formed, which in turn reduces the iron present in the reaction. Since the generation of **21** begins at a similar moment

where the production of biphenyl plateaus (~ 10 s), it is possible to determine the bulk oxidation state of the iron during the production of **21**. At the optimised $MgBr_2$ loading of 20 mol%, the plateau corresponds to the production of ~ 2.4 mM of biphenyl or an average of 0.75 electrons per iron centre; a reduction of Fe(III) to Fe(II). This suggests that, whilst Fe(0) can be accessed under the reaction conditions, it is more likely a thermodynamically accessible oxidation state, whereas the more kinetically relevant oxidation state of the iron could be two units higher. It should be noted that such a measurement only describes the average oxidation state of the system; it is still entirely possible for a variety of iron species with different oxidation states to exist in the reaction.

Examining the effect of $MgBr_2$ concentration on the initial rates of the reaction, a strong positive dependence is observed between a loading of 7.5 mol% and 20 mol% (Figure 3.7). Below this, no activity was observed, whilst above 20 mol% loading the initial rate begins to decrease. It is clear that, whilst essential for activity, increasing the loading of the additive eventually has an inhibitory effect, suggesting intervention at more than one point in the catalytic cycle.

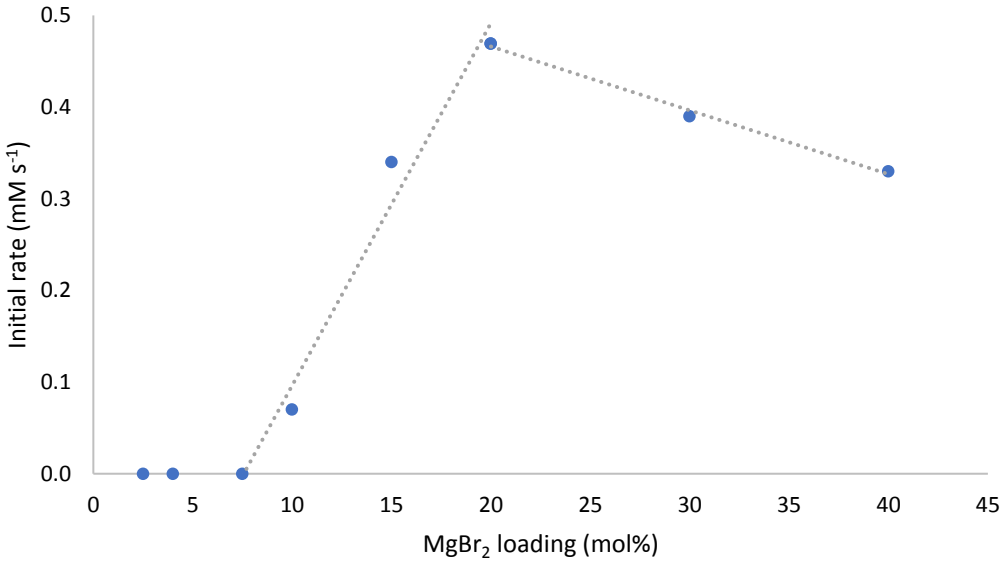

Figure 3.7: Initial rates at various $MgBr_2$ loadings. Data collected by Mattia Manzotti.

To see how the positive and negative influence of $MgBr_2$ loading affects the reaction mechanism, further kinetic analysis was performed to determine the order in [Fe/IMes], [**17**] and [**18**] at 15 mol% and 25 mol% $MgBr_2$; regions where the positive and inhibitory effects, respectively, are very pronounced.

Figure 3.8 shows that for the catalyst mixture [Fe/IMes] at 15 mol% $MgBr_2$ loading, there is approximately a 0.8 order dependence up to 10 mol% [Fe/IMes], beyond which the rate slows. At 25% mol% $MgBr_2$ loading, the order is approximately 0.7. The positive, almost 1st order dependence on Fe/IMes concentration suggests that a single Fe/IMes species is operative in the rate-determining step.

The non-integer order suggests that the role of the catalyst in the rate-determining step is complicated; possibly an equilibrium is occurring.

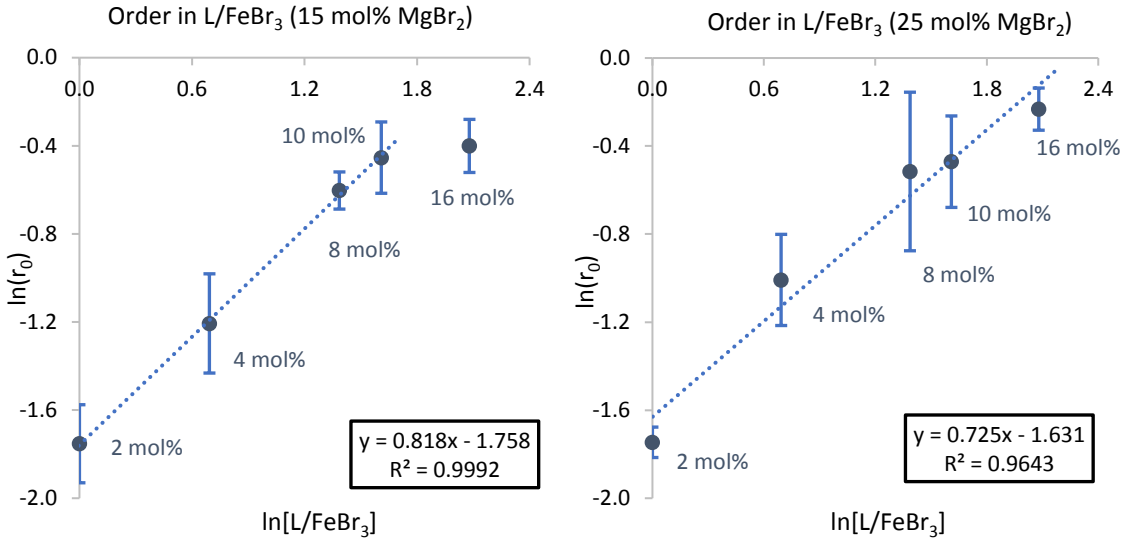

Figure 3.8: Order in [Fe/IMes] at 15 mol% (left) and 25 mol% (right) $MgBr_2$ loading. Data collected by Mattia Manzotti.

Figure 3.9 shows that for the electrophile **17** at 15 mol% $MgBr_2$ loading, the order is 0.5, increasing to approximately 0.6 at 25 mol% $MgBr_2$ loading. Again, the positive fractional order suggests that **17** is involved in the rate determining step and that an equilibrium may be occurring.

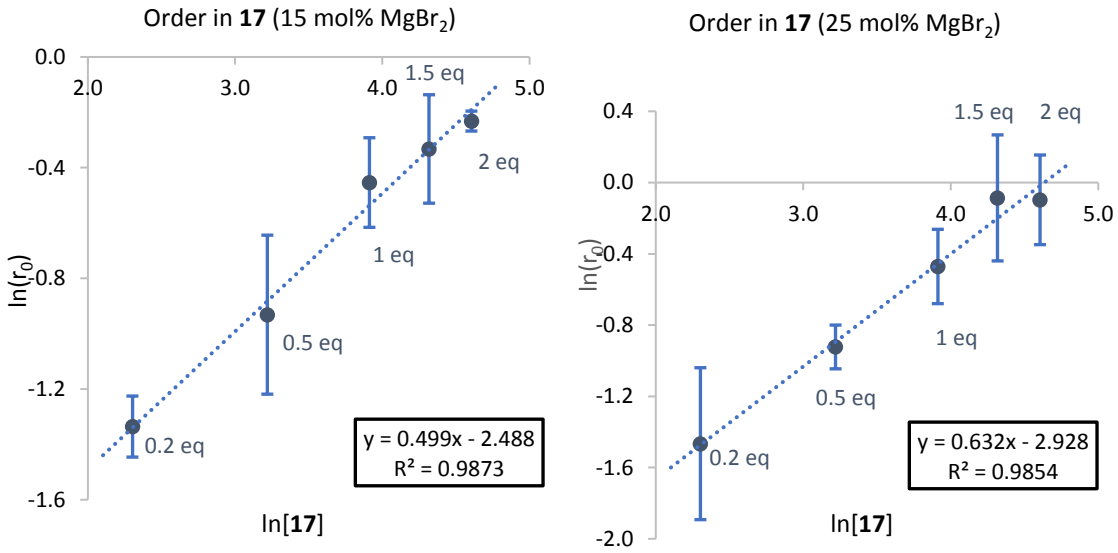

Figure 3.9: Order in **17** at 15 mol% (left) and 25 mol% (right) $MgBr_2$ loading. Data collected by Mattia Manzotti.

Finally, Figure 3.10 shows that the concentration of borate **18** is 1st order at 15 mol% $MgBr_2$ loading up to 2.5 equivalents, after which the rate starts to slow. A similar result is achieved when measuring the initial rates at a 25 mol% $MgBr_2$ loading, where the rate also plateaus at 2.5 equivalents of **18**.

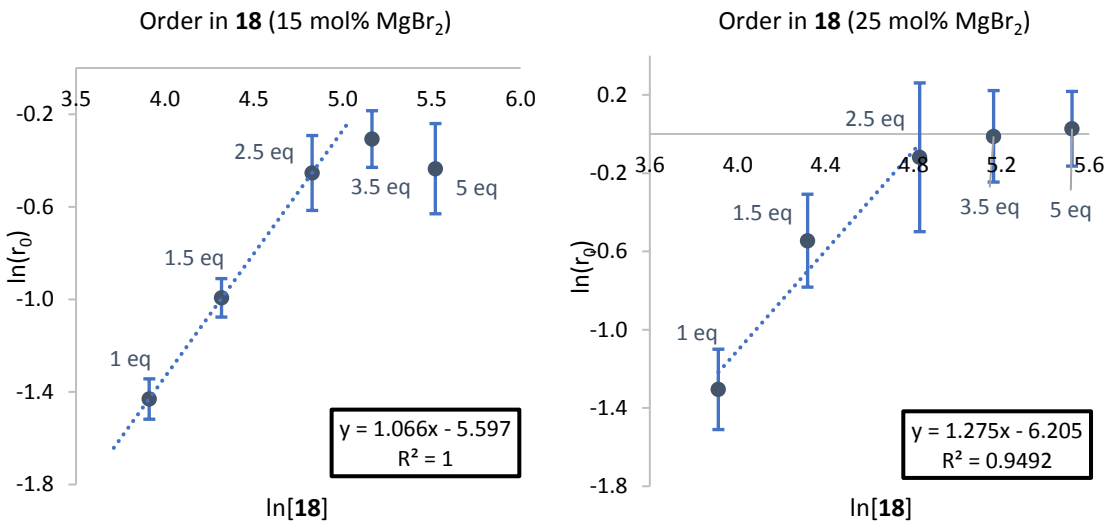

Figure 3.10: Order in **18** at 15 mol% (left) and 25 mol% (right) $MgBr_2$ loading. Data collected by Mattia Manzotti.

Taken together, analysis of initial rates show that all the reaction components at least take part in, or operate before, the rate-determining step of the reaction at both loadings of $MgBr_2$.

3.4 Role of the Directing Group: π-Coordination

In Chapter 2, a screen of alternative amide-based directing groups showed that aromaticity in the directing group was necessary for the reaction to proceed. The contrast between the reactivity of the *N*-pyrrole amide electrophile **17** (82% yield of biaryl cross-coupling) and *N*-pyrrolidine amide **31** (trace) makes this most unambiguous. It is therefore likely that π-coordination of the pyrrole amide group helps to tether the catalyst to allow aryl-chloride bond activation. Indeed, π-coordination of pyrroles to iron has been known for quite some time. Shortly after the first synthesis of ferrocene, reports of iron complexes bearing anionic pyrrole ligands, bonded by π-coordination, were reported.[152, 153] Since then, numerous structurally characterised η^5-pyrrole complexes have been disclosed, with a particularly noteworthy example reported recently by Walter and co-workers, who showed that even two pyrrole anions each bearing three sterically demanding ^{t}Bu groups can π-coordinate to a single Fe(II) atom.[154] There have also been reports of structurally characterised η^5-iron complexes of *N*-alkyl pyrroles,[155, 156] and, most encouragingly, η^5-iron complexes with *N*-acyl pyrrole ligands have been reported,[157, 158] although these have not been structurally characterised. Due to the literature precedence, it was envisioned that this process is likely taking place in the described reaction, and efforts were turned to finding experimental evidence in support of this.

Jacobi von Wangelin used a secondary kinetic isotope effect (KIE) experiment to show how π-coordination from a styrene directing group to an iron-centre was responsible for the biaryl cross-coupling of chlorostyrenes with aryl Grignard reagents (Scheme 3.8).[59] It was proposed that an equivalent secondary KIE experiment conducted between **17** and its deuterated analogue **17-d$_4$** could shed light on the role of the *N*-pyrrole amide.

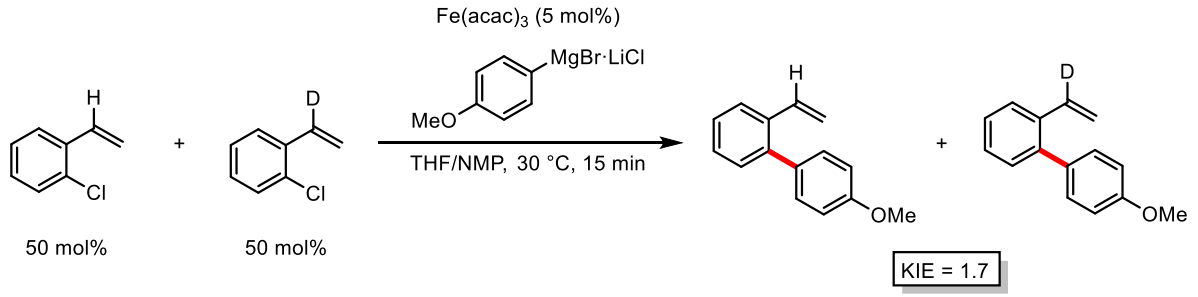

Scheme 3.8: Observed secondary KIE in Jacobi von Wangelin's iron-catalysed Kumada biaryl cross-coupling of chlorostyrenes.

There are two possible methods to measure the difference in rate in the Suzuki reaction of **17** and **17-d$_4$**. The first method would be to independently measure the rates of the two parallel Suzuki cross-coupling reactions of **17** and **17-d$_4$** and a KIE would be determined as the ratio of the two rates. The second method is a competitive reaction between an equimolar ratio of **17** and **17-d$_4$**. The initial rates of the Suzuki reaction are very fast and since the values for secondary KIEs are small, small errors in measurement could lead to erroneous results. Consequently, the second experiment was chosen, using

4-tolyl borate **45** as a nucleophile since the CH_3 protons on the tolyl group could be easily used for integration in the ^1H NMR spectrum. Quenching the reaction when the yield of **21**/**21-d$_4$** is ~ 30% prevents both substrates undergoing full conversion. The results from the experiment are summarised in Figure 3.11.

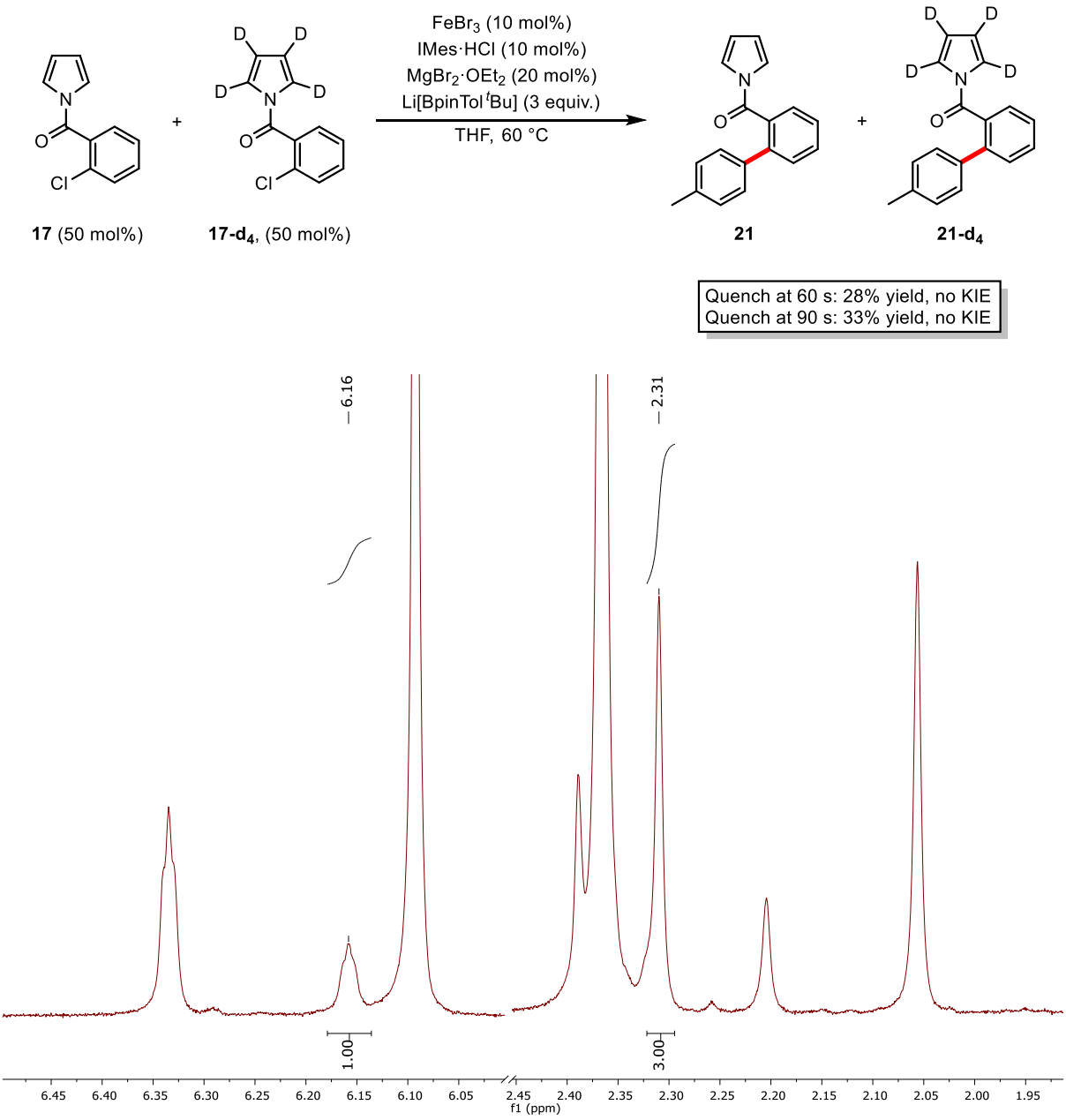

Figure 3.11: ^1H NMR spectrum of the crude Suzuki reaction between **17**/**17-d$_4$** and **45**, quenched at 60 s.

The Suzuki reaction of **17**/**17-d$_4$** with aryl borate **45** quenched at 60 s afforded **21**/**21-d$_4$** in 28% yield (determined by ^1H NMR). Integration of the CH_3 (tolyl) peak at δ 2.31 ppm and the 3,4-CH (pyrrole amide) peak at δ 6.16 ppm revealed that **17** and **17-d$_4$** had reacted at exactly the same rate (no KIE). The same result was obtained when the reaction was repeated and quenched at 90 s, affording **21**/**21-d$_4$** in 33% spectroscopic yield (no KIE). This shows that, under the optimised reaction conditions,

coordination of the iron-centre to the pyrrole amide is not the rate (or product) determining step of the reaction. In order to observe a secondary KIE, the experiment was repeated with a $MgBr_2$ loading of 15 mol%, where a strong positive influence of $MgBr_2$ was observed (Figure 3.12).

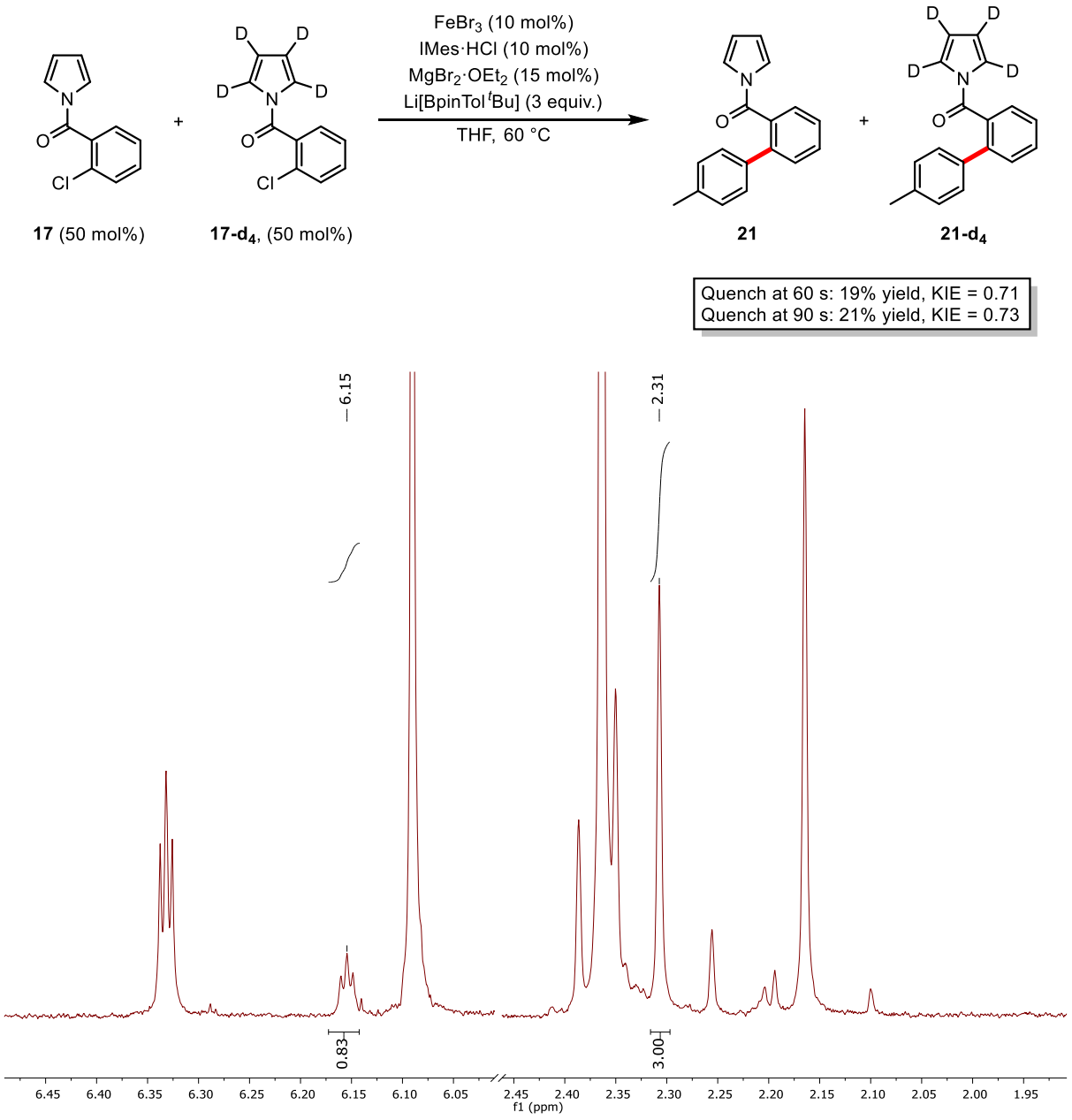

Figure 3.12: ^{1}H NMR spectrum of the crude Suzuki reaction between **17**/**17-d$_4$** and **45** (15 mol% $MgBr_2$ loading), quenched at 60 s.

Repeating the reaction at 15 mol% $MgBr_2$ loading revealed that **17** and **17-d$_4$** had reacted at different rates. Quenching at 60 s, the ratio of **21** to **21-d$_4$** was 0.83:1.17, corresponding to a KIE of 0.71. A similar result was obtained when the reaction was quenched at 90 s, affording a KIE of 0.73. This *inverse* secondary KIE shows that at a 15 mol% $MgBr_2$ loading, the rate (or product) determining step, or a process in pre-equilibrium with the rate (or product) determining step, involves a change in the hybridisation of the sp^2 pyrrole carbons, developing more p character in the transition state.[159] This is

consistent with π-coordination of pyrrole, directing the iron-catalyst before aryl chloride activation takes place.

3.5 Attempted Isolation of an Fe(0) Pyrrole Amide Complex

Encouraged by the observation of an inverse secondary KIE, the isolation of an Fe(0) pyrrole amide complex was attempted to help determine catalyst speciation. Having shown that Fe(0) was easily accessible by the formation of complex **86** (Section 3.2), a mixture of $FeCl_2$, IMes and *N*-pyrrole benzamide **27** was reacted with either KC_8, Na/Hg amalgam or borate **18** (Figure 3.13).

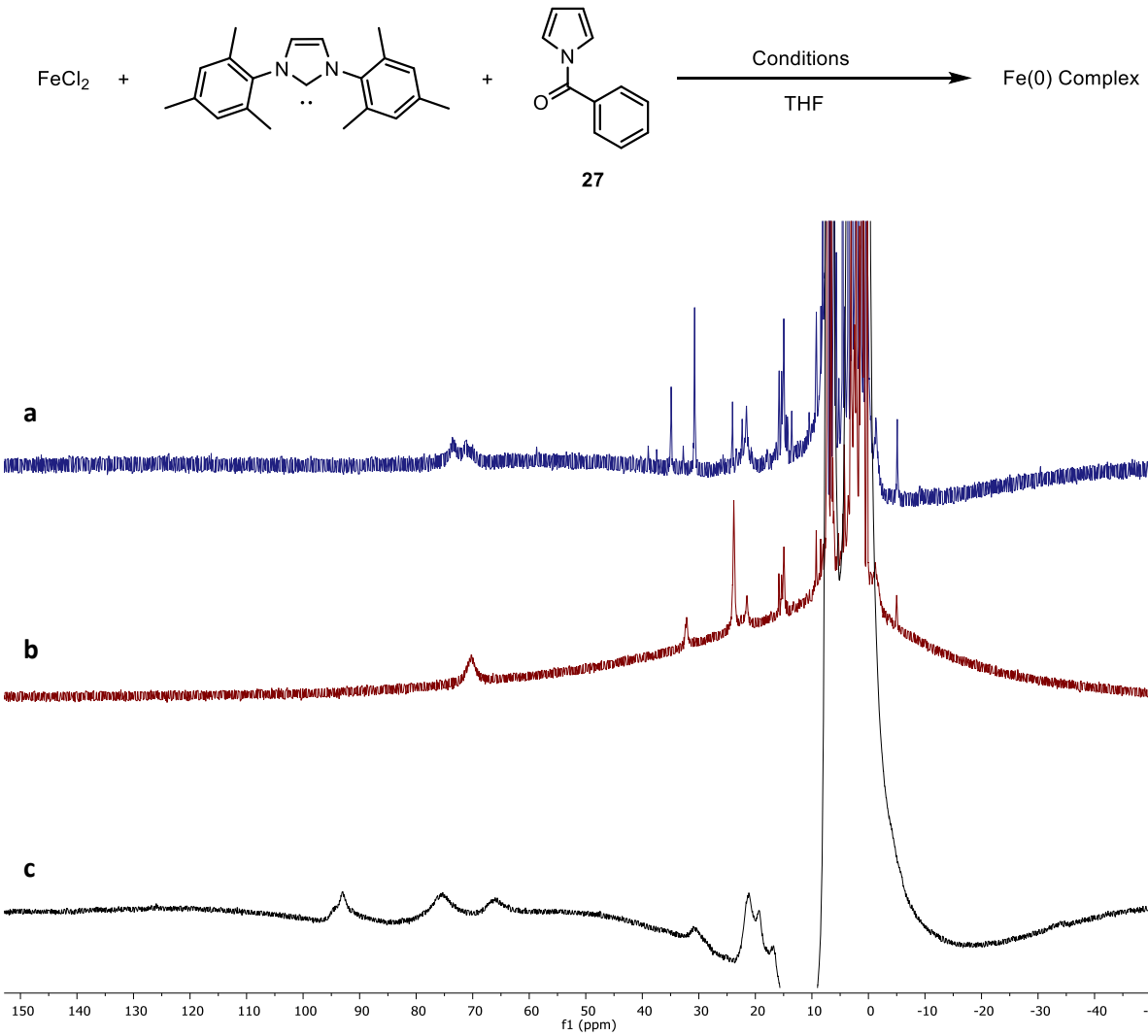

Figure 3.13: ^1H NMR spectrum of the reduction of $FeCl_2$ in the presence of IMes and **27** with a) KC_8, b) Na/Hg amalgam and c) borate **18**.

Addition of KC_8 to a THF solution of $FeCl_2$ and IMes in the presence of **27** at -40 °C afforded a colour change from dark brown to deep orange. After allowing the reaction to gradually warm to room temperature and stirring overnight, an aliquot was removed and the solvent removed *in vacuo*. The ^1H NMR in C_6D_6 revealed the presence several paramagnetically shifted peaks (Figure 3.13a), although no definitive assignment could be made at this stage. The number of paramagnetically shifted peaks and integrations suggests that more than one species had been produced in the reaction. Changing the reducing agent to Na/Hg amalgam generated a deep-red solution, from which a dark-brown solid was

isolated. The ^{1}H NMR of this compound (Figure 3.13b) shares similar paramagnetically shifted peaks to those observed in the reaction using KC_8 as a reductant, particularly at δ 70.5, 32.2, 23.8, 21.6, 15.8, 15.4, 15.0, -1.2 and -5.0 ppm. However, integration of the peaks and the number of environments suggests that more than one species had again been formed. Repeating the reduction using borate **18** and heating the mixture to 60 °C for 1.5 h gave a deep-red solution. Removal of an aliquot and recording the crude ^{1}H NMR in C_6D_6 revealed paramagnetically shifted peaks at δ 195.7, 93.0, 75.6, 65.4, 30.9, 21.4, 19.5 and 16.7 ppm (Figure 3.13c). Almost none of the paramagnetic peaks had similar shifts compared to the compounds produced in the previous reactions. Again, integration of the peaks suggests that more than one species had been produced in the reaction. Unfortunately, no crystals from any of the reactions suitable for single crystal X-ray diffraction could be grown, precluding further characterisation.

To circumvent the problem of multiple species being formed from the reduction of iron in the presence of an *N*-pyrrole amide, and to simplify the complicated spectra obtained, complex **86** was heated in the presence of **17-d$_4$** and the reaction monitored by ^{2}H NMR (Scheme 3.9). Unfortunately, no change in the ^{2}H NMR was observed, suggesting no reaction had taken place.

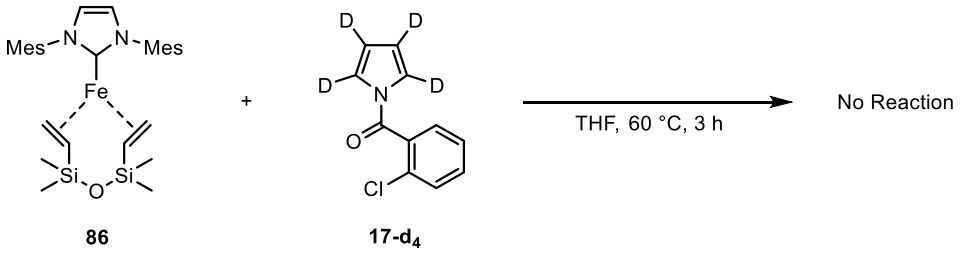

Scheme 3.9: Attempted reaction of **86** and **17-d$_4$**, monitored by ^{2}H NMR spectroscopy.

Repeating the reaction in the presence of 2 equiv. of $MgBr_2$ afforded the same result, with no change in the ^{2}H NMR spectrum observed after stirring for 3 h at 60 °C. In light of these results, the isolation of an Fe(0) pyrrole amide complex was not pursued further.

3.6 Role of the Directing Group: Amide-Coordination

The observation of a secondary KIE provides strong evidence for π-coordination of the pyrrole moiety tethering the iron catalyst to the substrate before arylation occurs. However, it is not possible to entirely rule out the possibility that coordination through the oxygen of the amide function is behind the regiocontrol observed in the reaction. The requirement of the amide group was demonstrated by subjecting **87** to the reaction conditions, affording biaryl **88** in 5% yield (Scheme 3.10).

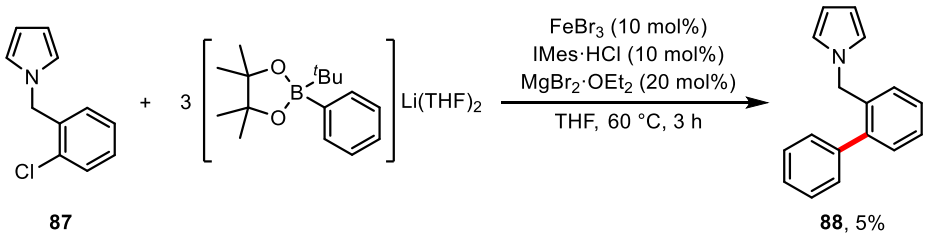

Scheme 3.10: Reaction of **87** under the optimised Suzuki reaction conditions. Spectroscopic yield determined by ^{1}H NMR spectroscopy using 1,3,5-trimethoxybenzene as an internal standard. **88** was also synthesised independently to confirm its presence in the catalytic reaction mixture.

The reactivity of other directing groups militates against the possibility that oxygen coordination alone is responsible for enabling the catalysis. Comparing the reactivity of substrates **31**, **32** and **17** in the reaction, it appears that productivity increases with increased C=O bond strength (Chart 3.1). If the directing group effect was entirely due to oxygen coordination, one would expect pyrrolidine substrate **31** to be the most active since the oxygen has the highest donor ability to the iron-centre.

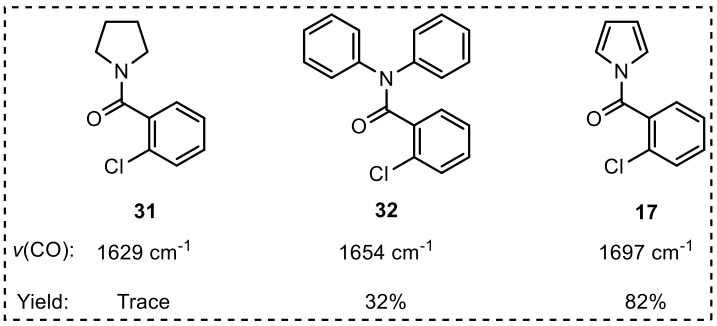

Chart 3.1: Substrates **31**, **32** and **17** with their productivity ranked against the ν(CO) stretch (measured using IR spectroscopy).

Furthermore, subjecting substrate **89** to the reaction conditions gave the mono-arylated product **90** in 72% yield with only trace amounts of diarylated **91** observed by GC-MS (Scheme 3.11). Importantly, arylation at only the C7 position was not observed, despite the fact that metal-catalysed C-H functionalisation using amide directing groups (*via* oxygen coordination) is well known.[160] These data, taken together with the secondary KIE, strongly suggest that oxygen coordination alone is not responsible for the observed directing group effect.

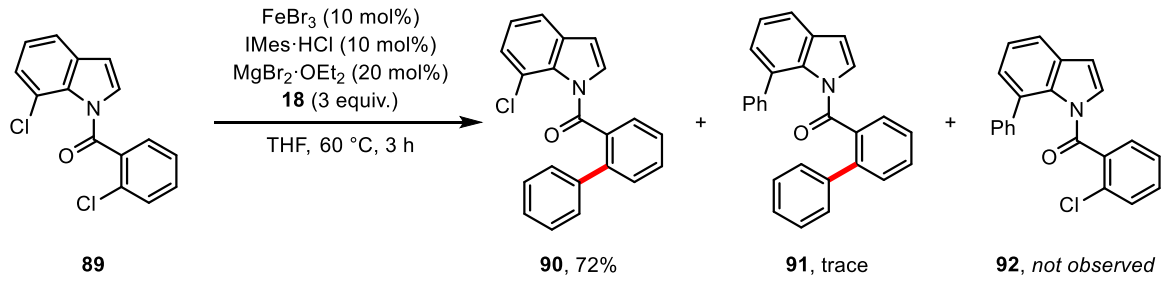

Scheme 3.11: Competition reaction of substrate **89**.

Another possible reason for the requirement of an amide group could be that the formation of an aminoketyl radical may electronically activate the substrate to allow aryl chloride bond scission. Formation of an aminoketyl radical could occur through a single electron transfer (SET) process where an electron is transferred into the π* orbital of the amide function, possibly following coordination of the iron-centre to the pyrrole and amide (Scheme 3.12a). Indeed, the use of the radical trap 2,2,6,6-tetramethyl-1-piperidinyloxy (TEMPO) completely shut down productivity, whereas styrene (acting as a potential arylborate radical scavenger)[161] had very little effect on the reaction outcome, allowing **21** to be furnished in 73% yield (Scheme 3.12b). These radical trapping reactions strongly suggest that a radical mechanism is involved in the reaction, most likely due to SET from iron. To probe the immediacy of aminoketyl radicals in the mechanism, a DFT study of compounds **17**, **31** and **32** was carried out.

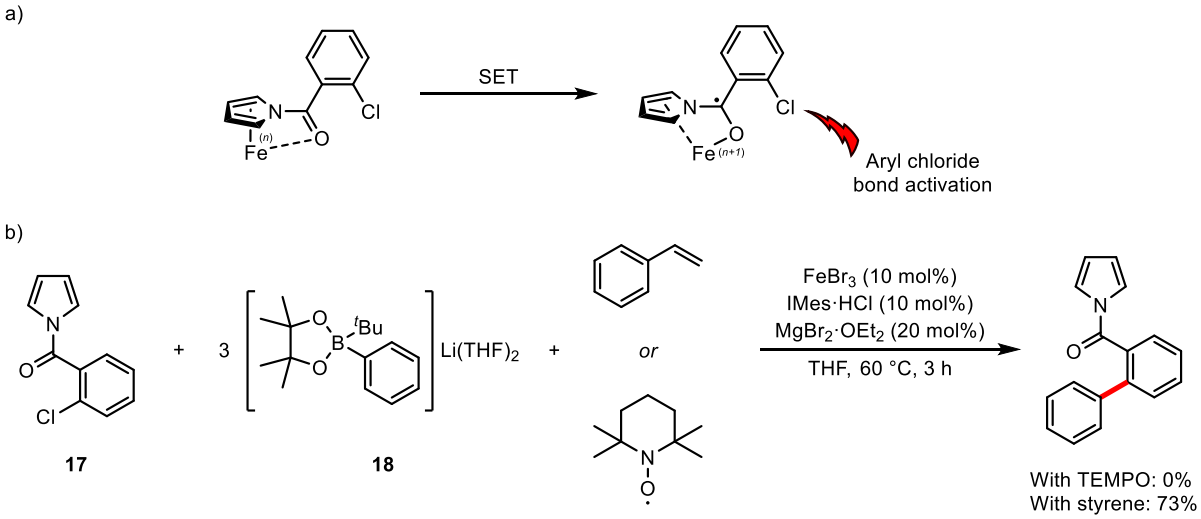

Scheme 3.12: a) SET from an iron species to generate an aminoketyl radical and b) the effect of adding radical trapping agents TEMPO and styrene to the reaction mixture.

Computationally probing the propensity of radical formation requires one to know:

1) The energy released or spent upon the addition of an electron to the neutral molecule to form a negative ion (the electron affinity).
2) The stability of the subsequent negatively charged radical produced.

This can be determined by calculating the electron affinities and electron dissociation energies of the neutral amides. In particular, the vertical electron affinity (VEA), adiabatic electron affinity (AEA) and vertical detachment energy (VDE). Invoking the Franck-Condon principle (the approximation that an electronic transition is most likely to occur without changes in the positions of the nuclei), the VEA is a measure of single-electron reduction prior to molecular rearrangement, whereas the AEA captures the energy of electron attachment followed by relaxation to the optimised radical geometry. The VDE is a measure of the stability of the resultant radical anion with respect to electron loss without molecular rearrangement.

To calculate VEA, AEA and VDE, the following equations are used:

VEA = E(optimised neutral amide) – E(radical anion at optimised geometry of neutral amide)

AEA = E(optimised neutral amide) – E(optimised radical anion)

VDE = E(neutral amide at geometry of optimised radical anion) – E(optimised radical anion).

Thus, geometry optimisation and electronic energy of the neutral amides and radical amide anions were calculated at the B3LYP level of theory using the 6-311G** basis set; a relatively large basis set lacking diffuse functions. Diffuse functions are usually required for calculations with anions as they include the next low lying vacant orbital in the calculation. However, with amides it has been found that it is possible (both experimentally and computationally) to get negative electron affinities.[162, 163] Computationally, it has been found that, when using a diffuse function for molecules with negative electron affinities, the excess electron tends to localise outside of the molecular framework. Using a large basis set without diffuse functions has been shown to confine the excess electron to the molecular framework and has shown to afford better agreement with experimentally calculated values.[162-164]

Table 3.2 summarises the values of VEA, AEA and VDE calculated for amides **17**, **31** and **32**. In the gas phase, the order of increasing electron affinity (i.e. the propensity for the substrate to accept an electron to become a radical anion) increases in the same order of productivity of the substrate in the catalysis. This is line with formation of an aminoketyl radical being in part responsible for the observed activity. The diphenyl amide **32** was calculated to form the most stable radical anion. The relative ordering of VEA, AEA and VDE was unperturbed when the energies were calculated in THF solvent using the standard implementation of the polarizable continuum model (PCM). Single point calculations on the optimised structures with THF solvation gave positive values for each VEA, AEA and VDE. This is consistent with the unstable state (i.e. negative electron affinity of the formed radical) becoming stable in solvent. The positive energy values in THF solvent allows for the use of diffuse functions to be used, and a comparison at this level of theory for **17** is also given in Table 3.2.

Table 3.2: Calculated electron affinites and electron dissociation energies for **17**, **31** and **32**.[a]

		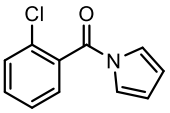 **17**	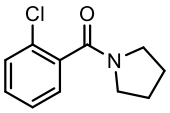 **31**	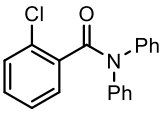 **32**
VEA (eV)	gas phase	-0.11	-0.91	-0.18
AEA (eV)	gas phase	0.52	-0.22	0.44
VDE (eV)	gas phase	0.95	0.48	1.16
VEA (eV)	THF solution[b]	2.39 (1.56)[c]	0.72	1.16
AEA (eV)	THF solution[b]	1.99 (2.16)[c]	1.29	1.80
VDE (eV)	THF solution[b]	1.60 (2.60)[c]	2.03	2.53

[a] Gas phase calculations at B3LYP/6-311G**. [b] Single point calculation using PCM on B3LYP/6-311G** optimised structures. [c] B3LYP-D3/6-311++G** optimised structure, with PCM included in optimisation (values in parentheses). DFT calculations carried out by Prof. Robin Bedford.

To calculate the singly occupied molecular orbitals (SOMO) of radicals **[17]**$^{\bullet-}$, **[31]**$^{\bullet-}$ and **[32]**$^{\bullet-}$, the geometries of the radicals were optimised in the gas phase with uB3LYP level of theory using the 6-311G** basis set. The population was calculated at roB3LYP/6-311G** with an isovalue of 0.05 (electron/bohr^3)^{½}. The SOMOs of radicals **[17]**$^{\bullet-}$, **[31]**$^{\bullet-}$ and **[32]**$^{\bullet-}$ are shown in Figure 3.14 and are all very similar, showing that the unpaired electron is delocalised across both the ketyl function and the in-plane aryl chloride, with essentially no contribution seen from the out-of-plane NR_2 group. Calculating the SOMO of **[17]**$^{\bullet-}$ in THF solvation (geometry optimised with THF solvation at uB3LYP-D3/6-311++G**, population calculated with THF solvation at roB3LYP-D3/6-311++G** with an isovalue of 0.05 (electron/bohr^3)^{½}) had very little effect on the SOMO, also showing the extra electron to be associated with the π-system of the aryl ketone (Figure 3.14). The generation of the aminoketyl radical could therefore be responsible for the activation of the aryl chloride bond.

a) b) c) d)

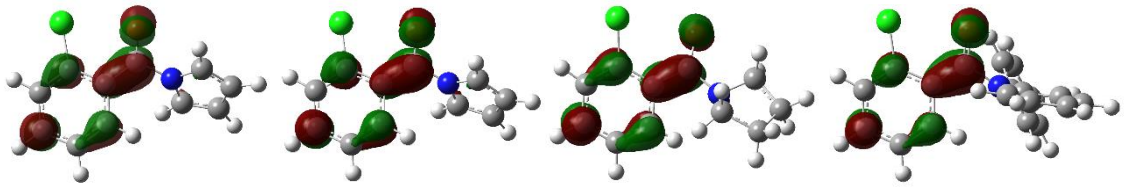

Figure 3.14: SOMOs for a) **17**, b) **17** (THF solvation), c) **31**, and d) **32** respectively. DFT calculations carried out by Professor Robin Bedford.

With a method to chart the relative reactivity of the halobenzamide substrates in hand, a model substrate was designed to test whether the generation of an aminoketyl radical alone is responsible for the observed reactivity. Using the calculated trends it was possible to show that for phthalimide substrate **93**, the propensity to form an aminoketyl radical was even greater than for substrate **17**, with the SOMO also showing the electron to be delocalised with the π-system of the aryl ketone (Table 3.3).

Table 3.3: Calculated electron affinites and electron dissociation energies for **[93]**$^{\bullet-}$.

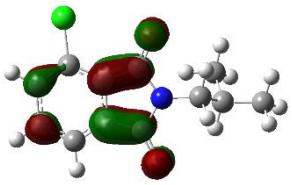

VEA (eV) (gas phase)	AEA (eV) (gas phase)	VDE (eV) (gas phase)	VEA (eV) (THF solvation)[b]	AEA (eV) (THF solvation)[b]	VDE (eV) (THF solvation)[b]
0.83	1.11	1.39	2.25	2.51	2.77

[a] Gas phase calculations at B3LYP/6-311G**. [b] Single point calculation using PCM on B3LYP/6-311G** optimised structures. DFT calculations carried out by Prof. Robin Bedford.

Phthalimide-based substrate **93** should undergo a significantly more facile single-electron reduction to form an aminoketyl than substrate **17**. The presence of a carbonyl group *ortho* to the C-Cl bond also means that the iron catalyst can be directed to arylate the substrate, but most importantly, the substrate lacks a suitable π-coordinating motif. Synthesis of phthalimide **93** was carried out by the condensation reaction of 3-chlorophthalic anhydride with isobutylamine in toluene at reflux temperature (Scheme 3.13a). When phthalimide **93** was subjected to the Suzuki reaction conditions, the reaction appeared strikingly different, with a deep blue colouration appearing a few seconds after the addition of borate **18**. None of the desired cross-coupled product was observed, with complete consumption of the electrophile and 26% of hydrodehalogenated product **95** obtained (Scheme 3.13b).

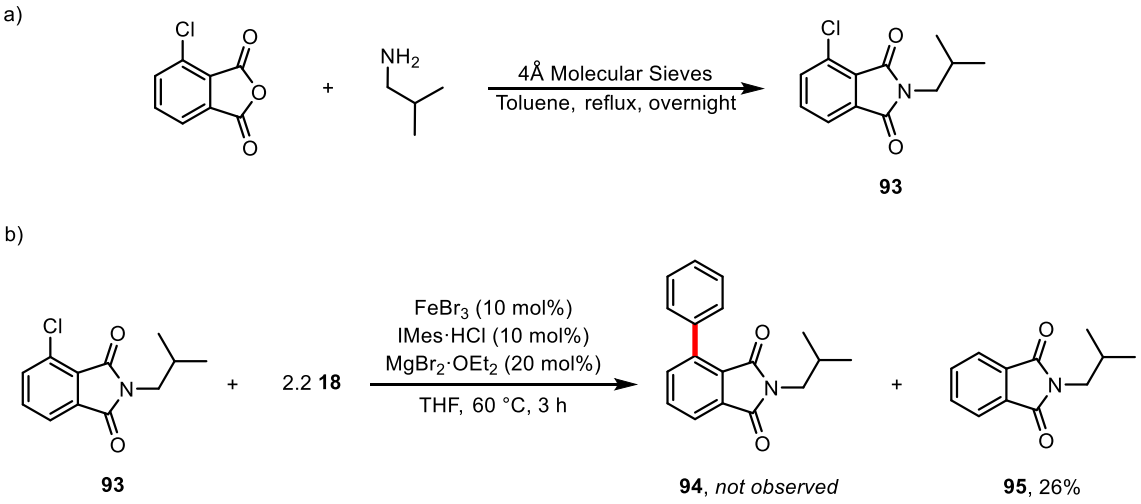

Scheme 3.13: a) Synthesis of **93** and b) Suzuki reaction of **93**.

At this point, it can be said that *both* the π-coordinating pyrrole and carbonyl group are essential for activity. Furthermore, a SmI_2 mediated reaction (SmI_2 has been used previously to generate aminoketyl radicals for use in organic synthesis as a single electron reductant)[165] afforded none of the cross-coupled product (Scheme 3.14), also showing that generation of an aminoketyl radical alone is not enough to engage biaryl cross-coupling with borate **18**.

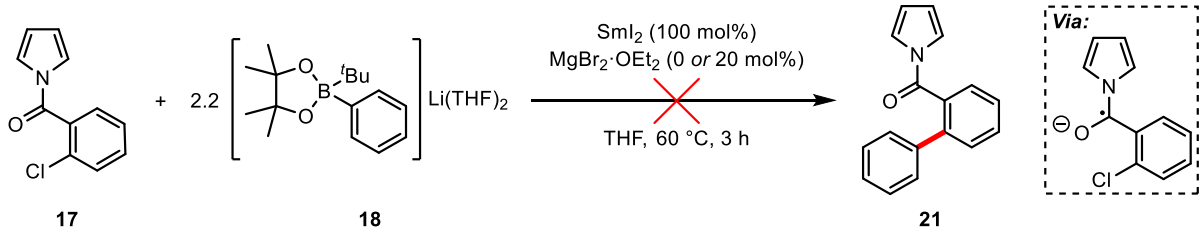

Scheme 3.14: Attempted SmI_2 mediated cross-coupling.

Taken together, a proposed mechanism for the role of the directing group is given in Scheme 3.15, where π-coordination followed by SET affords the aminoketyl species. Migration of the iron species via coordination to the oxygen atom on the amide group furnishes an intermediate where the C-Cl bond is electronically activated, and the iron species is tethered in close proximity to the activated bond. This explains the strict regiocontrol of the reaction, since the formation of an aminoketyl radical followed by an undirected C-Cl activation would also electronically activate the *meta*-Cl and *para*-Cl analogues of **17**. However, as discussed previously (Section 2.3) arylation at these positions does not occur.

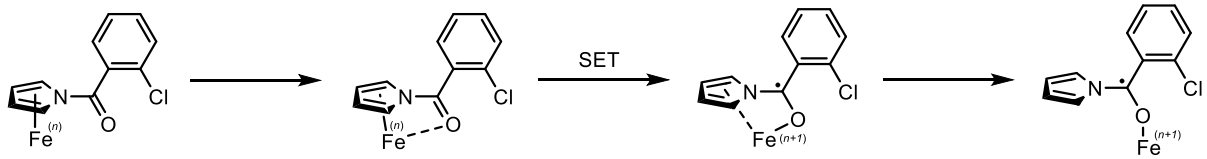

Scheme 3.15: Proposed mechanism for π-coordination followed by SET to form an aminokeyl radical species.

3.7 Proposed Catalytic Cycle

Figure 3.15 details a simplified, tentative catalytic cycle based on all the evidence discussed above. Although little information of the exact speciation of the iron-species in solution has been found, the strong ligand dependence, the negative result from the Hg drop experiment and the poor reactivity of pre-formed iron nanoparticles strongly suggest that the cycle takes place in the homogeneous phase with a ligated iron species.

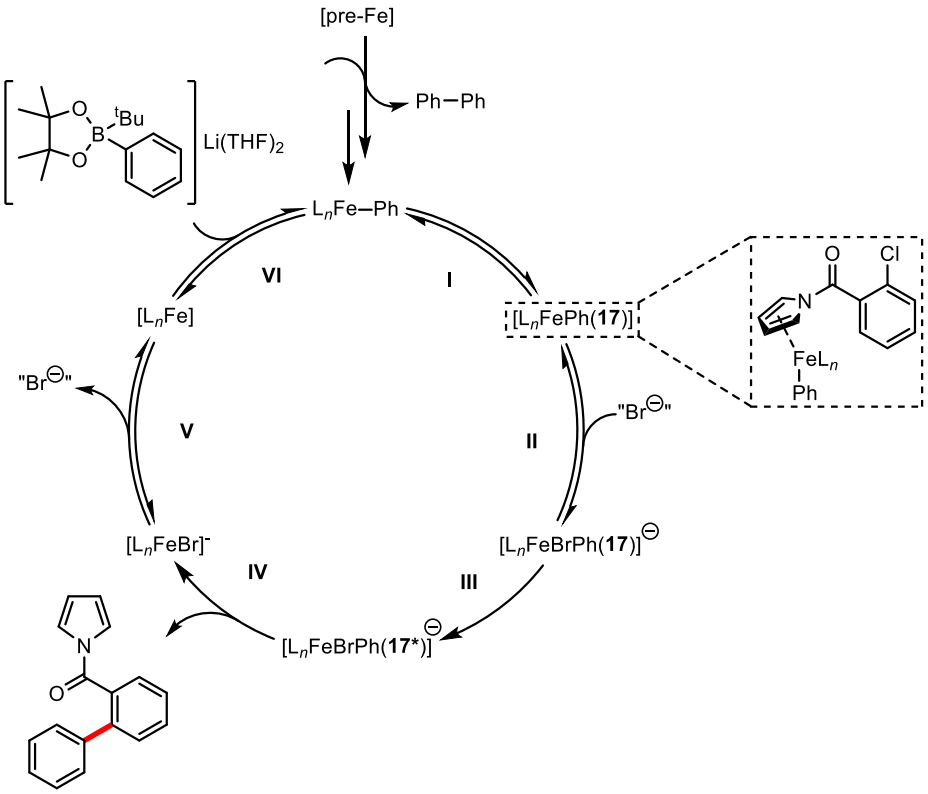

Figure 3.15: Proposed catalytic cycle for the iron-catalysed Suzuki biaryl cross-coupling reaction.

Upon addition of borate **18** to the reaction mixture, the pre-catalyst [pre-Fe] is arylated before reductively eliminating biphenyl, a process that is independent of $MgBr_2$ concentration, to furnish a catalytically active iron species [L_nFePh]. The amount of biphenyl produced during the reaction induction period (after which biphenyl production slows dramatically) suggests that the oxidation state of the formed species is Fe(II); reduction by an average of 0.75 electrons per iron centre from the Fe(III) pre-catalyst. However, is it possible that the oxidation state of the active catalyst could be higher, or lower, than Fe(II), as disproportionation reactions may occur to afford various species with different oxidation states. The catalytic cycle then proceeds as shown in Figure 3.15.

A summary of the evidence supporting each step is given below:

I. At $MgBr_2$ loadings below 20 mol%, the observed KIE shows that π-coordination of iron to the pyrrole moiety is, or is in pre-equilibrium with, the rate determining step, forming

species [L_nFePh(**17**)]. This is supported further by the directing group scope and investigations showing that oxygen coordination alone is not responsible for the observed activity.

II. The positive dependence on the reaction initial rate in $MgBr_2$ up to 20 mol% loading, and the observation that $MgBr_2$ is likely to be acting as a source of Br^- rather than a transmetallating agent in the reaction, suggests that following π-coordination, bromide donation to the iron-centre occurs forming [L_nFeBrPh(**17**)]$^-$; a reversible process. The fractional orders observed for [Fe] and [**17**] are also in agreement with processes **I** and **II** being in equilibrium.

III. The coordination of Br^- increases the electron density at the iron-centre, which in turn facilitates Ar-Cl bond activation, forming [L_nFeBrPh(**17***)]$^-$. This could also be due to the formation of an aminoketyl radical, activating the substrate for C-Cl bond scission and keeping the iron-centre in close proximity to the C-Cl bond by migration from the pyrrole moiety to the oxygen atom in the amide bond. Whether or not 'classical' oxidative addition into the C-Cl bond occurs cannot be determined at this point. Another mode of C-Cl cleavage could be through a SET mechanism that has been previously observed with cobalt.[166]

IV. [L_nFeBrPh(**17***)]$^-$ liberates the cross-coupled biaryl to form [L_nFeBr)]$^-$.

V. The observation of a negative fractional order at concentrations of $MgBr_2$ higher than 20 mol% suggests that $MgBr_2$ intervenes again in the cycle and plays an inhibitory role in the reaction. This can be explained by the equilibrium between [L_nFeBr)]$^-$ and [L_nFe]; increasing Br^- concentration pushes the position of the equilibrium towards [L_nFeBr)]$^-$, slowing down the reaction by impacting on the formation of [L_nFe].

VI. Release of Br^- from [L_nFeBr)]$^-$ would produce an electron poor species [L_nFe], from which transmetallation with **18** produces [L_nFePh], closing the cycle. The fractional orders obtained from the initial rates studies at 25 mol% $MgBr_2$ suggest that this step too, is in equilibrium.

3.8 Conclusions

A variety of mechanistic experiments has drawn back the curtain on the inner-workings of the substrate-directed iron-catalysed Suzuki biaryl cross-coupling reaction developed in Chapter 2.

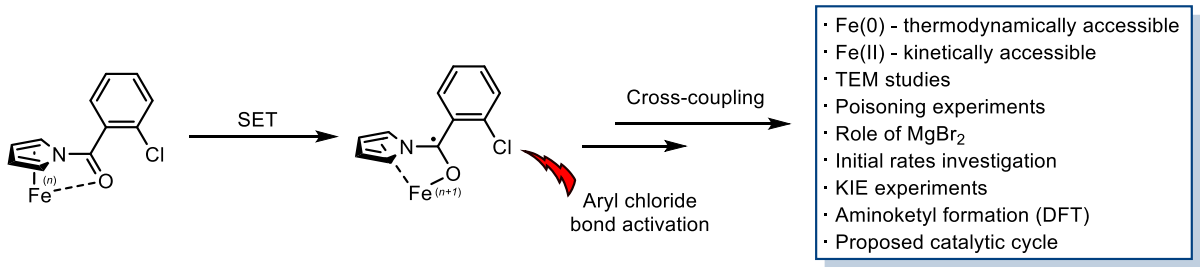

Scheme 3.16: Mechanism of aryl chloride bond activation in the substrate-directed iron-catalysed Suzuki biaryl cross-coupling reaction.

Whilst it was shown that the lowest thermodynamic accessible oxidation state of iron under the reaction conditions is Fe(0), kinetically it was shown that the oxidation state of the metal during catalysis is likely to be Fe(II). The facile reduction to Fe(0) points to the possibility that iron-nanoparticles could be a resting state in the reaction; TEM studies, Hg drop experiments and the use of pre-formed nanoparticles as pre-catalysts mitigated against this possibility, strongly suggesting that the biaryl cross-coupling occurs in the homogeneous phase. Unfortunately, investigations into the possible speciation of Fe(0) complexes under the reaction conditions proved unfruitful.

It is proposed that $MgBr_2$ acts as a bromide source rather than a transmetallating reagent. It was shown that the additive can either promote or inhibit the catalysis depending on its concentration. The role of the directing group was investigated heavily, with KIE experiments showing the importance of π-pyrrole coordination, whilst the ability of the substrate to form an aminoketyl radical through a SET process to activate the C-Cl bond (Scheme 3.16) was shown computationally.

Finally, the above data combined with an initial rates investigation at two different $MgBr_2$ loadings allowed for the proposal of a simplified catalytic cycle. To build on this, future endeavours should focus on the specific form and architecture of the iron-catalyst, which will spur on the development of new catalytic systems which would help with the development of an iron-catalysed Suzuki biaryl cross-coupling of *unactivated* aryl halide substrates.

Parts of this work have been published in *Nature Catalysis* **2018**, *1*, 429-437.

Chapter 4

Iron-Catalysed Asymmetric Cross-Coupling of 2-Bromo-1-Phenylpropane

4.1 Introduction

In 2015, Nakamura and co-workers disclosed the first example of an iron-catalysed cross-coupling between α-chloroesters and aryl Grignard reagents to afford optically active α-arylalkanoates (Scheme 4.1).[167] Controlling the enantioselectivity at the α-carbon was achieved by employing the P-chiral bisphosphine ligand (*R*,*R*)-BenzP*, with other chiral bisphosphine ligands such as (*R*,*R*)-QuinoxP*, (*S*,*S'*, *R*,*R'*)-Tangphos and (*S*,*S*)-^{i}Pr-DuPhos also giving chiral induction. A similar transformation has previously been described using cobalt catalysis.[168] The scope of the reaction was shown to be tolerant of both electron-rich and -poor Grignard nucleophiles whilst maintaining modest enantioselectivity in most cases. The scope regarding electrophiles was not extensively explored, thus it appears that the reaction is currently limited to bulky ester substrates.

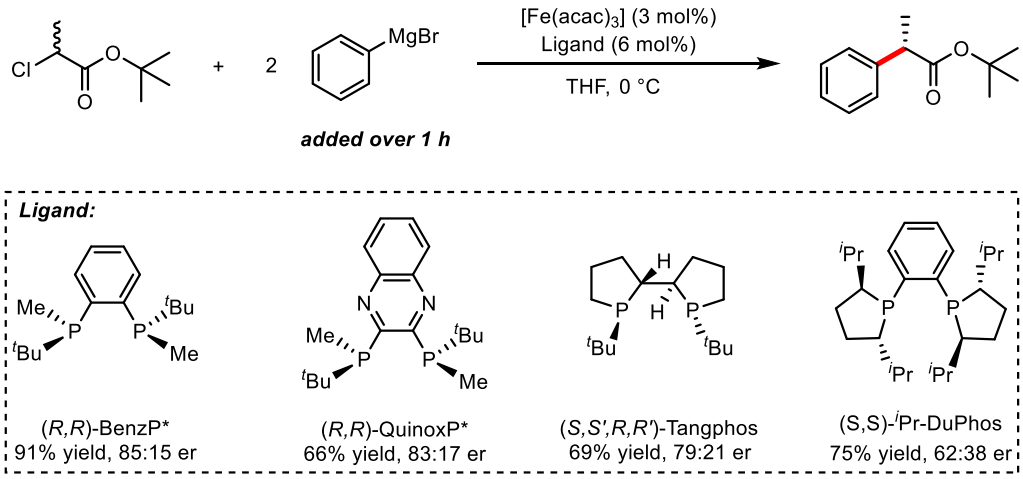

Scheme 4.1: Nakamura and co-workers' iron-catalysed enantioconvergent cross-coupling.[167]

Preliminary mechanistic investigations revealed that:

1) Selectivity of the product stereoisomer was determined in the C-C bond forming step.
2) No non-linear effects were observed in the dependence of the product's enantiomeric excess (ee) upon altering the ee of the ligand. Since the iron-catalyst is responsible for cross-coupling, the enantioselectivity must therefore be determined by the chiral ligand attached to an iron centre.
3) A radical probe (using an α-chloroalkanoate with a terminal alkenic moiety) provided good evidence for the formation of an alkyl radical intermediate at the α-carbon position where cross-coupling takes place.

An extensive computational study by Morokuma and Nakamura and co-workers[169] corroborated these findings and showed that the three-coordinate Fe(I) species [Fe(BenzP*)Cl] activates the electrophile's C-Cl bond to afford an alkyl radical on the α-carbon (Figure 4.1). Transmetallation with phenylmagnesium chloride furnishes the Fe(II) species [Fe(BenzP*)PhCl] which then combines with the alkyl radical through an inner-sphere mechanism where the chiral selectivity of the product is

determined by non-covalent interactions between the alkyl groups on the phosphine ligand and the alkyl radical, stabilising the transition state leading to the major isomer. Further transmetallation results in the formation of [$FePh_2$BenzP*] which leads to the unproductive formation of biphenyl, accounting for the need for the Grignard reagent to be added over the course of 1 h. A separate computational study by Gutierrez and co-workers[170] came to similar conclusions, where the origin of the enantioselectivity was also found to be induced during the C-C bond forming step in which several non-covalent interactions stabilise the transition state of the major product isomer. Whilst Gutierrez attributed arene π-interactions as the major stabilising contribution, Morokuma and Nakamura favoured the alkyl groups on the P-chiral ligand; both interacting with the electrophile in the transition state. In both cases it was found that the position of the bulky ^{t}Bu groups on the ligand contributed to destabilisation of the transition state of the minor chiral product.

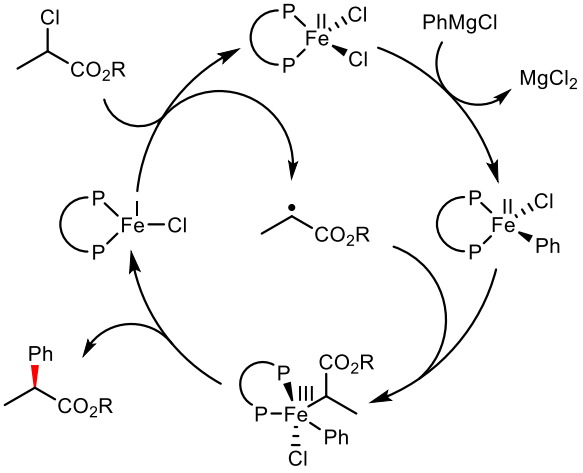

Figure 4.1: Morokuma and Nakamura's proposed catalytic cycle for the iron-catalysed asymmetric Kumada reaction.[169]

Currently, this remains the only example of an asymmetric cross-coupling reaction using iron-catalysis. Whilst Nakamura's enantioconvergent method represents a significant step forward in demonstrating the potential of iron as a catalyst in asymmetric cross-coupling reactions, the use of activated alkyl halides limits the applicability of the reaction. Also, 'hard' aryl Grignard nucleophiles could hinder its wider application due to problems with functional group tolerance. An exploration of 'soft' nucleophiles which could be employed instead would therefore also be useful to increase the attractiveness of the enantioconvergent method.

Since Nakamura's reaction occurs *via* a three-coordinate [Fe(BenzP*)Cl] species which abstracts a halide from an electrophile in a radical pathway, expanding the scope of Nakamura's asymmetric cross-coupling may therefore require a process that undergoes a similar mechanism. Encouragingly, Bedford and co-workers showed that in an iron-catalysed Suzuki arylation of alkyl halides, halide abstraction of the electrophile from a three-coordinate Fe(I) species also seems likely, furnishing a radical alkyl (Scheme 4.2).[97] Here, it was hypothesised that borate compounds could be employed as nucleophiles

with iron-complexes bearing P-chiral ligands to generate chiral centres in an enantioconvergent iron-catalysed Suzuki cross-coupling.

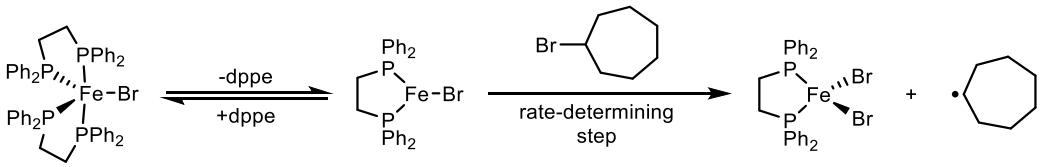

Scheme 4.2: Halide abstraction by an Fe(I) species to form an alkyl radical in Bedford's iron-catalysed Suzuki cross-coupling reaction.[97]

The facile arylation of 2-bromo-1-phenylpropane with borate **18** has previously been demonstrated by Bedford and co-workers using the iron complex [$FeCl_2(dppe)_2$] with co-catalytic $MgBr_2$. The pre-catalyst offers the possibility to alter the ligands to similar asymmetric architectures such as those used by Nakamura and co-workers. This electrophile represents a good starting point for broadening the scope of asymmetric iron-catalysed cross-coupling into more generic unactivated secondary halides. Inspired by the previous utilisation of an aromatic directing group (Chapters 2 & 3), it was hypothesised that an iron species of general formula [FeX_2(ligand*)] (X = Ar or halide, ligand* = P-chiral bis-chelating ligand) could coordinate to the arene group of the organic radical intermediate, directing the C-C bond forming event. Encouragingly, the asymmetric alkylation of 2-bromo-1-phenylpropane has previously been achieved by Fu and co-workers in nickel-catalysed Suzuki couplings using the alkyl organoboron reagent 9-borobicyclo[3.3.1]nonane derivative.[171] It was demonstrated that interaction of a nickel complex with the benzyl moiety was important due to the dependence of the correct positioning of the directing group (Scheme 4.3).

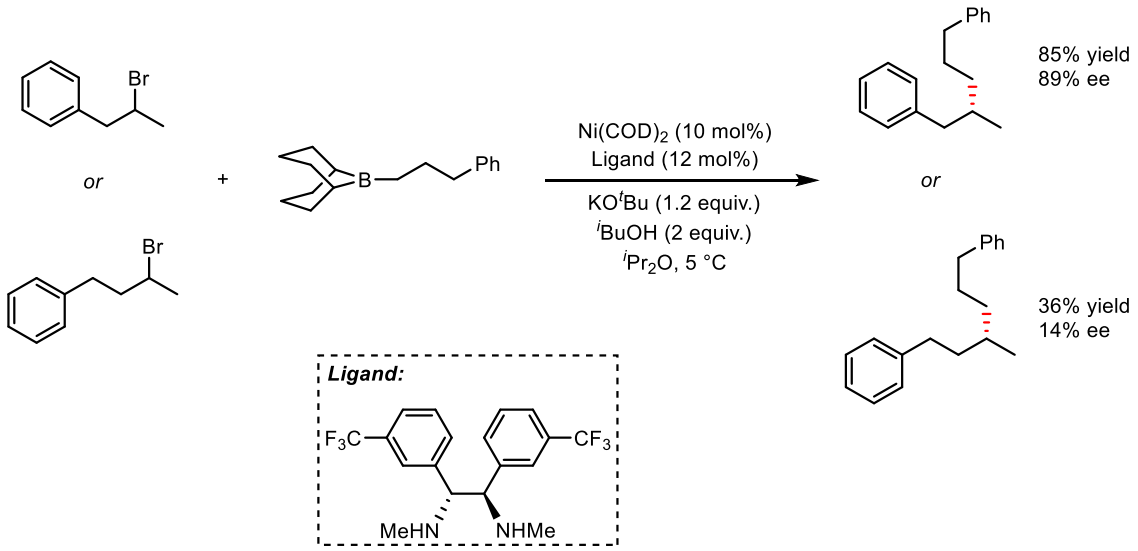

Scheme 4.3: Fu's directed asymmetric nickel-catalysed sp^3-sp^3 cross-coupling of 2-bromo-1-phenylpropane.[171]

4.2 Asymmetric Suzuki Cross-Coupling of 2-Bromo-1-phenylpropane

Bedford's procedure for the cross-coupling of 2-bromo-1-phenylpropane with borate **18** occurs in THF at 40 °C for 3 h using the isolated pre-catalyst [$FeCl_2$(dppe)] with co-catalytic $MgBr_2$. To see whether the conditions could be changed to allow for the iron salt and ligand to be added independently (thus enabling expedient screening of P-chiral ligands), $FeBr_2$ and 2 equivalents of either dppe or dpbz ligand were stirred in THF at room temperature for 1 h before the addition of 2-bromo-1-phenylpropane, $MgBr_2$ and **18** to furnish 1,2-diphenylpropane (Table 4.1).

Table 4.1: Iron-catalysed Suzuki cross-coupling of 2-bromo-1-phenylpropane.

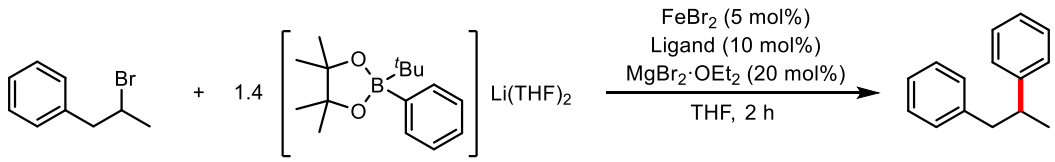

18

Entry	Ligand	Temperature	Appearance	Yield (%)[a]
1	dpbz	40 °C	Homogeneous	98
2	dpbz	rt	Homogeneous	61
3	dppe	rt	Homogeneous	42

Conditions: $FeBr_2$ (0.0075 mmol), ligand (0.015 mmol), $MgBr_2 \cdot OEt_2$ (0.03 mmol), 2-bromo-1-phenylpropane (0.15 mmol) and **18** (0.21 mmol) in THF for 2 h at the desired temperature. [a] Determined by ^{1}H NMR analysis (1,3,5-trimethoxybenzene internal standard).

Gratifyingly, under the same conditions the cross-coupling reaction could be carried out to furnish 1,2-diphenylpropane in 98% yield without requiring the independent synthesis of the iron-phosphine pre-catalyst (Table 4.1, entry 1). It was also found that when lowering the temperature, the reaction still afforded the product, albeit at reduced yield (entries 2 and 3). Importantly, each reaction stayed as a deep red homogenous solution indicating no formation of iron nanoparticles. A range of P-chiral bisphosphine ligands were then surveyed under various reaction conditions (Table 4.2).

Table 4.2: Asymmetric iron-catalysed Suzuki cross-coupling of 2-bromo-1-phenylpropane.

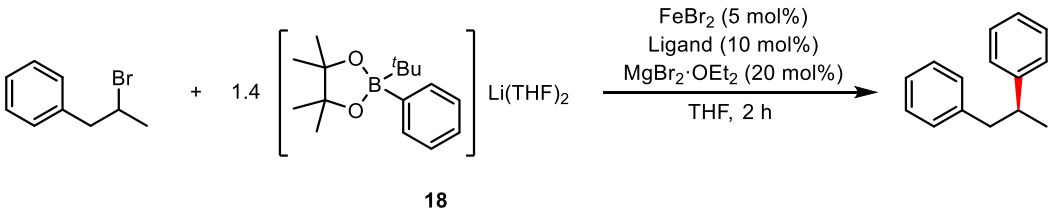

18

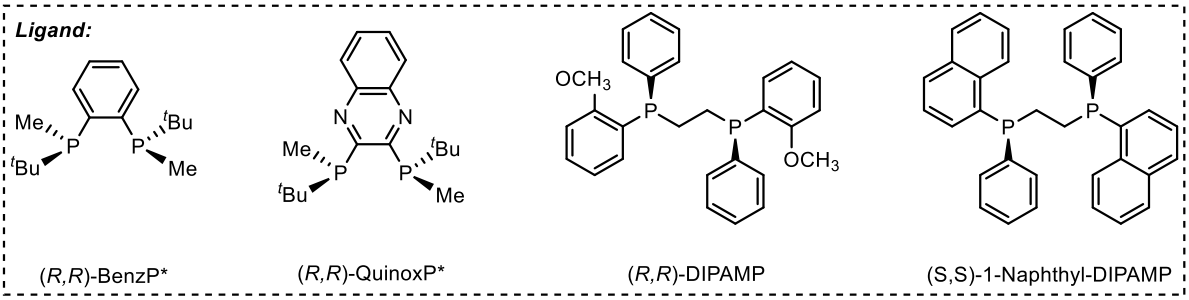

Entry	Ligand	Temperature (°C)	Yield (%)[a]	er[b]
1	(*R*,*R*)-BenzP*	40	0	N.A.
2	(*R*,*R*)-BenzP*	r.t.	0	N.A.
3[c]	(*R*,*R*)-BenzP*	r.t.	0	N.A.
4	(*R*,*R*)-QuinoxP*	40	7	50:50
5	(*R*,*R*)-QuinoxP*	r.t.	62	50:50
6[c]	(*R*,*R*)-QuinoxP*	r.t.	0	N.A.
7	(*R*,*R*)-QuinoxP*	0	0	N.A.
8	(*R*,*R*)-DIPAMP	r.t.	25	50:50
9[c]	(*R*,*R*)-DIPAMP	40	0	N.A.
10[d]	(*R*,*R*)-DIPAMP	0	0	N.A.
11	(*S*,*S*)-1-Naphthyl-DIPAMP	r.t.	49	50:50
12	(*S*,*S*)-1-Naphthyl-DIPAMP	40	75	50:50

Conditions: $FeBr_2$ (0.0075 mmol), ligand (0.015 mmol), $MgBr_2{\cdot}OEt_2$ (0.03 mmol), 2-bromo-1-phenylpropane (0.15 mmol) and **18** (0.21 mmol) in THF for 2 h at the desired temperature. [a] Determined by ^{1}H NMR analysis (1,3,5-trimethoxybenzene internal standard). [b] Determined by chiral supercritical fluid chromatography. [c] Added *via* syringe pump over 2 h. [d] Reaction left overnight.

Employment of the BenzP* ligand was deleterious to the reaction, affording no cross-coupled product even under identical conditions to those of Bedford and co-workers (Table 4.2, entries 1-3). Switching

to the more electron-withdrawing QuinoxP* ligand afforded the cross-coupled product in 62% yield after stirring at room temperature for 2 h, however no chiral induction was seen (entry 5). Adding the borate over a period over 2 h or running the reaction at 0 °C in an attempt to favour the production of a particular stereoisomer was also found to be deleterious to the reaction; enantiomeric ratios of 50:50 were produced (entries 6 and 7).

It appears that the steric bulk of the arene substituents of the phosphorus atoms of the ligand are important for achieving good yields. Thus, ligand architectures similar to dppe were investigated; (*R*,*R*)-1,2-bis[(2-methoxyphenyl)(phenylphosphino)]ethane (DIPAMP) and (*S*,*S*)-1,2-Bis[α-naphthyl(phenylphosphino)]ethane (1-naphthyl-DIMAMP) were trialled. Whilst DIPAMP afforded the product in 25% yield at room temperature (entry 8), no chiral induction was seen. Lowering the temperature (entry 10) or slow addition of borate **18** (entry 9) afforded none of the cross-coupled product. Conversely, 1-naphthyl-DIPAMP afforded the product at both room temperature and 40 °C (49% and 75% yield respectively) but with no chiral induction (entries 11 and 12).

It is apparent that the reaction is very sensitive to ligand environment when cross-coupling with borate nucleophiles, hampering the production of 1,2-diphenylpropane and offering no chiral induction. Mechanistically, this indicates that upon formation of an alkyl radical after the reaction of the alkyl halide with an Fe(I) species, the radical may then go on to react with borate nucleophile directly rather than an iron species bearing the P-chiral ligand.

4.3 Asymmetric Kumada Cross-Coupling of 2-Bromo-1-phenylpropane

Accordingly, our attention turned to the asymmetric Kumada-type cross-coupling of 2-bromo-1-phenylpropane with phenylmagnesium chloride. First attempts using QuinoxP* with either $FeBr_2$ or $[Fe(acac)_3]$ proved encouraging, with both reactions giving a slight asymmetric induction after slow addition of Grignard in THF as described by Nakamura and co-workers (Table 4.3, entries 1 and 2). Unfortunately, lowering the temperature to -40 or -78 °C didn't improve enantiomeric ratio, but instead lowered the yield (entries 4 – 6). As seen with the borate nucleophile, both DIPAMP (25% yield) and 1-naphthyl-DIPAMP (49% yield) gave the product as a racemic mixture.

Table 4.3: Asymmetric iron-catalysed Kumada cross-coupling of 2-bromo-1-phenylpropane.

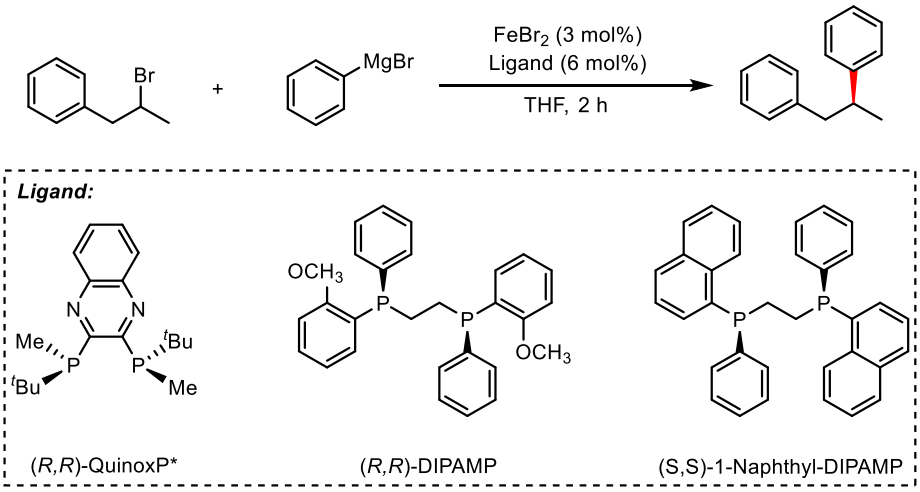

Entry	Ligand	Temperature (°C)	Yield (%)[a]	er[b]
1	(*R*,*R*)-QuinoxP*	0	77	45:55
2[c]	(*R*,*R*)-QuinoxP*	0	99	47:53
3	(*R*,*R*)-QuinoxP*	-40	63	45:55
4[d]	(*R*,*R*)-QuinoxP*	-40	57	45:55
5	(*R*,*R*)-QuinoxP*	-78	6	48:52
6[d]	(*R*,*R*)-QuinoxP*	-78	15	47:53
7	(*R*,*R*)-DIPAMP	r.t.	25	50:50
8	(*S*,*S*)-1-Naphthyl-DIPAMP	r.t.	49	50:50

Conditions: $FeBr_2$ (3 mol%), ligand (6%), 2-bromo-1-phenylpropane (0.3 mmol) and phenylmagnesium chloride (2 equiv.) in THF added over 1 h. [a] Determined by ^1H NMR analysis (1,3,5-trimethoxybenzene internal

standard). [b] Determined by chiral supercritical fluid chromatography. [c] 3 mol% [$Fe(acac)_3$] instead of $FeBr_2$. [d] Phenylmagnesium chloride added in one portion.

These data, from both the attempted Suzuki and Kumada cross-coupling reactions, indicate that the electrophile is not directing the iron-catalyst by arene π-coordination, thus not allowing the steric bulk on the P-chiral ligands to interact with the electrophile enough to cause an effect in the transition state leading to the production of an asymmetric cross-coupled product. Therefore, it seems that for now Nakamura's seminal work is currently limited to more activated and bulky α-chloroester electrophiles.

4.4 Conclusions

Nakamura's iron-catalysed enantioselective cross-coupling of racemic α-haloesters with aryl Grignard reagents to furnish optically active α-arylalkanoic acids represents the current state-of-the-art asymmetric cross-coupling using an iron-based catalyst. Attempts to broaden the scope by utilising a borate nucleophile and a simple alkane electrophile has not been achieved here despite a modest screen of asymmetric bidentate phosphine ligands.

Switching to the analogous Kumada-type reaction by utilising phenylmagnesium chloride as a nucleophile afforded the desired cross-coupled product in good yields but with only a very slight asymmetric induction when using QuinoxP* as a ligand. Future endeavours should therefore focus on screening other unactivated alkyl halide electrophiles in which a particular conformation may be stabilised in the transition state during the C-C bond forming event. Another avenue of investigation should also be the effect of zinc-based nucleophiles in a Negishi-type coupling.

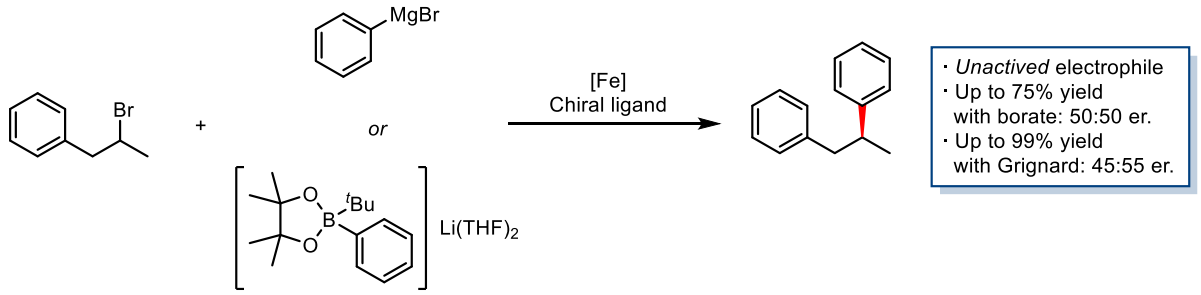

Scheme 4.4: Attempted asymmetric iron-catalysed Suzuki and Kumada cross-coupling of 2-bromo-1-phenylpropane.

Chapter 5

Comparison of an *N*-Heterocyclic Carbene and Germylene Ligand in Iron-Catalysed Cross-Couplings

5.1 Introduction

In 1968, Wanzlick reported the first example of an organometallic complex bearing an *N*-heterocyclic carbene (NHC) ligand (Figure 5.1a) produced by *in situ* deprotonation of imidazolium salts with $Hg(OAc)_2$.[172] Although many attempts to isolate a 'free' NHC were made,[173] it was not until 1991 that the first NHC, IAd, was isolated by Arduengo (Figure 5.1b),[174] who followed up shortly with his report on the first saturated NHC, SIMes, a few years later (Figure 5.1c).[175] Today, a plethora of NHC's are available commercially or easily synthesised on a multi-gram scale[124] and their applications in organometallic chemistry, main group chemistry and catalysis (organic and organometallic) are well established.[176]

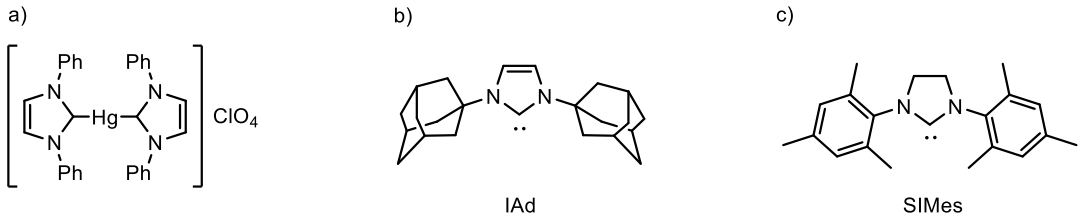

Figure 5.1: a) The first example of an NHC organometallic complex as reported by Wanzlick.[172] The first 'bottle-able' NHCs b) IAd and c) SIMes were reported by Arduengo many years later.[174, 175]

The first use of NHC ligands in iron-catalysed cross-coupling reactions was in 2005, where Bedford and co-workers showed that a preformed Fe-NHC complex or a combination of iron salts and NHC precursors were effective systems for cross-coupling reactions between alkyl halides and Grignard reagents (Scheme 5.1).

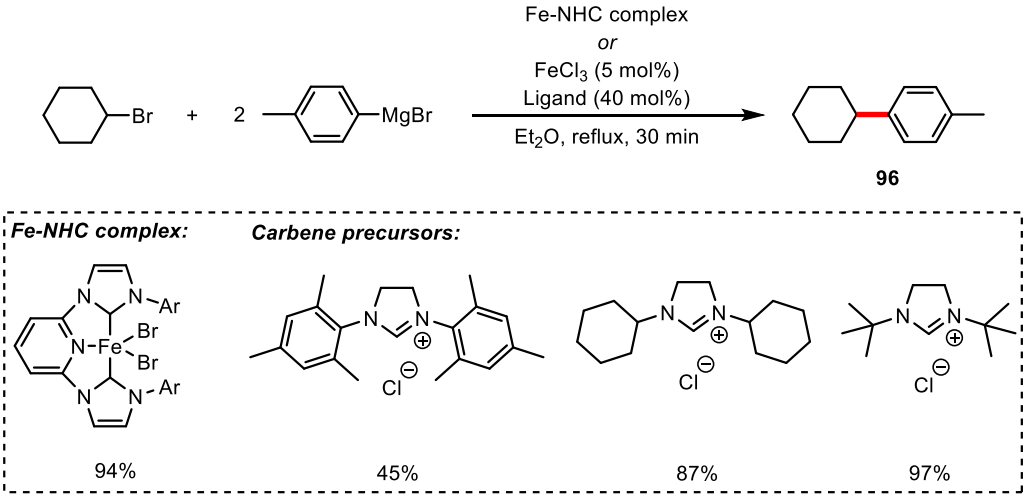

Scheme 5.1: Bedford's iron-catalysed cross-coupling of alkyl halides with Grignard reagents.

Subsequently, NHCs have been utilised in a wide variety of iron-catalysed reactions, not just limited to cross-couplings (Scheme 5.2a-c),[55, 61, 177] but also for oxidative esterification of aldehydes (Scheme

5.2d)[178] and hydrosilylation of ketones (Scheme 5.2e)[179]. As shown in Scheme 5.2, the differences in electronics of the NHC can have a vast influence on the performance of the catalytic reaction.

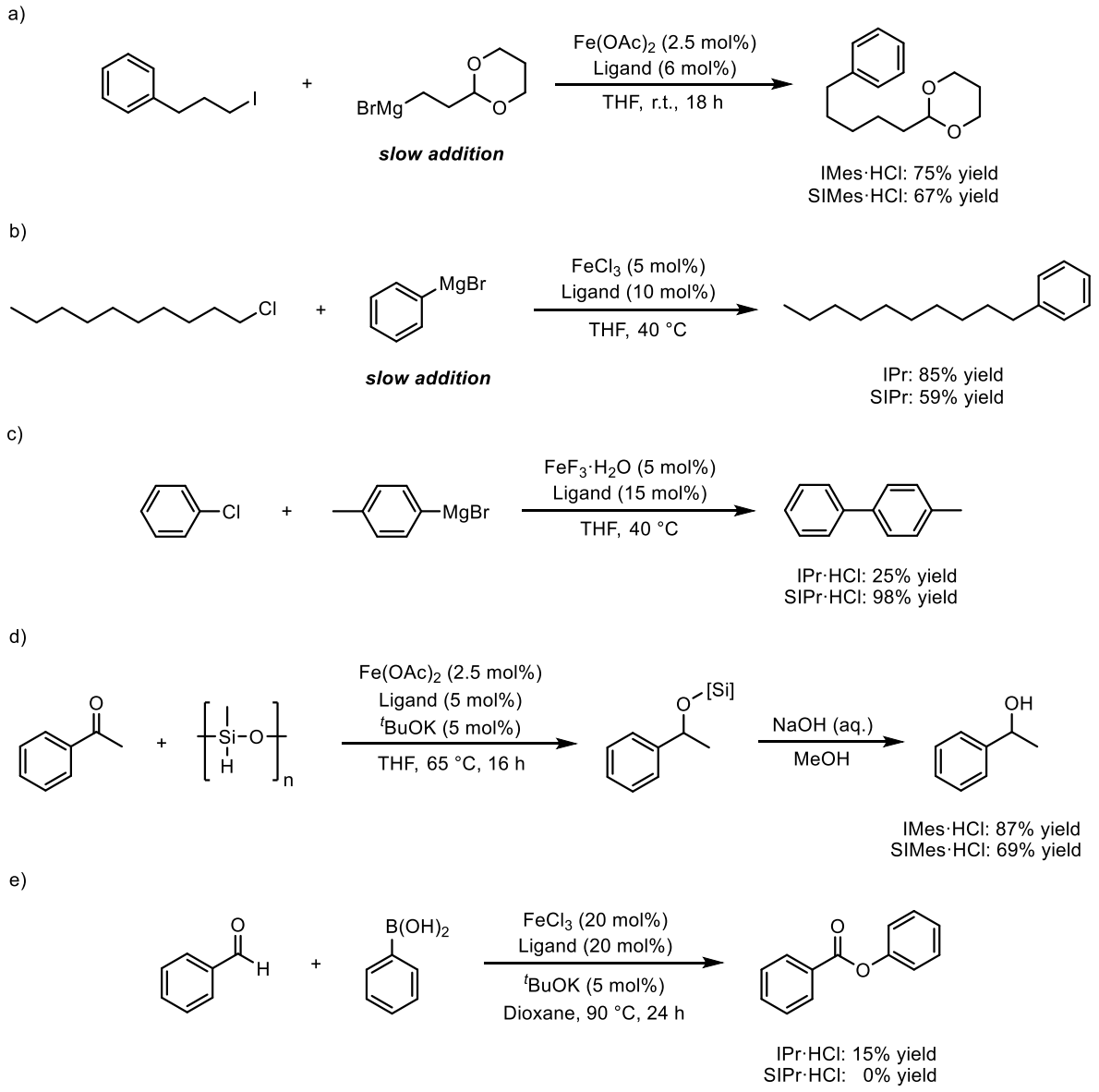

Scheme 5.2: Iron-catalysed reactions dependant on NHC ligands include a) alkyl-alkyl Kumada cross-coupling reported by Cahiez,[61] b) alkyl-aryl cross-coupling reported by Nakamura,[177] c) aryl-aryl cross-coupling reported by Nakamura,[55] d) silylation of ketones reported by Adolfsson[179] and e) oxidative esterification of aldehydes reported by Gois.[178]

NHCs are electron-rich, neutral two-electron σ-donors which coordinate to transition-metals by donation of the carbene electrons into an appropriate empty σ-symmetry orbital; a similar bonding regime to tertiary phosphines. NHCs are stronger σ-donors than phosphines, however phosphines are well known to also accept electron density from the metal they coordinate to through π-back-donation to their LUMO. In theory, π-back-donation into the carbene's empty p-orbital (LUMO) can occur, however, with NHCs the carbene is often flanked either side by a nitrogen atom which donate electron

density into the carbene orbital through π-bonding. This competing π-donation has caused many to believe that π-back-donation from the metal is negligible, although anomalies to this rule exist.[180, 181] The bonding between metals and NHCs has been extensively discussed by Nolan[182] and Díez-González[183] and is represented in Figure 5.2.

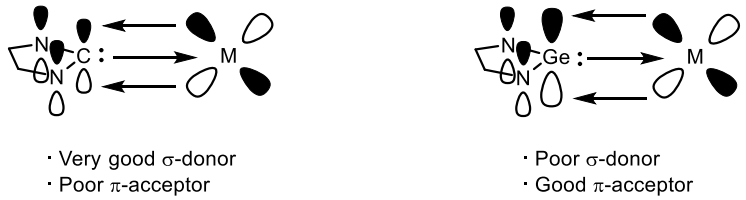

Figure 5.2: The differences in bonding between metals with carbene and germylene ligands.

Interestingly, if one goes down the Group 14 elements, this bonding regime changes. For example, germylene compounds (the first examples of which were synthesised in 1970s)[184], have weaker σ-donation but better π-acceptor ability than carbenes due to better orbital overlap between the germanium p-orbital and the metal d-orbital. When utilised as ligands, this could yield interesting activity in cross-coupling chemistry, particularly as germylenes favour metals in lower oxidation states (see Section 5.3). However, the use of germylene compounds as ligands in first row metal-catalysed cross-coupling chemistry remains completely uncharted. In this chapter, the NHC IMes was compared vis-à-vis with its germylene analogue **97** in both cobalt- and iron-catalysed cross-coupling reactions (Figure 5.3).

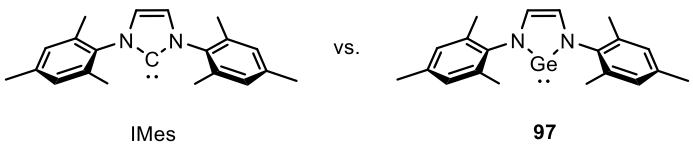

IMes **97**

Figure 5.3: The monodentate *N*-heterocyclic carbene and germylene ligands that will be investigated in this chapter.

5.2 Effect of Germylene in Cobalt- and Iron-Catalysed Cross-Couplings

5.2.1 Suzuki Cross-Coupling

The gram-scale synthesis of germylene ligand **97** was carried out by following the procedure of Tolman and co-workers where a stirred yellow solution of **98** in THF was treated with lithium metal to afford a deep red solution of reduced dimetallated **99** (Scheme 5.3).[185] Metathesis with $GeCl_2$·dioxane afforded the desired compound as an air- and moisture-sensitive orange solid with spectroscopic data matching the previously reported literature.[185] With the compound in hand, its ability to act as an effective ligand in cobalt- and iron-catalysed cross-coupling reactions was assessed.

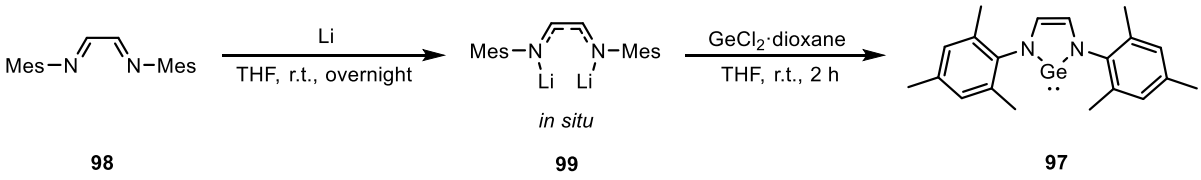

Scheme 5.3: Synthesis of the germylene IMes analogue **97** synthesised according to Tolman and co-workers.[185]

The first reaction **97** was utilised in was the substrate-directed Suzuki biaryl cross-coupling reaction developed in Chapter 2. Optimisation experiments (Chapter 2, Table 2.1) showed that the reaction has a strong ligand dependence and mechanistic studies (Chapter 3) indicate that it is unlikely that metal aggregates or nanoparticles are responsible for the catalysis. As previously discussed, the NHC precursor IMes·HCl was used for the majority of the study since it is stable to air and moisture. The carbene IMes was shown to be just as effective when employed as a ligand in the catalysis (82% yield), however when germylene **97** was used, biaryl **21** was only produced in 15% yield (Scheme 5.4). A similar yield (16%) was achieved when no ligand was used (Chapter 2, Table 2.1).

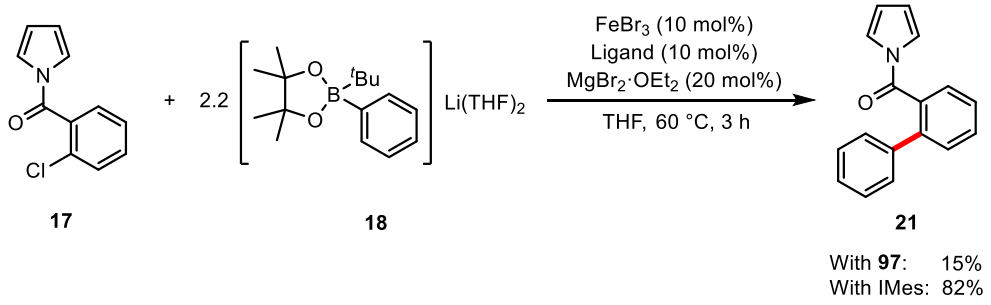

Scheme 5.4: Comparison of IMes and **97** in the iron-catalysed substrate-directed Suzuki biaryl cross-coupling reaction developed in Chapter 2.

A similar sp^2-sp^2 cross-coupling reaction, the cobalt-catalysed Suzuki biaryl reaction developed by Bedford and co-workers,[115] was trialled next (Scheme 5.5). This reaction too shows a strong ligand dependence, with a variety of NHC precursors giving excellent to almost quantitative yields of the cross-coupled biaryl product. Again, the free carbene IMes proved to be a capable ligand, affording **100**

in 73% yield after 48 h. The germylene ligand however gave **100** in 20% yield under identical conditions. Having proved ineffective in Suzuki-type cross-coupling reactions, attention was turned to iron-catalysed Kumada-type chemistry.

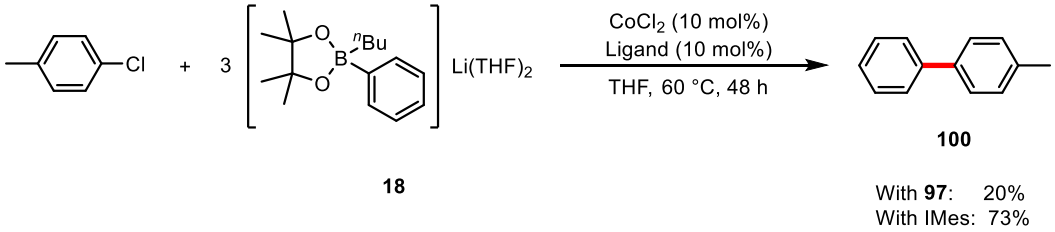

Scheme 5.5: Comparison of IMes and **97** in the cobalt-catalysed Suzuki biaryl cross-coupling reaction developed by Bedford and co-workers.

5.2.2 Kumada Cross-Coupling

As mentioned in Section 5.1, Bedford showed how NHCs could facilitate iron-catalysed arylation of alkyl halides. Given the general applicability of different ligand types, and the effectiveness of carbene ligands in this transformation, both IMes and **97** were trialled in the cross-coupling reaction of cyclohexyl bromide and *p*-tolylmagnesium bromide (Scheme 5.6a).

In stark contrast to the Suzuki-type reactions trialled, both IMes and **97** proved to be effective ligands in the reaction, affording **96** in 70% and 65% yield respectively. However, it is possible that under these conditions, the formation of iron nanoparticles is occurring and that these could be responsible for the observed catalysis. Indeed, the reaction mixtures both turned very dark upon the addition of the Grignard reagent, suggesting that iron nanoparticles may have formed. To circumvent this possibility, the reaction was repeated by adding the Grignard reagent over 1 h *via* syringe pump (Scheme 5.6b). In this case, both reaction mixtures containing either IMes or **97** did not turn black. Interestingly, under these conditions, the germylene ligand outperformed IMes, affording **96** in 70% and 49% yield respectively.

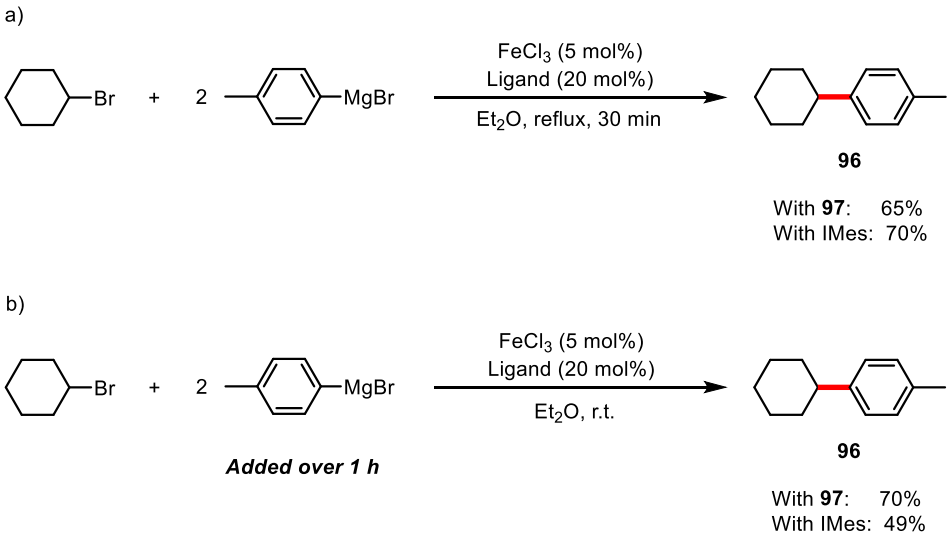

Scheme 5.6: Iron-catalysed cross-coupling of cyclohexyl bromide with *p*-tolylmagnesium bromide using either IMes or **97** as ligand by either a) addition of Grignard in one portion or b) slow addition of Grignard over 1 h.

A reaction profile showing the formation of **96** using IMes or **97** is shown in Figure 5.4. When utilising IMes as a ligand, the production of **96** was observed within the first 5 minutes of the reaction before plateauing at around 50 minutes. Interestingly, with the germylene ligand an induction period is seen with only trace amounts of **96** being produced 5 minutes into the reaction. After this period however, the production of **96** begins but at a faster rate than with the IMes ligand, with both IMes and **97** affording the same amount of **96** within 20 minutes. The formation of **96** plateaus slightly earlier, at around 40 minutes into the reaction when **97** is used. It appears that at the start of the reaction (where the concentration of Grignard reagent is low) the formation of an active catalyst occurs immediately for the $FeCl_3$ and IMes mixture. Conversely, a higher concentration of Grignard reagent is required to furnish the active catalyst for the $FeCl_3$ and **97** mixture. Insight into the possible speciation of the iron catalysts under the reaction conditions is given when the reaction is repeated *without* any ligand present. Not only does the production of **96** occur without an induction period, it also produces the cross-coupled product at a similar rate to the $FeCl_3$/**97** system, with a very similar profile and plateauing at around 40 minutes. Again, the production of **96** without ligand is better than when using IMes as a ligand, but surprisingly, is also better than when either the germylene or carbene ligand is used.

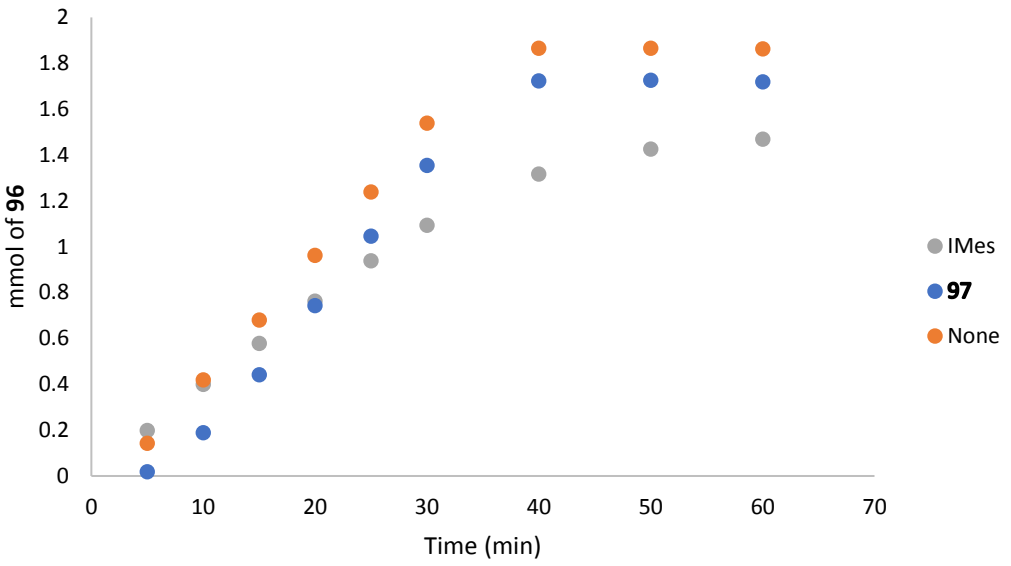

Figure 5.4: Formation of **96** over time with either IMes, **97** or no ligand.

As discussed in Chapter 1, mechanistic studies by Bedford and co-workers showed that in iron-catalysed couplings of alkyl halides and aryl Grignard reagents, *N,N,N',N'*-tetramethylethylenediamine (TMEDA) does not coordinate to the iron complexes present in the reaction mixture.[84] Instead, it was shown that the homoleptic iron 'ate' complex $[Fe(Mes)_3]^-$ (**4**) was the sole species present in a THF solution of $FeCl_3$, TMEDA and 8 equivalents mesitylmagnesium bromide (MesMgBr). However, the mesitylene ligand is sterically demanding and can stabilise organometallic complexes by making reductive elimination of the bulky ligands challenging. This means that when smaller aryl Grignard reagents are used, alternative organometallic complexes may be formed instead, especially if catalysis proceeds by the formation of Fe(0) nanoparticles (which the use of a bulky Grignard reagent may prevent). Indeed, when Bedford and co-workers reacted *p*-tolylmagnesium bromide with $FeCl_3$ in the presence or absence of TMEDA, EPR spectroscopy revealed the presence of an S=½ species, consistent with the formation of an Fe(I) complex. Nevertheless, the additional stability afforded by using bulky mesityl ligands may still provide useful insight into catalyst speciation during the reaction.

The similarity between the profiles of the production of **96** using **97** and no ligand suggest that a common intermediate may be responsible for the catalysis. One would expect both IMes and **97** to form a stronger bond to iron than TMEDA, yet it is possible that in the case of **97**, the bond from an electron poor Fe(III) centre (and subsequently an Fe(II) centre, *vide infra*) to the Ge(II) atom is not as strong as expected. To investigate this possibility, mixtures of $FeCl_3$ and **97** with varying amounts of MesMgBr were monitored by ^1H NMR. The results are shown in Figure 5.5.

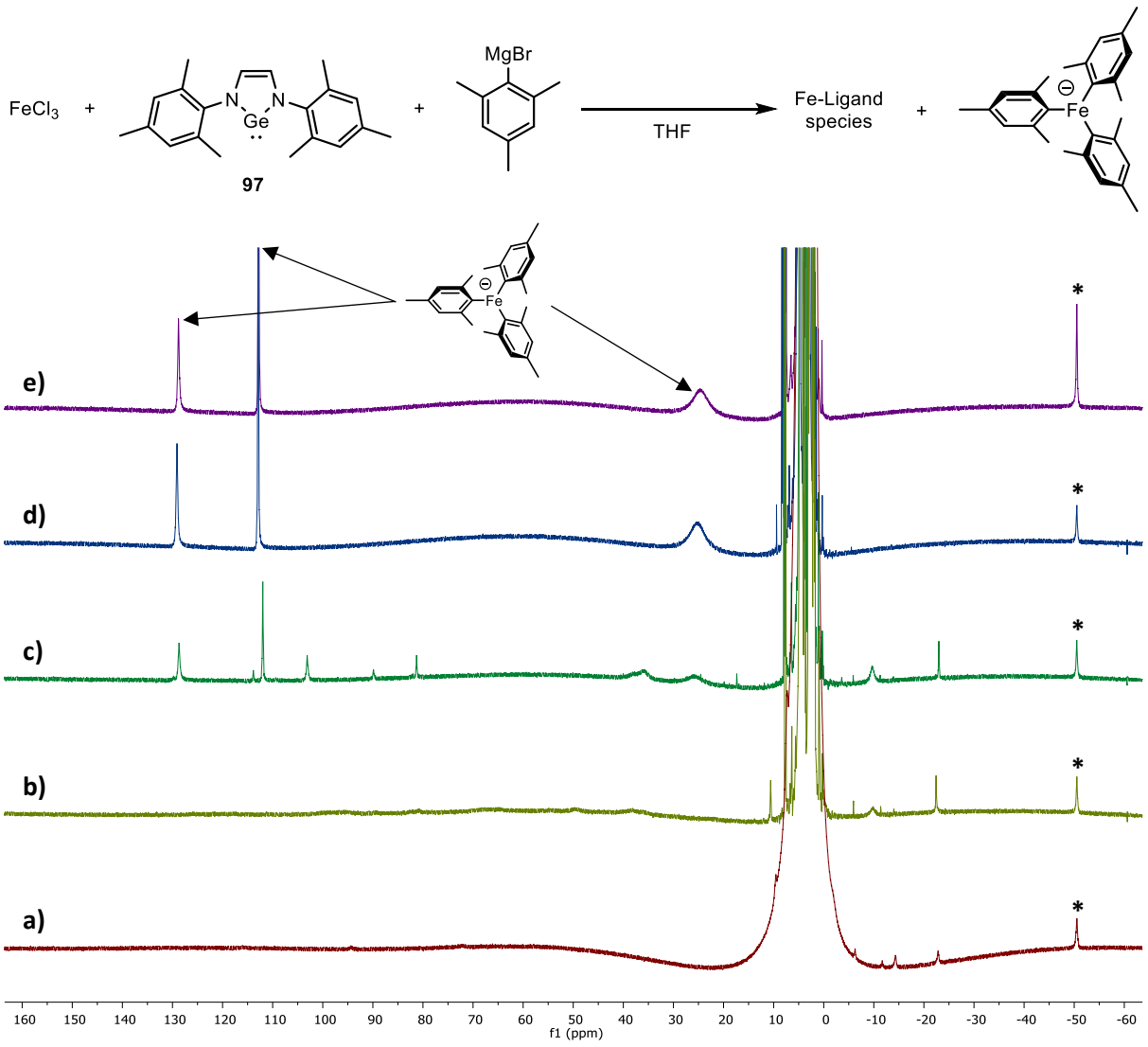

Figure 5.5: ^{1}H NMR spectrum of the reaction mixture of $FeCl_3$ and **97** with a) 1 equivalent of MesMgBr, b) 2 equivalents of MesMgBr, c) 3 equivalents of MesMgBr, d) 5 equivalents of MesMgBr and e) 10 equivalents of MesMgBr. The * denotes the peak for cobaltocene (internal standard).

The ^{1}H NMR spectrum of a mixture of $FeCl_3$ and **97** with 1 equivalent of MesMgBr showed paramagnetically shifted peaks at δ -6.30, -11.71, -14.36 and -22.91 ppm (Figure 5.5a). The first equivalent of MesMgBr likely serves to reduce the Fe(III) to Fe(II) with concomitant formation of bimesityl. With 2 equivalents of MesMgBr, the peak at δ -22.9 ppm remained, however the only other predominant paramagnetic peak observed was a broadened peak at δ -9.82 ppm (Figure 5.5b). Increasing the amount of MesMgBr to 3 equivalents, these two peaks remained. However, downfield in the spectrum, another species observable by ^{1}H NMR was present (Figure 5.5c). One of these is the homoleptic iron 'ate' complex **4**, with two sharp peaks at δ 128.82 and 112.81 ppm, and a broadened peak at δ 24.74 ppm. By integrating against a cobaltocene standard (seen at δ -50.53 ppm), the amount of **4** in solution can be calculated. With 3 equivalents of MesMgBr, ~ 38% of the iron in solution is **4**. At both 5 and 10 equivalents of MesMgBr, the sole species observable in the ^{1}H NMR is **4** (Figure 5.5d)

and (Figure 5.5e), accounting for all the iron. This suggests that at lower concentrations of Grignard, an unproductive organometallic species is formed, accounting for the induction period seen with the production of **96**. As the concentration of Grignard increases, to at least 5 equivalents per iron centre, the active iron catalyst is formed, which from the data shown in Figure 5.5 is likely to be species which *does not* bear the germylene ligand **97**. This also fits with the reactivity observed when germylene **97** was used in place of IMes in the cobalt- and iron- catalysed Suzuki-cross coupling reactions. In both cases, yields of the cross-coupled product in both these strongly ligand dependant reactions were similar to the yields achieved when no ligand was used.

A comparison of the behaviour between **97** and IMes was sought by repeating this procedure with IMes. The results arising from this are shown in Figure 5.6.

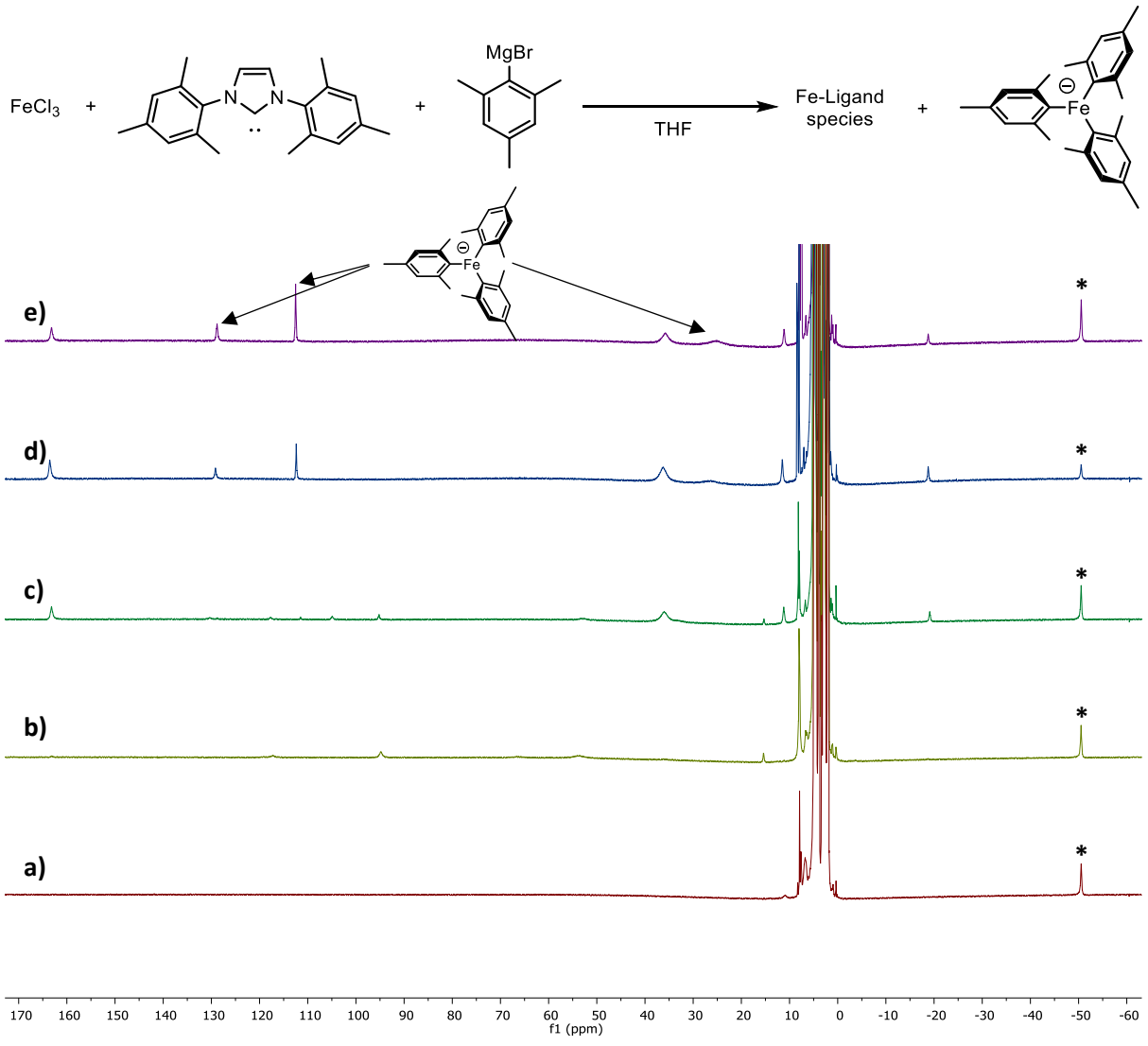

Figure 5.6: ^{1}H NMR spectrum of the reaction mixture of $FeCl_3$ and IMes with a) 1 equivalent of MesMgBr, b) 2 equivalents of MesMgBr, c) 3 equivalents of MesMgBr, d) 5 equivalents of MesMgBr and e) 20 equivalents of MesMgBr. The * denotes the peak for cobaltocene (internal standard).

Whilst no paramagnetic species were observable upon the addition of 1 equivalent of MesMgBr to a mixture of $FeCl_3$ and IMes in THF (Figure 5.6a), the addition of 2 equivalents of MesMgBr formed species which were observable in paramagnetic region with broadened peaks at δ 117.15, 94.77, 66.26, 53.60 and 15.38 ppm (Figure 5.6b). At 3 equivalents of MesMgBr, only trace amounts of **4** was observed, with predominant peaks seen at δ 163.20, 35.82, 11.20 and -19.14 ppm (Figure 5.6c). The addition 5 equivalents of MesMgBr revealed the presence of **4**, accounting for ~ 41% of the iron in solution (Figure 5.6d). This is in stark contrast to the species present in the $FeCl_3$/**97** mixture where at 5 equivalents of MesMgBr the only observable species is **4**. For the $FeCl_3$/IMes mixture, peaks at δ 163.20, 35.82 and -19.14 ppm are still present which are tentatively assigned to [(IMes)Fe$(Mes)_2$] based on spectroscopic data of the analogous compound [(IPr)Fe$(Mes)_2$].[†] Most strikingly however, when increasing the amount of MesMgBr to 20 equivalents, the ^{1}H NMR spectrum looks mostly unchanged (Figure 5.6e). These results show that IMes forms a more stable complex with iron compared to **97**, most likely because of the stronger σ-donation from the carbene compared to the germylene, and the electron-poor Fe(II) only providing weak π-back-bonding to the Ge(II) centre.

As mentioned previously, the bulkiness of the mesityl ligand helps to stabilise organometallic complexes that may not actually form under normal catalytic conditions. This is compounded by the fact that they usually do not make effective cross-coupling partners, with reactions either being very sluggish or not working at all (see Chapter 1). Indeed, the cross-coupling reaction of MesMgBr and cyclohexyl bromide afforded none of the desired product **101** after 24 hours with either IMes, **97** or no ligand (Scheme 5.7a). When using the less sterically demanding electrophile bromooctane however, compound **102** was produced in 11% yield when using **97** and 19% yield when using IMes (Scheme 5.7b).

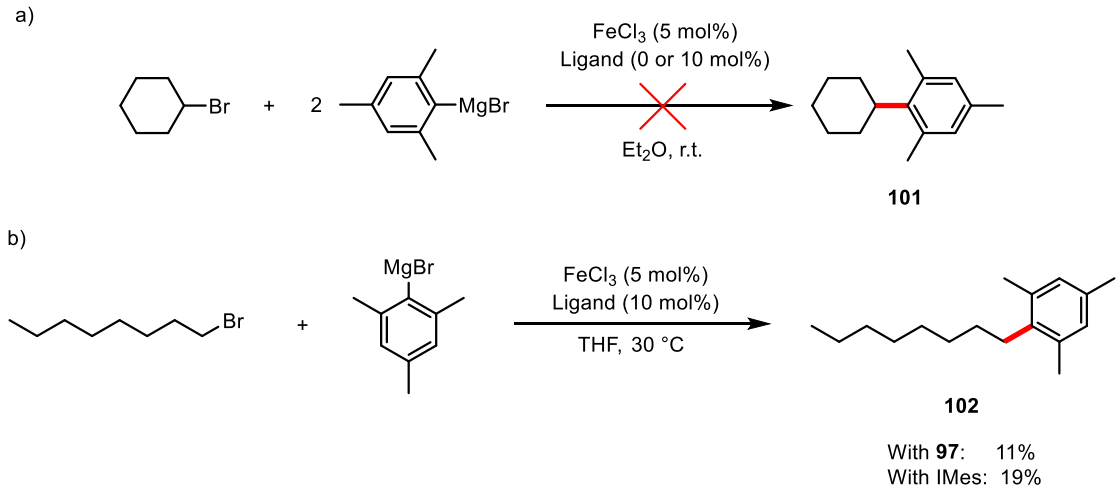

Scheme 5.7: Iron-catalysed cross-coupling of MesMgBr with a) bromocyclohexane and b) bromooactane.

[†] Unpublished data. [(IPr)Fe$(Mes)_2$] isolated and characterised by Nimisha Raj Sharma.

A reaction profile showing the production of **102** over time is shown in Figure 5.7. In contrast to when *p*-tolylmagnesium bromide is used as a nucleophile, no induction period is observed when employing the germylene ligand. There is a slight increase in the production of **102** when using IMes. However, this concurs with previous observations that whilst mesityl ligands are useful for probing the possible organometallic speciation present in catalytic reaction mixtures, care must be taken as they are not representative of the overall synthetic methodology.

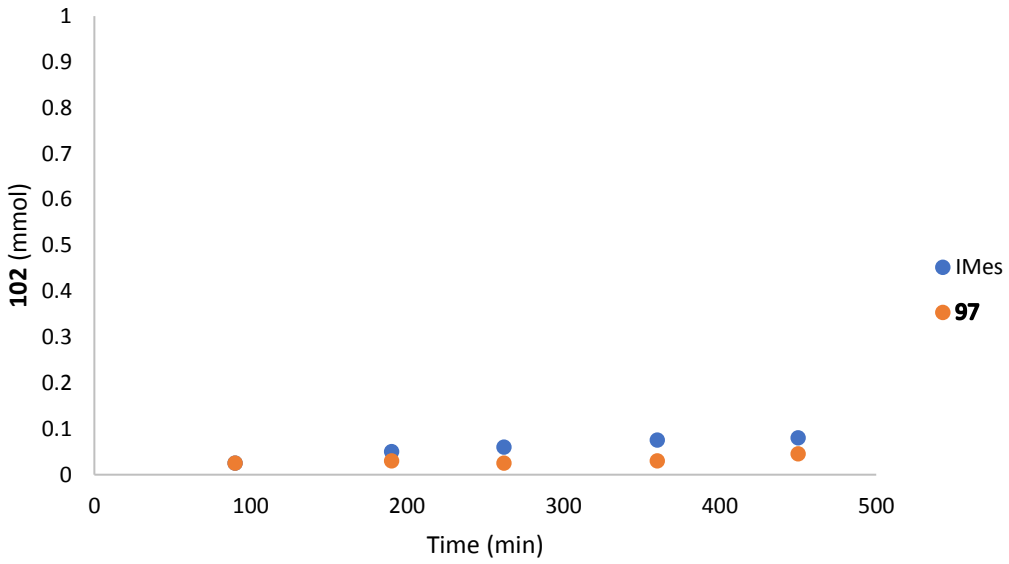

Figure 5.7: Formation of **102** over time with either IMes or **97** as ligand.

Overall, conditions have been developed where the germylene ligand **97** outperforms its carbene analogue IMes in an iron-catalysed Kumada cross-coupling reaction. Intriguingly, it appears that the weaker coordination of the germylene ligand to iron is responsible for this observed activity. Synthesis of two different organometallic iron complexes bearing germylene **97** was attempted next to gain insight into the nature of the bonding between the two elements.

5.3 Attempted Isolation of Iron-Germylene Complexes

The first example of a germanium-iron complex was reported by Helling and co-workers in 1962.[186] The reduction of cyclopentadienyl iron dicarbonyl dimer with sodium amalgam before addition of triphenylgermanium bromide produces the air- and moisture-stable complex **103** (Figure 5.8a). Since then, there has been interest in ligand architectures where the germylene atom is flanked by two nitrogen atoms, allowing for intramolecular donation of electron density to the germylene atom (c.f. NHCs). This stabilises the singlet form of the carbene, increasing the germylene's Lewis basicity, i.e. its σ-donor ability, allowing for better coordination to other metals. One such example is from Barrau and co-workers where a heterogermylene is supported by a β-diiminate ligand; a reaction with Fe_2CO_9 affords the halogermylene-iron complex **104** (Figure 5.8b).[187] Interestingly, the metal-metal bond distance in this complex is small, and calculations suggest that the ligand possesses strong σ-donation with weaker π-acceptor potential. Another example of an effective *N*,*N*'-chelating ligand is the amidinato ligand which stabilises a heterogermylene in complex **105** (Figure 5.8c).[188] Finally, an alternative way of increasing electron density at the germylene-centre is by using a highly σ-donating NHC co-ligand coordinated to a heterogermylene, shown in Figure 5.8d.[188] As can be seen, Fe(0) supported by CO ligands is a common occurrence for iron-germylene complexes.

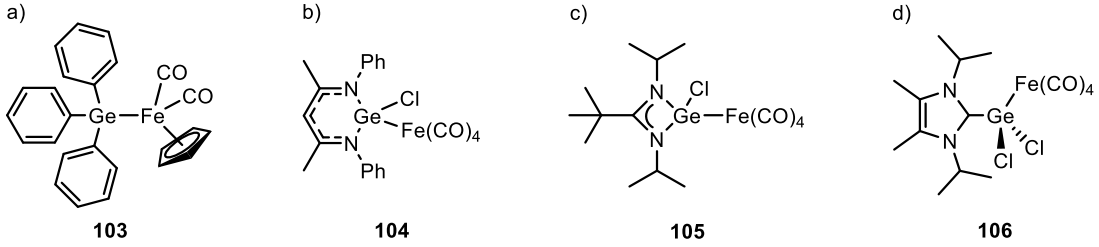

Figure 5.8: Examples of iron-germylene complexes by a) Helling[186], b) Barrau[187] and c-d) Madec[188].

Although examples of iron germylene complexes exist, there have been no reports of any bearing the germylene ligand **97**. The only example of an organometallic complex bearing ligand **97** is a copper complex reported by Tolman and co-workers.[185] To gain further insight into the organometallic complexes that may be formed when reacting a solution of $FeCl_3$ and **97** with fewer than 5 equivalents of mesitylmagnesium bromide, the synthesis of complex **107** was attempted. Iron NHC compounds bearing mesityl ligands have been prepared previously by Radius and co-workers by adding the carbene to the homoleptic iron dimer $[Fe_2(Mes)_4]$. Here, C_6D_6 was added to $[Fe_2(Mes)_4]$ and 2 or 4 equivalents of **97** in vial in a glovebox and the solution left for 1 hour. The ^{1}H NMR spectrum of the crude reaction mixture of $[Fe_2(Mes)_4]$ with 2 equivalents of **97** is shown in Figure 5.9.

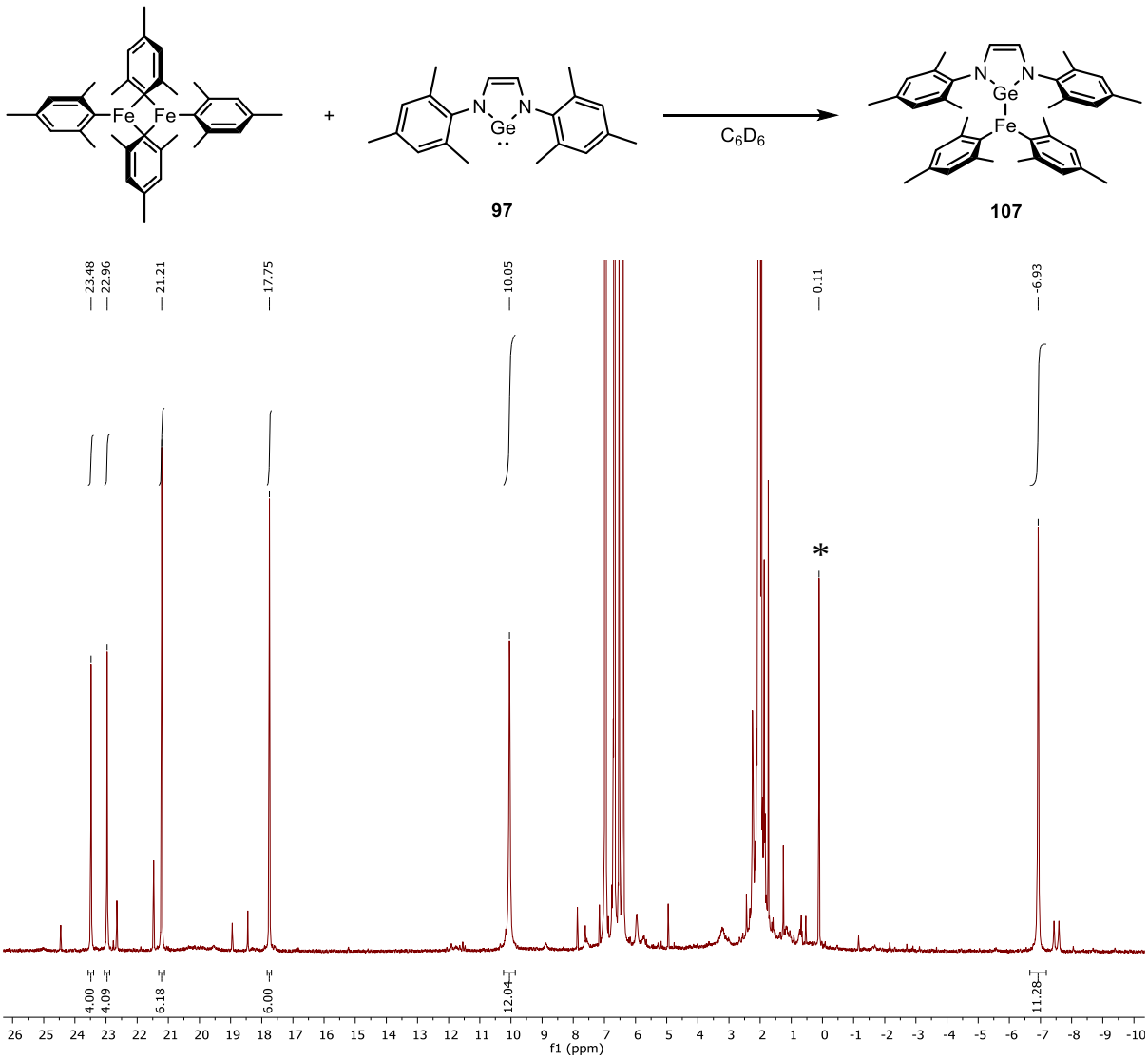

Figure 5.9: ^{1}H NMR spectrum of the crude reaction mixture of $[Fe_2(Mes)_4]$ and 2 equivalents of **97** with resonances tentatively assigned to **107**. * denotes the presence of vacuum grease.

The ^{1}H NMR spectrum revealed the complete consumption of $[Fe_2(Mes)_4]$ and the presence of paramagnetically shifted peaks which are tentatively assigned to compound **107**. Two singlets at δ 23.48 and 22.96 ppm correspond to 4H (Ar-H), whilst another set of two singlets at δ 21.21 (6H) and 17.75 (6H) ppm can be assigned to the *para* methyl protons on the mesityl rings on both the iron atom and ligand. Finally, the *ortho* methyl groups on the mesityl rings on both the ligand and iron-centre are given as two singlets at δ 10.05 (12H) and -6.93 ppm (12H). No definitive peak in the spectrum could be assigned for the backbone protons on the *N*-heterocyclic ring of the germylene ligand, with a spectrum width of – 45 to 195 ppm showing little else in the paramagnetic region. It is likely that the peak is hidden by the large peaks seen for the residual ligand. The ^{1}H NMR spectrum showed little change after the reaction mixture was left overnight, and addition of 4 equivalents of **97** to $[Fe_2(Mes)_4]$ gave an identical ^{1}H NMR spectrum to that obtained in Figure 5.9. This is in line with only one germylene ligand being able to coordinate iron when bulky mesitylene ligands are present.

Unfortunately, due to the relatively low conversion to complex **107** (determined spectroscopically by the ratio of **107** to unreacted **97**), the isolation of pure **107** was not achieved, precluding any further characterisation. As discussed earlier, many isolated examples of iron germylene complexes contain an electron-rich Fe(0) centre. This presumably facilitates enhanced π-back-donation from the Fe(0) centre to the Ge(II) atom; compared with π-back-bonding from a more electron-poor Fe(II) centre to a Ge(II) atom. Therefore, complex **108**, the germylene analogue of Deng's Fe(0) complex[143] (see Section 3.2) was targeted, first using using Na/Hg amalgam as a reducing agent.

The addition of a THF solution of $FeCl_2$, **97** and dvtms to Hg/Na caused the yellow solution to gradually turn a very dark yellow/brown. After leaving the reaction to stir at room temperature overnight, the solution was filtered through Celite and the solvent removed *in vacuo* which unfortunately only recovered ligand **97**. Repeating the procedure with the highly reducing agent KC_8 also gave a change from a yellow to dark brown mixture. The ^{1}H NMR of an aliquot removed from the reaction mixture (Figure 5.10) showed peaks in the paramagnetic region at δ -6.55, -12.33 and -14.39 ppm, however at a much lower intensity than observed in crude mixtures for the synthesis of Deng's complex (Section 3.2). Unfortunately, attempts at isolating the pure paramagnetic complex were not successful, precluding any further characterisation.

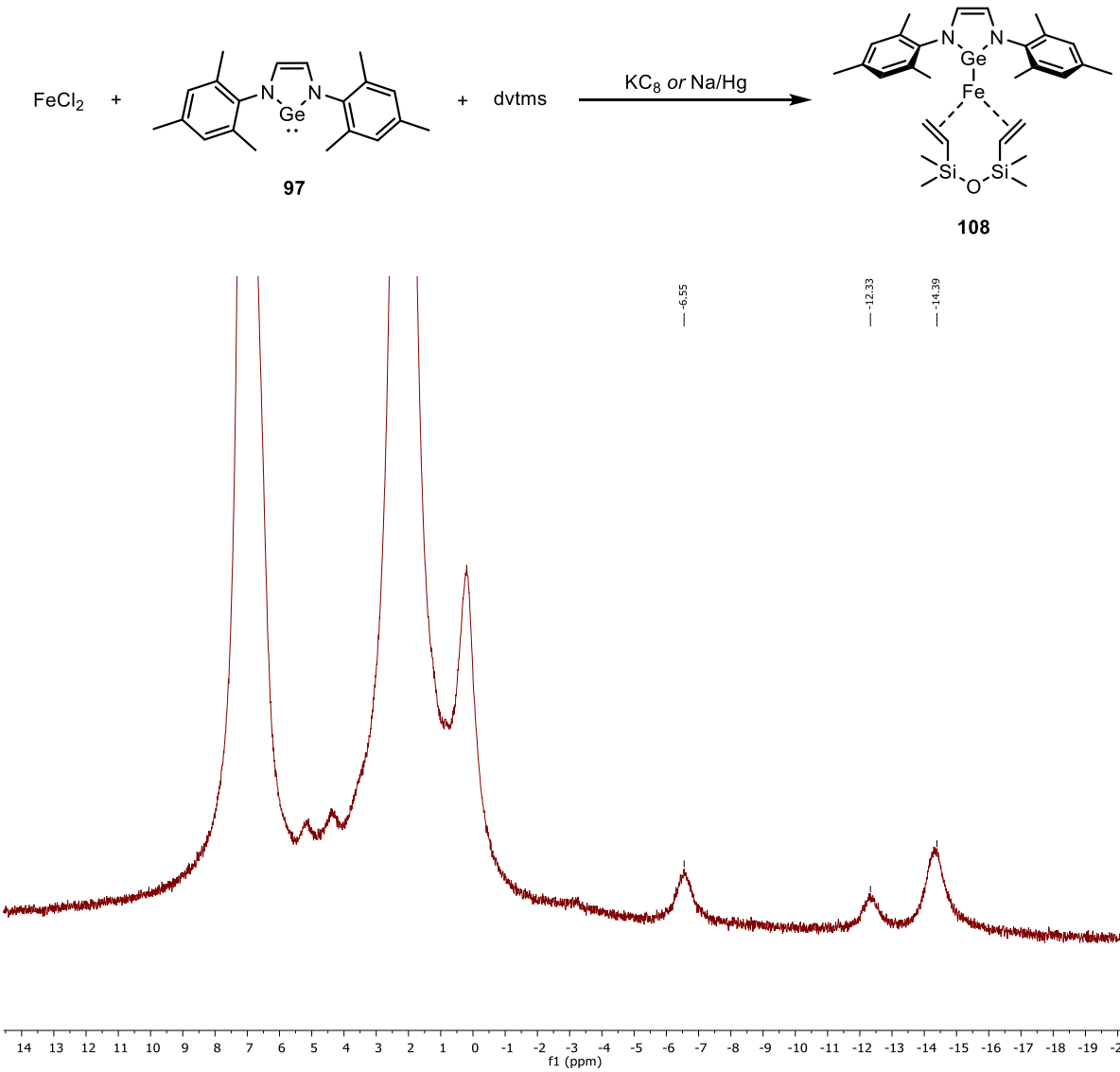

Figure 5.10: ^{1}H NMR spectrum of the crude reaction mixture of Fe(0) complex **108**.

5.4 Conclusions

In conclusion, two analogous *N*-heterocyclic ligands, bearing either C or Ge as the coordinating element, have been investigated by comparing their activity in cobalt- and iron-catalysed cross-coupling reactions (Figure 5.11). Whilst the commonly employed carbene ligand IMes proved to be superior at facilitating cobalt- and iron-catalysed Suzuki biaryl cross-coupling reactions (where a strong ligand dependence is observed), the germylene ligand **97** was more successful when used in an iron-catalysed cross-coupling reaction between cyclohexyl bromide and *p*-tolylmagnesium bromide. Insight into this behaviour was given by showing that IMes forms a stronger bond with iron than **97**. In the presence of only 5 equivalents of a sterically demanding Grignard reagent (MesMgBr) to an $FeCl_3$ and **97** mixture, **4** is the sole observable paramagnetic species. Conversely, even with 20 equivalents of MesMgBr to a $FeCl_3$ and IMes mixture, **4** appears to be in equilibrium with what is tentatively assigned as [(IMes)Fe$(Mes)_2$]. The difference in catalytic activity between the two ligands could therefore be attributed to the ease in which homoleptic 'ate' complexes are formed in the reaction mixture, although further studies with less sterically demanding Grignard reagents would be needed to confirm this.

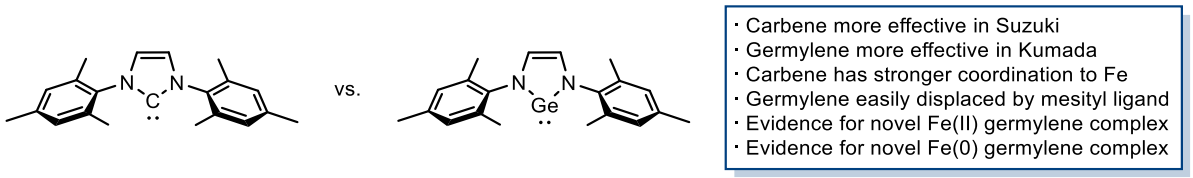

Figure 5.11: A comparison between IMes and **97** as ligands for cobalt- and iron-catalysed cross-coupling reactions.

Although attempts to isolate two novel iron germylene complexes were not successful here, strong evidence for the formation of [(**97**)Fe$(Mes)_2$] was gained through ^{1}H NMR analysis of the reaction between [$Fe_2(Mes)_4$] and **97**. Evidence for the formation of [(**97**)Fe(dvtms)] was also shown from the reduction of $FeCl_2$ by KC_8 the presence of **97** and dvtms. Future endeavours should focus on the isolation of these compounds to gain insight into the structure of these complexes. This would facilitate an analysis of the differences in bonding between the germylene and carbene when coordinated to an iron centre. Also, given the apparent weaker coordination of **97** compared to IMes, synthesis of iron germylene complexes bearing electron-rich Fe(0) centres should be prioritised.

Chapter 6
Future Work

6.1 Substrate-Directed Iron-Catalysed Suzuki Biaryl Cross-Coupling

In Chapter 2, it was shown that iron-catalysed Suzuki biaryl cross-coupling is an achievable goal. However, to be considered a replacement for palladium-based Suzuki cross-couplings, the first caveat that needs to be overcome is the requirement of the directing group. Indeed, it was shown that removal of the directing group causes a drastic drop in yield of the cross-coupled product (Scheme 6.1). Yet importantly, the reaction is still able to turnover. This shows that with catalyst design, the issues with aryl halide activation can be overcome and a method for iron-catalysed Suzuki biaryl synthesis is within reach.

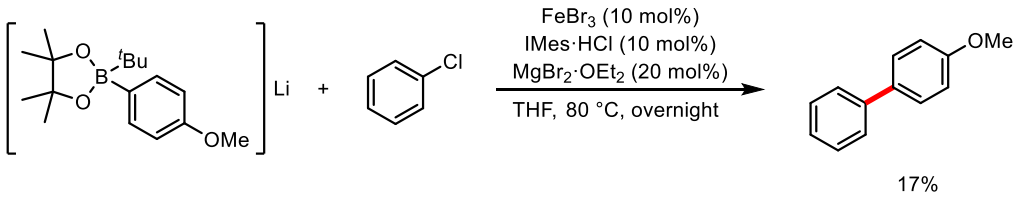

Scheme 6.1: Undirected Suzuki cross-coupling.

The second caveat is the requirement for pyrophoric ^{t}BuLi to activate the boronate ester. Unpublished results from the Bedford group shows that the addition of conventional bases does not promote Earth abundant metal Suzuki cross-couplings, however an important contribution from Duong and co-workers shows that KOMe can be utilised to great effect with the correct boronate ester.[114] Future endeavours should therefore focus on screening a range of boronate esters with a variety of bases in both directed and undirected iron-catalysed Suzuki biaryl cross-coupling reactions.

In Chapter 3, a mechanistic study allowed for the proposal of a catalytic cycle for the Suzuki reaction. Lacking from this study however was information on the iron-based species in the reaction. It seems highly likely that the IMes ligand is bound to the iron-centre during the reaction, and that Fe(II) appears to be the bulk oxidation state of the metal during the reaction, whilst oxidation state Fe(0) is also accessible. Therefore, synthesis of potential intermediates of a variety of oxidation states bearing IMes and the examination of their reactivity could aid the discovery of catalyst architectures that could be active in the undirected reaction.

6.2 Iron-Catalysed Asymmetric Cross-Coupling of 2-Bromo-1-Phenylpropane

In Chapter 4, an attempt to broaden the scope of Nakamura's enantioconvergent cross-coupling was unsuccessful. It appears that for now, the methodology is restricted to α-arylalkanoates substrates. However, an investigation into the Negishi- and Suzuki-variant of the enantioconvergent reaction with α-arylalkanoates would still be useful to help expand the scope of this reaction (Scheme 6.2).

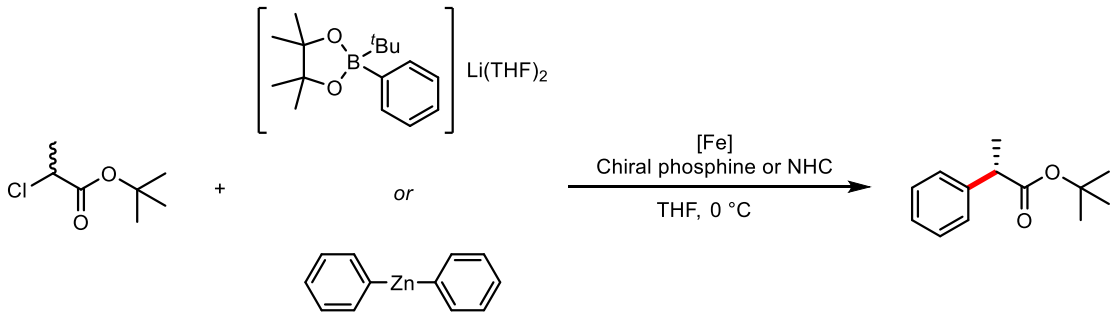

Scheme 6.2: Suzuki- and Negishi-type enantioconvergent cross-coupling.

Also, Nakamura only investigated P-chiral ligands for the enantioconvergent cross-coupling. With the success shown in Chapter 2 using NHC ligands in a Suzuki reaction, the use of asymmetric NHCs could enable the production of chiral products with higher ee than the modest ee's achieved by Nakamura.

6.3 Comparison of an *N*-Heterocyclic Carbene and Germylene Ligand in Iron-Catalysed Cross-Couplings

In Chapter 5, a comparison between the activity of an *N*-heterocyclic carbene and an *N*-heterocyclic germylene ligand in cobalt- and iron-catalysed cross-couplings was carried out. Intriguingly, mechanistic investigations showed how the germylene ligand is far more labile compared to its carbene analogue. To fully assess the effect of germylene ligands in iron-catalysis, a range, such as those shown in Figure 6.1, should be investigated. These represent the germylene analogues of the most utilised carbene ligands in iron-catalysed cross-couplings.

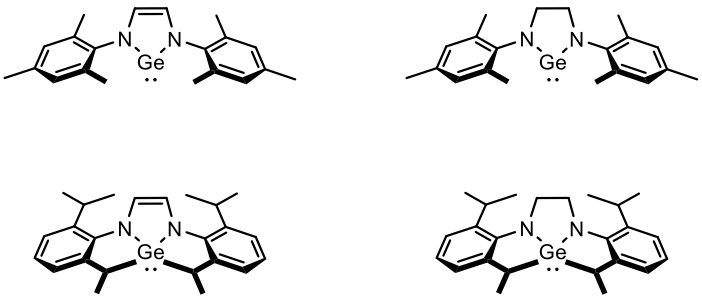

Figure 6.1: Suggested germylene ligands to be investigated in iron-catalysed cross-coupling reactions.

From an organometallic perspective, it would be very interesting to isolate a new class of iron-germylene compounds. In Chapter 5 it was found that the lability of the ligand was problematic for the isolation of new iron-germylene complexes. Two avenues of investigation are offered; the first would be to utilize [Fe_2CO_9] as an iron source since there has been much success in using this complex to coordinate germylene moieties (Scheme 6.3a). Second, the germylene ligand shown in Scheme 6.3b has been shown by Szilvási and Benedek to be a very strong σ-donor (almost as strong as IPr).[189] Therefore, this should be investigated for the synthesis of Fe(II)/Fe(III)-germylene complexes which are exceedingly rare.

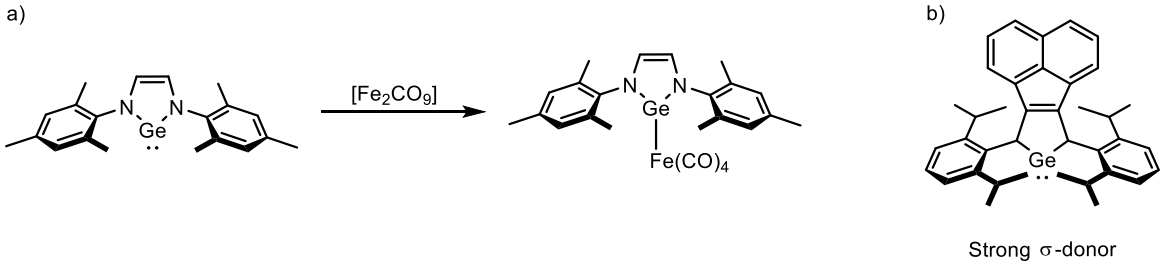

Scheme 6.3: a) Reaction of germylene ligand with [Fe_2CO_9] and b) germylene ligand shown by Szilvási and Benedek to be a particularly strong σ-donor[189].

Chapter 7
Experimental

7.1 General Considerations

All reactions were carried out in an inert atmosphere of nitrogen or argon using standard Schlenk-line or glovebox techniques unless specified otherwise. All reagents purchased from commercial suppliers were used as received without further purification. THF, CH_2Cl_2, toluene and hexane and were dried using an Anhydrous Engineering alumina column drying system and all other solvents were dried over 3 Å or 4 Å molecular sieves. TLC was performed on Silica Gel 60 F^{254} (Merck) and visualised using UV light (254 nm). Flash column chromatography was performed using technical grade silica gel, pore size 60 Å, 230-400 mesh particle size. Preparative TLC was performed using Analtech Uniplates with a 2,000 μm layer thickness of silica gel with fluorescent indicator and visualised using UV light (254 nm). NMR spectra were recorded on Bruker Nano 400, Varian 400-MR or Bruker Advance III HD 500 cryo spectrometers. Chemical shifts (δ) are quoted in parts per million (ppm), referenced to the residual solvent peak and coupling constants (*J*) are given in Hz. Multiplicities are abbreviated as: a (apparent), br (broad), s (singlet), d (doublet), t (triplet), q (quartet), p (pentet), h (heptet), m (multiplet) or combinations thereof. In a number of cases the ^{13}C resonance for the carbon atom directly bonded to boron was not observed due to the effect of quadrupolar relaxation. Mass spectrometry was performed by the University of Bristol mass spectrometry service by electrospray ionisation (ESI) using a micrOTOF II spectrometer. Infrared spectra were recorded using a Perkin Elmer Spectrum Two FT-IR spectrometer. Melting points were determined using a Stuart Scientific Melting Point Apparatus SMP3. GC-FID analysis was performed using an Agilent Technologies 7820A, with quantification implemented using calibration curves obtained from a minimum of five different concentrations of the samples being investigated with dodecane used as an internal standard. TEM samples were imaged using a JEOL 2100 TEM operating at 200 kV. TEM images were acquired using a Gatan Orius SC1000 digital camera. EDX analysis and elemental mapping were performed in HAADF-STEM mode with a spot size of 1.5 nm using an Oxford Instruments Aztec X-ray system.

7.2 Substrate-Directed Iron-Catalysed Suzuki Biaryl Cross-Coupling: Methodology

4-Methoxyphenylboronic acid pinacol ester;[190] *Li[Bpin(2-Me-thiophene)]*[t]*Bu] (**49**);*[133] *2-chloro-N-phenylbenzamide (**33**);*[129] *2-chloro-4-cyanobenzoic acid;*[191] *diimine **22**;*[124] *diimine **23**;*[126] *diamine **24**;*[127] *IXyl(2,6)·HCl;*[124] *SIXyl(3,5)·HCl;*[126] *ITol·HCl*[125] *and activated B_2pin_2 **80***[137] *were prepared according to literature procedures.*

7.2.1 Preparation of Activated Aryl Borates

Note: The residual THF content in borate **18** was determined by single crystal X-ray analysis. The broadened resonances for the THF protons are observable in the NMR spectra, but not for all borate compounds (i.e. borate **44**, and borates synthesised in hexane solvent). Integration of the observable THF resonances often produced values lower than expected, suggesting that exchange is occurring with the THF-d8 solvent used for the NMR experiments.

Preparation of **18**

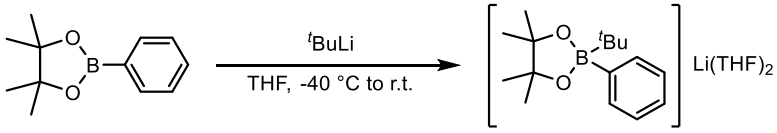

To a 500 ml Schlenk-flask was added phenylboronic acid pinacol ester (18.366 g, 90 mmol) and THF (120 ml). The solution was cooled to -40 °C (acetonitrile/liq. N_2 bath) and *tert*-butyllithium (Caution! 1.7 M in pentane, 49.4 ml, 84 mmol) was added slowly causing the solution to turn pale-yellow. The solution was stirred for 45 min and then warmed to room temperature and stirred for another 45 min before being concentrated to ~ 40 ml in volume. This was layered with hexane (~ 40 ml) and left overnight allowing a layer of crystals to form (suitable for single crystal X-ray diffraction). The Schlenk-flask was then placed in the freezer for 2 h causing the rest of the product to precipitate. The solvent was removed via cannula filtration and the solids washed with hexane (3 x 30 ml). Drying the solid overnight under vacuum afforded the titled compound (29.483 g, 82%) as an air- and moisture-sensitive colourless solid, which decomposes within 20 mins under air. **^{1}H NMR** (400 MHz, THF-d_8) δ 7.38 (d, *J* = 6.7 Hz, 2H), 6.94 (t, *J* = 7.3 Hz, 2H), 6.82 – 6.78 (m, 1H), 3.64 – 3.60 (m, 4H), 1.79 – 1.76 (m, 4H), 1.13 (s, 6H), 0.83 (s, 6H), 0.63 (s, 9H). **^{13}C{^{1}H} NMR** (101 MHz, THF-d_8) δ 133.4, 125.9, 123.2, 78.5, 68.4, 30.9, 28.6, 28.2, 26.5. **^{11}B{^{1}H} NMR** (128 MHz, THF-d_8) δ 8.10.

Preparation of **44**

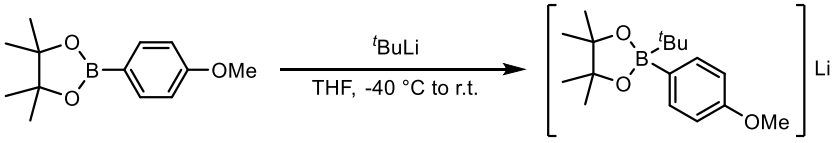

To a 500 ml Schlenk-flask was added 4-methoxyphenylboronic acid pinacol ester (17.558 g, 75 mmol) and THF (120 ml). The solution was cooled to -40 °C (acetonitrile/liq. N_2 bath) and *tert*-butyllithium (Caution! 1.7 M in pentane, 41.2 ml, 70 mmol) was added slowly causing the solution to turn pale-yellow. The solution was stirred for 30 min and then warmed to room temperature and stirred for 45 min before the volatiles were removed *in vacuo* affording a pale-yellow viscous gum. Hexane (40 ml) was added and the mixture sonicated for 1 h resulting in the formation of a precipitate. The solvent was removed *via* cannula filtration and the solid dried *in vacuo* overnight affording the title compound (16.939 g, 81%) as an as an air- and moisture-sensitive colourless solid. **^{1}H NMR** (400 MHz, THF-d_8) δ 7.28 (d, J = 8.4 Hz, 2H), 6.57 (d, J = 8.4 Hz, 2H), 3.65 (s, 3H), 1.14 (s, 6H), 0.85 (s, 6H), 0.63 (s, 9H). **^{13}C{^{1}H} NMR** (101 MHz, THF-d_8) δ 157.4, 133.9, 111.7, 78.5, 54.9, 30.9, 28.7, 28.2. **^{11}B{^{1}H} NMR** (128 MHz, THF-d_8) δ 8.13.

Preparation of **45**

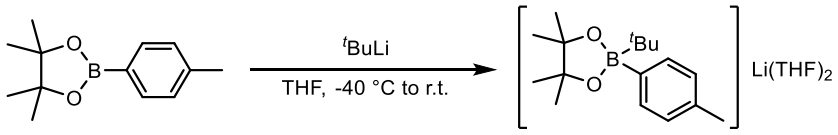

To a Schlenk-flask was added 4-methylphenylboronic acid pinacol ester (1.4395 g, 6.6 mmol) and THF (15 ml). The solution was cooled to -40 °C (acetonitrile/liq. N_2 bath) and *tert*-butyllithium (Caution! 2.57 M in pentane, 2.33 ml, 6 mmol) was added slowly causing the solution to turn pale-yellow. The solution was stirred for 30 min and then warmed to room temperature and stirred for 45 min before the volatiles were removed *in vacuo* affording a pale-yellow viscous gum. Hexane (20 ml) was added and the mixture sonicated for 1 h resulting in the formation of a precipitate. The solvent was removed *via* cannula filtration and the solid dried *in vacuo* affording the title compound (2.185 g, 85%) as an as an air- and moisture-sensitive cream-coloured solid. **^{1}H NMR** (400 MHz, THF-d_8) δ 7.24 (d, J = 7.6 Hz, 2H), 6.78 (d, J = 7.5 Hz, 2H), 3.63 – 3.59 (m, 4H), 2.18 (s, 3H), 1.78 – 1.75 (m, 4H), 1.11 (s, 6H), 0.82 (s, 6H), 0.60 (s, 9H). **^{13}C{^{1}H} NMR** (101 MHz, THF-d_8) δ 133.0, 131.1, 126.5, 78.1, 68.0, 30.6, 28.6, 27.8, 26.2, 21.2. **^{11}B{^{1}H} NMR** (128 MHz, THF-d_8) δ 8.21.

Preparation of **48**

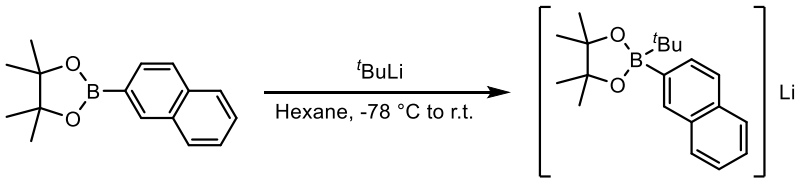

To a Schlenk-flask was added 2-naphthylboronic acid pinacol ester (1.677 g, 6.6 mmol) and hexane (40 ml). The solution was cooled to -78 °C and *tert*-butyllithium (Caution! 1.7 M in pentane, 3.53 ml, 6 mmol) was added slowly. The mixture was stirred for 30 min and then warmed to room temperature and stirred overnight, after which a white precipitate was present. The solvent was removed *via* cannula

filtration and the remaining solid washed with hexane (3 x 15 ml) and dried *in vacuo* affording the title compound (1.958 g, 93%) as an air- and moisture-sensitive colourless solid. **^{1}H NMR** (400 MHz, THF-d_8) δ 7.99 (s, 1H), 7.95 (d, J = 8.1 Hz, 1H), 7.81 (d, J = 8.3 Hz, 2H), 7.65 (d, J = 8.1 Hz, 1H), 7.40 – 7.31 (m, 2H), 1.38 (s, 6H), 1.04 (s, 6H), 0.89 (s, 9H). **^{13}C{^{1}H} NMR** (101 MHz, THF-d_8) δ 134.5, 134.5, 132.9, 130.5, 128.2, 128.1, 124.2, 124.1, 123.2, 78.7, 31.0, 28.7, 28.2. **^{11}B{^{1}H} NMR** (128 MHz, THF-d_8) δ 8.19.

Preparation of **46**

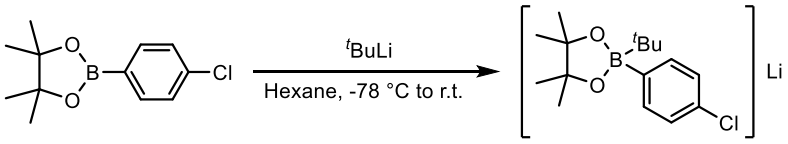

To a Schlenk-flask was added 4-chlorophenylboronic acid pinacol ester (1.572 g, 6.6 mmol) and hexane (30 ml). The solution was cooled to -78 °C and *tert*-butyllithium (Caution! 1.7 M in pentane, 3.53 ml, 6 mmol) was added slowly. The mixture was stirred for 30 min and then warmed to room temperature and stirred overnight, after which a white precipitate was present. The solvent was removed *via* cannula filtration and the remaining solid washed with hexane (3 x 15 ml) and dried *in vacuo* affording the title compound (1.143 g, 63%) as an air- and moisture-sensitive colourless solid. **^{1}H NMR** (400 MHz, THF-d_8) δ 7.37 (d, J = 8.2 Hz, 2H), 6.90 (d, J = 8.2 Hz, 2H), 1.10 (s, 6H), 0.79 (s, 6H), 0.59 (s, 9H). **^{13}C{^{1}H} NMR** (101 MHz, THF-d_8) δ 135.3, 128.8, 125.4, 78.5, 30.7, 28.7, 28.3. **^{11}B{^{1}H} NMR** (128 MHz, THF-d_8) δ 7.56.

Preparation of **73**

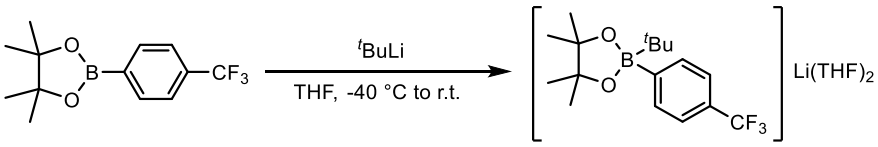

To a Schlenk-flask was added 4-trifluoromethylphenylboronic acid pinacol ester (1.7957 g, 6.6 mmol) and THF (15 ml). The solution was cooled to -40 °C (acetonitrile/liq. N_2 bath) and *tert*-butyllithium (Caution! 2.57 M in pentane, 2.33 ml, 6 mmol) was added slowly causing the solution to turn pale-yellow. The solution was stirred for 30 min and then warmed to room temperature and stirred for another 30 min before being concentrated to ~ 5 ml in volume. This was layered with hexane (~ 8 ml) and left overnight allowing a layer of crystals to form. The Schlenk-flask was then placed in the freezer for 6 h causing the rest of the product to precipitate. The solvent was removed via cannula filtration and the solids washed with hexane (2 x 10 ml). Drying the solid overnight under vacuum afforded the titled compound as an air- and moisture-sensitive colourless solid. **^{1}H NMR** (400 MHz, THF-d_8) δ 7.59 (d, J = 7.6 Hz, 2H), 7.18 (d, J = 7.7 Hz, 2H), 3.63 – 3.60 (m, 4H), 1.79 – 1.76 (m, 4H), 1.09 (s, 6H), 0.76 (s, 6H), 0.59 (s, 9H). **^{13}C{^{1}H} NMR** (101 MHz, THF-d_8) δ 133.9, 121.7, 78.5, 68.4, 30.7, 28.7, 28.4, 26.6,

26.0 (C-F splitting not observed due to low concentration of sample). **^{11}B{^{1}H} NMR** (128 MHz, THF-d_8) δ 7.42. **^{19}F{^{1}H} NMR** (377 MHz, THF) δ -61.53.

7.2.2 General Procedure 1 (GP1): Preparation of N-Pyrrole Amide Substrates

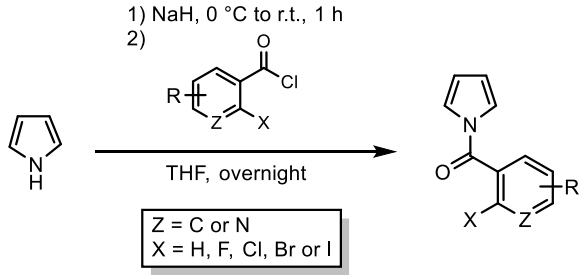

To a 100 ml round-bottom flask was added pyrrole (0.347 ml, 5 mmol) and THF (20 ml). The solution was cooled to 0 °C and sodium hydride (60% dispersion in mineral oil, 200 mg, 5 mmol) was added in one portion. The mixture was stirred for 30 min during which effervescence was observed, and then warmed to room temperature and stirred for a further 30 min. The mixture was then cooled to 0 °C and the appropriate aryl acid chloride (5.5 mmol) was added in one portion. The resulting mixture was warmed to room temperature and stirred overnight. The reaction was quenched by the addition of 1 M HCl (10 ml) and the organics extracted from the aqueous layer with CH_2Cl_2 (3 x 15 ml). The organic fractions were combined, dried over $MgSO_4$, filtered and the solvent removed under reduced pressure to afford the crude compound which was purified by flash column chromatography.

7.2.3 General Procedure 2 (GP2): Preparation of *N*-Pyrrole Amide Substrates

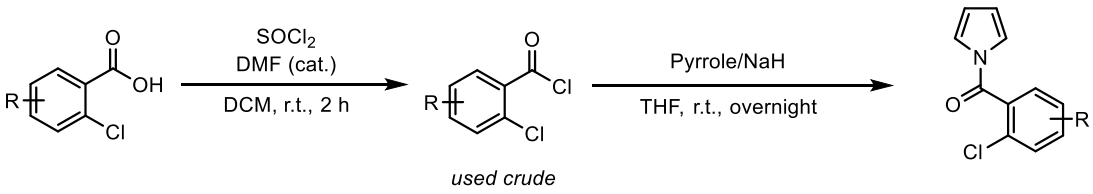

To a 100 ml round-bottom flask was added the appropriate benzoic acid (5.5 mmol), CH_2Cl_2 (20 ml) and DMF (5 drops). Thionyl chloride (4.01 ml, 55 mmol) was added slowly and the solution stirred for 2 h at room temperature. The solvent and excess thionyl chloride were then removed *in vacuo* and the residue dissolved in THF (20 ml). In a separate 100 ml round-bottom flask was added pyrrole (0.347 ml, 5 mmol) and THF (20 ml). The solution was cooled to 0 °C and sodium hydride (60% dispersion in mineral oil, 200 mg, 5 mmol) was added in one portion. The mixture was stirred for 30 min during which effervescence was observed, and then warmed to room temperature and stirred for a further 30 min. The mixture was then cooled to 0 °C and the crude acid chloride mixture was added *via* cannula. The reaction was warmed to room temperature and was left stirring overnight before being quenched by the addition of 1 M HCl (10 ml) and the organics extracted from the aqueous layer with CH_2Cl_2 (3 x 15 ml). The organic fractions were combined, dried over $MgSO_4$, filtered and the solvent removed

under reduced pressure to afford the crude compound which was purified by flash column chromatography.

7.2.4 *N*-Pyrrole Amides Obtained from GP1 and GP2

(2-Chlorophenyl)(1*H*-pyrrol-1-yl)methanone (**17**)

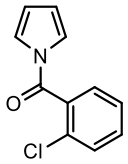

Prepared according to **GP1** from 2-chlorobenzoyl chloride. Flash column chromatography (10% Et_2O in petroleum ether) afforded the title compound as a colourless solid (0.683 g, 66%). **^{1}H NMR** (400 MHz, $CDCl_3$) δ 7.51 – 7.45 (m, 3H), 7.41 – 7.37 (m, 1H), 7.12 (bs, 2H), 6.33 (t, *J* = 2.4 Hz, 2H). **^{13}C{^{1}H} NMR** (101 MHz, $CDCl_3$) δ 165.3, 133.8, 131.9, 131.6, 130.2, 129.1, 126.9, 120.5 (b), 114.0. **IR (neat) ν_{max}**: 1698 ν(C=O), 1466, 1333, 1303, 1076, 1055, 883, 735, 652 cm^{-1}. Data in accordance with previously reported values.[192]

(2-Chlorophenyl)(1*H*-pyrrol-1-yl-d_4)methanone (**17-d_4**)

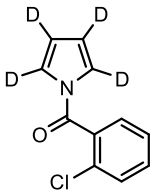

Prepared according to **GP1** from pyrrole-d_5 and 2-chlorobenzoyl chloride (14.88 mmol scale). In this case, after leaving the reaction overnight the resulting mixture was filtered (washing through with CH_2Cl_2) and purified by flash column chromatography (5% EtOAc in petroleum ether) followed by recrystallisation from petroleum ether to afford the title compound as a beige solid (2.193 g, 70%). **^{1}H NMR** (500 MHz, $CDCl_3$) δ 7.51 – 7.45 (m, 3H), 7.41 – 7.38 (m, 1H). **^{13}C{^{1}H} NMR** (126 MHz, $CDCl_3$) δ 165.3, 134.0, 132.0, 131.7, 130.3, 129.1, 127.0, 120.2 (bt, *J* = 29.3 Hz), 113.7 (t, *J* = 26.3 Hz). **HRMS (*m*/*z*)**: (ESI+) calculated for $C_{11}H_5ClD_4NO$ $[M+H]^+$: 210.0618. Found: 210.0608. **m.p.**: 44 – 45 °C. **IR (neat) ν_{max}**: 1697 ν(C=O), 1410, 1357, 1248, 1062, 886, 764, 604 cm^{-1}.

(2-Bromophenyl)(1*H*-pyrrol-1-yl)methanone

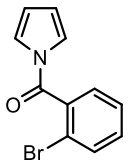

Prepared according to **GP1** from 2-bromobenzoyl chloride. Flash column chromatography (10% Et_2O in petroleum ether) afforded the title compound as a beige solid (0.949 g, 76%). **^{1}H NMR** (400 MHz,

$CDCl_3$) δ 7.67 (d, *J* = 7.7 Hz, 1H), 7.45 – 7.37 (m, 3H), 7.11 (bs, 2H), 6.33 (t, *J* = 2.4 Hz, 2H). **$^{13}C\{^1H\}$ NMR** (101 MHz, $CDCl_3$) δ 166.1, 136.2, 133.4, 132.1, 129.2, 127.6, 120.7 (b), 120.0, 114.2. **HRMS (*m*/*z*)**: (ESI+) calculated for $C_{11}H_8BrNNaO$ $[M+Na]^+$: 271.9681. Found: 271.9680. **m.p.**: 53 – 54 °C. **IR (neat) ν_{max}**: 1696 ν(C=O), 1466, 1335, 1304, 1098, 883, 734, 689, 645, 587 cm^{-1}.

(2-Iodophenyl)(1*H*-pyrrol-1-yl)methanone

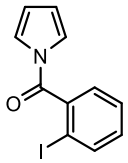

Prepared according to **GP1** from 2-iodobenzoyl chloride. Flash column chromatography (10% Et_2O in petroleum ether) afforded the title compound as a beige solid (0.891 g, 60%). **^1H NMR** (400 MHz, $CDCl_3$) δ 7.93 (d, *J* = 8.0 Hz, 1H), 7.48 (td, *J* = 7.5, 1.1 Hz, 1H), 7.39 (dd, *J* = 7.6, 1.8 Hz, 1H), 7.23 (td, *J* = 7.8, 1.8 Hz, 1H), 7.10 (bs, 2H), 6.34 (t, *J* = 2.4 Hz, 2H). **$^{13}C\{^1H\}$ NMR** (101 MHz, $CDCl_3$) δ 167.5, 140.2, 139.8, 132.0, 128.7, 128.2, 120.8, 114.2, 92.7. **HRMS (*m*/*z*)**: (ESI+) calculated for $C_{11}H_8INNaO$ $[M+Na]^+$: 319.9543. Found: 319.9538. **m.p.**: 43 – 44 °C. **IR (neat) ν_{max}**: 1694 ν(C=O), 1467, 1338, 1301, 1096, 1072, 883, 730, 682, 639, 588 cm^{-1}.

(2-Fluorophenyl)(1*H*-pyrrol-1-yl)methanone

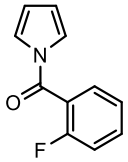

Prepared according to **GP1** from 2-fluorobenzoyl chloride. Flash column chromatography (10% Et_2O in petroleum ether) afforded the title compound as a beige solid (0.673 g, 71%). **^1H NMR** (400 MHz, $CDCl_3$) δ 7.57 – 7.51 (m, 2H), 7.27 (t, *J* = 7.9 Hz, 1H), 7.22 – 7.17 (bm, 3H), 6.32 (t, *J* = 2.2 Hz, 2H). **$^{13}C\{^1H\}$ NMR** (101 MHz, $CDCl_3$) δ 163.9, 159.6 (d, *J* = 252.9 Hz), 133.5 (d, *J* = 8.4 Hz), 130.4 (d, *J* = 2.3 Hz), 124.6 (d, *J* = 3.6 Hz), 122.4 (d, *J* = 15.3 Hz), 120.8, 116.6 (d, *J* = 21.1 Hz), 113.9. **$^{19}F\{^1H\}$ NMR** (377 MHz, $CDCl_3$) δ -112.4. **HRMS (*m*/*z*)**: (ESI+) calculated for $C_{11}H_9FNO$ $[M+H]^+$: 190.0663. Found: 190.0671. **m.p.**: 35 – 36 °C. **IR (neat) ν_{max}**: 3153, 1684 ν(C=O) 1612, 1470, 1334, 1090, 885, 745, 712, 657, 588, 535 cm^{-1}.

Phenyl(1*H*-pyrrol-1-yl)methanone (**27**)

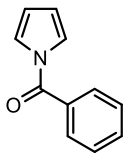

Prepared according to **GP1** from benzoyl chloride. Flash column chromatography (5% Et_2O in petroleum ether) afforded the title compound as a colourless oil (0.580 g, 68%). **^{1}H NMR** (400 MHz, $CDCl_3$) δ 7.77 – 7.74 (m, 2H), 7.61 (td, *J* = 7.5, 1.3 Hz, 1H), 7.53 – 7.49 (m, 2H), 7.29 (t, *J* = 2.3 Hz, 2H), 6.35 (t, *J* = 2.3 Hz, 2H). **^{13}C{^{1}H} NMR** (101 MHz, $CDCl_3$) δ 167.9, 133.5, 132.5, 129.7, 128.7, 121.5, 113.4. Data in accordance with previously reported values.[193]

(3-Chlorophenyl)(1*H*-pyrrol-1-yl)methanone

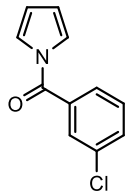

Prepared according to **GP1** from 3-chlorobenzoyl chloride. Flash column chromatography (10% Et_2O in petroleum ether) afforded the title compound as a colourless solid (0.683 g, 66%). **^{1}H NMR** (400 MHz, $CDCl_3$) δ 7.73 (t, *J* = 1.7 Hz, 1H), 7.62 (dt, *J* = 7.6, 1.5 Hz, 1H), 7.58 (dq, *J* = 8.1, 1.1 Hz, 1H), 7.46 (t, *J* = 7.8 Hz, 1H), 7.26 (t, *J* = 2.4 Hz, 2H), 6.37 (t, *J* = 2.6 Hz, 2H). **^{13}C{^{1}H} NMR** (101 MHz, $CDCl_3$) δ 165.8, 134.4, 134.4, 132.0, 129.6, 129.2, 127.3, 120.9, 113.4. Data in accordance with previously reported values.[194]

(4-Chlorophenyl)(1*H*-pyrrol-1-yl)methanone

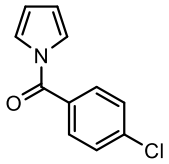

Prepared according to **GP1** from 4-chlorobenzoyl chloride. Flash column chromatography (10% Et_2O in petroleum ether) afforded the title compound as a colourless solid (0.683 g, 66%). **^{1}H NMR** (400 MHz, $CDCl_3$) δ 7.71 (d, *J* = 8.5 Hz, 2H), 7.50 (d, *J* = 8.5 Hz, 2H), 7.25 (t, *J* = 2.4 Hz, 2H), 6.36 (t, *J* = 2.3 Hz, 2H). **^{13}C{^{1}H} NMR** (101 MHz, $CDCl_3$) δ 166.9, 139.0, 131.8, 131.2, 129.1, 121.4, 113.7. Data in accordance with previously reported values.[195]

(2-Chloro-4,5-dimethoxyphenyl)(1*H*-pyrrol-1-yl)methanone

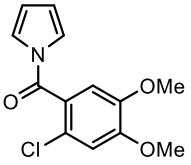

Prepared according to **GP2** from 2-chloro-4,5-dimethoxybenzoic acid. Flash column chromatography (10% EtOAc in petroleum ether) afforded the title compound as a grey solid (0.680 g, 48%). **^{1}H NMR** (400 MHz, $CDCl_3$) δ 7.15 (bs, 2H), 6.94 (d, *J* = 3.3 Hz, 2H), 6.33 (t, *J* = 2.1 Hz, 2H), 3.94 (s, 3H), 3.88

(s, 3H). **^{13}C{^{1}H} NMR** (101 MHz, $CDCl_3$) δ 165.4, 151.6, 148.0, 125.5, 124.0, 120.8, 113.9, 113.0, 111.8, 56.6, 56.6. **HRMS (*m*/*z*)**: (ESI+) calculated for $C_{13}H_{12}ClNNaO_3$ $[M+Na]^+$: 288.0398. Found: 288.0411. **m.p.**: 97 – 99 °C. **IR (neat) ν_{max}**: 2941, 1698 ν(C=O), 1466, 1298, 1261, 1217, 1168, 1098, 1208, 848, 791, 734, 660 cm^{-1}.

(2-Chloro-4-methoxyphenyl)(1*H*-pyrrol-1-yl)methanone

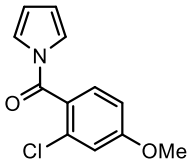

Prepared according to **GP2** from 2-chloro-4-methoxybenzoic acid. Flash column chromatography (10% EtOAc in petroleum ether) afforded the title compound as a colourless solid (0.498 g, 42%). **^{1}H NMR** (400 MHz, $CDCl_3$) δ 7.40 (d, *J* = 8.6 Hz, 1H), 7.14 (bs, 2H), 7.01 (d, *J* = 2.4 Hz, 1H), 6.90 (dd, *J* = 8.6, 2.4 Hz, 1H), 6.32 (t, *J* = 2.3 Hz, 2H), 3.87 (s, 3H). **^{13}C{^{1}H} NMR** (101 MHz, $CDCl_3$) δ 165.4, 162.1, 133.4, 130.8, 126.0, 120.8, 115.8, 113.8, 113.0, 56.0. **HRMS (*m*/*z*)**: (ESI+) calculated for $C_{12}H_{10}ClNNaO_2$ $[M+Na]^+$: 258.0292. Found: 258.0295. **m.p.**: 51 – 53 °C. **IR (neat) ν_{max}**: 3005, 1688 ν(C=O), 1330, 1304, 1242, 1093, 1029, 897, 847, 828, 746 cm^{-1}.

(2-Chloro-5-methoxyphenyl)(1*H*-pyrrol-1-yl)methanone

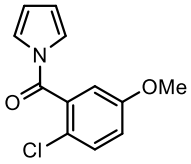

Prepared according to **GP2** from 2-chloro-5-methoxybenzoic acid. Flash column chromatography (5% EtOAc in petroleum ether) afforded the title compound as a beige solid (0.514 g, 44%). **^{1}H NMR** (400 MHz, $CDCl_3$) δ 7.37 (d, *J* = 8.8 Hz, 1H), 7.14 (bs, 2H), 7.00 (dd, *J* = 8.8, 3.0 Hz, 1H), 6.97 (d, *J* = 3.0 Hz, 1H), 6.33 (t, *J* = 2.3 Hz, 2H), 3.82 (s, 3H). **^{13}C{^{1}H} NMR** (101 MHz, $CDCl_3$) δ 165.2, 158.4, 134.6, 131.2, 122.7, 120.6 (b), 118.2, 114.1, 56.0. **HRMS (*m*/*z*)**: (ESI+) calculated for $C_{12}H_{10}ClNNaO_2$ $[M+Na]^+$: 258.0292. Found: 258.0294. **m.p.**: 50 – 51 °C. **IR (neat) ν_{max}**: 2850, 1699 ν(C=O), 1471, 1418, 1328, 1100, 1061, 1024, 915, 809, 738 cm^{-1}.

(2-Chloro-5-methylphenyl)(1*H*-pyrrol-1-yl)methanone

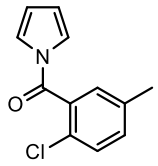

Prepared according to **GP2** from 2-chloro-5-methylbenzoic acid. Flash column chromatography (5% Et_2O in petroleum ether) afforded the title compound as a colourless oil (0.844 g, 77%). **^{1}H NMR** (400

MHz, $CDCl_3$) δ 7.37 – 7.35 (m, 1H), 7.29 – 7.26 (bm, 2H), 7.13 (bs, 2H), 6.33 (t, *J* = 2.3 Hz, 2H), 2.38 (s, 3H). **$^{13}C\{^1H\}$ NMR** (101 MHz, $CDCl_3$) δ 165.7, 137.3, 133.7, 132.8, 130.0, 129.6, 128.5, 120.7 (b), 114.0, 21.0. **HRMS (*m*/*z*)**: (ESI+) calculated for $C_{12}H_{10}ClNNaO$ $[M+Na]^+$: 242.0343. Found: 242.0342. **IR (neat) ν_{max}**: 2925, 1702 ν(C=O), 1467, 1405, 1330, 1097, 1057, 920, 814, 741 cm^{-1}.

(2-Chloro-4-methylphenyl)(1*H*-pyrrol-1-yl)methanone

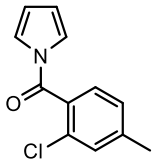

Prepared according to **GP2** from 2-chloro-4-methylbenzoic acid. Flash column chromatography (5% Et_2O in petroleum ether) afforded the title compound as a colourless oil (0.628 g, 57%). **^1H NMR** (400 MHz, $CDCl_3$) δ 7.35 (d, *J* = 7.8 Hz, 1H), 7.31 (s, 1H), 7.18 (d, *J* = 7.8 Hz, 1H), 7.13 (bs, 2H), 6.32 (t, *J* = 2.4 Hz, 2H), 2.42 (s, 3H). **$^{13}C\{^1H\}$ NMR** (126 MHz, $CDCl_3$) δ 165.5, 142.7, 131.4, 130.8, 130.6, 129.0, 127.5, 120.5, 113.7, 21.3. **HRMS (*m*/*z*)**: (ESI+) calculated for $C_{12}H_{10}ClNNaO$ $[M+Na]^+$: 242.0343. Found: 242.0349. **IR (neat) ν_{max}**: 3143, 2925, 1694 ν(C=O), 1602, 1470, 1403, 1333, 1307, 1093, 898, 827, 748, 715 cm^{-1}.

(2-Chloro-3-methylphenyl)(1*H*-pyrrol-1-yl)methanone

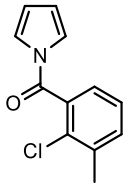

Prepared according to **GP2** from 2-chloro-3-methylbenzoic acid. Flash column chromatography (5% Et_2O in petroleum ether) afforded the title compound as a colourless solid (0.637 g, 58%). **^1H NMR** (400 MHz, $CDCl_3$) δ 7.42 – 7.38 (m, 1H), 7.29 – 7.27 (m, 2H), 7.12 (bs, 2H), 6.32 (t, *J* = 2.3 Hz, 2H), 2.45 (s, 3H). **$^{13}C\{^1H\}$ NMR** (101 MHz, $CDCl_3$) δ 165.8, 137.8, 134.4, 133.1, 131.4, 126.7, 126.5, 120.6 (b), 114.0, 20.4. **HRMS (*m*/*z*)**: (ESI+) calculated for $C_{12}H_{10}ClNNaO$ $[M+Na]^+$: 242.0343. Found: 242.0348. **m.p.**: 53 – 54 °C. **IR (neat) ν_{max}**: 3143, 1704 ν(C=O), 1467, 1339, 1092, 1072, 1045, 918, 794, 737 cm^{-1}.

1-(3-Chloro-4-(1*H*-pyrrole-1-carbonyl)phenyl)ethan-1-one

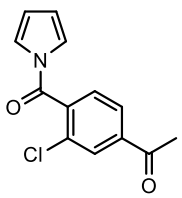

Prepared according to **GP2** from 4-acetyl-2-chlorobenzoic acid (2.48 mmol scale). In this case, oxalyl chloride (2.1 ml, 24.8 mmol) was used instead of thionyl chloride. Flash column chromatography (20% EtOAc in petroleum ether) afforded the title compound as a grey solid (0.147 g, 24%). **^{1}H NMR** (400 MHz, $CDCl_3$) δ 8.06 (s, 1H), 7.95 (d, *J* = 7.9 Hz, 1H), 7.57 (d, *J* = 7.9 Hz, 1H), 7.09 (bs, 2H), 6.35 (bs, 2H), 2.65 (s, 3H). **^{13}C{^{1}H} NMR** (101 MHz, $CDCl_3$) δ 196.0, 164.6, 140.0, 137.8, 132.5, 130.1, 129.5, 126.8, 120.5 (b), 114.6, 27.0. **HRMS (*m*/*z*)**: (ESI+) calculated for $C_{13}H_{11}ClNO_2$ $[M+H]^+$: 248.0473. Found: 248.0479. **m.p.**: 122 – 124 °C. **IR (neat) ν_{max}**: 3137, 1680 ν(C=O), 1406, 1390, 1337, 1242, 1102, 883, 845, 803, 745, 680 cm^{-1}.

3-Chloro-4-(1*H*-pyrrole-1-carbonyl)benzonitrile

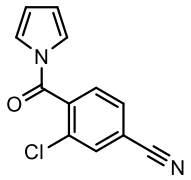

Prepared according to **GP2** from 2-chloro-4-cyanobenzoic acid (2.28 mmol scale). In this case, oxalyl chloride (1.9 ml, 22.8 mmol) was used instead of thionyl chloride. Flash column chromatography (5% EtOAc in petroleum ether) afforded the title compound as a beige solid (0.219 g, 42%). **^{1}H NMR** (400 MHz, $CDCl_3$) δ 7.81 (s, 1H), 7.71 (dd, *J* = 7.9, 1.5 Hz, 1H), 7.59 (d, *J* = 7.9 Hz, 1H), 7.07 (bs, 2H), 6.37 (t, *J* = 2.5 Hz, 2H). **^{13}C{^{1}H} NMR** (101 MHz, $CDCl_3$) δ 163.6, 138.2, 133.7, 132.9, 130.7, 129.9, 120.4 (b), 116.7, 116.1, 114.9. **HRMS (*m*/*z*)**: (ESI+) calculated for $C_{12}H_7ClN_2NaO$ $[M+Na]^+$: 253.0139. Found: 253.0142. **m.p.**: 78 – 79 °C. **IR (neat) ν_{max}**: 3143, 3073, 2240 ν(C≡N), 1702 ν(C=O), 1469, 1404, 1386, 1330, 1101, 1059, 894, 825, 741, 592 cm^{-1}.

(2,5-Dichlorophenyl)(1*H*-pyrrol-1-yl)methanone

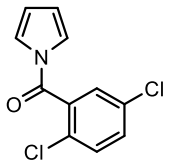

Prepared according to **GP1** from 2,5-dichlorobenzoyl chloride. Flash column chromatography (5% EtOAc in petroleum ether) afforded the title compound as a beige solid (0.897 g, 75%). **^{1}H NMR** (400 MHz, $CDCl_3$) δ 7.47 – 7.42 (m, 3H), 7.11 (bs, 2H), 6.35 (t, *J* = 2.4 Hz, 2H). **^{13}C{^{1}H} NMR** (101 MHz, $CDCl_3$) δ 164.0, 135.3, 133.3, 132.1, 131.5, 130.0, 129.1, 120.5 (b), 114.5. **HRMS (*m*/*z*)**: (ESI+) calculated for $C_{11}H_7Cl_2NNaO$ $[M+Na]^+$: 261.9797. Found: 261.9798. **m.p.**: 56 – 57 °C. **IR (neat) ν_{max}**: 3064, 1698 ν(C=O), 1687, 1468, 1408, 1330, 1301, 1097, 900, 830, 783, 741, 587 cm^{-1}.

(5-Bromo-2-chlorophenyl)(1*H*-pyrrol-1-yl)methanone

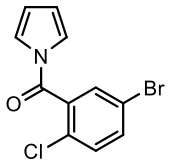

Prepared according to **GP1** from 2-chloro-5-bromobenzoyl chloride. Flash column chromatography (5% EtOAc in petroleum ether) afforded the title compound as a colourless solid (0.997 g, 70%). **^{1}H NMR** (400 MHz, $CDCl_3$) δ 7.61 – 7.58 (m, 2H), 7.38 – 7.35 (m, 1H), 7.11 (bs, 2H), 6.35 (t, *J* = 2.4 Hz, 2H). **^{13}C{^{1}H} NMR** (101 MHz, $CDCl_3$) δ 163.8, 135.6, 135.0, 131.9, 131.8, 130.7, 120.8, 120.5 (b), 114.5. **HRMS (*m*/*z*)**: (ESI+) calculated for $C_{11}H_7BrClNNaO$ $[M+Na]^+$: 305.9292. Found: 305.9285. **m.p.**: 63 – 64 °C. **IR (neat) ν_{max}**: 3146, 3062, 1702 ν(C=O), 1687, 1468, 1407, 1328, 1304, 1098, 893, 740, 587 cm^{-1}.

(2-Chloro-5-fluorophenyl)(1*H*-pyrrol-1-yl)methanone

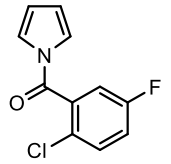

Prepared according to **GP1** from 2-chloro-5-fluorobenzoyl chloride (4.55 mmol scale). Flash column chromatography (5% EtOAc in petroleum ether) afforded the title compound as a pale-yellow solid (0.653 g, 64%). **^{1}H NMR** (400 MHz, $CDCl_3$) δ 7.47 (dd, *J* = 9.8, 4.7 Hz, 1H), 7.22 – 7.17 (m, 2H), 7.11 (bs, 2H), 6.35 (t, *J* = 2.4 Hz, 2H). **^{13}C{^{1}H} NMR** (101 MHz, $CDCl_3$) δ 164.0, 161.0 (d, *J* = 250.4 Hz), 135.3 (d, *J* = 7.2 Hz), 132.0 (d, *J* = 8.2 Hz), 126.8 (d, *J* = 3.6 Hz), 120.5 (b), 119.3 (d, *J* = 22.8 Hz), 116.5 (d, *J* = 25.0 Hz), 114.5. **^{19}F{^{1}H} NMR** (377 MHz, $CDCl_3$) δ -113.4. **HRMS (*m*/*z*)**: (ESI+) calculated for $C_{11}H_7ClFNNaO$ $[M+Na]^+$: 246.0092. Found: 246.0082. **m.p.**: 32 – 33 °C. **IR (neat) ν_{max}**: 3387, 3066, 1699 ν(C=O), 1467, 1417, 1339, 1101, 826, 736, 652, 587 cm^{-1}.

(2-Chloro-4-fluorophenyl)(1*H*-pyrrol-1-yl)methanone

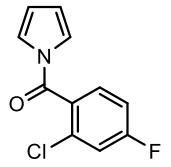

Prepared according to **GP1** from 2-chloro-4-fluorobenzoyl chloride. Flash column chromatography (5% EtOAc in petroleum ether) afforded the title compound as a beige solid (0.729 g, 65%). **^{1}H NMR** (400 MHz, $CDCl_3$) δ 7.47 (dd, *J* = 8.5, 5.8 Hz, 1H), 7.25 (dd, *J* = 8.3, 2.3 Hz, 1H), 7.14 – 7.10 (bm, 3H), 6.34 (d, *J* = 2.1 Hz, 2H). **^{13}C{^{1}H} NMR** (101 MHz, $CDCl_3$) δ 165.0, 163.6 (d, *J* = 217.6 Hz), 133.4 (d, *J* = 10.6 Hz), 130.9 (d, *J* = 9.2 Hz), 130.2 (d, *J* = 3.8 Hz), 120.6 (b), 118.0 (d, *J* = 24.9 Hz), 114.6

(d, *J* = 21.8 Hz), 114.3. **^{19}F{^{1}H} NMR** (377 MHz, $CDCl_3$) δ -106.3. **HRMS (*m*/*z*)**: (ESI+) calculated for $C_{11}H_7ClFNNaO$ $[M+Na]^+$: 246.0092. Found: 246.0101. **m.p.**: 30 – 31 °C. **IR (neat) ν_{max}**: 3364, 3106, 1685 ν(C=O), 1468, 1330, 1095, 912, 852, 823, 737. 587, 579 cm^{-1}.

(2-Chloro-5-(trifluoromethyl)phenyl)(1*H*-pyrrol-1-yl)methanone

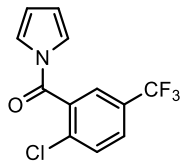

Prepared according to **GP1** from 2-chloro-5-(trifluoromethyl)benzoyl chloride. Flash column chromatography (5% Et_2O in petroleum ether) afforded the title compound as a beige solid (0.891 g, 65%). **^{1}H NMR** (400 MHz, $CDCl_3$) δ 7.76 – 7.73 (m, 2H), 7.66 – 7.63 (m, 1H), 7.10 (bs, 2H), 6.37 (t, *J* = 2.2 Hz, 2H). **^{13}C{^{1}H} NMR** (101 MHz, $CDCl_3$) δ 163.9, 135.7 (q, *J* = 1.5 Hz), 134.8, 131.1, 129.9 (q, *J* = 33.9 Hz), 128.7 (q, *J* = 3.6 Hz), 126.3 (q, *J* = 3.7 Hz), 123.3 (q, *J* = 272.5 Hz), 120.5 (b), 114.7. **^{19}F{^{1}H} NMR** (377 MHz, $CDCl_3$) δ -62.7. **GCMS (*m*/*z*)**: calculated for $C_{12}H_7ClF_3NO$: 273.0. Found: 273.1. **m.p.**: 50 – 51 °C. **IR (neat) ν_{max}**: 3153, 1705 ν(C=O), 1470, 1300, 1120, 1077, 901, 831, 713, 735, 713, 651, 593, 519 cm^{-1}.

(2-Chloro-4-(pyrrolidin-1-yl)phenyl)(1*H*-pyrrol-1-yl)methanone

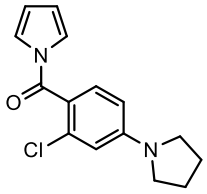

Prepared according to **GP2** from 2-chloro-4-(pyrrolidin-1-yl)benzoic acid (1.08 mmol scale). In this case, the carboxylic acid and thionyl chloride mixture was stirred for 4 h. This example was quenched with 1M KOH and the organics extracted as previously described. Flash column chromatography (10% EtOAc in petroleum ether) afforded the title compound as a dark beige solid (0.153 g, 52%). **^{1}H NMR** (400 MHz, $CDCl_3$) δ 7.32 (d, *J* = 8.6 Hz, 1H), 7.19 (t, *J* = 2.4 Hz, 2H), 6.58 (d, *J* = 2.3 Hz, 1H), 6.44 (dd, *J* = 8.6, 2.4 Hz, 1H), 6.29 (t, *J* = 2.3 Hz, 2H), 3.37 – 3.29 (m, 4H), 2.07 – 2.03 (m, 4H). **^{13}C{^{1}H} NMR** (101 MHz, $CDCl_3$) δ 166.1, 150.2, 134.2, 131.8, 121.1, 118.9, 113.0, 112.7, 109.4, 47.9, 25.6. **HRMS (*m*/*z*)**: (ESI+) calculated for $C_{15}H_{15}ClN_2NaO$ $[M+Na]^+$: 297.0765. Found: 297.0777. **m.p.**: 69 – 71 °C. **IR (neat) ν_{max}**: 2972, 2840, 1694 ν(C=O), 1598, 1324, 1298, 1086, 1072, 1028, 741, 659 cm^{-1}.

(2-Chloro-5-(methylthio)phenyl)(1*H*-pyrrol-1-yl)methanone

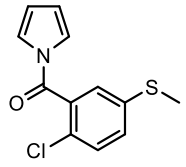

Prepared according to **GP2** from 2-chloro-5-(methylthio)benzoic acid. Flash column chromatography (5% Et_2O in petroleum ether) afforded the title compound as a beige solid (0.701 g, 56%). **^{1}H NMR** (400 MHz, $CDCl_3$) δ 7.38 (d, *J* = 8.5 Hz, 1H), 7.32 (dd, *J* = 8.5, 2.3 Hz, 1H), 7.28 (d, *J* = 2.3 Hz, 1H), 7.13 (bs, 2H), 6.34 (t, *J* = 2.4 Hz, 2H), 2.49 (s, 3H). **^{13}C{^{1}H} NMR** (101 MHz, $CDCl_3$) δ 165.0, 138.8, 134.4, 130.4, 129.6, 127.8, 126.2, 120.6 (b), 114.2, 15.9. **HRMS (*m*/*z*)**: (ESI+) calculated for $C_{15}H_{15}ClNNaOS$ $[M+Na]^+$: 274.0064. Found: 274.0069. **m.p.**: 88 – 89 °C. **IR (neat) ν_{max}**: 2923, 1693 ν(C=O), 1468, 1344, 1102, 902, 821, 785, 745, 590 cm^{-1}.

(4-Chloro-[1,1'-biphenyl]-3-yl)(1*H*-pyrrol-1-yl)methanone

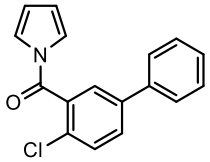

Prepared according to **GP2** from 4-chloro-[1,1'-biphenyl]-3-carboxylic acid (1.05 mmol scale). In this case, the carboxylic acid and thionyl chloride mixture was stirred for 4 h. Flash column chromatography (4% EtOAc in petroleum ether) afforded the title compound as a colourless gum (0.179 g, 61%). **^{1}H NMR** (400 MHz, $CDCl_3$) δ 7.72 (d, *J* = 1.6 Hz, 1H), 7.63 – 7.59 (m, 3H), 7.54 – 7.42 (m, 4H), 7.20 (bs, 2H), 6.36 (t, *J* = 2.4 Hz, 2H). **^{13}C{^{1}H} NMR** (101 MHz, $CDCl_3$) δ 165.4, 145.3, 138.7, 132.3, 132.3, 129.7, 129.3, 128.9, 128.8, 127.4, 125.6, 120.7, 114.1. **HRMS (*m*/*z*)**: (ESI+) calculated for $C_{17}H_{12}ClNNaO$ $[M+Na]^+$: 304.0500. Found: 304.0504. **IR (neat) ν_{max}**: 1705 ν(C=O), 1601, 1467, 1401, 1329, 1305, 1094, 1057, 886, 740, 697, 591 cm^{-1}.

(2-Chloropyridin-3-yl)(1*H*-pyrrol-1-yl)methanone

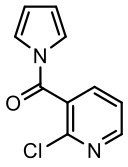

Prepared according to **GP1** from 2-chloronicotinoyl chloride. Flash column chromatography (20% EtOAc in petroleum ether) followed by recrystallisation from petroleum ether afforded the title compound as a colourless solid (0.814 g, 79%). **^{1}H NMR** (400 MHz, $CDCl_3$) δ 8.58 (dd, *J* = 4.9, 2.0 Hz, 1H), 7.82 (dd, *J* = 7.6, 2.0 Hz, 1H), 7.40 (dd, *J* = 7.6, 4.9 Hz, 1H), 7.10 (bs, 2H), 6.36 (t, *J* = 2.5 Hz, 2H). **^{13}C{^{1}H} NMR** (101 MHz, $CDCl_3$) δ 163.7, 151.7, 148.1, 138.0, 130.5, 122.4, 120.5, 114.7. **HRMS (*m*/*z*)**: (ESI+) calculated for $C_{10}H_7ClN_2NaO$ $[M+Na]^+$: 229.0139. Found: 229.0140. **m.p.**: 77 – 78 °C. **IR (neat) ν_{max}**: 1694 ν(C=O), 1470, 1401, 1346, 1306, 1106, 1069, 880, 813, 732, 589 cm^{-1}.

7.2.5 Preparation of Halobenzamide Substrates

(2-Chlorophenyl)(1*H*-indol-1-yl)methanone (**30**)

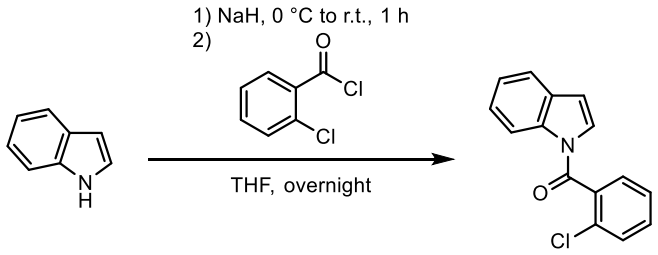

Prepared according to **GP1** from indole and 2-benzoylchloride. Flash column chromatography (10% EtOAc in petroleum ether) followed by recrystallisation from petroleum ether afforded the title compound as a pale-pink solid (0.738 g, 58%). **^{1}H NMR** (400 MHz, $CDCl_3$) δ 8.42 (bs, 1H), 7.59 (d, *J* = 7.6 Hz, 1H), 7.54 – 7.38 (m, 5H), 7.33 (td, *J* = 7.5, 1.2 Hz, 1H), 6.99 (bs, 1H), 6.61 (d, *J* = 3.9 Hz, 1H). **^{13}C{^{1}H} NMR** (101 MHz, $CDCl_3$) δ 166.2, 135.7, 135.1, 131.9, 131.5, 131.3, 130.4, 129.1, 127.4, 126.8, 125.5, 124.6, 121.2, 116.7 (b), 101.0. **HRMS (*m/z*)**: (ESI+) calculated for $C_{15}H_{11}ClNO$ $[M+H]^+$: 256.0524. Found: 256.0526. **m.p.**: 65 – 67 °C. **IR (neat) ν_{max}**: 1682 ν(C=O), 1452, 1382, 1343, 1204, 1045, 750, 730, 660, 623, 421 cm^{-1}.

2-Chloro-*N*,*N*-diphenylbenzamide (**32**)

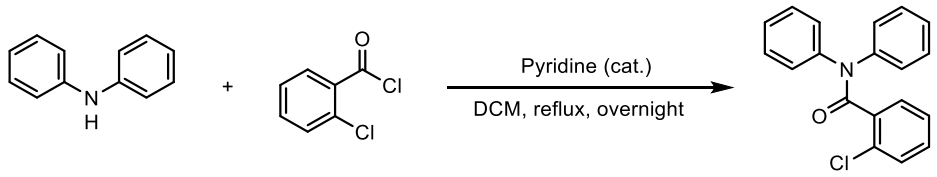

Prepared according to a modified literature procedure.[128] To a three-necked round-bottom flask was added 2-chlorobenzoyl chloride (1.52 ml, 12 mmol), pyridine (50 µl, 0.6 mmol) and CH_2Cl_2 (25 ml). The mixture was stirred whilst diphenylamine (2.031 g, 12 mmol) was added portion-wise causing the solution to turn yellow. The solution was heated to reflux and left stirring overnight before being cooled to room temperature and quenched by the addition of 2 M NaOH (30 ml). The organics were extracted from the aqueous layer with CH_2Cl_2 (3 x 20 ml), dried over Na_2SO_4 and the solvent removed under reduced pressure gave the crude compound as a pale-yellow solid. The compound was purified by recrystallisation from ethanol affording the title compound as a pale-yellow solid (2.22 g, 60%). **^{1}H NMR** (400 MHz, DMSO-d_6) δ 7.57 – 7.55 (m, 1H), 7.41 – 7.14 (m, 13H). **^{13}C{^{1}H} NMR** (101 MHz, DMSO-d_6) δ 166.9, 142.3 (b), 142.1 (b), 136.4, 130.4, 129.3, 129.3, 129.1, 129.1, 128.4 (b), 127.5 (b), 126.8 (b), 126.7. **IR (neat) ν_{max}:** 1654 ν(C=O), 1589, 1490, 1344, 747, 691, 618, 518 cm^{-1}. Data in accordance with previously reported values.[196]

2-Chloro-*N*-tosylbenzamide (**34**)

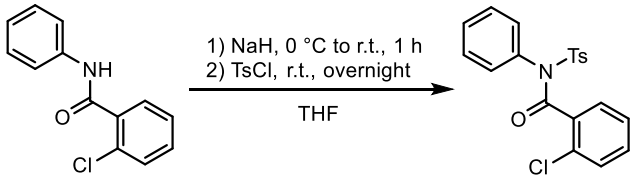

To a round-bottom flask was added 2-chloro-*N*-phenylbenzamide (324 mg, 1.4 mmol) and THF (10 ml). The solution was cooled to 0 °C and sodium hydride (60% dispersion in mineral oil, 56 mg, 1.4 mmol) was added in one portion. The mixture was stirred for 30 min during which effervescence was observed, and then warmed to room temperature and stirred for a further 30 min. The mixture was then cooled to 0 °C and *p*-toluenesulfonyl chloride (267 mg, 1.4 mmol) was added portion-wise. The reaction was warmed to room temperature and left stirring overnight and then quenched by the addition of saturated NH_4Cl (5 ml). The organics were extracted from the aqueous layer with CH_2Cl_2 (3 x 10 ml), the combined organic layers dried over Na_2SO_4, filtered and the solvent removed under reduced pressure to give the crude product. Purification by flash column chromatography (20% EtOAc in petroleum ether) afforded the title compound as a colourless solid (361 mg, 67%). **^{1}H NMR** (400 MHz, $CDCl_3$) δ 7.95 (d, *J* = 8.4 Hz, 2H), 7.38 (d, *J* = 8.3 Hz, 2H), 7.27 – 7.23 (m, 5H), 7.15 – 7.08 (m, 3H), 7.04 (td, *J* = 7.2, 1.7 Hz, 1H), 2.48 (s, 3H). **^{13}C{^{1}H} NMR** (101 MHz, $CDCl_3$) δ 167.2, 145.4, 136.1, 135.6, 135.0, 131.0, 130.7, 130.3, 129.8, 129.8, 129.7, 129.6, 129.3, 128.6, 126.4, 22.0. **HRMS (*m*/*z*)**: (ESI+) calculated for $C_{20}H_{17}ClNO_3S$ $[M+H]^+$: 386.0612. Found: 386.0612. **m.p.**: 161 – 162 °C. **IR (neat) ν_{max}**: 1694 ν(C=O), 1363, 1292, 1167, 1115, 955, 811, 767, 689, 655, 551, 541 cm^{-1}.

(2-chlorophenyl)(1H-pyrazol-1-yl)methanone (**35**)

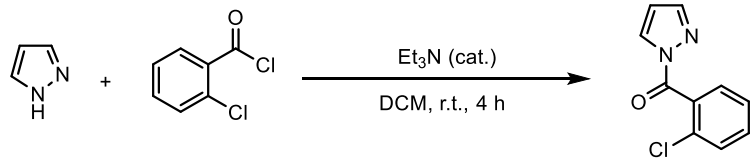

In a 100 ml round-bottom flask, pyrazole (1.021 g, 15 mmol) was dissolved in CH_2Cl_2 (40 ml) and the solution cooled to 0 °C. Et_3N (2.1 ml, 15 mmol) was added followed by 2-chlorobenzoyl chloride (2.0 ml, 16 mmol) causing the formation of a white precipitate and the mixture warmed to room temperature and stirred for 4 h. The reaction was quenched by the addition of water (20 ml), the organic layer separated and washed with 0.5 M HCl, 2 M NaOH and then brine before drying over Na_2SO_4. The solvent was removed under reduced pressure to give the crude product which was purified by flash column chromatography (10% acetone in petroleum ether) affording a colourless oil which turned to a colourless solid upon standing (1.4 g, 45%). **^{1}H NMR** (400 MHz, $CDCl_3$) δ 8.39 (dd, *J* = 2.9, 0.7 Hz, 1H), 7.76 (dd, *J* = 1.5, 0.7 Hz, 1H), 7.54 – 7.52 (m, 1H), 7.49 – 7.48 (m, 2H), 7.42 – 7.38 (m, 1H), 6.54 (dd, *J* = 2.9, 1.5 Hz, 1H). **^{13}C{^{1}H} NMR** (101 MHz, $CDCl_3$) δ 165.8, 145.4, 133.3, 132.1, 132.1, 130.1,

129.8, 129.4, 126.7, 110.6. **HRMS (*m/z*)**: (ESI+) calculated for $C_{10}H_7ClN_2NaO$ $[M+Na]^+$: 229.0139. Found: 229.0150. **m.p.**: 54 – 55 °C. **IR (neat) ν_{max}**: 3130, 1716, 1415, 1382, 1346, 888, 765, 736, 708, 652 cm^{-1}.

(2-Chlorophenyl)(pyrrolidin-1-yl)methanone (**31**)

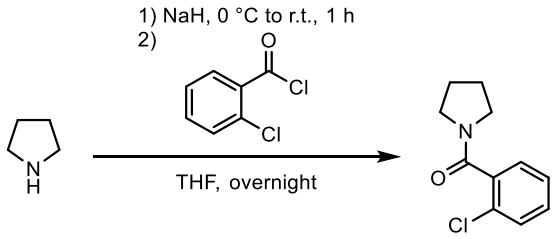

Prepared according to **GP1** from pyrrolidine and 2-chlorobenzoyl chloride. This example was quenched with sat. $NaHCO_3$ and the organics extracted as previously described. Flash column chromatography (60% EtOAc in petroleum ether) afforded the title compound as a colourless oil (0.774 g, 74%). **^{1}H NMR** (400 MHz, $CDCl_3$) δ 7.40 – 7.36 (m, 1H), 7.33 – 7.28 (m, 3H), 3.66 (t, *J* = 6.9 Hz, 2H), 3.19 (t, *J* = 6.6 Hz, 2H), 2.00 – 1.85 (m, 4H). **^{13}C{^{1}H} NMR** (101 MHz, $CDCl_3$) δ 166.8, 137.6, 130.2, 129.8, 127.7, 127.3, 48.0, 45.6, 26.0, 24.7. **HRMS (*m/z*)**: (ESI+) calculated for $C_{11}H_{13}ClNO$ $[M+H]^+$: 210.0680. Found: 210.0685. **IR (neat) ν_{max}:** 2972, 2877, 1629 ν(C=O), 1420, 1055, 1032, 768, 747, 700, 644 cm^{-1}.

1-(2-Chlorobenzyl)-1H-pyrrole (**87**)

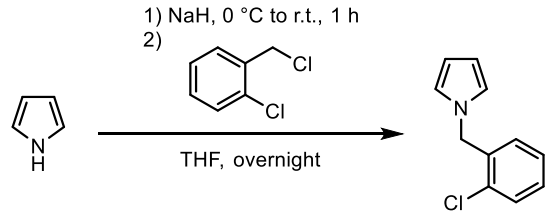

Prepared according to **GP1** from 2-chlorobenzyl chloride. Flash column chromatography (petroleum ether) afforded the title compound as a colourless oil (0.312 g, 33%). **^{1}H NMR** (400 MHz, $CDCl_3$) δ 7.38 (dd, *J* = 7.4, 1.7 Hz, 1H), 7.21 (pd, *J* = 7.4, 1.8 Hz, 2H), 6.76 (dd, *J* = 7.1, 1.9 Hz, 1H), 6.72 (t, *J* = 2.1 Hz, 2H), 6.22 (t, *J* = 2.1 Hz, 2H), 5.18 (s, 2H). **^{13}C{^{1}H} NMR** (101 MHz, $CDCl_3$) δ 136.3, 132.6, 129.5, 129.0, 128.5, 127.4, 121.5, 108.9, 51.0. **GCMS (*m/z*)**: calculated for $C_{11}H_{10}ClN$: 191.1. Found: 191.1. **IR (neat) ν_{max}:** 1498, 1444, 1350, 1292, 1276, 1087, 1049, 1038, 968, 718, 619 cm^{-1}.

(7-Chloro-1*H*-indol-1-yl)(2-chlorophenyl)methanone (**89**)

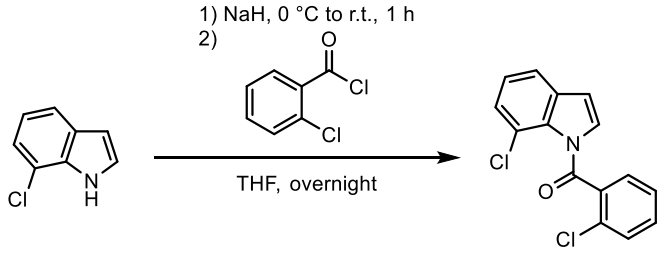

Prepared according to **GP1** from 7-chloroindole and 2-benzoylchloride. Flash column chromatography (5% EtOAc in petroleum ether) afforded the title compound as a pale-pink solid (1.106 g, 76%). **^{1}H NMR** (400 MHz, $CDCl_3$) δ 7.62 – 7.60 (m, 1H), 7.54 – 7.49 (m, 3H), 7.42 – 7.37 (m, 2H), 7.28 – 7.26 (m, 1H), 7.10 (d, *J* = 3.7 Hz, 1H), 6.62 (d, *J* = 3.7 Hz, 1H). **^{13}C{^{1}H} NMR** (101 MHz, $CDCl_3$) δ 164.3, 134.6, 134.1, 133.3, 132.9, 132.9, 131.0, 131.0, 129.0, 127.1, 127.0, 125.0, 121.5, 119.8, 108.5. **HRMS (*m*/*z*)**: (ESI+) calculated for $C_{15}H_{10}Cl_2NO$ $[M+H]^+$: 290.0134. Found: 290.0135. **m.p.**: 74 – 76 °C. **IR (neat) ν_{max}:** 1698 ν(C=O), 1578, 1470, 1409, 1318, 1175, 1110, 1043, 940, 864, 777, 718, 632 cm^{-1}.

4-Chloro-2-isobutylisoindoline-1,3-dione (**93**)

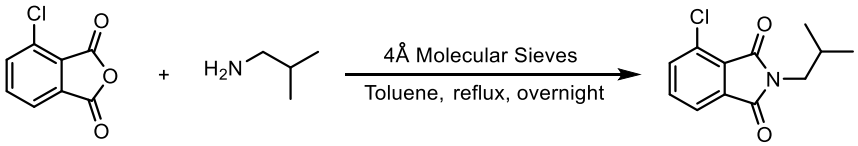

To a 100 ml round-bottom flask was added 3-chlorophthalic acid anhydride (0.9128 g, 5 mmol), toluene (20 ml) and 4Å molecular sieves. Isobutylamine (0.75 ml, 7.5 mmol) was added whilst stirring and the reaction heated to reflux and left overnight. The resulting mixture was filtered, and the volatiles removed under reduced pressure to afford the crude product which was purified by flash column chromatography (10% EtOAc in petroleum ether) affording the title compound as a pale-yellow solid (0.963 g, 81%). **^{1}H NMR** (400 MHz, $CDCl_3$) δ 7.77 – 7.73 (m, 1H), 7.63 (d, *J* = 4.2 Hz, 2H), 3.50 (d, *J* = 7.3 Hz, 2H), 2.12 (m, 1H), 0.94 (d, *J* = 6.7 Hz, 6H). **^{13}C{^{1}H} NMR** (101 MHz, $CDCl_3$) δ 167.3, 166.3, 135.8, 134.9, 134.3, 131.4, 127.8, 121.8, 45.7, 27.9, 20.3. **HRMS (*m*/*z*)**: (ESI+) calculated for $C_{12}H_{13}ClNO_2$ $[M+H]^+$: 238.0629. Found: 238.0640. **m.p.**: 66 – 67 °C. **IR (neat) ν_{max}:** 2965, 2929, 1703 ν(C=O), 1459, 1433, 1394, 1056, 906, 851, 818, 740, 626, 590, 550 cm^{-1}.

7.2.6 Iron-Catalysed Suzuki Biaryl Cross-Coupling - Optimisation

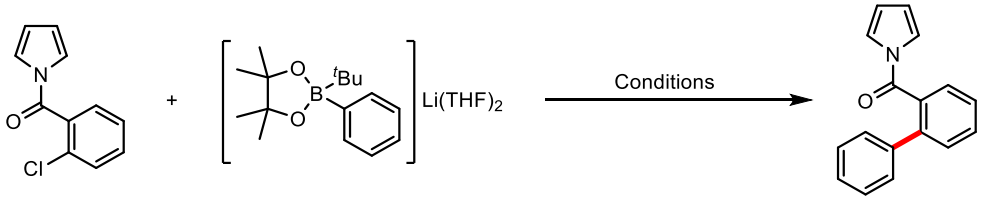

To a Schlenk-tube was added the appropriate ligand or ligand precursor followed by the appropriate iron salt and THF (0.63 ml). The mixture was stirred at room temperature for 1 h before $MgBr_2 \cdot OEt_2$ (0.1 M solution in THF), **17** (0.125 mmol, 25.7 mg) and **18** (0.4 M in solution in THF) were added sequentially. The Schlenk-tube was sealed and the reaction stirred for 3 h at the desired temperature. The resulting mixture was cooled to room temperature before dodecane (0.125 mmol, 28 µl) was added, the mixture thoroughly stirred and an aliquot (~ 0.2 ml) passed through a pad of Celite (eluting with CH_2Cl_2) for GC analysis.

7.2.7 General Procedure 3 (GP3): Iron-Catalysed Suzuki Biaryl Cross-Coupling

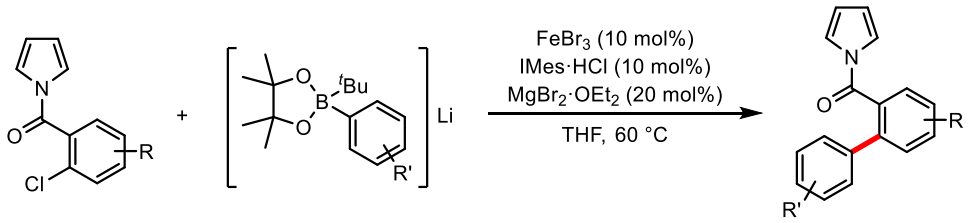

To a Schlenk-tube was added IMes·HCl (13.6 mg, 0.04 mmol) and $FeBr_3$ (0.02 M in THF, 2 ml, 0.04 mmol). The mixture was stirred at room temperature for 1 h before $MgBr_2 \cdot OEt_2$ (0.1 M in THF, 0.8 ml, 0.08 mmol), the appropriate halobenzamide substrate (0.4 mmol) and activated boronate (0.4 M in THF, 2.2 ml, 0.88 mmol) were added sequentially. The reaction was stirred for 3 h at 60 ºC (except when using boronate **44**: 2 h) and then quenched by the addition of 1 M HCl (10 ml). The organics were extracted from the aqueous layer with CH_2Cl_2 (3 x 10 ml), the combined organics layers dried over $MgSO_4$ and filtered. 1,3,5-Trimethoxybenzene (67.3 mg, 0.4 mmol) was added and an aliquot taken for analysis by ^{1}H NMR spectroscopy. The crude mixture was purified by flash column chromatography (and if necessary preparative TLC) to yield the desired biaryl cross-coupled product.

7.2.8 Biaryls Obtained from GP3

[1,1'-Biphenyl]-2-yl(1*H*-pyrrol-1-yl)methanone (**21**)

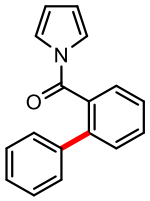

Prepared according to **GP3**; spectroscopic yield 82%. Flash column chromatography (5% Et_2O in petroleum ether) afforded the title compound as a colourless solid (69 mg, 70%). **^{1}H NMR** (400 MHz, $CDCl_3$) δ 7.62 – 7.45 (m, 4H), 7.34 – 7.24 (m, 5H), 7.01 (bs, 2H), 6.14 (t, *J* = 2.4 Hz, 2H). **^{13}C{^{1}H} NMR** (101 MHz, $CDCl_3$) δ 168.6, 141.1, 139.6, 133.6, 131.2, 130.4, 128.9, 128.8, 128.6, 128.0, 127.4, 120.8 (b), 113.4. **HRMS (*m*/*z*)**: (ESI+) calculated for $C_{17}H_{13}NNaO$ $[M+Na]^+$: 270.0889. Found:

270.0891. **m.p.**: 62 – 63 °C. **IR (neat)** ν_{max}: 1693 ν(C=O), 1468, 1330, 1305, 1086, 1068, 880, 740, 702, 664, 581 cm^{-1}.

(4,5-Dimethoxy-[1,1'-biphenyl]-2-yl)(1*H*-pyrrol-1-yl)methanone (**50**)

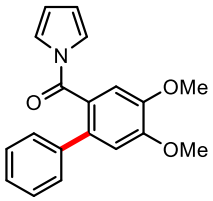

Prepared according to **GP3**; spectroscopic yield 89%. Flash column chromatography (25% EtOAc in heptane) afforded the title compound as a yellow solid (79 mg, 64%). **^{1}H NMR** (500 MHz, $CDCl_3$) δ 7.32 – 7.22 (m, 5H), 7.09 (s, 1H), 7.00 (bs, 2H), 6.97 (s, 1H), 6.09 (t, *J* = 2.4 Hz, 2H), 3.98 (s, 3H), 3.94 (s, 3H). **^{13}C{^{1}H} NMR** (126 MHz, $CDCl_3$) δ 168.4, 151.1, 148.3, 139.6, 134.9, 128.7, 128.5, 127.7, 125.5, 120.8 (b), 113.2, 113.0, 112.1, 56.5, 56.4. **HRMS (*m*/*z*)**: (ESI+) calculated for $C_{19}H_{18}NO_3$ $[M+H]^+$: 308.1281. Found: 308.1284. **m.p.**: 120 – 122 °C. **IR (neat)** ν_{max}: 1681 ν(C=O), 1604, 1324, 1305, 1212, 1144, 1086, 1038, 874, 790, 736, 704, 643, 530 cm^{-1}.

(5-Methoxy-[1,1'-biphenyl]-2-yl)(1*H*-pyrrol-1-yl)methanone (**51**)

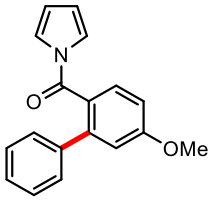

Prepared according to **GP3**; spectroscopic yield 81%. Flash column chromatography (25% EtOAc in heptane) followed by a second flash column (40% CH_2Cl_2 in heptane) afforded the title compound as a yellow oil (68 mg, 61%). **^{1}H NMR** (400 MHz, $CDCl_3$) δ 7.53 (d, *J* = 8.4 Hz, 1H), 7.34 – 7.27 (m, 5H), 7.02 (bs, 2H), 7.01 (d, *J* = 2.6 Hz, 1H), 6.96 (dd, *J* = 8.4, 2.6 Hz, 1H), 6.12 (t, *J* = 2.4 Hz, 2H), 3.91 (s, 3H). **^{13}C{^{1}H} NMR** (101 MHz, $CDCl_3$) δ 168.2, 161.4, 143.3, 139.4, 130.9, 128.5, 128.2, 127.8, 125.7, 120.6, 115.6, 112.8, 112.5, 55.5. **HRMS (*m*/*z*)**: (ESI+) calculated for $C_{18}H_{16}NO_2$ $[M+H]^+$: 278.1176. Found: 278.1178. **IR (neat)** ν_{max}: 1689 ν(C=O), 1600, 1466, 1327, 1297, 1215, 1086, 1032, 891, 729, 699, 595 cm^{-1}.

(4-Methoxy-[1,1'-biphenyl]-2-yl)(1*H*-pyrrol-1-yl)methanone (**52**)

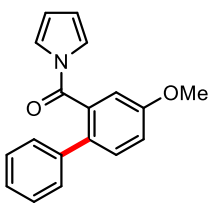

Prepared according to **GP3** on a 0.2 mmol scale; spectroscopic yield 80%. Flash column chromatography (15% EtOAc in heptane) followed by preparative TLC (toluene) afforded the title compound as a yellow oil (27 mg, 49%). **^{1}H NMR** (400 MHz, $CDCl_3$) δ 7.43 (d, *J* = 8.5 Hz, 1H), 7.29 – 7.20 (m, 5H), 7.13 (dd, *J* = 8.5, 2.6 Hz, 1H), 7.08 (d, *J* = 2.6 Hz, 1H), 6.99 (bs, 2H), 6.12 (bt, 2H), 3.87 (s, 3H). **^{13}C{^{1}H} NMR** (101 MHz, $CDCl_3$) δ 168.2, 158.6, 139.0, 134.2, 133.2, 131.4, 128.5, 128.3, 127.3, 120.5 (b), 117.1, 113.5, 113.2, 55.6. **HRMS (*m*/*z*)**: (ESI+) calculated for $C_{18}H_{16}NO_2$ $[M+H]^+$: 278.1176. Found: 278.1170. **IR (neat) ν_{max}**: 1702 ν(C=O), 1606, 1482, 1467, 1332, 1293, 1232, 1085, 1050, 818, 769, 744, 703 cm^{-1}.

(5-Methyl-[1,1'-biphenyl]-2-yl)(1*H*-pyrrol-1-yl)methanone (**53**)

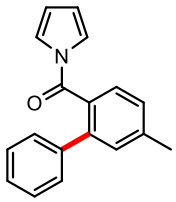

Prepared according to **GP3** on a 0.2 mmol scale; spectroscopic yield 94%. Flash column chromatography (5% EtOAc in heptane) followed by preparative TLC (40% CH_2Cl_2 in heptane) afforded the title compound as a pale-yellow oil (28 mg, 54%). **^{1}H NMR** (500 MHz, $CDCl_3$) δ 7.46 (d, *J* = 7.8 Hz, 1H), 7.32 – 7.23 (m, 7H), 7.01 (bs, 2H), 6.12 (t, *J* = 2.4 Hz, 2H), 2.48 (s, 3H). **^{13}C{^{1}H} NMR** (126 MHz, $CDCl_3$) δ 168.6, 141.4, 141.0, 139.5, 130.9, 130.6, 128.9, 128.5, 128.3, 127.8, 127.7, 120.6 (b), 113.0, 21.5. **HRMS (*m*/*z*)**: (ESI+) calculated for $C_{18}H_{16}NO$ $[M+H]^+$: 262.1226. Found: 262.1232. **IR (neat) ν_{max}**: 1740, 1669 ν(C=O), 1607, 1313, 909, 822, 766, 731, 701 cm^{-1}.

(4-Methyl-[1,1'-biphenyl]-2-yl)(1*H*-pyrrol-1-yl)methanone (**54**)

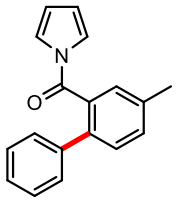

Prepared according to **GP3**; spectroscopic yield 91%. Flash column chromatography (5% EtOAc in petroleum ether) followed by preparative TLC (35% CH_2Cl_2 in petroleum ether) afforded the title compound as a yellow oil (70 mg, 67%). **^{1}H NMR** (400 MHz, $CDCl_3$) δ 7.40 (s, 2H), 7.37 (s, 1H), 7.32 – 7.21 (m, 5H), 6.99 (bs, 2H), 6.11 (t, *J* = 2.4 Hz, 2H), 2.44 (s, 3H). **^{13}C{^{1}H} NMR** (126 MHz, $CDCl_3$) δ 168.9, 139.5, 138.2, 137.4, 133.5, 132.0, 130.3, 129.4, 128.7, 128.6, 127.8, 120.7 (b), 113.3, 21.2. **HRMS (*m*/*z*)**: (ESI+) calculated for $C_{18}H_{16}NO$ $[M+H]^+$: 262.1226. Found: 262.1214. **IR (neat) ν_{max}**: 1698 ν(C=O), 1466, 1328, 1086, 1072, 922, 820, 765, 738, 702, 592, 523 cm^{-1}.

(6-Methyl-[1,1'-biphenyl]-2-yl)(1*H*-pyrrol-1-yl)methanone (**55**)

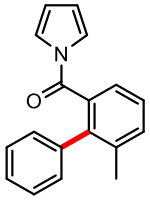

Prepared according to **GP3**; spectroscopic yield 60%. Flash column chromatography (4% EtOAc in petroleum ether) followed by preparative TLC (toluene) afforded the title compound as a yellow gum (30 mg, 28%). **^{1}H NMR** (400 MHz, $CDCl_3$) δ 7.44 (ddd, *J* = 7.1, 2.0, 0.8 Hz, 1H), 7.38 – 7.23 (m, 5H), 7.16 – 7.14 (m, 2H), 6.98 (bs, 2H), 6.16 (t, *J* = 2.4 Hz, 2H), 2.20 (s, 3H). **^{13}C{^{1}H} NMR** (101 MHz, $CDCl_3$) δ 168.2, 140.3, 138.2, 137.4, 134.9, 132.5, 129.4, 128.3, 127.7, 127.2, 125.2, 120.8 (b), 113.2, 20.8. **HRMS (*m*/*z*)**: (ESI+) calculated for $C_{18}H_{15}NNaO$ $[M+Na]^+$: 284.1046. Found: 284.1047. **IR (neat) ν_{max}**: 1704 ν(C=O), 1465, 1399, 1327, 1072, 926, 792, 592 cm^{-1}.

4'-Methoxy-6-(1*H*-pyrrole-1-carbonyl)-[1,1'-biphenyl]-3-carbonitrile (**57**)

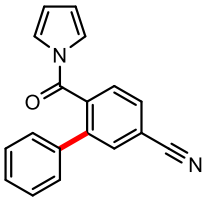

Prepared according to **GP3**; spectroscopic yield 72%. Flash column chromatography (20% Et_2O in petroleum ether) afforded the title compound as a beige solid (75 mg, 69%). **^{1}H NMR** (400 MHz, $CDCl_3$) δ 7.82 (d, *J* = 1.5 Hz, 1H), 7.77 (dd, *J* = 7.9, 1.6 Hz, 1H), 7.67 (d, *J* = 7.9 Hz, 1H), 7.35 – 7.29 (m, 5H), 6.92 (bs, 2H), 6.17 (bs, 2H). **^{13}C{^{1}H} NMR** (101 MHz, $CDCl_3$) δ 166.7, 142.1, 137.6, 137.2, 133.9, 130.8, 129.4, 129.1, 129.0 (b), 128.4, 120.3, 117.9, 115.1, 114.2. **HRMS** (*m*/*z*): (ESI+) calculated for $C_{18}H_{12}N_2NaO$ $[M+Na]^+$: 295.0842. Found: 295.0835. **m.p.**: 106 – 109 °C. **IR (neat) ν_{max}**: 3143, 2237 ν(C≡N), 1690 ν(C=O), 1601, 1466, 1324, 1304, 1206, 1149, 1071, 888, 832, 738, 694, 636, 600 cm^{-1}.

(4-Chloro-[1,1'-biphenyl]-2-yl)(1*H*-pyrrol-1-yl)methanone (**58**)

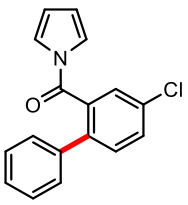

Prepared according to **GP3** on a 0.2 mmol scale; spectroscopic yield 72%. Flash column chromatography (5% EtOAc in heptane) followed by preparative TLC (30% CH_2Cl_2 in heptane) afforded the title compound as a pale-yellow oil (28 mg, 49%). **^{1}H NMR** (400 MHz, $CDCl_3$) δ 7.59 –

7.55 (m, 2H), 7.45 (d, *J* = 8.6 Hz, 1H), 7.31 – 7.27 (m, 5H), 6.99 (bs, 2H), 6.15 (bt, 2H). **^{13}C{^{1}H} NMR** (126 MHz, $CDCl_3$) δ 167.1, 139.4, 138.4, 134.9, 133.7, 131.8, 131.3, 128.9, 128.7, 128.4, 128.3, 120.6 (b), 113.8. **HRMS (*m*/*z*)**: (ESI+) calculated for $C_{17}H_{12}ClNNaO$ $[M+Na]^+$: 304.0500. Found: 304.0498. **IR (neat) ν_{max}**: 1744, 1667 ν(C=O), 1470, 1331, 1307, 1259, 1094, 1009, 803, 764, 525, 476 cm^{-1}.

(4'-Methoxy-[1,1'-biphenyl]-2-yl)(1*H*-pyrrol-1-yl)methanone (**59**)

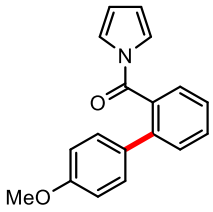

Prepared according to **GP3**; spectroscopic yield 99%. Flash column chromatography (5% EtOAc in petroleum ether) afforded the title compound as a yellow oil (73 mg, 66%). **^{1}H NMR** (400 MHz, $CDCl_3$) δ 7.59 – 7.40 (m, 4H), 7.24 (d, *J* = 8.7 Hz, 2H), 7.01 (bs, 2H), 6.82 (d, *J* = 8.7 Hz, 2H), 6.14 (t, *J* = 2.3 Hz, 2H), 3.76 (s, 3H). **^{13}C{^{1}H} NMR** (101 MHz, $CDCl_3$) δ 168.8, 159.5, 140.7, 133.5, 132.0, 131.1, 130.3, 129.7, 128.8, 126.9, 120.7 (b), 114.3, 113.4, 55.4. **HRMS (*m*/*z*)**: (ESI+) calculated for $C_{18}H_{16}NO_2$ $[M+H]^+$: 278.1176. Found: 278.1176. **IR (neat) ν_{max}**: 1701 ν(C=O), 1609, 1518, 1466, 1330, 1304, 1246, 1180, 1085, 1034, 885, 834, 741 cm^{-1}.

(4-Bromo-4'-methoxy-[1,1'-biphenyl]-2-yl)(1*H*-pyrrol-1-yl)methanone (**60**)

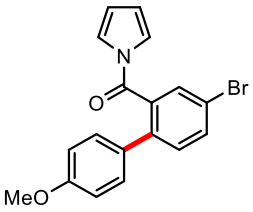

Prepared according to **GP3**; spectroscopic yield 55%. Flash column chromatography (10% Et_2O in petroleum ether) followed by a second flash column (4% EtOAc in petroleum ether) and preparative TLC (4% EtOAc in petroleum ether) afforded the title compound as a pale-yellow oil (29 mg, 20%). **^{1}H NMR** (400 MHz, $CDCl_3$) δ 7.69 (dd, *J* = 8.2, 2.1 Hz, 1H), 7.66 (d, *J* = 1.8 Hz, 1H), 7.35 (d, *J* = 8.3 Hz, 1H), 7.21 (d, *J* = 8.8 Hz, 2H), 6.99 (bs, 2H), 6.82 (d, *J* = 8.8 Hz, 2H), 6.16 (bt, 2H), 3.77 (s, 3H). **^{13}C{^{1}H} NMR** (126 MHz, $CDCl_3$) δ 167.1, 159.7, 139.5, 135.0, 134.1, 131.9, 131.4, 130.8, 129.6, 120.9, 120.6 (b), 114.4, 113.8, 55.4. **HRMS (*m*/*z*)**: (ESI+) calculated for $C_{18}H_{14}BrNNaO_2$ $[M+Na]^+$: 378.0100. Found: 378.0112. **IR (neat) ν_{max}**: 2924, 2853, 1699 ν(C=O), 1608, 1518, 1467, 1401, 1327, 1301, 1246, 1179, 1086, 1036, 907, 822, 732, 531 cm^{-1}.

(4-Fluoro-4'-methoxy-[1,1'-biphenyl]-2-yl)(1*H*-pyrrol-1-yl)methanone (**61**)

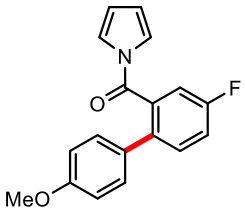

Prepared according to **GP3**; spectroscopic yield 80%. Flash column chromatography (5% EtOAc in petroleum ether) afforded the title compound as a colourless gum (70 mg, 59%). **^{1}H NMR** (400 MHz, $CDCl_3$) δ 7.44 (dd, *J* = 8.5, 5.3 Hz, 1H), 7.29 – 7.23 (m, 2H), 7.20 (d, *J* = 8.7 Hz, 2H), 6.99 (bs, 2H), 6.81 (d, *J* = 8.7 Hz, 2H), 6.15 (t, *J* = 2.1 Hz, 2H), 3.76 (s, 3H). **^{13}C{^{1}H} NMR** (101 MHz, $CDCl_3$) δ 167.0 (d, *J* = 2.2 Hz), 161.2 (d, *J* = 249.1 Hz), 159.3, 136.6 (d, *J* = 3.6 Hz), 134.6 (d, *J* = 7.0 Hz), 132.0 (d, *J* = 7.8 Hz), 130.7, 129.5, 120.4 (b), 117.9 (d, *J* = 21.0 Hz), 115.5 (d, *J* = 23.6 Hz), 114.1, 113.6, 55.2. **^{19}F{^{1}H} NMR** (377 MHz, $CDCl_3$) δ -114.8. **HRMS (*m*/*z*)**: (ESI+) calculated for $C_{18}H_{15}FNO_2$ $[M+H]^+$: 296.1081. Found: 296.1080. **IR (neat) ν_{max}**: 1698 ν(C=O), 1608, 1482, 1467, 1326, 1245, 1178, 1073, 1036, 825, 739, 536 cm^{-1}.

(5-Fluoro-4'-methoxy-[1,1'-biphenyl]-2-yl)(1*H*-pyrrol-1-yl)methanone (**62**)

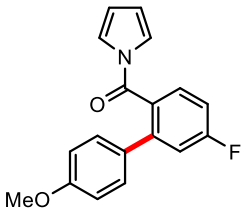

Prepared according to **GP3**; spectroscopic yield 82%. Flash column chromatography (5% EtOAc in petroleum ether) twice afforded the title compound as a colourless gum (70 mg, 59%). **^{1}H NMR** (400 MHz, $CDCl_3$) δ 7.53 (dd, *J* = 8.5, 5.6 Hz, 1H), 7.24 (d, *J* = 8.7 Hz, 2H), 7.18 (dd, *J* = 9.6, 2.5 Hz, 1H), 7.12 (td, *J* = 8.3, 2.6 Hz, 1H), 6.99 (bs, 2H), 6.83 (d, *J* = 8.7 Hz, 2H), 6.15 (t, *J* = 2.4 Hz, 2H), 3.77 (s, 3H). **^{13}C{^{1}H} NMR** (101 MHz, $CDCl_3$) δ 168.0, 164.0 (d, *J* = 251.7 Hz), 159.9, 143.7 (d, *J* = 8.4 Hz), 131.1 (d, *J* = 9.2 Hz), 130.9 (d, *J* = 1.9 Hz), 129.6, 127.2, 120.7 (b), 117.2 (d, *J* = 22.1 Hz), 114.4, 114.0 (d, *J* = 21.9 Hz), 113.6, 55.5. **^{19}F{^{1}H} NMR** (377 MHz, $CDCl_3$) δ -108.6. **HRMS (*m*/*z*)**: (ESI+) calculated for $C_{18}H_{15}FNO_2$ $[M+H]^+$: 296.1081. Found: 296.1081. **IR (neat) ν_{max}**: 1696 ν(C=O), 1607, 1517, 1466, 1327, 1304, 1246, 1178, 1087, 901, 833, 740 cm^{-1}.

(4'-Methoxy-4-(trifluoromethyl)-[1,1'-biphenyl]-2-yl)(1*H*-pyrrol-1-yl)methanone (**63**)

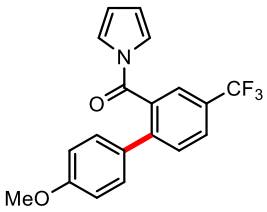

Prepared according to **GP3**; spectroscopic yield 48%. Flash column chromatography (5% EtOAc in petroleum ether) afforded the title compound as a colourless gum (59 mg, 42%). **^{1}H NMR** (400 MHz, $CDCl_3$) δ 7.83 (dd, *J* = 8.1, 1.3 Hz, 1H), 7.79 (s, 1H), 7.61 (d, *J* = 8.0 Hz, 1H), 7.26 (d, *J* = 8.8 Hz, 2H), 6.98 (bs, 2H), 6.84 (d, *J* = 8.8 Hz, 2H), 6.16 (t, 2H), 3.77 (s, 3H). **^{13}C{^{1}H} NMR** (101 MHz, $CDCl_3$) δ 167.4, 160.1, 144.1, 134.0, 130.9, 130.5, 129.7, 129.4 (q, *J* = 33.3 Hz), 127.8 (q, *J* = 3.5 Hz), 125.8 (q, *J* = 3.8 Hz), 123.9 (q, *J* = 272.3 Hz), 120.5 (b), 114.5, 114.0, 55.5. **^{19}F{^{1}H} NMR** (377 MHz, $CDCl_3$) δ -62.5. **HRMS (*m*/*z*)**: (ESI+) calculated for $C_{19}H_{15}F_3NO_2$ $[M+H]^+$: 346.1049. Found: 346.1048. **IR (neat) ν_{max}**: 1698 ν(C=O), 1608, 1523, 1467, 1342, 1318, 1300, 1247, 1169, 1124, 1083, 1036, 902, 829, 740 cm^{-1}.

(4'-Methoxy-5-(pyrrolidin-1-yl)-[1,1'-biphenyl]-2-yl)(1*H*-pyrrol-1-yl)methanone (**64**)

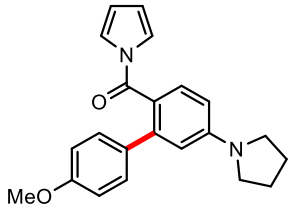

Prepared according to **GP3**; spectroscopic yield 67%. Flash column chromatography (10% EtOAc in petroleum ether) followed by a second flash column (15% EtOAc in petroleum ether) afforded the title compound as a bright-yellow oil (88 mg, 64%). **^{1}H NMR** (400 MHz, $CDCl_3$) δ 7.43 (d, *J* = 9.2 Hz, 1H), 7.24 (d, *J* = 5.3 Hz, 2H), 7.08 (t, *J* = 2.4 Hz, 2H), 6.81 (d, *J* = 8.7 Hz, 2H), 6.53 – 6.50 (m, 2H), 6.11 (t, *J* = 2.4 Hz, 2H), 3.77 (s, 3H), 3.40 – 3.36 (m, 4H), 2.06 – 2.03 (m, 4H). **^{13}C{^{1}H} NMR** (101 MHz, $CDCl_3$) δ 168.8, 159.0, 149.5, 143.4, 133.3, 131.6, 129.4, 120.8, 119.3, 113.7, 112.9, 112.1, 109.2, 55.2, 47.6, 25.5. **HRMS (*m*/*z*)**: (ESI+) calculated for $C_{22}H_{23}N_2O_2$ $[M+H]^+$: 347.1754. Found: 347.1749. **IR (neat) ν_{max}**: 2965, 2836, 1683 ν(C=O), 1598, 1502, 1463, 1380, 1324, 1297, 1244, 1176, 1084, 1070, 884, 830, 728 cm^{-1}.

(4'-Methoxy-4-(methylthio)-[1,1'-biphenyl]-2-yl)(1*H*-pyrrol-1-yl)methanone (**65**)

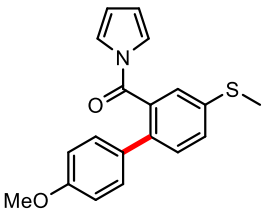

Prepared according to **GP3**; spectroscopic yield 51%. Flash column chromatography (5% EtOAc in petroleum ether) afforded the title compound as a beige solid (54 mg, 42%). **^{1}H NMR** (400 MHz, $CDCl_3$) δ 7.44 (dd, *J* = 8.2, 2.0 Hz, 1H), 7.39 (d, *J* = 8.2 Hz, 1H), 7.36 (d, *J* = 1.9 Hz, 1H), 7.22 (d, *J* = 8.8 Hz, 2H), 7.00 (bs, 2H), 6.81 (d, *J* = 8.8 Hz, 2H), 6.14 (bt, 2H), 3.77 (s, 3H), 2.53 (s, 3H). **^{13}C{^{1}H} NMR** (101 MHz, $CDCl_3$) δ 168.4, 159.4, 138.1, 137.1, 133.9, 131.4, 130.6, 129.6, 129.0, 126.0, 120.6 (b), 114.3, 113.6, 55.4, 15.9. **HRMS (*m*/*z*)**: (ESI+) calculated for $C_{19}H_{18}NO_2S$ $[M+H]^+$: 324.1053.

Found: 324.1052. **m.p.**: 114 – 116 °C. **IR (neat)** ν_{max}: 1712 ν(C=O), 1466, 1331, 1299, 1242, 1094, 1070, 1030, 816, 744, 590, 537 cm^{-1}.

(4-Methoxy-[1,1':4',1''-terphenyl]-2'-yl)(1*H*-pyrrol-1-yl)methanone (**66**)

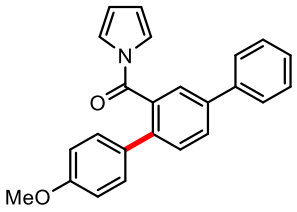

Prepared according to **GP3**; spectroscopic yield 47%. Flash column chromatography (5% EtOAc in petroleum ether) afforded the title compound as a colourless gum (64 mg, 45%). **^{1}H NMR** (400 MHz, $CDCl_3$) δ 7.71 – 7.60 (m, 5H), 7.51 – 7.47 (m, 2H), 7.42 (tt, *J* = 7.4, 1.3 Hz, 1H), 7.31 (d, *J* = 8.8 Hz, 2H), 7.08 (bs, 2H), 6.86 (d, *J* = 8.8 Hz, 2H), 6.18 (t, *J* = 2.4 Hz, 2H), 3.79 (s, 3H). **^{13}C{^{1}H} NMR** (101 MHz, $CDCl_3$) δ 168.7, 159.6, 144.0, 141.3, 140.1, 132.2, 132.0, 129.7, 129.4, 129.2, 129.1, 128.3, 127.5, 125.5, 120.7 (b), 114.3, 113.4, 55.4. **HRMS (*m*/*z*)**: (ESI+) calculated for $C_{24}H_{20}NO_2$ $[M+H]^+$: 354.1489. Found: 354.1500. **IR (neat)** ν_{max}: 1697 ν(C=O), 1604, 1464, 1326, 1302, 1246, 1178, 1086, 1028, 884, 834, 737, 697 cm^{-1}.

(2-(4-Methoxyphenyl)pyridin-3-yl)(1*H*-pyrrol-1-yl)methanone (**67**)

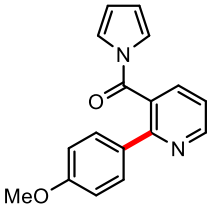

Prepared according to **GP3**; spectroscopic yield 46%. In this case, the reaction was quenched with 1 M HCl (10 ml) and the organics extracted from the aqueous layer with CH_2Cl_2 (3 x 10 ml). The aqueous layer was then made alkaline by the addition of 1 M KOH and the organics extracted again with CH_2Cl_2 (3 x 10 ml). Flash column chromatography (25% EtOAc in petroleum ether) afforded the title compound as a colourless gum (29 mg, 27%). **^{1}H NMR** (400 MHz, $CDCl_3$) δ 8.83 (dd, *J* = 4.8, 1.7 Hz, 1H), 7.86 (dd, *J* = 7.7, 1.7 Hz, 1H), 7.55 (d, *J* = 8.8 Hz, 2H), 7.35 (dd, *J* = 7.7, 4.8 Hz, 1H), 7.00 (bs, 2H), 6.85 (d, *J* = 8.8 Hz, 2H), 6.18 (bt, 2H), 3.78 (s, 3H). **^{13}C{^{1}H} NMR** (101 MHz, $CDCl_3$) δ 167.5, 160.5, 156.5, 151.3, 137.0, 131.0, 129.8, 128.5, 120.8, 120.2 (b), 114.1, 113.8, 55.2. **HRMS (*m*/*z*)**: (ESI+) calculated for $C_{17}H_{14}N_2NaO_2$ $[M+Na]^+$: 301.0947. Found: 301.0961. **IR (neat)** ν_{max}: 1696 ν(C=O), 1428, 1331, 1252, 1177, 1091, 1022, 882, 781, 737, 583 cm^{-1}.

(4'-Methyl-[1,1'-biphenyl]-2-yl)(1*H*-pyrrol-1-yl)methanone (**69**)

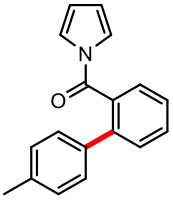

Prepared according to **GP3**, stirring for 3 h; spectroscopic yield 82%. **69** can also be prepared using the activated boronate prepared *in situ* as follows: To a Schlenk-tube was added IMes·HCl (13.6 mg, 0.04 mmol) and $FeBr_3$ (0.02 M in THF, 2 ml, 0.04 mmol) and the mixture stirred at room temperature for 1 h before the addition of $MgBr_2{\cdot}OEt_2$ (0.1 M in THF, 0.8 ml, 0.08 mmol) and **17** (82.3 mg 0.4 mmol). To a separate Schlenk-tube was added 4-tolylboronic acid pinacol ester (424.4 mg, 1.56 mmol) and THF (3 ml). The solution was cooled to -40 °C (acetonitrile/liq. N_2 bath) and *tert*-butyllithium (Caution! 1.7 M in pentane, 0.71 ml, 1.2 mmol) was added slowly. The solution was stirred for 30 min and then warmed to room temperature and then stirred for another 30 min. The activated boronate was then added to the first Schlenk-tube which was then sealed, and the reaction stirred for 3 h at 60 ºC before quenching by the addition of 1 M HCl (10 ml). The organics were extracted from the aqueous layer with CH_2Cl_2 (3 x 10 ml), the combined organic layers dried over $MgSO_4$ and filtered. 1,3,5-Trimethoxybenzene (67.3 mg, 0.4 mmol) was added and an aliquot taken for analysis by ^{1}H NMR (spectroscopic yield 84%). The crude mixture was purified by flash column chromatography (5% Et_2O in petroleum ether) to yield the title compound as a yellow oil (68 mg, 65%). **^{1}H NMR** (400 MHz, $CDCl_3$) δ 7.60 – 7.42 (m, 4H), 7.21 (d, *J* = 8.1 Hz, 2H), 7.11 (d, *J* = 7.9 Hz, 2H), 7.03 (bs, 2H), 6.16 (t, *J* = 2.4 Hz, 2H), 2.31 (s, 3H). **^{13}C{^{1}H} NMR** (101 MHz, $CDCl_3$) δ 168.7, 141.1, 137.8, 136.7, 133.5, 131.1, 130.4, 129.5, 128.8, 128.4, 127.1, 120.8 (b), 113.4, 21.4. **HRMS (*m/z*)**: (ESI+) calculated for $C_{18}H_{16}NO$ $[M+H]^+$: 262.1226. Found: 262.1237. **IR (neat) ν_{max}**: 1702 ν(C=O), 1466, 1327, 1303, 1085, 1072, 876, 820, 738, 709, 662 cm^{-1}.

(2-(Naphthalen-2-yl)phenyl)(1*H*-pyrrol-1-yl)methanone (**70**)

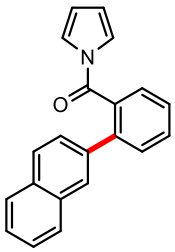

Prepared according to **GP3**, stirring for 3 h; spectroscopic yield 52% (using 3,4,5-trichloropiridine as internal standard). Flash column chromatography (5% EtOAc in petroleum ether) followed by preparative TLC (50% toluene in petroleum ether) afforded the title compound as a colourless gum (40 mg, 37%). **^{1}H NMR** (400 MHz, $CDCl_3$) δ 7.81 – 7.77 (m, 4H), 7.67 – 7.59 (m, 3H), 7.52 – 7.44 (m,

4H), 7.04 (bs, 2H), 6.11 (t, *J* = 2.4 Hz, 2H). **$^{13}C\{^{1}H\}$ NMR** (101 MHz, $CDCl_3$) δ 168.6, 141.0, 137.1, 133.9, 133.5, 132.8, 131.2, 130.8, 128.9, 128.5, 128.4, 127.9, 127.8, 127.4, 126.6, 126.5, 126.5, 120.7 (b), 113.5. **HRMS (*m*/*z*)**: (ESI+) calculated for $C_{21}H_{15}NNaO$ $[M+Na]^+$: 320.1046. Found: 320.1046. **IR (neat) ν_{max}**: 1699 ν(C=O), 1465, 1327, 1304, 1085, 1072, 884, 735, 659, 478 cm^{-1}.

(4'-Chloro-[1,1'-biphenyl]-2-yl)(1*H*-pyrrol-1-yl)methanone (**71**)

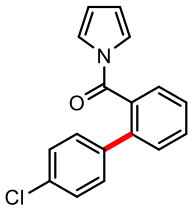

Prepared according to **GP3**, stirring for 3 h; spectroscopic yield 52%. Flash column chromatography (5% EtOAc in petroleum ether) afforded a gummy mixture (82 mg) of **71** and **17** (60:40). Co-elution of **71** and **17** in multiple eluent systems frustrated attempts of isolation of the pure desired compound. *Selected* **^{1}H NMR** (400 MHz, $CDCl_3$) δ 7.00 (bs, 2H), 6.17 (t, *J* = 2.4 Hz, 2H). *Selected* **$^{13}C\{^{1}H\}$ NMR** (126 MHz, $CDCl_3$) δ 168.3, 120.7 (b), 113.7. **HRMS (*m*/*z*)**: (ESI+) calculated for $C_{17}H_{12}ClNNaO$ $[M+Na]^+$: 304.0500. Found: 304.0508.

7.2.9 Alternative Preparation of Biaryls

The independent synthesis of compounds **21**, **30**, **32**, **88** and **89** was carried out to allow the determination of spectroscopic yield from low yielding cross-coupling procedures (**32** and **88**), GC calibration for optimisation studies (**21**) and for purposes of identification (**88** and **89**).

Preparation of **21**

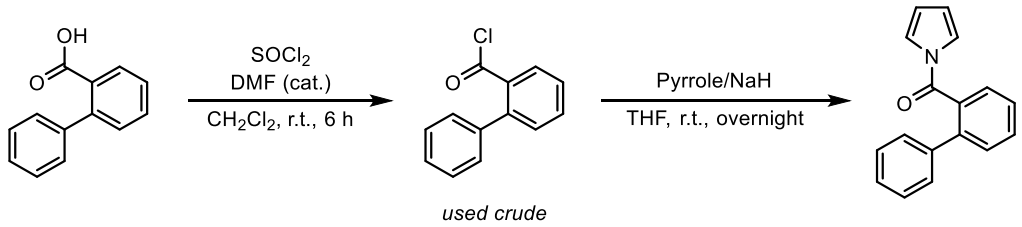

In a 100 ml round-bottom flask, biphenyl-2-carboxylic acid (1.00 g, 5.04 mmol) was dissolved in CH_2Cl_2 (10 ml) and the solution cooled to 0 °C. DMF (a few drops) was added followed by thionyl chloride (3.66 ml, 50.4 mmol) causing effervescence. The solution was warmed to room temperature and stirred for 6 h before the solvent and excess thionyl chloride were removed *in vacuo* and the residue dissolved in THF (20 ml). In a separate 100 ml round-bottom flask was added pyrrole (0.35 ml, 5.04 mmol) and THF (20 ml). The solution was cooled to 0 °C and sodium hydride (60% dispersion in mineral oil, 201 mg, 5.03 mmol) was added in one portion. The mixture was stirred for 30 min during which effervescence was observed, and then warmed to room temperature and stirred for a further 30 min. The mixture was then cooled to 0 °C and the crude acid chloride mixture in THF was added *via*

cannula. The reaction was stirred at room temperature overnight before being quenched by the addition of 1 M HCl (10 ml). The organics were extracted from the aqueous layer with CH_2Cl_2 (3 x 25 ml), the combined organic layers dried over $MgSO_4$, filtered and the solvent removed under reduced pressure to afford the crude compound. Purification by flash column chromatography (10% Et_2O in petroleum ether) afforded a dark oil which became a solid upon standing. The compound was further purified by recrystallisation from petroleum ether affording a colourless solid (0.550 g, 44%). Spectroscopic data as above.

Preparation of **30**

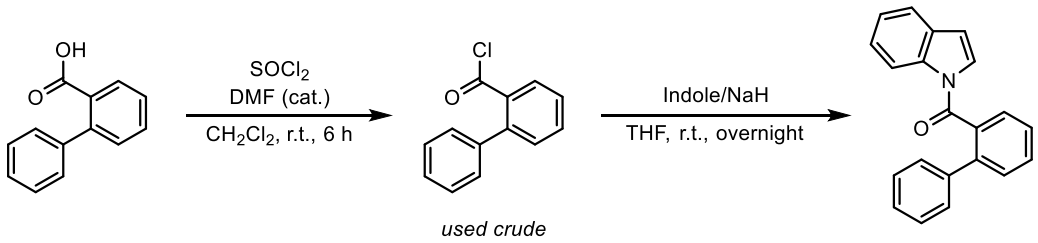

The preparation of **30** was carried out in the same way as the preparation of **17**, using indole instead of pyrrole. Flash column chromatography (10% EtOAc in petroleum ether) followed by recrystallisation from petroleum ether afforded the desired compound as a colourless solid (0.554 g, 37%). **^{1}H NMR** (400 MHz, $CDCl_3$) δ 8.31 (bs, 1H), 7.66 – 7.61 (m, 2H), 7.57 – 7.47 (m, 3H), 7.38 – 7.16 (m, 7H), 6.97 (bs, 1H), 6.40 (d, *J* = 3.8 Hz, 1H). **^{13}C{^{1}H} NMR** (101 MHz, $CDCl_3$) δ 169.3, 140.7, 139.4, 135.7, 134.7, 131.1, 130.9, 130.4, 128.7, 128.5, 127.9, 127.7, 127.1, 125.0, 124.0, 120.9, 116.4 (b), 109.0. **HRMS (*m*/*z*)**: (ESI+) calculated for $C_{21}H_{15}NNaO$ $[M+Na]^+$: 320.1046. Found: 320.1047. **m.p.**: 96 – 98 °C **IR (neat) ν_{max}**: 1695 ν(C=O), 1446, 1335, 1204, 889, 870, 741, 697, 673, 632, 423 cm^{-1}.

Preparation of **32**

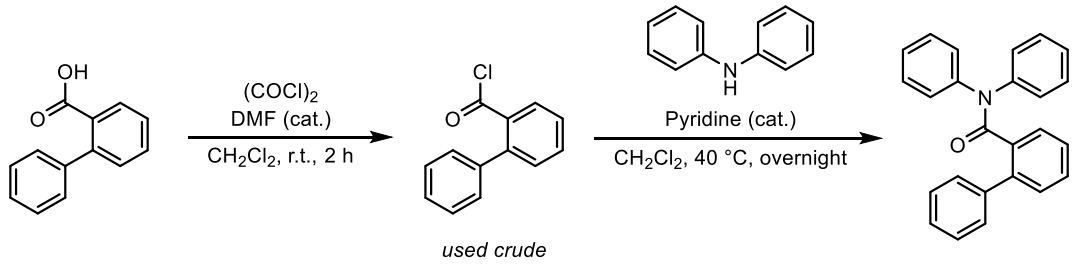

In a 50 ml round-bottom flask, biphenyl-2-carboxylic acid (0.991 g, 5 mmol) was dissolved in CH_2Cl_2 (10 ml) and DMF (a few drops) added. The solution was stirred whilst oxalyl chloride (0.5 ml, 6 mmol) was added dropwise causing effervescence and the solution stirred for 2 h at room temperature before all the volatiles were removed *in vacuo* and the resulting residue dissolved in CH_2Cl_2 (15 ml). Pyridine (a few drops) was added followed by diphenylamine (0.8461 g, 5 mmol) and the resulting solution was warmed to 40 °C and stirred overnight. The solution was then allowed to cool to room temperature before being quenched by the addition of 1 M NaOH (10 ml) and the organics extracted from the

aqueous layer with EtOAc (3 x 20 ml). After drying over $MgSO_4$, the volatiles were removed under reduced pressure and the crude mixture purified by flash column chromatography (20% ethyl acetate in petroleum ether) followed by recrystallisation from ethanol to afford the desired compound as colourless crystals (0.876 g, 50%). **^{1}H NMR** (400 MHz, $CDCl_3$) δ 7.72 (dd, *J* = 7.4, 1.7 Hz, 1H), 7.45 – 7.28 (m, 7H), 7.27 – 7.24 (m, 2H), 7.19 (bs, 3H), 7.13 (dd, *J* = 7.3, 1.6 Hz, 1H), 6.96 (bs, 1H), 6.91 (bs, 2H), 6.28 (bs, 2H). **^{13}C{^{1}H} NMR** (101 MHz, $CDCl_3$) δ 171.4, 143.1 (b), 142.1 (b), 140.0, 139.0, 136.3, 129.9, 129.8, 129.6, 129.5, 129.1 (b), 128.5 (b), 128.4, 128.2 (b), 127.9, 127.4, 126.8 (b), 126.5 (b), 126.2 (b). **HRMS (*m/z*)**: (ESI+) calculated for $C_{25}H_{19}NNaO$ $[M+Na]^+$: 372.1359. Found: 372.1372. **m.p.**: 161 – 162 °C. **IR (neat) ν_{max}**: 1648 ν(C=O), 1490, 1345, 760, 745, 695, 502 cm^{-1}.

Preparation of **88**

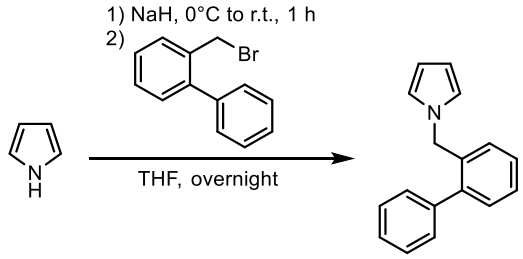

The preparation of **88** was carried out in the same way as the preparation of **17** (according to **GP1**, section 7.2.2) from 2-phenylbenzylbromide (2.5 mmol scale). Flash column chromatography (1% Et_2O in petroleum ether) afforded the title compound as a yellow solid (0.230 g, 48%). **^{1}H NMR** (400 MHz, $CDCl_3$) δ 7.45 – 7.24 (m, 8H), 7.03 (dd, *J* = 6.7, 1.8 Hz, 1H), 6.52 (t, *J* = 2.1 Hz, 2H), 6.13 (t, *J* = 2.1 Hz, 2H), 4.99 (s, 2H). **^{13}C{^{1}H} NMR** (101 MHz, $CDCl_3$) δ 141.6, 140.6, 135.4, 130.3, 129.2, 128.5, 128.3, 128.0, 127.7, 127.5, 121.2, 108.4, 51.3. **HRMS (*m/z*)**: (ESI+) calculated for $C_{17}H_{16}N$ $[M+H]^+$: 234.1292. Found: 234.1277. **m.p.**: 56 – 57 °C. **IR (neat) ν_{max}:** 1497, 1475, 1435, 1287, 1089, 1068, 1008, 754, 724, 699, 613 cm^{-1}.

Preparation of **89**

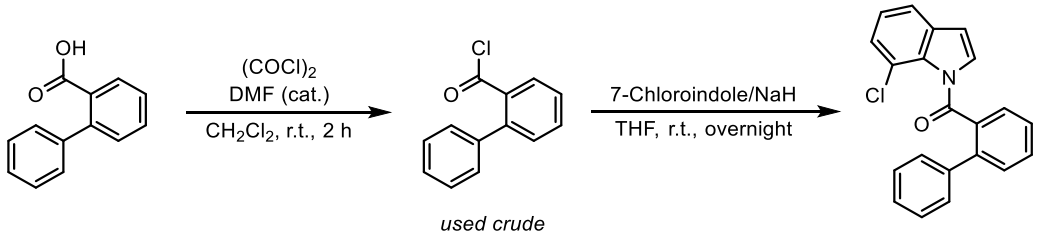

In a 50 ml round-bottom flask, biphenyl-2-carboxylic acid (0.496 g, 2.5 mmol) was dissolved in CH_2Cl_2 (5 ml) and DMF (a few drops) added. The solution was stirred whilst oxalyl chloride (0.25 ml, 3 mmol) was added dropwise causing effervescence and the solution stirred for 2 h at room temperature before all the volatiles were removed *in vacuo* and the resulting residue dissolved in THF (10 ml). In a separate 50 ml round-bottom flask was added 7-chloroindole (0.379 g, 2.5 mmol) and THF (10 ml). The solution

was cooled to 0 °C and sodium hydride (60% dispersion in mineral oil, 100 mg, 2.5 mmol) was added in one portion. The mixture was stirred for 30 min during which effervescence was observed, and then warmed to room temperature and stirred for a further 30 min. The mixture was then cooled to 0 °C and the crude acid chloride mixture in THF was added *via* cannula. The reaction was stirred at room temperature overnight before being quenched by the addition of 1 M HCl (10 ml). The organics were extracted from the aqueous layer with CH_2Cl_2 (3 x 15 ml), the combined organic layers dried over $MgSO_4$, filtered and the solvent removed under reduced pressure to afford the crude compound. Purification by flash column chromatography (10% Et_2O in petroleum ether) afforded the desired compound as a pale-pink solid (0.252 g, 30%). **^{1}H NMR** (400 MHz, $CDCl_3$) δ 7.81 (d, *J* = 8.1 Hz, 1H), 7.65 (td, *J* = 7.5, 1.4 Hz, 1H), 7.53 – 7.49 (m, 2H), 7.36 – 7.26 (m, 4H), 7.21 – 7.09 (m, 4H), 6.96 (d, *J* = 3.7 Hz, 1H), 6.33 (d, *J* = 3.7 Hz, 1H). **^{13}C{^{1}H} NMR** (101 MHz, $CDCl_3$) δ 167.4, 142.5, 139.27, 134.3, 133.8, 132.7, 132.1, 130.9, 130.8, 129.1, 128.7, 128.3, 127.7, 127.7, 126.7, 124.4, 121.1, 119.5, 107.6. **HRMS (*m*/*z*)**: (ESI+) calculated for $C_{21}H_{14}ClNNaO$ $[M+Na]^+$: 354.0656. Found: 354.0656. **m.p.**: 115 – 116 °C. **IR (neat) ν_{max}:** 1690 ν(C=O), 1411, 1314, 1175, 940, 870, 742, 695, 641 cm^{-1}.

7.2.10 Optimisation of Ketone Synthesis from 17 by Nucleophilic Addition of Borate 18

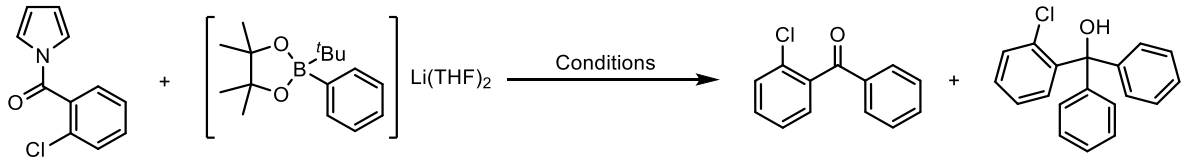

To a Schlenk-tube was added **17** (51.4 mg, 0.25 mmol) and THF (2 ml). The desired amount of **18** was added in portion and the resulting reaction was stirred at the desired temperature. After leaving for the desired amount of time, dodecane (57 µl, 0.25 mmol) was added an aliquot (~ 0.1 ml) removed from the reaction. This was quenched by through a pad of silica gel (EtOAc as eluent) and the crude mixture analysed by GC.

7.2.11 Optimisation of Undirected Iron-Catalysed Suzuki Biaryl Cross-Coupling

In a glovebox, a 7.5 ml vial was charged with $FeBr_3$ (3 mg, 0.01 mmol), IMes·HCl (3.4 mg, 0.01 mmol), $MgBr_2{\cdot}OEt_2$ (5.2 mg, 0.02 mmol) and borate **74** (58.2 mg, 0.2 mmol). Solvent (2 ml) was added followed by chlorobenzene (10 µl, 0.1 mmol) and the resulting mixture stirred at 100 °C (except when THF was used: 80 °C) in a heating block overnight. Dodecane (22.7 µl, 0.1 mmol) was added and

aliquot (~ 0.1 ml) removed from the crude mixture. This was quenched by eluting through a plug of silica gel (EtOAc as eluent) and the crude mixture was analysed by GC.

7.3 Substrate-Directed Iron-Catalysed Suzuki Biaryl Cross-Coupling: Mechanism

*[(IMes)Fe(dvtms)] (**86**) was prepared according to a literature procedure.*[143]

7.3.1 Formation of Complex 86 with 18 as Reductant/Base

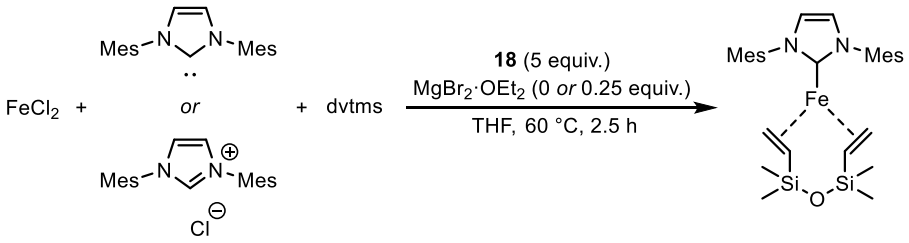

In a glovebox, a Schlenk-tube was charged with IMes (76.1 mg, 0.25 mmol). The tube was sealed, taken out of the glovebox and THF (2 ml) added. $FeCl_2$ (31.7 mg, 0.25 mmol) and 1,3-divinyltetramethyldisiloxane (58 µL, 0.25 mmol) were added and the resulting mixture was stirred for 1 h at room temperature. $MgBr_2{\cdot}OEt_2$ (0.1 M in THF, 0.625 ml, 0.0625 mmol or 0 mmol) was added followed by **18** (515.5 mg, 1.25 mmol) and the mixture heated to 60 °C for 2.5 h during which the colour changed to dark brown and then dark green. An aliquot was taken, the solvent removed *in vacuo* and the residue dissolved in C_6D_6 for ^{1}H NMR analysis. The procedure was repeated on a 0.1 mmol scale using IMes·HCl (34 mg, 0.1 mmol) instead of IMes in the absence of $MgBr_2{\cdot}OEt_2$.

7.3.2 Iron-Catalysed Suzuki Biaryl Cross-Coupling with 86 as Pre-Catalyst

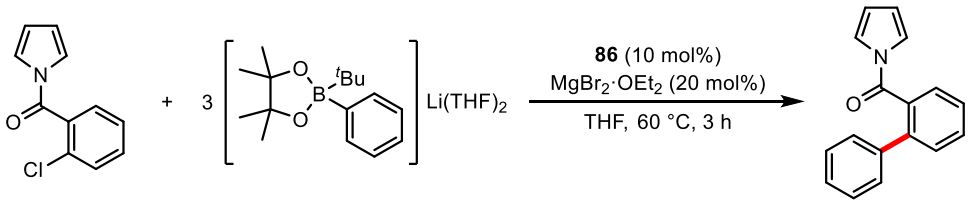

In a glovebox, a Schlenk-tube equipped with a stirrer bar was charged with **86** (11.6 mg, 0.02 mmol). The tube was sealed, taken out of the glovebox and THF (1 ml) was added. $MgBr_2{\cdot}OEt_2$ (0.1 M in THF, 0.4 ml, 0.04 mmol) and **17** (41.1 mg, 0.2 mmol) were added before the addition of **18** (0.4 M in THF, 1.5 ml, 0.6 mmol). The Schlenk-tube was sealed, the reaction stirred for 3 h at 60 ºC and then quenched by the addition of 1 M HCl (10 ml). The organics were extracted from the aqueous layer with CH_2Cl_2 (3 x 10 ml), the combined organics layers dried over $MgSO_4$ and filtered. 1,3,5-Trimethoxybenzene (33.6 mg, 0.2 mmol) was added and an aliquot taken for analysis by ^{1}H NMR showing **21** to be formed in 73% yield.

7.3.3 TEM of Catalytic Reaction Mixture

In a glovebox, a 7.5 ml vial was charged with IMes·HCl (3.4 mg, 0.01 mmol). $FeBr_3$ (0.02 M in THF, 500 µl, 0.01 mmol) was added and the mixture stirred for 1 h at room temperature before the addition of $MgBr_2{\cdot}OEt_2$ (0.1 M in THF, 200 µl, 0.02 mmol). To a separate 7.5 ml vial was added **17** (20.6 mg, 0.1 mmol) and **18** (0.4 M in THF, 550 µl, 0.22 mmol). The first vial was heated to 60 °C in a heating block for 5 mins with stirring before the addition of the **17**/**18** mixture. An aliquot (50 µl) was taken from the resulting reaction mixture at 90 s and drop-cast onto carbon-covered 3 mm Cu grids and the solvent allowed to evaporate. The grids were removed from the glovebox in a sealed Ar-filled vial and handled briefly in air whilst loaded into a single-tilt specimen holder before transfer into the TEM column.

7.3.4 Hg Drop Test

The catalytic coupling of **17** and **18** was carried out as described in Section 7.3.7, adding Hg (one drop) from a Pasteur pipette into the reaction mixture 58 s after the addition of **18**. Aliquots were taken for GC analysis before and after the addition of Hg. The addition of Hg did not affect the production of **21**.

7.3.5 PEG-Stabilised Iron-Nanoparticles as Pre-Catalyst

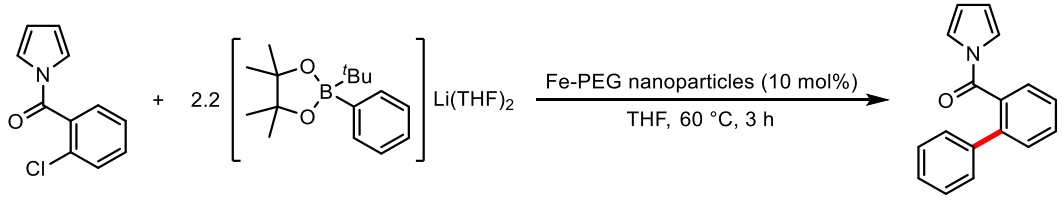

A suspension of iron nanoparticles was prepared according to a literature method:[93] In a glovebox, a Schlenk-tube was charged with $FeCl_3$ (8.1 mg, 0.05 mmol) and polyethylene glycol (pre-dried by toluene azeotrope, M_w = 10,000, 3 mg, 0.05 mmol). The tube was sealed, taken out of the glovebox and CH_2Cl_2 (2 ml) was added. The mixture was stirred for 2 min before the volatiles were removed *in vacuo*. Et_2O (2 ml) was added before 4-tolylmagnesium bromide (0.5 M in Et_2O, 0.3 ml, 0.15 mmol) and the resulting mixture stirred for 1 h at room temperature, affording a suspension of black material.

To a separate Schlenk-tube was added **17** (102.8 mg, 0.5 mmol) and **18** (0.4 M in THF, 2.75 ml, 1.1 mmol) and the resulting mixture was added to the first Schlenk-tube which was then sealed. The reaction was stirred at 60 °C for 3 h and then quenched by the addition of 1 M HCl (10 ml). The organics were extracted from the aqueous layer with CH_2Cl_2 (3 x 10 ml), the combined layers dried over $MgSO_4$ and filtered. 1,3,5-Trimethoxybenzene (84.1 mg, 0.5 mmol) was added and an aliquot taken for analysis by ^{1}H NMR spectroscopy revealing the formation of **21** in 9% yield. The use of PEG as a ligand afforded **21** in 16% yield.

7.3.6 Cross-Coupling Reactions with Alternative Nucleophiles

Cross-Coupling of **17** with phenylmagnesium bromide

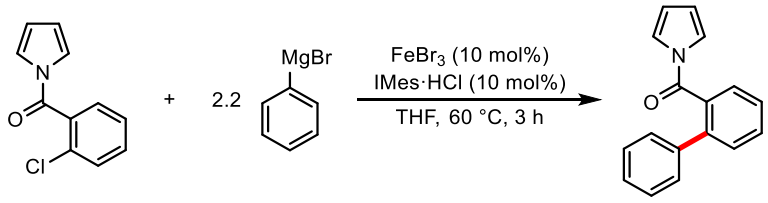

To a Schlenk-tube was added IMes·HCl (6.8 mg, 0.02 mmol) and $FeBr_3$ (0.02 M in THF, 1 ml, 0.02 mmol). The mixture was stirred at room temperature for 1 h before **17** (41.1 mg, 0.2 mmol) and phenylmagnesium bromide (1.06 M in THF, 0.42 ml, 0.44 mmol) were added sequentially. The Schlenk-tube was sealed, and the reaction stirred for 3 h at 60 °C and then quenched by the addition of 1 M HCl (5 ml). The organics were extracted from the aqueous layer with CH_2Cl_2 (3 x 5 ml), the combined layers dried over $MgSO_4$ and filtered. 1,3,5-Trimethoxybenzene (33.6 mg, 0.2 mmol) was added and an aliquot taken for analysis by ^{1}H NMR spectroscopy revealing the production of **21** in 45% yield.

Cross-Coupling of **17** with diphenylzinc

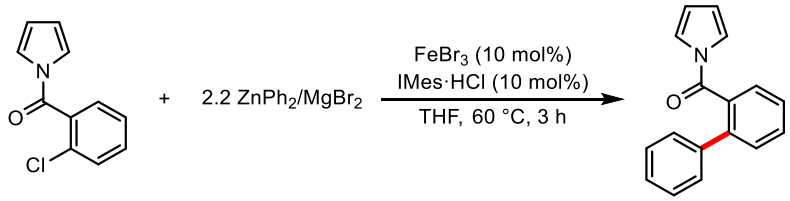

In a glovebox, a Schlenk-tube was charged with $ZnBr_2$ (49.5 mg, 0.22 mmol). The tube was sealed, taken out of the glovebox and THF (1 ml) was added. Phenylmagnesium bromide (1.0 M in THF, 0.44 ml, 0.44 mmol) was added and the resulting mixture stirred for 1 h. To a separate Schlenk-tube was added IMes·HCl (3.4 mg, 0.01 mmol) and $FeBr_3$ (0.02 M in THF, 0.5 ml, 0.01 mmol). The mixture was stirred at room temperature for 1 h before the addition of **17** (20.6 mg, 0.1 mmol) and the mixture from the first Schlenk-tube. The Schlenk-tube was sealed, and the reaction stirred for 3 h at 60 °C and then quenched by the addition of 1 M HCl (5 ml). The organics were extracted from the aqueous layer with CH_2Cl_2 (3 x 5 ml), the combined layers dried over $MgSO_4$ and filtered. 1,3,5-Trimethoxybenzene (16.8 mg, 0.1 mmol) was added and an aliquot taken for analysis by ^{1}H NMR spectroscopy revealing the formation of **21** in 6% yield.

Cross-Coupling of **17** with MgBr[Al(4-tol)$_4$]

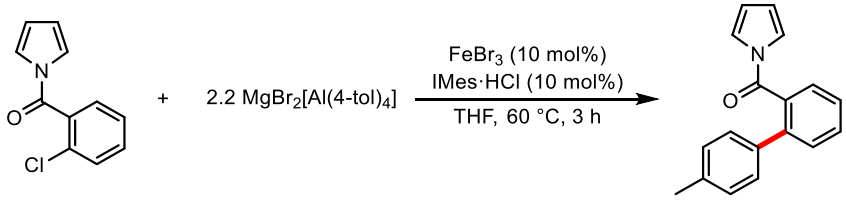

In a glovebox, a Schlenk-tube was charged with $AlBr_3$ (58.7 mg, 0.22 mmol). The tube was sealed, taken out of the glovebox and THF (1 ml) was added. The solution was cooled to 0 °C and 4-tolylmagnesium bromide (1.0 M in THF, 0.88 ml, 0.88 mmol) was added and the resulting mixture then warmed to room temperature and stirred for 30 min. To a separate Schlenk-tube was added IMes·HCl (3.4 mg, 0.01 mmol) and $FeBr_3$ (0.02 M in THF, 0.5 ml, 0.01 mmol). The mixture was stirred at room temperature for 1 h before the addition of **17** (20.6 mg, 0.1 mmol) and the mixture from the first Schlenk-tube. The Schlenk-tube was sealed, and the reaction stirred for 3 h at 60 °C and then quenched by the addition of 1 M HCl (5 ml). The organics were extracted from the aqueous layer with CH_2Cl_2 (3 x 5 ml), the combined layers dried over $MgSO_4$ and filtered. 1,3,5-Trimethoxybenzene (16.8 mg, 0.1 mmol) was added and an aliquot taken for analysis by ^{1}H NMR spectroscopy revealing no formation of **21**.

7.3.7 Influence of $MgBr_2$ on the Suzuki Cross-Coupling Reaction

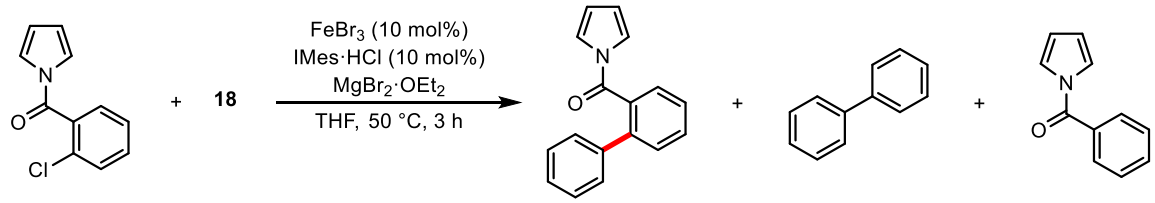

To a Schlenk-tube was added IMes·HCl (17.0 mg, 0.05 mmol, 5 mM) and $FeBr_3$ (14.8 mg, 0.05 mmol, 5 mM) in THF (2.0 ml). The mixture was stirred for 1 h at room temperature before the addition of dodecane (42.6 mg, 0.25 mmol, 25 mM), **17** (102.8 mg, 0.50 mmol, 50 mM), the appropriate amount of $MgBr_2{\cdot}OEt_2$ and THF (total reaction volume 10.0 ml). The mixture was warmed to 50 °C before the rapid addition of **18** in one portion (515.4 mg, 1.25 mmol, 125 mM). The progress of the reaction was monitored by the drawing of aliquots (0.1 ml) which were quenched by injecting into 3.5 ml vials containing 1.0 M HCl (~ 1 ml). The organics were extracted into CH_2Cl_2 and analysed by GC.

7.3.8 Kinetic Analysis of the Suzuki Cross-Coupling Reaction

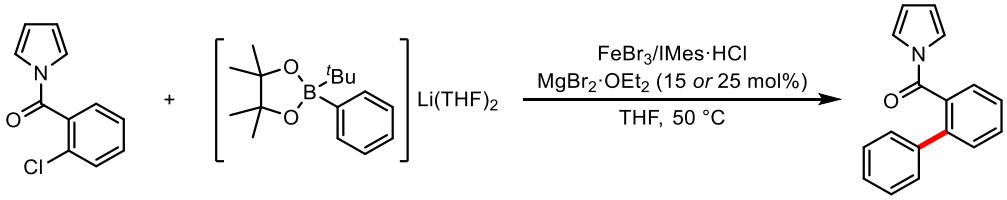

Kinetic analysis were performed as described in Section 7.3.7, varying the concentration of $FeBr_3$/IMes·HCl, **17** and **18** at either 15 or 25 mol% $MgBr_2 \cdot OEt_2$ loading.

7.3.9 Secondary Deuterium Kinetic Isotope Effect

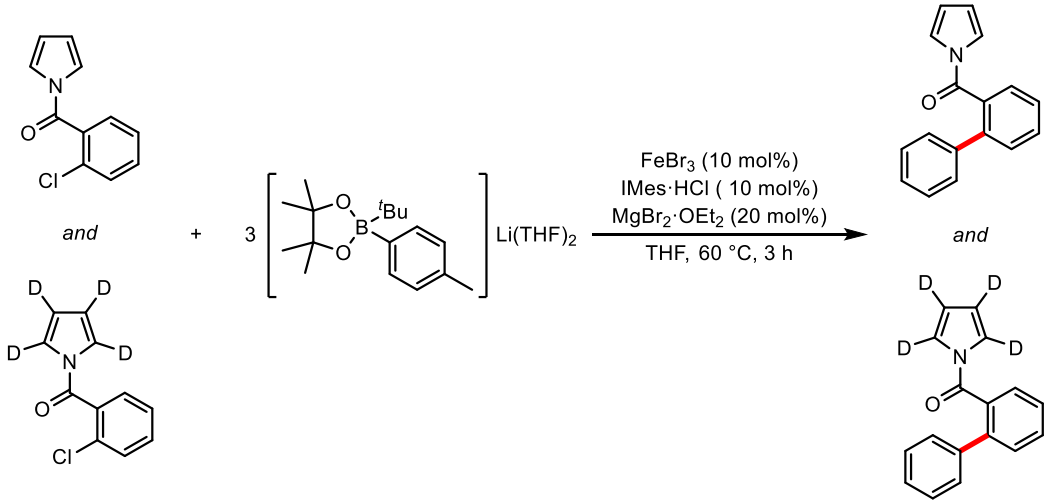

To a Schlenk-tube was added IMes·HCl (13.6 mg, 0.04 mmol) and $FeBr_3$ (0.02 M in THF, 2 ml, 0.04 mmol) and the resulting mixture stirred at room temperature for 1 h. To a separate Schlenk-tube was added 4-tolylboronic acid pinacol ester (1.5671 g, 5.76 mmol) and THF (8 ml). The solution was cooled to -40 °C (acetonitrile/liq. N_2 bath) and *tert*-butyllithium (Caution! 1.7 M in pentane, 2.82 ml, 4.8 mmol) was added slowly. The solution was stirred for 30 min before being warmed to room temperature and then stirred for another 30 min. The appropriate amount of $MgBr_2 \cdot OEt_2$ (0.1 M in THF) **17** (41.1 mg 0.2 mmol) and **17-d$_4$** (42.0 mg 0.2 mmol) was added to the first Schlenk-tube and the mixture heated to 60 °C for 5 min before rapid addition of a portion of the activated boronate solution (2 ml, 1.2 mmol) causing the mixture to turn black. This was then quenched at the appropriate time by the rapid addition of water (10 ml) *via* syringe. The organics were then extracted into CH_2Cl_2 (3 x 10 ml), the combined layers dried over Na_2SO_4 and filtered. 1,3,5-Trimethoxybenzene (67.3 mg, 0.4 mmol) was added and an aliquot taken for analysis by ^{1}H NMR spectroscopy.

7.3.10 Attempted Isolation of an Iron(0) Pyrrole Amide Complex

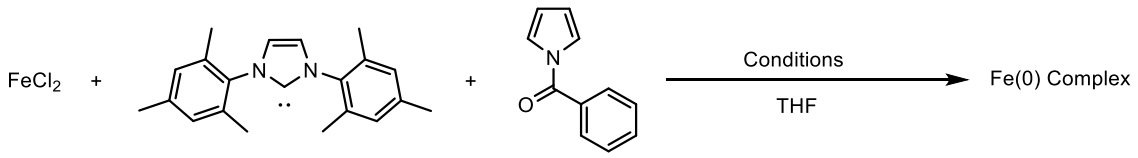

Na/Hg amalgam:

In a glovebox, a Schlenk-tube was charged with IMes (304.4 mg, 1 mmol). The tube was sealed, taken out of the glovebox and THF (7 ml) added. $FeCl_2$ (126.8 mg, 1 mmol) and **27** (197 µL, 1 mmol) were added and the resulting mixture was stirred for 1 h at room temperature. The resulting solution was added to a separate Schlenk containing Na/Hg amalgam (55.1 mg Na in 56 g Hg) *via* cannula, the colour

changing from dark brown to an intense red. The mixture was stirred overnight at room temperature before filtering through Celite and removing the volatiles *in vacuo*. The residue was washed with hexane (10 ml) to afford a dark brown powder.

KC_8:

In a glovebox, a Schlenk-tube was charged with IMes (76.1 mg, 0.25 mmol). The tube was sealed, taken out of the glovebox and THF (2 ml) added. $FeCl_2$ (31.7 mg, 0.25 mmol) and **27** (49 µL, 0.25 mmol) were added and the resulting mixture was stirred for 1 h at room temperature. The resulting dark brown solution was cooled to -40 °C (acetonitrile/liq. N_2 bath) and KC_8 (67.6 mg, 0.5 mmol) was added in one portion, causing the mixture to turn deep orange/brown. The reaction was stirred overnight, gradually warming to room temperature. An aliquot was taken, the solvent removed *in vacuo* and the residue dissolved in C_6D_6 for ^1H NMR analysis.

Borate/$MgBr_2$:

In a glovebox, a Schlenk-tube was charged with IMes (76.1 mg, 0.25 mmol). The tube was sealed, taken out of the glovebox and THF (2 ml) added. $FeCl_2$ (31.7 mg, 0.25 mmol) and **27** (49 µL, 0.25 mmol) were added and the resulting mixture was stirred for 1 h at room temperature. $MgBr_2 \cdot OEt_2$ (0.1 M in THF, 0.625 ml, 0.0625 mmol) was added followed by **18** (0.4 M in THF, 3.1 ml, 1.25 mmol) and the mixture heated to 60 °C for 1.5 h. An aliquot was taken, the solvent removed *in vacuo* and the residue dissolved in C_6D_6 for ^1H NMR analysis.

7.3.11 Radical Trap Experiments

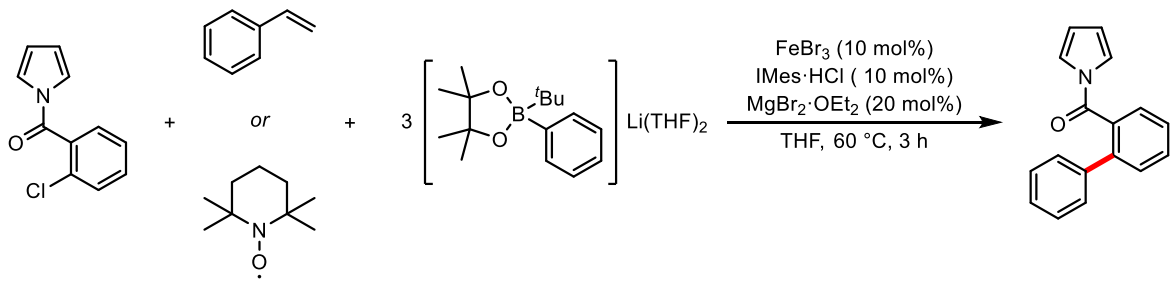

Reactions performed according to **GP3** (0.2 mmol scale) with either styrene (35 µl, 0.3 mmol) or TEMPO (46.9 mg, 0.3 mmol) added to the reaction mixture before the addition of **18**. The addition of styrene had little effect on the reaction (furnishing **21** in 73% yield) whereas the addition of the TEMPO switched off the production of **21** (0% yield).

7.3.12 DFT Calculations

DFT calculations were carried out as described in Section 3.6. The optimised Cartesian coordinates for the compounds under investigation and their radical analogues are given at:

https://static-content.springer.com/esm/art%3A10.1038%2Fs41929-018-0081-x/MediaObjects/41929_2018_81_MOESM1_ESM.pdf

7.4 Iron-Catalysed Asymmetric Cross-Coupling of 2-Bromo-1-Phenylpropane

Racemic 1,2-diphenylpropane for chiral resolution by chiral SFC was prepared according to a literature procedure.[97]

7.4.1 Suzuki-type Cross-Coupling

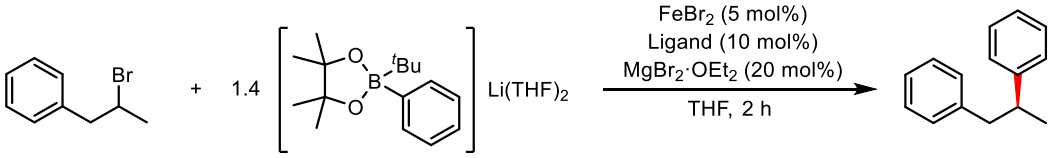

To a Schlenk-tube was added the appropriate ligand (0.015 mmol) and $FeBr_2$ (0.008 M in THF, 0.94 ml, 0.0075 mmol) and the mixture stirred until all solids dissolved (typically <1 min). $MgBr_2 \cdot OEt_2$ (0.1 M in THF, 0.3 ml, 0.03 mmol), 2-bromo-1-phenylpropane (23 µl, 0.15 mmol) and borate **18** (0.2 M in THF, 1.05 ml, 0.21 mmol) were added sequentially and the reaction was stirred at the intended temperature for 2 h before the addition 1,3,5-trimethoxybenzene (dissolved in ~ 1 ml CH_2Cl_2, 25.2 mg, 0.15 mmol). An aliquot was passed through a pad of silica eluting with CH_2Cl_2 and the solvent evaporated under reduced pressure. The residue was then dissolved in methanol and an aliquot taken for chiral SFC analysis. The rest of the methanol solution was evaporated to dryness and dissolved in $CDCl_3$ for analysis by ^1H NMR.

7.4.2 Kumada-type Cross-Coupling

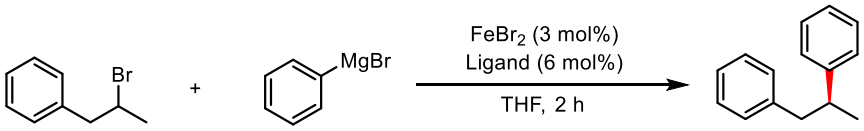

To a Schlenk-tube was added the appropriate ligand (0.03 mmol) and $FeBr_2$ (0.008 M in THF, 1.88 ml, 0.015 mmol) and the mixture stirred until all solids dissolved (typically <1 min). 2-Bromo-1-phenylpropane (46 µl, 0.3 mmol) was added and the solution cooled to the desired temperature before phenylmagnesium chloride (2 M in THF, 0.3 ml, 0.6 mmol) was added dropwise over the course of one hour causing the mixture to turn black. After stirring for an additional 10 mins, 1,3,5-trimethoxybenzene (dissolved in ~ 1 ml CH_2Cl_2, 50.4 mg, 0.3 mmol) was added and an aliquot passed through a pad of silica gel eluting with CH_2Cl_2. The solvent was removed under reduced pressure, the residue dissolved in methanol and an aliquot taken for chiral SFC analysis. The rest of the methanol solution was evaporated to dryness and dissolved in $CDCl_3$ for analysis by ^1H NMR.

7.5 Comparison of an *N*-Heterocyclic Carbene and Germylene Ligand in Iron-Catalysed Cross-Couplings

*Germylene **97** was prepared according to a literature procedure.[185] The iron-catalysed Suzuki biaryl cross coupling and cobalt-catalysed Suzuki biaryl cross-coupling reactions were performed as previously described. Cross-coupled **96** was collected from several reactions and purified by flash column chromatography (petroleum ether as eluent) for GC calibration.*

7.5.1 Reaction Profile of Cross-Coupling Between Cyclobromohexane and *p*-Toluenemagnesium Bromide

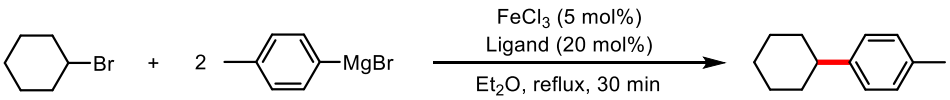

To a Schlenk-tube was added ligand (0 or 0.2 mmol), $FeCl_3$ (16.2 mg, 0.1 mmol) and CH_2Cl_2 (4 ml). After standing for 2 min, the solvent was removed *in vacuo* and Et_2O (6 ml) was added. The mixture was stirred for 2 min before bromocyclohexane (245 µl, 2 mmol) and dodecane (454 µl, 2 mmol) was added and the resulting mixture stirred for 5 min. *p*-Tolylmagnesium bromide (1 M in THF, 4 ml, 4 mmol) was added *via* syringe pump over 1 h and the reaction stirred (room temperature: 19 °C), during which time aliquots (0.1 ml) were removed from the reaction mixture and quenched with 1M HCl. The organics were extracted into CH_2Cl_2, filtered through a pad of $MgSO_4$ and analysed by GC.

7.5.2 Reaction Profile of Cross-Coupling Between Cyclobromohexane and Mesitylmagnesium Bromide

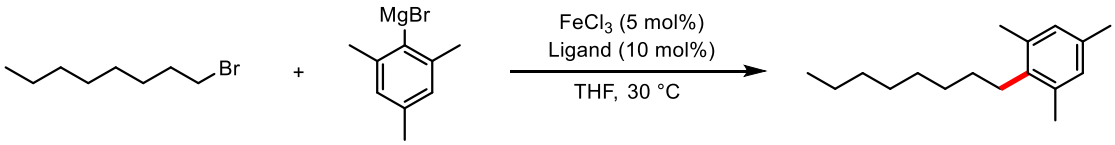

To a Schlenk-tube was added ligand (0.1 mmol), $FeCl_3$ (8 mg, 0.05 mmol), 1,3,5-trimethoxybenzene (84.1 mg, 0.5 mmol) and THF (3 ml). Mesitylmagnesium bromide (0.95 M in THF, 1.26 ml, 1.2 mmol) was added in one portion and after stirring for 30 min at room temperature, the mixture was heated to 30 °C and 1-bromooctane (173 µl, 1 mmol) was added. Aliquots (0.1 ml) were removed from the reaction mixture and quenched with 1M HCl, the organics extracted into CH_2Cl_2, filtered through a pad of $MgSO_4$ and the solvent removed. The residue was dissolved in $CDCl_3$ and analysed by ^1H NMR.

7.5.3 ^{1}H NMR Analysis of $FeCl_3$, Carbene/Germylene and Mesitylmagnesium Bromide Mixtures

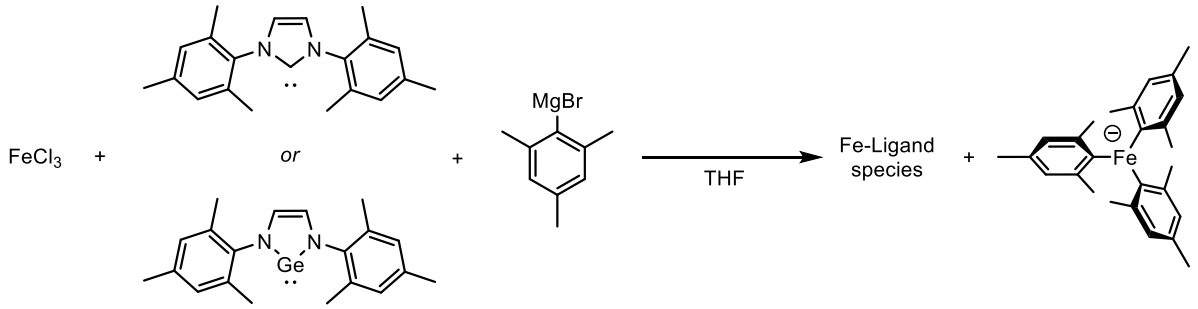

In a glovebox, a 7.5 ml vial was charged with $FeCl_3$ (4.1 mg, 0.025 mmol) and ligand (0.025 mmol). The appropriate amount of THF was added, followed by appropriate amount of mesitylmagnesium bromide (0.95 M in THF), making the total volume of the reaction mixture to 1 ml. The vial was sealed, vigorously shaken and an aliquot (~ 0.5 ml) added to an NMR tube with a sealed capillary containing cobaltocene (0.0025 or 0.005 mmol). The NMR tube sealed, removed from the glovebox and the mixture analysed by ^{1}H NMR.

7.5.4 ^{1}H NMR Analysis of $[Fe_2Mes_4]$ and 97

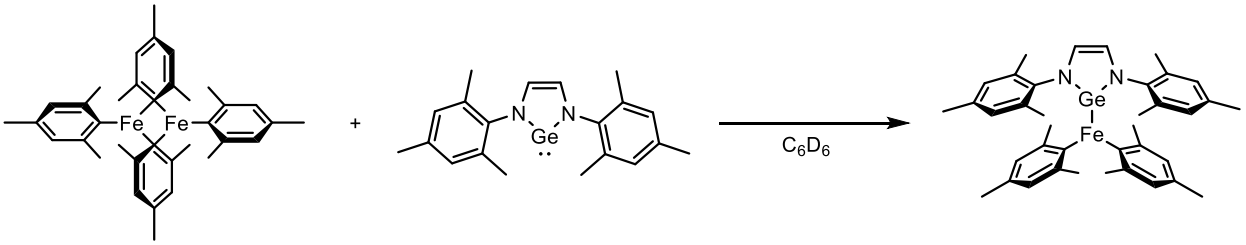

In a glovebox, a 7.5 ml vial was charged with $[Fe_2Mes_4]$ (7.6 mg, 0.0129 mmol) and **97** (0.0258 or 0.0516 mmol). C_6D_6 was added (~ 0.75 ml), the vial was sealed, vigorously shaken and left to stand for 1 h at room temperature. The mixture was transferred to an NMR tube, sealed, removed from the glovebox and the mixture analysed by ^{1}H NMR.

7.5.5 Attempted Synthesis of 108

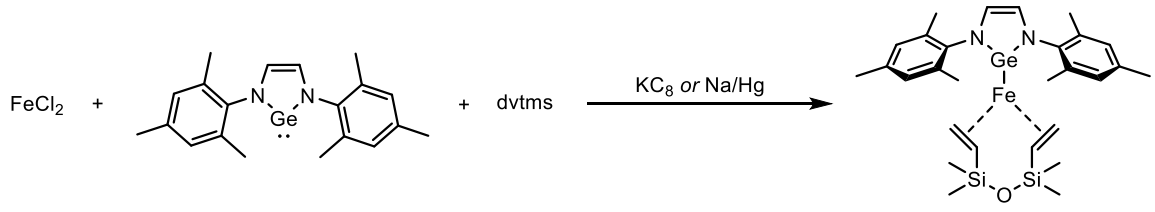

The attempted synthesis of **108** using Na/Hg was performed according to Deng and co-workers.[143] ^{1}H NMR analysis of the reduction with KC_8 (in place of place of **18** and $MgBr_2$) was performed as described in Section 7.3.1.

7.6 Crystallographic Data

Identification code	**18**	**21**	**36**	**86**
Empirical formula	$C_{24}H_{42}BLiO_4$	$C_{17}H_{13}NO$	$C_{21}H_{15}NO$	$C_{29}H_{42}FeN_2OSI_2$
Formula weight	412.32	247.28	297.34	546.67
Temperature/K	200(2)	100(2)	100(2)	100(2)
Crystal system	monoclinic	triclinic	monoclinic	triclinic
Space group	$P2_1/n$	P-1	$P2_1/n$	P-1
a/Å	9.3874(6)	9.2826(2)	6.1377(2)	8.7765(2)
b/Å	19.1079(12)	11.5379(3)	13.3562(4)	10.7292(3)
c/Å	14.2909(8)	11.9866(3)	17.9907(6)	17.4228(5)
α/°	90	80.959(1)	90	95.5463(15)
β/°	90.240(5)	89.996(1)	91.366(1)	96.2315(16)
γ/°	90	82.124(1)	90	111.6055(14)
Volume/Å^3	2563.4(3)	1255.57(5)	1474.39(8)	1499.68(7)
Z	4	4	4	2
ρ_{calc}g/cm^3	1.068	1.308	1.340	1.211
μ/mm^{-1}	0.069	0.081	0.082	0.606
F(000)	904.0	520.0	624.0	584.0
Crystal size/mm^3	0.50 × 0.35 × 0.22	0.95 × 0.70 × 0.56	0.60 × 0.36 × 0.26	0.45 × 0.30 × 0.16
Radiation	MoKα (λ = 0.71073)	MoKα (λ = 0.71073)	MoKα (λ = 0.71073)	MoKα (λ = 0.71073)
2θ range for data collection/°	2.132 to 51.47	3.442 to 55.98	3.798 to 55.98	2.378 to 52.744
Index ranges	$-8 \le h \le 11$, $-23 \le k \le 23$, $-17 \le l \le 16$	$-12 \le h \le 12$, $-15 \le k \le 15$, $-15 \le l \le 14$	$-8 \le h \le 3$, $-17 \le k \le 17$, $-23 \le l \le 23$	$-10 \le h \le 10$, $-13 \le k \le 13$, $0 \le l \le 21$
Reflections collected	19245	22889	13381	6012

R_{int} / R_{sigma}	0.0551 / 0.0528	0.0150 / 0.0133	0.0227 / 0.0205	0.0778 / 0.0397
Data/restraints/ parameters	4882/136/315	6031/0/343	3550/0/208	6012/12/327
Goodness-of-fit on F^2	1.015	1.025	1.033	1.065
Final R indexes [I>=2σ (I)]	R_1 = 0.0787, wR_2 = 0.2047	R_1 = 0.0422, wR_2 = 0.1078	R_1 = 0.0367, wR_2 = 0.0891	R_1 = 0.0412, wR_2 = 0.0943
Final R indexes [all data]	R_1 = 0.1205, wR_2 = 0.2404	R_1 = 0.0461, wR_2 = 0.1111	R_1 = 0.0446, wR_2 = 0.0938	R_1 = 0.0575, wR_2 = 0.1043
Largest diff. peak/hole / e $Å^{-3}$	0.66/-0.24	0.38/-0.25	0.33/-0.20	0.42/-0.40

References

1. Wu, X.-F; Anbarasan, P.; Neumann, H.; Beller, M. *Angew. Chem., Int. Ed.* **2010**, *49*, 9047-9050.
2. Johansson Seechurn, C.; Kitching, M. O.; Colacot, T. J.; Snieckus, V. *Angew. Chem., Int. Ed.* **2012**, *51*, 5062-5085.
3. Ullman, F.; Sponagel, P. *Ber. Dtsch. Chem. Ges.* **1905**, *38*, 2211-2212.
4. Ullman, F.; Bielecki, J. *Ber. Dtsch. Chem. Ges.* **1901**, *34*, 2174-2185.
5. Corriu, R. J. P. *J. Organomet. Chem.* **2002**, *653*, 20-22.
6. Kharasch, M. S.; Fields, E. K. *J. Am. Chem. Soc.* **1941**, *63*, 2316-2320.
7. Kharasch, M. S.; Sosnovsky, G. *J. Am. Chem. Soc.* **1958**, *80*, 756-756.
8. Kharasch, M. S; Fuchs, C. F. *J. Am. Chem. Soc.* **1943**, *65*, 504-507.
9. Meerwein, H.; Büchner, E.; van Emster, K. *J. Prakt. Chem.* **1939**, *152*, 237-266.
10. Corriu, R. J. P.; Masse, J. P. *J. Chem. Soc., Chem. Commun*. **1972**, 144a-144a.
11. Tamao, K.; Sumitani, K.; Kumada, M. *J. Am. Chem. Soc.* **1972**, *94*, 4374-4376.
12. Tamao, K.; Kiso, Y.; Sumitani, K.; Kumada, M. *J. Am. Chem. Soc.* **1972**, *94*, 9268-9269.
13. Heck, R. F. *J. Am. Chem. Soc.* **1968**, *90*, 5518-5526.
14. Heck, R. F. *J. Am. Chem. Soc.* **1968,** *90*, 5526-5531.
15. Heck, R. F. *J. Am. Chem. Soc.* **1968**, *90*, 5531-5534.
16. Heck, R. F. *J. Am. Chem. Soc.* **1968**, *90*, 5535-5538.
17. Heck, R. F. *J. Am. Chem. Soc.* **1968**, *90*, 5538-5542.
18. Heck, R. F. *J. Am. Chem. Soc.* **1968**, *90*, 5542-5546.
19. Heck, R. F. *J. Am. Chem. Soc.* **1968**, *90*, 5546-5548.
20. Heck, R. F.; Nolley, J. P. *J. Org. Chem.* **1972**, *37*, 2320-2322.
21. Sonogashira, K.; Tohda, Y.; Hagihara, N. *Tetrahedron Lett.* **1975**, *16*, 4467-4470.
22. Negishi, E.-I. In *Aspects of Mechanism and Organometallic Chemistry*; Brewster, J. H., Eds.; Springer US: Boston, MA, 1978; pp 285-317.
23. Yamamura, M.; Moritani, I.; Murahashi, S.-I. *J. Organomet. Chem.* **1975**, *91*, C39-C42.
24. Murahashi, S.; Yamamura, M.; Yanagisawa, K.; Mita, N.; Kondo, K. *J. Org. Chem.* **1979**, *44*, 2408-2417.
25. Negishi, E.-I.; Baba, S. *J. Chem. Soc., Chem. Commun.* **1976**, 596b-597b.
26. King, A. O.; Okukado, N.; Negishi, E.-I. *J. Chem. Soc. Chem. Commun.* **1977**, 683-684.
27. Negishi, E.-I.; King, A. O.; Okukado, N. *J. Org. Chem.* **1977**, *42*, 1821-1823.
28. Milstein, D.; Stille, J. K. *J. Am. Chem. Soc.* **1978**, *100*, 3636-3638.
29. Miyaura, N.; Suzuki, A. *J. Chem. Soc., Chem. Commun.* **1979**, 866-867.
30. Miyaura, N.; Suzuki, A. *Chem. Rev.* **1995**, *95*, 2457-2483.
31. Hatanaka, Y.; Hiyama, T. *J. Org. Chem.* **1988**, *53*, 918-920.
32. Roughley, S. D.; Jordan, A. M. *J. Med. Chem.* **2011**, *54*, 3451-3479.
33. Nicolaou, K. C.; Bulger, P. G.; Sarlah, D. *Angew. Chem., Int. Ed.* **2005**, *44*, 4442-4489.
34. Torborg, C.; Beller, M. *Adv. Synth. Catal.* **2009**, *351*, 3027-3043.

35. Busacca, C. A.; Fandrick, D. R.; Song, J. J.; Senanayake, C. H. *Adv. Synth. Catal.* **2011**, *353*, 1825-1864.

36. Beutler, U.; Mazacek, J.; Penn, G.; Schenkel, B.; Wasmuth, D. *CHIMIA Int. J. Chem.* **1996**, *50*, 154-156.

37. Negishi, E.-I.; Alimardanov, A.; Xu, C. *Org. Lett.* **2000**, *2*, 65-67.

38. Garrett, C. E.; Prasad, K. *Adv. Synth. Catal.* **2004**, *346*, 889-900.

39. Tamura, M.; Kochi, J. K. *J. Am. Chem. Soc.* **1971**, *93*, 1487-1489.

40. Fabre, J.-L.; Julia, M.; Verpeaux, J.-N. *Tetrahedron Lett.* **1982**, *23*, 2469-2472.

41. Molander, G. A.; Rahn, B. J.; Shubert, D. C.; Bonde, S. E. *Tetrahedron Lett.* **1983**, *24*, 5449-5452.

42. Fiandanese, V.; Miccoli, G.; Naso, F.; Ronzini, L. *J. Organomet. Chem.* **1986**, *312*, 343-348.

43. Cahiez, G.; Avedissian, H. *Synthesis* **1998**, 1199-1205.

44. Fürstner, A.; Leitner, A. *Angew. Chem., Int. Ed.* **2002**, *41*, 609-612.

45. Fürstner, A.; Leitner, A.; Méndez, M.; Krause, H. *J. Am. Chem. Soc.* **2002**, *124*, 13856-13863.

46. Cárdenas, D. J. *Angew. Chem., Int. Ed.* **2003**, *42*, 384-387.

47. Nagano, T.; Hayashi, T. *Org. Lett.* **2004**, *6*, 1297-1299.

48. Nakamura, M.; Matsuo, K.; Ito, S.; Nakamura, E. *J. Am. Chem. Soc.* **2004**, *126*, 3686-3687.

49. Bedford, R. B.; Bruce, D. W.; Frost, R. M.; Goodby, J. W.; Hird, M. *Chem. Commun.* **2004**, 2822-2823.

50. Martin, R.; Fürstner, A. *Angew. Chem., Int. Ed.* **2004**, *43*, 3955-3957.

51. Bedford, R. B.; Bruce, D. W.; Frost, R. M.; Hird, M. *Chem. Commun.* **2005**, 4161-4163.

52. Bedford, R. B.; Betham, M.; Bruce, D. W.; Danopoulos, A. A.; Frost, R. M.; Hird, M. *J. Org. Chem.* **2006**, *71*, 1104-1110.

53. Corbet, J.-P.; Mignani, G. *Chem. Rev.* **2006**, *106*, 2651-2710.

54. Cepanec, I. In *Synthesis of Biaryls*; Cepanec, I., Eds.; Elsevier Science Ltd: Oxford, 2004, pp 139-207.

55. Hatakeyama, T.; Nakamura, M. *J. Am. Chem. Soc.* **2007**, *129*, 9844-9845.

56. Hatakeyama, T.; Hashimoto, S.; Ishizuka, K.; Nakamura, M. *J. Am. Chem. Soc.* **2009**, *131*, 11949-11963.

57. Chua Y.-Y.; Duong, H. A. *Chem. Commun.* **2014**, *50*, 8424-8427.

58. Chua Y.-Y.; Duong, H. A. *Chem. Commun.* **2016**, *52*, 1466-1469.

59. Gülak, S.; Jacobi von Wangelin, A. *Angew. Chem., Int. Ed.* **2011**, *51*, 1357-1361.

60. Dongol, K. G.; Huishi, K.; Manisankar, S.; Chai, C. L. L. *Adv. Synth. Catal.* **2007**, *349*, 1015-1018.

61. Guisán-Ceinos, M.; Tato, F.; Buñuel, E.; Calle, P.; Cárdenas, D. J. *Chem. Sci.* **2013**, *4*, 1098-1104.

62. Nakamura, M.; Ito, S.; Matsuo, K.; Nakamura, E. *Synlett* **2005**, 1794-1798.

63. Hatakeyama, T.; Nakagawa, N.; Nakamura, M. *Org. Lett.* **2009**, *11*, 4496-4499.

64. Bedford, R. B.; Huwe, M.; Wilkinson, M. C. *Chem. Commun.* **2009**, 600-602.

65. Hatakeyama, T.; Kondo, Y.; Fujiwara, Y.-I.; Takaya, H.; Ito, S.; Nakamura, E.; Nakamura, M. *Chem. Commun.* **2009**, 1216-1218.

66. Clifton, J.; Habraken, E. R. M.; Pringle, P. G.; Manners, I. *Catal. Sci. Technol.* **2015**, *5*, 4350-4353.

67. Bedford, R. B.; Carter, E.; Cogswell, P. M.; Gower, N. J.; Haddow, M. F.; Harvey, J. N.; Murphy, D. M.; Neeve, E. C.; Nunn, J. *Angew. Chem., Int. Ed.* **2013**, *52*, 1285-1288.

68. Bedford, R. B.; Hall, M. A.; Hodges, G. R.; Huwe, M.; Wilkinson, M. C. *Chem. Commun.* **2009**, 6430-6432.

69. Hatakeyama, T.; Hashimoto, T.; Kondo, Y.; Fujiwara, Y.; Seike, H.; Takaya, H.; Tamada, Y.; Ono, T.; Nakamura, M. *J. Am. Chem. Soc.* **2010**, *132*, 10674-10676.

70. Bedford, R. B.; Brenner, P. B.; Carter, E.; Clifton, J.; Cogswell, P. M.; Gower, N. J.; Haddow, M. F.; Harvey, J. N.; Kehl, J. A.; Murphy, D. M.; Neeve, E. C.; Neidig, M. L.; Nunn, J.; Snyder, B. E. R.; Taylor, J. *Organometallics*, **2014**, *33*, 5767-5780.

71. Hatakeyama, T.; Hashimoto, T.; Kathriarachchi, K. K. A. D. S.; Zenmyo, T.; Seike, H.; Nakamura, M. *Angew. Chem., Int. Ed.* **2012**, *51*, 8834-8837.

72. Kawamura, S.; Ishizuka, K.; Takaya, H.; Nakamura, N. *Chem. Commun.* **2010**, *46*, 6054-6056.

73. Hatakeyama, T.; Okada, Y.; Yoshimoto, Y.; Nakamura, N. *Angew. Chem., Int. Ed.* **2011**, *50*, 10973-10976.

74. Carril, M.; Correa, A.; Bolm, C. *Angew. Chem.* **2008**, *120*, 4940-4943.

75. Hatakeyama, T.; Yoshimoto, Y.; Gabriel, T.; Nakamura, M. *Org. Lett.* **2008**, *10*, 5341-5344.

76. Xie, X.; Xu, X.; Li, H.; Xu, X.; Yang, J.; Li, Y. *Adv. Synth. Catal.* **2009**, *351*, 1263-1267.

77. Loska, R.; Roa Volla, C. M.; Vogel, P. *Adv. Synth. Catal.* **2008**, *350*, 2859-2864.

78. Waldhart, G. W.; Mankad, N. P. *J. Organomet. Chem.* **2015**, *793*, 171-174.

79. Piontek, A.; Bisz, E.; Szostak, M. *Angew. Chem., Int. Ed.* **2018**, *57*, 11116-11128.

80. Gangula, S.; Neelam, U. K.; Baddam, S. R.; Dahanukar, V. H.; Bandichhor, R. *Org. Process Res. Dev.* **2015**, *19*, 470-475.

81. Kim, M. J.; Lee, J.; Kang, S. Y.; Lee, S.-H.; Son, E.-J.; Jung, M. E.; Lee, S. H.; Song, K.-S.; Lee, M.; Han, H.-K.; Kim, J.; Lee, J. *Bioorg. Med. Chem. Lett.* **2010**, *20*, 3420-3425.

82. Bisz, E.; Szostak, M. *ChemSusChem* **2018**, *11*, 1290-1294.

83. Noda, D.; Sunada, Y.; Hatakeyama, T.; Nakamura, M.; Nagashima, H. *J. Am. Chem. Soc.* **2009**, *131*, 6078-6079.

84. Bedford, R. B.; Brenner, P. B.; Carter, E.; Cogswell, P. M.; Haddow, M. F.; Harvey, J. N.; Murphy, D. M.; Nunn, J.; Woodall, C. H. *Angew. Chem., Int. Ed.* **2014**, *53*, 1804-1808.

85. Bedford, R. B. *Acc. Chem. Res.* **2015**, *48*, 1485-1493.

86. Ding, K.; Zannat, F.; Morris, J. C.; Brennessel, W. W.; Holland, P. L. *J. Organomet. Chem.* **2009**, *694*, 4204-4208.

87. Muñoz III, S. B.; Daifuku, S. L.; Sears, J. D.; Baker, T. M.; Carpenter, S. H.; Brennessel, W. W.; Neidig, M. L. *Angew. Chem., Int. Ed.* **2018**, *57*, 6496-6500.

88. Daifuku, S. L.; Al-Afyouni, M. H.; Snyder, B. E. R.; Kneebone, J. L.; Neidig, M. L. *J. Am. Chem. Soc.* **2014**, *136*, 9132-9143.

89. Przyojski, J. A.; Veggeberg, K. P.; Arman H. D.; Tonzetich, Z. J. *ACS Catal*. **2015**, *5*, 5938-5946.

90. Bogdanović, B.; Schwickardi, M. *Angew. Chem., Int. Ed.* **2000**, *39*, 4610-4612.

91. Casitas, A.; Rees, J. A.; Goddard, R.; Bill, E.; DeBeer, S.; Fürstner, A. *Angew. Chem., Int. Ed.* **2017**, *56*, 10108-10113.

92. Fürstner, A.; Martin, R.; Krause, H.; Seidel, G.; Goddard, R.; Lehmann, C. W. *J. Am. Chem. Soc.* **2008**, *130*, 8773-8787.

93. Bedford, R. B.; Betham, M.; Bruce, D. W.; Davis, S. A.; Frost, R. M.; Hird, M. *Chem. Commun.* **2006**, 1398-1400.

94. Smith, R. S.; Kochi, J. K. *J. Org. Chem.* **1976**, *41*, 502-509.

95. Muñoz III, S. B.; Daifuku, S. L.; Brennessel, W. W.; Neidig, M. L. *J. Am. Chem. Soc.* **2016**, *138*, 7492-7495.

96. Adams, C. J.; Bedford, R. B.; Carter, E.; Gower, N. J.; Haddow, M. F.; Harvey, J. N.; Huwe, M.; Cartes, M. Á.; Mansell, S. M.; Mendoza, C.; Murphy, D. M.; Neeve, E. C.; Nunn, J. *J. Am. Chem. Soc.* **2012**, *134*, 10333-10336.

97. Bedford, R. B.; Brenner, P. B.; Carter, E.; Carvell, T. W.; Cogswell, P. M.; Gallagher, T.; Harvey, J. N.; Murphy, D. M.; Neeve, E. C.; Nunn, J.; Pye, D. R. *Chem. Eur. J.* **2014**, *20*, 7935-7938.

98. Hatakeyama, T.; Fujiwara, Y.-I.; Okada, Y.; Itoh, T.; Hashimoto, T.; Kawamura, S.; Ogata, K.; Takaya, H.; Nakamura, M. *Chem. Lett.* **2011**, *40*, 1030-1032.

99. Nakagawa, N.; Hatakeyama, T.; Nakamura, M. *Chem. Lett.* **2015**, *44*, 486-488.

100. Hashimoto, T.; Hatakeyama, T.; Nakamura, M. *J. Org. Chem.* **2012**, *77*, 1168-1173.

101. Kneebone, J. L.; Brennessel, W. W.; Neidig, M. L. *J. Am. Chem. Soc.* **2017**, *139*, 6988-7003.

102. Daifuku, S. L.; Kneebone, J. L.; Snyder, B. E. R.; Neidig, M. L. *J. Am. Chem. Soc.* **2015**, *137*, 11432-11444.

103. Han, F.-S. *Chem. Soc. Rev.* **2013**, *42*, 5270-5298.

104. Mastalir, M.; Stöger, B.; Pittenauer, E.; Allmaier, G.; Kirchner, K. *Org. Lett.* **2016**, *18*, 3186-3189.

105. Zhou, J.; Berthel, J. H. J.; Kuntze-Fechner, M. W.; Friedrich, A.; Marder T. B.; Radius, U. *J. Org. Chem.* **2016**, *81*, 5789-5794.

106. Shi, S.; Meng, G.; Szostak, M. *Angew. Chem., Int. Ed.* **2016**, *55*, 6959-6963.

107. Malan, F. P.; Singleton, E.; van Rooyen P. H.; Landman, M. *J. Organomet. Chem.* **2016**, *813*, 7-14.

108. Shields, J. D.; Gray, E. E.; Doyle, A. G. *Org. Lett.* **2015**, *17*, 2166-2169.

109. Thapa, S.; Shrestha, B.; Gurung, S. K.; Giri, R. *Org. Biomol. Chem.* **2015**, *13*, 4816-4827.

110. Gurung, S. K.; Thapa, S.; Shrestha, B.; Giri, R. *Org. Chem. Front.* **2015**, *2*, 649-653.

111. Zhou, Y.; You, W.; Smith, K. B.; Brown, M. K. *Angew. Chem., Int. Ed.* **2014**, *53*, 3475-3479.

112. Gurung, S. K.; Thapa, S.; Kafle, A.; Dickie, D. A.; Giri, R. *Org. Lett.* **2014**, *16*, 1264-1267.

113. Neely, J. M.; Bezdek, M. J.; Chirik, P. J. *ACS Cent. Sci*. **2016**, *2*, 935-942.

114. Duong, H. A.; Wu W.; Teo, Y.-Y. *Organometallics* **2017**, *36*, 4363-4366.

115. Asghar, S.; Tailor, S. B.; Elorriaga, D.; Bedford, R. B. *Angew. Chem., Int. Ed.* **2017**, *56*, 16367-16370.

116. Edaravone Acute Infarction Study Group *Cerebrovasc. Dis.* **2003**, *15*, 222-229.

117. https://www.accessdata.fda.gov/drugsatfda_docs/label/2017/209176lbl.pdf

118. Kylmälä, T.; Valkonen, A.; Rissanen, K.; Xu, Y.; Franzén, R. *Tetrahedron Lett.* **2008**, *49*, 6679-6681.

119. Bézier, D; Darcel, C. *Adv. Synth. Catal.* **2009**, *351*, 1732-1736.

120. Bedford, R. B.; Nakamura, M.; Gower, N. J.; Haddow, M. F.; Hall, M. A.; Huwe, M.; Hashimoto, T.; Okopie, R. A. *Tetrahedron Lett.* **2009**, *50*, 6110-6111.

121. Guo, Y.; Young D. J.; Hor, A. T. S. *Tetrahedron Lett.* **2008**, *49*, 5620-5621.

122. Bedford, R. B.; Gallagher, T.; Pye, D. R.; Savage, W. *Synthesis* **2015**, *47*, 1761-1765.

123. Berlin, J. M.; Campbell, K.; Ritter, T.; Funk, T. W.; Chlenov, A.; Grubbs, R. H. *Org. Lett.* **2007**, *9*, 1339-1342.

124. Hintermann, L. *Beilstein J. Org. Chem.* **2007**, *3*, 22.

125. Arduengo, A. J., III U.S. Patent 5,077,414, 1991.

126. Berlin, J. M.; Grubbs, R. H.; Schrodi, Y; Steward, I. C. W. O Patent 2007075427, 2007.

127. Hickman, A. J.; Sanford, M. S. *ACS Catal.* **2011**, *1*, 170-174.

128. Tian, J.-Y.; Luo, Q.-C.; Liang, H.-Z.; Chen, X.-H. *Med. Plant* **2011**, *2*, 9-12.

129. Li, X.; Zou, G. *Chem. Commun.* **2015**, *51*, 5089-5092.

130. Weires, N. A.; Baker, E. L.; Garg, N. K. *Nat. Chem.* **2016**, *8*, 75-79.

131. Dander, J. E.; Garg, N. K. *ACS Catal.* **2017**, *7*, 1413-1423.

132. Meng, G.; Szostak, R.; Szostak, M. *Org. Lett.* **2017**, *19*, 3596-3599.

133. Procter, R. J.; Dunsford, J. J.; Rushworth, P. J.; Hulcoop, D. G.; Layfield, R. A.; Ingleson, M. J. *Chem. Eur. J.* **2017**, *23*, 15889-15893.

134. Yonezawa, S.; Komurasaki, T.; Kawada, K.; Tsuri, T.; Fuji, M.; Kugimiya, A.; Haga, N.; Mitsumori, S.; Inagaki, M.; Nakatani, T.; Tamura, Y.; Takechi, S.; Taishi, T.; Ohtani, M. *J. Org. Chem.* **1998**, *63*, 5831-5837.

135. Tian, S.-Z.; Pu, X.; Luo, G.; Zhao, L.-X.; Xu, L.-H.; Li, W.-J.; Luo, Y. *J. Agric. Food Chem.* **2013**, *61*, 3006-3012.

136. Denmark, S. E.; Butler, C. R. *Chem. Commun.* **2009**, 20-33.

137. Bedford, R. B.; Brenner, P. B.; Carter, E.; Gallagher, T.; Murphy, D. M.; Pye, D. R. *Organometallics* **2014**, *33*, 5940-5943.

138. Atack, T. C.; Lecker, R. M.; Cook, S. P. *J. Am. Chem. Soc.* **2014**, *136*, 9521-9523.

139. Yoshida, T.; Ilies, L.; Nakamura, E. *ACS Catal.* **2017**, *7*, 3199-3203.

140. Dunsford, J. J.; Cade, I. A.; Fillman, K. L.; Neidig, M. L.; Ingleson, M. J. *Organometallics* **2014**, *33*, 370-377.

141. Dunsford, J. J.; Clark, E. R.; Ingleson, M. J. *Dalton Trans.* **2015**, *44*, 20577-20583.

142. Blom, B.; Tan, G.; Enthaler, S.; Inoue, S.; Epping, J. D.; Driess, M. *J. Am. Chem. Soc.* **2013**, *135*, 18108-18120.

143. Zhang, H.; Ouyang, Z.; Liu, Y.; Zhang, Q.; Wang, L.; Deng, L. *Angew. Chem., Int. Ed.* **2014**, *53*, 8432-8436.

144. Hashimoto, T.; Hoshino, R.; Hatanaka, T.; Ohki, Y.; Tatsumi, K. *Organometallics* **2014**, *33*, 921-929.

145. Mo, Z.; Ouyang, Z.; Wang, L.; Fillman, K. L.; Neidig, M. L.; Deng, L. *Org. Chem. Front.* **2014**, *1*, 1040-1044.

146. Ouyang, Z.; Du, J.; Wang, L.; Kneebone, J. L.; Neidig, M. L.; Deng, L. *Inorg. Chem.* **2015**, *54*, 8808-8816.

147. Przyojski, J. A.; Arman, H. D.; Tonzetich, Z. J. *Organometallics* **2012**, *31*, 3264-3271.

148. Danopoulos, A. A.; Braunstein, P.; Wesolek, M.; Monakhov, K. Y.; Rabu, P.; Robert, V. *Organometallics* **2012**, *31*, 4102-4105.

149. Dunsford, J. J.; Evans, D. J.; Pugh, T.; Shah, S. N.; Chilton, N. F.; Ingleson, M. J. *Organometallics* **2016**, *35*, 1098-1106.

150. Crabtree, R. H. *Chem. Rev.* **2012**, *112*, 1536-1554.

151. Gieshoff, T. N.; Villa, M.; Welther, A.; Plois, M.; Chakraborty, U.; Wolf, R.; Jacobi von Wangelin, A. *Green Chem.* **2015**, *17*, 1408-1413.

152. Joshi, K. K.; Pauson, P. L.; Qazi, A. R.; Stubbs, W. H. *J. Organomet. Chem.* **1964**, *1*, 471-475.

153. King, R. B.; Bisnette, M. B. *Inorg. Chem.* **1964**, *3*, 796-800.

154. Kreye, M.; Baabe, D.; Schweyen, P.; Freytag, M.; Daniliuc, C. G.; Jones, P. G.; Walter, M. D. *Organometallics* **2013**, *32*, 5887-5898.

155. Kuhn, N.; Horn, E. M.; Zauder, E.; Bläser, D.; Boese, R. *Angew. Chem., Int. Ed.* **1988**, *27*, 579-580.

156. Kowalski, K.; Suwaki, N.; Zakrzewski, J.; White, A. J. P.; Long, N. J.; Mann, D. J. *Dalton Trans.* **2007**, 743-748.

157. Kuhn, N.; Schulten, M.; Zauder, E.; Augart, N.; Boese, R. *Chem. Ber.* **1989**, *122*, 1891-1896.

158. Kuhn, N.; Kuhn, A.; Lampe, E.-M. *Chem. Ber.* **1991**, *124*, 997-1002.

159. Gómez-Gallego, M.; Sierra, M. A. *Chem. Rev.* **2011**, *111*, 4857-4963.

160. Leitch, J. A.; Bhonoah, Y.; Frost, C. G. *ACS Catal.* **2017**, *7*, 5618-5627.

161. Sandford, C.; Rasappan, R.; Aggarwal, V. K. *J. Am. Chem. Soc.* **2015**, *137*, 10100-10103.

162. Li, X.; Cai, Z.; Sevilla, M. D. *J. Phys. Chem. A* **2002**, *106*, 1596-1603.

163. Li, P.; Bu, Y.; Ai, H. *J. Phys. Chem. A* **2004**, *108*, 1200-1207.

164. Chiara, J. L.; García, Á.; Cristóbal-Lumbroso, G. *J. Org. Chem.* **2005**, *70*, 4142-4151.

165. Shi, S; Szostak, M. *Org. Lett.* **2015**, *17*, 5144-5147.

166. Zhu, D.; Budzelaar, P. H. M. *Organometallics* **2010**, *29*, 5759-5761.

167. Jin, M.; Adak, L.; Nakamura, M. *J. Am. Chem. Soc.* **2015**, *137*, 7128-7134.

168. Mao, J.; Liu, F.; Wang, M.; Wu, L.; Zheng, B.; Liu, S.; Zhong, J.; Bian, Q.; Walsh, P. J. *J. Am. Chem. Soc.* **2014**, *136*, 17662-17668.

169. Sharma, A. K.; Sameera, W. M. C.; Jin, M.; Adak, L.; Okuzono, C.; Iwamoto, T.; Kato, M.; Nakamura, M.; Morokuma, K. *J. Am. Chem. Soc.* **2017**, *139*, 16117-16125.

170. Lee, W.; Zhou, J.; Gutierrez, O. *J. Am. Chem. Soc.* **2017**, *139*, 16126-16133.

171. Saito, B.; Fu, G. C. *J. Am. Chem. Soc.* **2008**, *130*, 6694-6695.

172. Wanzlick, H.-W.; Schönherr, H.-J. *Angew. Chem.* **1968**, *80*, 154-154.

173. Kirmse, W. *Angew. Chem., Int. Ed.* **2010**, *49*, 8798-8801.

174. Arduengo, A. J.; Harlow, R. L.; Kline, M. *J. Am. Chem. Soc.* **1991**, *113*, 361-363.

175. Arduengo, A. J.; Goerlich, J. R.; Marshall, W. J. *J. Am. Chem. Soc.* **1995**, *117*, 11027-11028.

176. Hopkinson, M. N.; Richter, C.; Schedler, M.; Glorius, F. *Nature* **2014**, *510*, 485-496.

177. Ghorai, S. K.; Jin, M.; Hatakeyama, T.; Nakamura, M. *Org. Lett.* **2012**, *14*, 1066-1069.

178. Rosa, J. N.; Reddy, R. S.; Candeias, N. R.; Cal, P. M. S. D.; Gois, P. M. P. *Org. Lett.* **2010**, *12*, 2686-2689.

179. Elina, B.; Lorenzo, Z.; Hans, A. *Appl. Organomet. Chem.* **2011**, *25*, 748-752.

180. Nemcsok, D.; Wichmann, K.; Frenking, G. *Organometallics* **2004**, *23*, 3640-3646.

181. Khramov, D. M.; Lynch, V. M.; Bielawski, C. W. *Organometallics* **2007**, *26*, 6042-6049.

182. Díez-González, S.; Marion, N.; Nolan, S. P. *Chem. Rev.* **2009**, *109*, 3612-3676.

183. Jacobsen, H.; Correa, A.; Poater, A.; Costabile, C.; Cavallo, L. *Coord. Chem. Rev.* **2009**, *253*, 687-703.

184. Jutzi, P.; Steiner, W. *Angew. Chem.* **1976**, *88*, 720-721.

185. York, J. T.; Young, V. G.; Tolman, W. B. *Inorg. Chem.* **2006**, *45*, 4191-4198.

186. Seyferth, D.; Hofmann, H. P.; Burton, R.; Helling, J. F. *Inorg. Chem.* **1962**, *1*, 227-231.

187. Saur, I.; Rima, G.; Miqueu, K.; Gornitzka, H.; Barrau, J. *J. Organomet. Chem.* **2003**, *672*, 77-85.

188. El Ezzi, M.; Kocsor, T.-G.; D'Accriscio, F.; Madec, D.; Mallet-Ladeira, S.; Castel, A. *Organometallics* **2015**, *34*, 571-576.

189. Benedek, Z.; Szilvási, T. *Organometallics* **2017**, *36*, 1591-1600.

190. Hu, J.; Gao, B.; Li, L.; Ni, C.; Hu, J. *Org. Lett.* **2015**, *17*, 3086-3089.

191. Frantz, M.-C.; Rodrigo, J.; Boudier, L.; Durroux, T.; Mouillac, B.; Hibert, M. *J. Med. Chem.* **2010**, *53*, 1546-1562.

192. Zuo, B.; Chen, J.; Liu, M.; Ding, J.; Wu, H.; Su, W. *J. Chem. Res.* **2009**, 14-16.

193. Ren, W.; Yamane, M. *J. Org. Chem.* **2010**, *75*, 8410-8415.

194. Lee, C. K; Jun, J. H.; Yu, J. S. *J. Het. Chem.* **2000**, *37*, 15-24.

195. Wu, Y.; Wang, S.; Zhang, L.; Yang, G.; Zhu, X.; Zhou, Z.; Zhu, H.; Wu, S. *Eur. J. Org. Chem.* **2010**, 326-332.

196. Racine, E.; Monnier, F.; Vors, J.-P.; Taillefer, M. *Org. Lett.* **2011**, *13*, 2818-2821.